

Letter from the Editors

Dear readers,
The Editorial Board and the Editorial Council are delighted to bring to your attention the ninth issue of *Acta Naturae*. We have maintained the conventional format of previous issues, and we offer several reviews, original articles, and the popular Forum section, which we believe will be of great interest. Regretfully, and in spite of numerous attempts, we were unable to get clinicians, experts in the sphere of experimental medicine, involved with this issue. We are on the lookout for serious research made by Russian and foreign scientists in the field of fundamental medicine for our subsequent issues. It is no coincidence that a new department has been established in the Russian Academy of Sciences, with a mission to focus efforts in this field. Therefore, we invite the members of this newly founded department to share the most interesting developments and their views in our Forum section in subsequent issues of this journal.

We offer to your attention the review made by V.V. Pleshkan *et al.*, which is devoted to gene therapy for melanoma. In our opinion, the review is representative of the modern tendencies that exist in the directed therapy of malignant tumors. The review by M.V. Nesterchuk *et al.* deals with the rather interesting field of the posttranslational modifications of ribosomal proteins of the prokaryotic cell. Regardless of the vast pool of studies devoted to the prokaryotic ribosome, including the contemporary X-ray diffraction studies, the functional role of the posttranslational modifications of ribosomal proteins still remains a puzzle. The review by L.A. Dykman and N.G. Khlebtsov is devoted to gold nanoparticles and their application in biology and medicine. The review contains a considerable amount of bibliographic data; we believe it will be of equal interest to seasoned researchers, undergraduates, and PhD students.

The insightful population genetics study by V.A. Stepanov *et al.* opens the section of experimental articles in this issue. The articles devoted to the components of innate immunity are conventionally published in this issue. The article by O.V. Samsonova *et al.* is devoted to the structural and functional studies of the antimicrobial peptide Ltc1-K that is toxic to eukaryotic cells. The article by K.V. Lobanov *et al.* deals with the topic of the mechanism-dependent therapeutic effect of drugs. The studies in the field of the physical chemistry of trans-membrane proteins (K.S. Mineev *et al.*) are traditionally strong. Composite authors (O.A. Zorina *et al.*) present clinical research through the use of modern methods of DNA diagnostics. It is exulting that articles relating to physiology have begun to appear in the journal. The article by Yu.G. Odnoshivkina *et al.* devoted to the activation of β_2 -adrenoreceptors should be mentioned in this context.

The Forum section offers you information on the visit by a delegation from the National Institute of Health (NIH, U. S.) to the Russian Academy of Sciences. The authors of the article look into the prospects of future international collaboration and emphasize the fact that, after an affectedly long interruption in official scientific contacts, both parties have finally found it worthwhile to resume dialogue. The section also features an interview with Deputy Minister of Education and Science of the Russian Federation Sergei Ivannets devoted to the crucial issue of financial support for contemporary science and the problem of the “150-million-rouble grants.” Although some of the views in the interview are not shared by the members of the Editorial Board and the Editorial Council of this journal, we have always stood for the diversity multipolarity of views in this section, and we intend to continue publishing interesting materials and articles devoted to topics that have the attention of Russian researchers.

Save 10% on Subscription for 2011

Details at www.actanaturae.ru

RESEARCH ARTICLES

Docking approaches are further improved by implementing new algorithms of the conformational search and new scoring functions (methods to estimate the free energy of ligand binding). Scoring functions may include either components of molecular mechanics force fields [2] or empirical terms, e.g. hydrogen bonds classified by their geometrical parameters [4]. In this work we studied stacking interactions, which usually are not properly taken into account in widely used scoring functions.

THE PARAMETERS OF STACKING INTERACTIONS

Of all the various types of interaction in biomolecular complexes (such as hydrogen bonds, salt bridges, etc.), the stacking of aromatic substances deserves special attention. Most drugs include aromatic fragments in their chemical structure, and stacking often plays a notable role in their recognition by protein-targets. We have recently shown that an explicit account of stacking in scoring functions increases the efficiency of ATP docking [6]. The aromatic interactions were identified by the mutual orientation of two cycles described by geometrical parameters: the height h and displacement d of one cycle relative to the other, and the angle between their planes (Fig. 1).

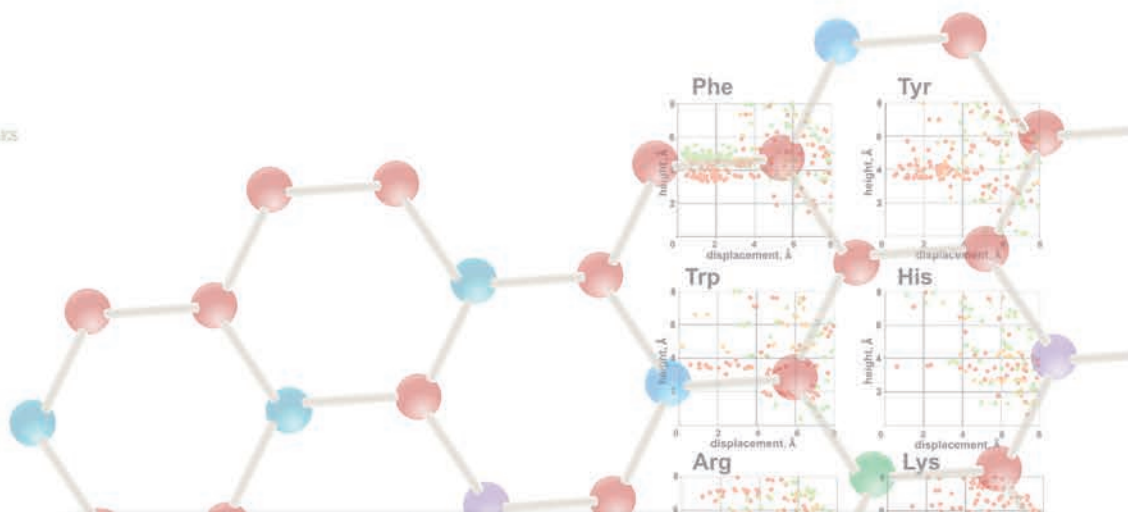
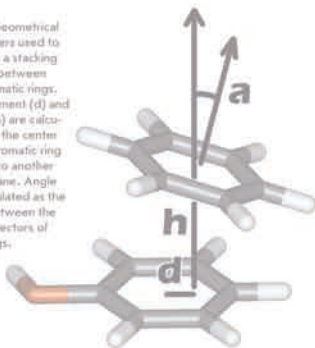
However, the range of these parameters, which corresponds to the presence or absence of a stacking contact, is still not very well defined and usually taken as arbitrary [6, 7]. Defining it more accurately would assist in developing more efficient scoring functions and should increase the prediction quality of the spatial structures of protein-ligand complexes by molecular modeling methods. With this aim in view, we performed an analysis of the spatial structures of protein-ligand complexes determined experimentally with atomic resolution where ligands contained adenine or guanine as a substructure.

One well-known example of stacking interactions is the parallel packing of purine and pyrimidine nucleobases in DNA [8, 9]. Some aromatic compounds tend to orient perpendicular to each other (T-shaped stacking), as has been shown for amino acids in proteins [7, 10] and for model systems of carbon aromatic cycles (benzene and naphthalene) [11–14]. Besides, such compounds participate in cation- π interactions, where a positively charged group interacts with the negatively charged cloud of aromatic π -electrons [15–17].

Taking all that into account, we analyzed the distribution of geometrical parameters h , d , and α for contacts of adenine and guanine moieties of ligands with the aromatic side-chains of receptor amino acids Phe, Tyr, Trp, and His, as well as with the positively charged guanidino group of Arg and amino group of Lys. The results obtained for guanine are presented in Fig. 2.

It can be seen that two distinct orientations are typical for Phe: parallel and perpendicular to the guanine plane (Fig. 2, shown in red and green, respectively). The displacement d lies in the same range 0–3 Å for both types of contacts. Meanwhile, they clearly differ in the value of height h , which is ≈ 4.8 for parallel Å and ≈ 5.5 Å for perpendicular orientation. Similar distributions were obtained for Tyr, Trp, and His, though the data are sparser in these cases. However, the T-shaped contact is not as typical for Tyr, Trp, and His as it is for Phe.

Fig. 1. Geometrical parameters used to describe a stacking contact between two aromatic rings. Displacement (d) and height (h) are calculated for the center of one aromatic ring relative to another ring's plane. Angle α is calculated as the angle between the normal vectors of both rings.



APRIL/JUNE 2009, No 1

ActaNaturae

SYNTHETIC ANTIBODIES
FOR CLINICAL USE

REGULATING TELOMERASE IN ONCOGENESIS
P. 91

THE STRUCTURE OF THE MITOCHONDRIAL GENOME AS AN ACTIVATOR OF OPISTHORCHIASIS
P. 99

STACKING INTERACTIONS IN COMPLEXES OF FIBERS WITH ADENINE AND GUANINE CONTAINING LIGANDS

charged side
of various
of folded
responds to
corresponds to
in the planes of bolts

Founders

Ministry of Education and
Science of the Russian Federation,
Lomonosov Moscow State University,
Park Media Ltd

Editorial Council

Chairman: A.I. Grigoriev
Editors-in-Chief: A.G. Gabibov, S.N. Kochetkov

V.V. Vlassov, P.G. Georgiev, M.P. Kirpichnikov,
A.A. Makarov, A.I. Miroshnikov, V.A. Tkachuk,
M.V. Ugryumov

Editorial Board

Managing Editor: V.D. Knorre
Publisher: A.I. Gordeyev

K.V. Anokhin (Moscow, Russia)
I. Bezprozvanny (Dallas, Texas, USA)
I.P. Bilenkina (Moscow, Russia)
M. Blackburn (Sheffield, England)
S.M. Deyev (Moscow, Russia)
V.M. Govorun (Moscow, Russia)
O.A. Dontsova (Moscow, Russia)
K. Drauz (Hanau-Wolfgang, Germany)
A. Friboulet (Paris, France)
M. Issagouliants (Stockholm, Sweden)
A.L. Konov (Moscow, Russia)
M. Lukic (Abu Dhabi, United Arab Emirates)
P. Masson (La Tronche, France)
K. Nierhaus (Berlin, Germany)
V.O. Popov (Moscow, Russia)
I.A. Tikhonovich (Moscow, Russia)
A. Tramontano (Davis, California, USA)
V.K. Švedas (Moscow, Russia)
J.-R. Wu (Shanghai, China)
N.K. Yankovsky (Moscow, Russia)
M. Zouali (Paris, France)

Project Head: E.A. Novoselova

Editor: N.Yu. Deeva

Strategic Development Director: E.L. Pustovalova

Designer: K.K. Oparin

Photo Editor: I.A. Solovey

Art and Layout: K. Shnaider

Copy Chief: Daniel M. Medjo

Address: 119991 Moscow, Russia, Leninskiye Gory, Nauchny
Park MGU, vlad.1, stroeniye 75G.

Phone/Fax: +7 (495) 930 80 06

E-mail: vera.knorre@gmail.com, enovoselova@strf.ru,
biomem@mail.ru

Reprinting is by permission only.

© ACTA NATURAE, 2011

Номер подписан в печать 18 мая 2011 г.

Тираж 200 экз. Цена свободная.

Отпечатано в типографии «МЕДИА-ГРАНД»

Letter from the Editors 1

FORUM

Boosting Class 6

V. N. Danilenko

Collaboration between Russian and U.S.
Scientists in Biomedical Research 9

REVIEWS

V.V. Pleshkan, I.V. Alekseenko,
M.V. Zinovyeva, T.V. Vinogradova,
E.D. Sverdlov

Promoters with Cancer Cell-Specific Activity
for Melanoma Gene Therapy 13

M. V. Nesterchuk, P. V. Sergiev,
O. A. Dontsova

Posttranslational Modifications of Ribosomal
Proteins in *Escherichia coli* 22

L. A. Dykman, N. G. Khlebtsov

Gold Nanoparticles in Biology and Medicine:
Recent Advances and Prospects 34

RESEARCH ARTICLES

V. A. Stepanov, O. P. Balanovsky,
A. V. Melnikov, A. Yu. Lash-Zavada,
V. N. Khar'kov, T. V. Tyazhelova,
V. L. Akhmetova, O. V. Zhukova,
Yu. V. Shneider, I. N. Shil'nikova,

S. A. Borinskaya, A. V. Marusin,
M. G. Spiridonova, K. V. Simonova,
I. Yu. Khitrinskaya, M. O. Radzhabov,
A. G. Romanov, O. V. Shtygasheva,
S. M. Koshel', E. V. Balanovskaya,
A. V. Rybakova, E. K. Khusnutdinova,
V. P. Puzyrev, N. K. Yankovsky

**Characteristics of Populations
of the Russian Federation over the Panel
of Fifteen Loci Used for DNA Identification
and in Forensic Medical Examination56**

O. V. Samsonova, K. S. Kudryashova,
A. V. Feofanov

**N-Terminal Moiety of Antimicrobial
Peptide Ltc1-K Increases its Toxicity
for Eukaryotic Cells68**

K.V. Lobanov, L. Errais Lopes,
N.V. Korol'kova, B.V. Tyaglov,
A.V. Glazunov, R.S. Shakulov, A.S. Mironov

**Reconstruction of Purine Metabolism
in *Bacillus subtilis* to Obtain
the Strain Producer of AICAR - a New Drug
with a Wide Range of Therapeutic
Applications79**

K.S. Mineev, E.V. Bocharov, P.E. Volynsky,
M.V. Goncharuk, E.N. Tkach, Ya.S. Ermolyuk,
A.A. Schulga, V.V. Chupin, I.V. Maslennikov,
R.G. Efremov, A.S. Arseniev

**Dimeric Structure of the Transmembrane
Domain of Glycophorin A in Lipidic and
Detergent Environments90**

O. A. Zorina, A. A. Kulakov,
O. A. Boriskina, D. V. Rebrikov

**Relationship between the Pathogenic
Representatives of Periodontal Pockets
Microbiocenosis in Patients with Periodontitis
with Varying Degrees of Severity99**

Yu. G. Odnoshivkina, A. M. Petrov,
A. L. Zefirov

**The Effects of β_2 -Adrenoreceptor Activation
on the Contractility, Ca-Signals
and Nitric Oxide Production
in the Mouse Atria103**

Guidelines for Authors..... 113

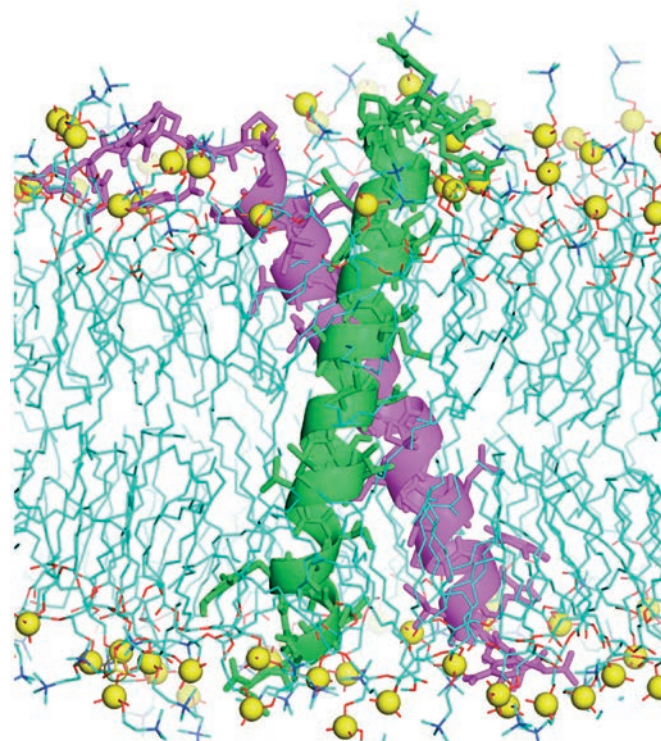


IMAGE ON THE COVER PAGE
Ribbon diagram of the GpA_{tm} dimer after MD-relaxation
in DMPC bilayer (Mineev *et al.*)

Boosting Class

The Ministry of Education and Science of the Russian Federation has announced the second stage of the open public grant competition (each grant is up to 150 million rubles). The research will be carried out in Russian universities and will be spearheaded by leading scientists from all over the world. In his interview with the head of the project "Science and technologies of the Russian Federation" Konstantin Kiselev, Deputy Minister of Education and Science Sergei Ivanets spoke about the characteristics of the project and how to adjust this innovative competition to Russian realities.

Konstantin KISELEV: Sergei Vladimirovich, the implementation of Resolution of the Government of the Russian Federation № 220 commenced last summer. It is an open competition aimed at the establishment of research subdivisions headed by world-class scientists in higher educational institutions. Since the financial support for this competition is considerable even in comparison with competitions held in scientifically developed countries, the attention of the scientific community is equally high.

In 2010, the Ministry of Education and Science of the Russian Federation held the first stage of the competition; 40 winners were announced. Not all researchers were successful in their attempts to secure grants within the framework of the selection that took place last year; however, they all will be able to participate in the second stage, which will be held this year.

Let us refresh the memories of our readers and touch upon the problems that emerged during the implementation of the competition.

Sergei IVANETS:

Indeed, this competition was unprecedented for Russian research

and development and higher professional education both in terms of the scale of the tasks to be solved and in terms of the allocated funds. The participants included researchers, among which were world-recognized scientific leaders. When organizing the competition, the most important task for us was to make it open and transparent. I hope that we were successful to a large extent, since the system of evaluation and selection of the applications was based on high-quality expertise involving a considerable number of Russian and foreign experts, and some world-leading scientists. Of course, there were critical comments concerning the holding of the contest; we will be able to address a number of these criticisms when we hold the competition in 2011.

However, we believe that the overall results of the 2010 competition were satisfactory.

What was the aim of this competition? What results did it seek to achieve?

This event is one of the most complex organizational events that have been financially supported by the Government of the Russian Federation since 2008 with the aim of modernizing higher education. The other major components

of this complex are already known to you. The complex nature of the event was due to the fact that it involved the competition of innovative programs of development of higher educational institutions within the framework of the priority national project "Education," the establishment of federal and national research universities, and the development of an innovative infrastructure at higher educational institutions.

We believe that modern education can be competitive only when combined with research activity. This activity should be promoted, i.e., financially supported. In order to promote this concept, in 2009, a competition was held among Russian higher educational institutions and the winners were announced, which were subsequently converted into the national research institutes. The next stage comprised not just the stimulation of university researchers, but also the involvement of the best foreign scientists. Firstly, these researchers will implement a world-class research project, and secondly, they will establish a laboratory that will be competitive on the world stage. Moreover, the modernization of infrastructure supplies (instruments, equipment, and communications) will take place. For a higher educational institution, the appearance of a "star" in its staff is an opportunity to provide the entire research team with cutting-edge knowledge and first-grade practice in performing research and preparing publications.

Some observers have been critical: "Why is it higher educational institutions only? Why is it not research organizations that belong to the system of state academies?"

Our aim was not to exclude the financing of research in research organizations in favor of that in higher educational institutions. The aim of this competition is to foster

an increase in the level of higher educational institutions and control the quality of education, ensuring that it remains competitive at the international level.

Meanwhile, other organizational and financial instruments are used to support research in state academies of sciences.

You have mentioned the involvement of a large number of experts, including foreign ones, in the selection and assessment of the applications. To what extent was this activity “unusual” for the Ministry?

In general, we have a rather representative and wide expert base which has been used in the Russian Federal when holding various competitions in the research and development sector and in the higher professional education sector. However, during this competition we had an additional problem to solve: that of contacting experts. The involvement of a large number of international experts was necessary for the success of the first stage of the contest. The experts were either contacted directly, or, through special organizations which deal with the organization of the expertise of research projects by nature of their professional activity. This was how the task was solved, and now we have contacts and business relations with these experts. We are certain that this will be a considerable advantage for us at the second stage of the competition.

Sometimes a conflict of interests may emerge even in perfect expertise. It is inevitable. Did the Ministry have to fight against it somehow?

Yes, sometimes it may happen: the circle of experts and executors of large international projects is not boundless. In our case, an expert pledges that he will report on a possible conflict of interests, if one exists, and will not contribute expertise to that certain project.



Sergei Ivanets

We also avoid conflicts of interests due to the fact that half of our expert group includes foreign researchers who do not have any direct relationship with Russian higher educational institutions. Moreover, the expert group leaders pay careful attention to ethical issues, since in the scientific community, reputation is more valuable than those hypothetical advantages that may be acquired through the award of unfair points to a certain project.

Is the geography of expertise wide?

Yes, the geography is appreciably wide and corresponds to the terms of the competition. All countries that are considered key players in terms of science and technology have been embraced: the United States of America, the European Union, sections of Latin America, and a number of experts from South Eastern Asia.

The President of Russia and the Government of the Russian Federation support the idea of involving

foreign scientists and experts. The problem is that people who come to Russia, especially those who are used to a certain standard of existing institutional settings and institutions, may have difficulties adapting to the conditions that exist in our country.

Speaking about the day to day life of a foreign scientist in our country, we see no particular problems: the grant amount is appreciably large to solve these problems, especially if a foreign scientist has to be in Russia for 4 months per year in total (not necessarily consecutively).

Of course, there are some limitations that can cause certain difficulties, such as those associated with the migration legislation requirements, or those connected with the import/export of biological samples and reagents. Unfortunately, I cannot say that all these problems have already been solved. However, we are making progress and they are being solved, step by step.

Concerning the disposition of money, are there any limitations?

The only limitation is that the fund for remuneration of labor could be no more than 60% of the total grant. In all other respects, the money can be spent on infrastructure, retraining programs, and the purchase of reagents and materials. The higher educational institution is responsible for matching the expenses and the contract terms, all expenditures being approved only by the project leader.

Last year, since the competition actually ended in the very end of the year, whereas the applications (including those for the stages of fund expenditure) were filed much earlier, we managed to get permission for higher educational institutions and scientists who won in the competition to change the application format before signing the contract. This measure was undertaken so that these funds could be redistributed for the following period at the stage when the winners are announced in order not to lose them.

We managed to solve this appreciably complicated problem, which was not caused by the scientists.

Will the second stage of the competition somehow differ from the first stage?

It seems very important to us that there are no fundamental differences, since the competition is a whole. The participants of the first stage should be placed under the same conditions as the participants of the second stage.

Are you apprehensive that something could go wrong, and how bad could it be? There can be different combinations, when a highly rated specialist is invited into a higher educational institution which has failed to provide normal conditions. Or the specialist fails to put together an appropriate team. Or it could turn out that the results are not worth the money that was spent.

For the efficient implementation of the competition in accordance with its terms, a share of the funds is sent to the monitoring organizations that are in charge of control-

ling the project at all its stages. There are indices that allow the monitors to precisely trace whether there has been progress in the specified direction or whether some adjustments are necessary.

In the scientific sector, there are a number of risks, and measures are to be taken to minimize them. We consider international expertise to be the most correct one. With the guarantees ensured by this expertise, one may expect that there should be no failures.

When do you plan to summarize the second stage?

We took into account the shortcomings of the first stage, and we increased the time for preparation of applications by two months. Applications deadline is now mid-July. The expertise then occurs, followed by summarization.

This year, the expertise will take less time, since last year we had to simultaneously perform the selection of experts. Therefore, I am positive that this year we will strike a balance much earlier. ●

Collaboration between Russian and U.S. Scientists in Biomedical Research

V. N. Danilenko

Vavilov Institute of General Genetics, Russian Academy of Sciences

E-mail: valerid@rutenia.ru

During the past two decades, tens of thousands of Russian scientists, including leading researchers in the field of biomedicine, have left Russia to work abroad. Some scientists maintained contact with institutes of the Russian Academy of Sciences (RAS) and the Russian Academy of Medical Sciences (RAMS); however, such interactions were usually initiated by the scientist. Recently, there has been a shift in the pattern of international collaboration; the meeting between the representatives of the National Institute of Health (USA) and the Russian Academy of Sciences, held on April 25–26, 2011, in Moscow, is evidence of this change.

BACKGROUND

On July 6, 2009, during the visit by U.S. President B. Obama to Moscow, the establishment of the US–Russia Bilateral Presidential Commission was declared. The move was intended to contribute towards the strengthening of relations (including scientific relations) between Russia and the United States. Eighteen working groups are now at work within the Commission. The Health Working Group headed by Minister of Healthcare and Social Development of the Russian Federation T.A. Golikova and Minister of Health and Human Services of the United States of America K. Sebelius is focused on collaboration in protecting the health of Russian and U.S. residents; and “the entire planet,” as is stated in the document. The deputy administrator of the working group is the Deputy Minister of Healthcare and Social Development of the Russian Federation V.I. Skvortsova. In July 2009, a Memorandum of Mutual

Understanding between the Ministry of Health and Human Services of the United States of America and the Ministry of Healthcare and Social Development of the Russian Federation was also signed. In the document, collaboration on healthcare and medical sciences is underlined.

On September 22, 2010, the Foundation for the National Institutes of Health announced the establishment of the US–Russia Medical Science Forum within the framework of the US–Russia Bilateral Presidential Commission in order to facilitate collaboration in the sphere of biomedical research. The Forum was initiated by the National Institutes of Health Fogarty International Center and representatives of the U.S. pharmaceutical business. This private–public partnership aims at advancing collaboration between Russian and U.S. scientists in the field of morbidity control, treatment and prevention, clinical and applied research, the development

of new medical technologies, and the design of innovative drugs.

The organizers believe that this meeting should facilitate the establishment of close contacts between Russian and American governmental institutions, as well as between Russian and American scientists. Conferences will be held annually in order to elaborate the strategy of joint scientific research during the forum; the organizers also believe that it will help breach the gap between actual research and the practical implementation of this research. The elaboration of research priorities, formation of joint research projects, including those involving the pharmaceutical business, are among the significant tasks facing the Forum.

In July 2010, representatives of the U.S. National Institute of Health met with the vice-president of the RAS, Academician A.I. Grigoriev. The meeting initiated a scientific dialogue concerning the resumption of collaboration. In October 2010, during a visit by the RAS president, Academician Yu.S. Osipov, to the United States of America, the administration of the U.S. National Institute of Health expressed interest in establishing official collaboration. The working visits of a number of Russian scientists, RAS Academicians V.V. Vlasov and M.V. Ugryumov, RAMS Academicians G.T. Sukhikh and V.A. Tutel’yan, and corresponding member S.V. Netesov to the U.S. National Institute of Health facilitated the elaboration of a platform for collaboration.



Vice-president of the RAS,
Academician A.I. Grigoriev

Much work in this direction has been carried out by the formed Program and Organizational Committees, with outstanding scientists of the RAS, RAMS, and Moscow State University among the members

WORKING CONFERENCE DEVOTED TO FORUM PREPARATION

The working conference that was held between April 25 and 26, 2011, in Moscow at the Russian Academy of Sciences was an important step towards fostering closer relations between the research communities of the two countries. The major goal of the conference was to prepare the Russian–American Forum on collaboration in the field of biomedical research. The Russian Academy of Sciences, the Ministry of Healthcare and Social Development of the Russian Federation, and the Russian Academy of Medical Sciences were among the organizers on behalf of Russia; the Foundation for National Institutes of Health, the National Institute of

Health, and the Institute of Medicine of the United States National Academy of Sciences, on behalf of the United States of America.

The vice-president of the RAS, Academician A. I. Grigoriev, and the director of the U.S. National Institute of Health Fogarty International Center, Dr. Rodger Glass, were elected as co-chairpersons of the Working Conference.

The deputy chairperson of the Working Group on Healthcare of the US–Russia Bilateral Presidential Commission and Deputy Minister of Healthcare of the Russian Federation V.I. Skvortsova set the major directions of the strategy of interaction between Russian and American scholars within the framework of the Forum. In his report, A.I. Grigoriev highlighted the problems of infrastructural supply for research in Russia, the priorities in biomedical research, and she also emphasized the role of fundamental science as the basis for innovative developments. Dr. Rodger Glass presented a report devoted to the structure of the National Institute of Health, the subject areas of research, and the directions of the bilateral partnership at the initial stage of the Forum's activity.

More than 90 participants sat through the Working Conference; among them were outstanding Russian and U.S. scholars and government officials. A Considerable degree of interest was shown by the business community, including such pharmaceutical and biotechnological companies as Amgen, Amway, Bach Pharma, Becton Dickinson, Bristol-Myers Squibb, Boston Scientific, Coca-Cola, Eli Lilly, GalenBio, Genzyme, Johnson & Johnson, PepsiCo, and Pfizer.

The following research orientations were selected as topics of discussions at the Conference: fundamental neurology, organism development and childhood pathology; oncology; infections and



Director of the Fogarty International
Center NIH R. Glass

epidemiology; physiology and pathology of the cardiovascular system; healthy lifestyle; and translational medicine. The following scholars made oral reviews of the research carried out in Russia and the United States of America in the selected directions: Academician M.V. Ugryumov (Brain Sciences), RAMS Academician A.A. Baranov (Human development), Academician G.P. Georgiev, and Dr. Ted Trimble (Oncology), RAMS Academician V.V. Zverev and Dr. Robert Fontaine (Infectious Diseases and Epidemiology), Academician V.A. Tkachuk and Dr. Susan Shurin (Cardiovascular Diseases), RAMS Academician V.A. Tutel'yan and Dr. Van Hubbard (Healthy Lifestyle), and RAMS Academician G.P. Sukhikh (Clinical and Translational Studies). A separate section was devoted to business, with 12 reports both on fundamental science and applied clinical and translational studies. The representatives of the business community proposed col-

laboration and joint participation in the elaboration and promotion of joint projects.

The American delegation visited the Shemyakin and Ovchinnikov Institute of Bioorganic Chemistry, RAS, the Engelhardt Institute of Molecular Biology, RAS, the Institute of Gene Biology, RAS, the Vavilov Institute of General Genetics, RAS, Lomonosov Moscow State University (Faculty of Fundamental Medicine), Blokhin Russian Cancer Research Center, RAMS, Cardiology Research Center, Ministry of Healthcare and Social Development, the Child Health Research Center, RAMS, and the Nutrition Research Center, RAMS. During these meetings, the participants discussed the specific problems of the scientific partnership.

To conclude, the co-chairpersons of the Conference formulated recommendations for the development of the Forum's structure and determined the most important work stages.

The initial stage of collaboration is meant to determine priority projects that are of mutual interest to leading research institutions and groups in both countries, and to involve partners from non-governmental organizations and the private sector. Provisions have been made for other governmental institutions and non-governmental organizations to join the collaboration, including the Foundation for the National Institutes of Health, the U.S. Agency for International Development, and private sector organizations.

The formation of a bilateral working committee which will be made up of representatives of organizations on both the Russian and American sides, as well as business, has been scheduled. The Committee will elaborate the criteria for selecting projects, partners, the terms of project financing, and will ensure that the deadline for the prepara-

tion of the Forum conference in November 2011 in Moscow is met.

SIGNING THE RAS–NIH MEMORANDUM

On April 26, 2011, in Moscow, in the old residence of the RAS Presidium, the scientific collaboration already underway was officially formalized through the signing of the memorandum on collaboration in the sphere of fundamental biomedical research between the Russian Academy of Sciences and the U.S. National Institute of Health.

On the Russian part, the following personalities participated in the signing: vice-president of the RAS, Academician A.I. Grigoriev, vice-president of the RAS, Academician A.F. Andreev; the Counsellor to the president of the RAS in foreign economic activity, Academician M.V. Ugryumov; Deputy Head of the Board for Foreign Relations of the RAS, V.V. Shapovalenko; Academic Secretary of the Council under the RAS Presidium "Medical Engineering, Technology, and Pharmaceuticals," Professor V.N. Danilenko, and the representative of the Department of Foreign

Relations of the RAS, Yu.K. Shiy-an.

On the U.S. side, the following personalities participated in the signing of the Memorandum: Director of the Fogarty International Center R. Glass, President of the Office of Global Health of the Ministry of Health and Human Services of the United States of America N. Dolaire, President of the Institute of Medicine of the U.S. National Academy of Sciences H. Feinberg, Director of the National Heart, Lungs, and Blood Institute S. Shurin, Director of the Foundation for the U.S. National Institute of Health S. Campbell, Professor at the Medicine Institute G. Cassell, Deputy Head of the U.S. Mission to Russia M. Mitman, and Coordinator of the Fogarty International Center M. Levintova.

After a 12-year gap, this document made public the official collaboration between the two largest research organizations in Russia and the United States of America in the field of biomedical studies.

The scope of the priorities in the collaboration had been outlined at the initial stage. They include on-



Signing the RAS-NIH Memorandum

cologic, cardiovascular, neurologic and infectious diseases; innovation pharmaceuticals, translational research, bio-safety, and the health of large population groups (megapolises, stress situations, and geographic features). It is assumed that the priorities in the collaboration could be adjusted if necessary.

THE FORUM SCHEDULED FOR NOVEMBER 2011

The Conference within the framework of the U.S.-Russia Scientific Forum for Biomedical and Behavioral Research will be held in Moscow in November of 2011. The organizing committee of the Forum is currently being formed. It will include representatives of the Russian Academy of Sciences, the Ministry of Healthcare and Social Development of the Russian Federation, the Russian Academy of Medical Sci-

ences, the U.S. National Institute of Health, the Institute of Medicine of the U.S. National Academy of Sciences, and private companies.

The Foundation for NIH has begun accepting applications from organizations and companies for participation in the Forum. The terms of participation and the application forms can be downloaded at <http://www.medtechpharm-ras.ru> (in Russian) and <http://www.fnih.org/work/programs-development/us-russia-scientific-forum> (in English). The most promising projects and proposals will be selected to participate in the Forum. Proposals for the Forum may comprise applications for scientific conferences, researchers exchange programs, research projects, educational programs, and professional-development courses.

The platform for partner collaboration between Russian and U.S.

scientists has been prepared; however, given the immutable importance of the human factor, leaders willing to and capable of organizing such collaboration are being actively sought. As mentioned by many participants at the Conference, a great contribution to the organization of the collaboration was made by Professor Gail Caspell, who has devoted more than 10 years to joint U.S.-Russian research in the field of the study and treatment of tuberculosis. It is of considerable importance that the world's largest pharmaceutical companies are showing interest in joint Russian-American projects. Medico-biological science in any country can develop only if there is demand from the government, industry, and medicine aimed at ensuring the health of populations.●

Promoters with Cancer Cell-Specific Activity for Melanoma Gene Therapy

V.V. Pleshkan^{1,2*}, I.V. Alekseenko^{1,2}, M.V. Zinovyeva¹, T.V. Vinogradova¹, E.D. Sverdlov^{1,2}

¹ Shemyakin and Ovchinnikov Institute of Bioorganic Chemistry, Russian Academy of Sciences

² Institute of Molecular Genetics, Russian Academy of Sciences

*E-mail: vpleshkan@gmail.com

Received 01.04.2011

ABSTRACT Melanoma is one of the most aggressive tumors. It develops from pigment-forming cells (melanocytes) and results in a high number of lethal outcomes. The use of genetic constructs with the ability to specifically kill melanoma cells, but not normal cells, might increase the lifespan of patients, as well as improve their quality of life. One of the methods to achieve a selective impact for therapeutic genes on cancer cells is to utilize a transcriptional control mechanism using promoters that are specifically activated only in cancerous cells. In this review, promoters of the genes that are preferentially expressed in melanoma cells are described. These promoters, and other highly melanoma-specific regulatory elements, reduce the unspecific expression of therapeutic genes in normal tissues. Moreover, cancer-specific promoters and their elements are advantageous for the development of universal anticancer drugs. Examples of the use of double promoters that have a high potential as instruments in cancer gene therapy are also given in this review.

KEYWORDS melanoma; gene therapy; tissue-specific promoters; specific expression of a transgene

ABBREVIATIONS Ad – adenovirus; CRAds – conditionally replicative adenoviruses; DT-A – diphtheria toxin A chain; HSVtk – herpes simplex virus thymidine kinase; SCLC – small cell lung cancer; MC1R – melanocortin 1 receptor; MIA – melanoma inhibitory activity, MITF – microphthalmia-associated transcription factor; TERT – human telomerase reverse transcriptase; TSP – tumor specific promoter; TSS – transcription start site

INTRODUCTION

A steady increase in deaths caused by malignant skin melanoma has recently been in evidence around the world, including in Russia. Malignant melanoma belongs to the most aggressive variety of tumors; the five-year survival rate of patients is less than 50%. Melanoma especially stands out by its early metastasizing; therefore, chemotherapy and radiation therapy are not very effective against the disease [1–3].

In the longer term, an important role could be played by gene therapy methods based on the introduction of a therapeutic gene (transgene) into melanoma cells in patients. Therapeutic constructs may contain genes that compensate for the reduction in the expression of suppressor genes, which results in tumor development. Or conversely, they may contain genes whose products neutralize the increased expression of an undesirable gene (oncogene) [4–7]. The approach in which the so-called suicide genes are used is considered to be one of the most universal strategies among genetic strategies for killing cancer cells [8–10]. In this case, a gene is introduced into a tumor cell; which encodes an enzyme that is not typical for the normal cell and is capable of converting the compound that has no toxicity towards healthy cells (prodrug) into a toxin that results in the killing of tumor cells containing a suicide gene. Thus,

the selective killing of cancer cells in which the suicide gene acts is provided [11–13]. The gene encoding the herpes simplex virus thymidine kinase (*HSVtk*) and the gene encoding yeast cytosine desaminase (*FCY1*) are the most widely known and the most frequently used suicide genes. As opposed to cellular thymidine kinase, *HSVtk* has the ability to phosphorylate the antiherpes drugs acyclovir and ganciclovir. The cells transformed by the *HSVtk* gene die in the presence of these agents, since cellular kinases convert the phosphorylated acyclovir and ganciclovir into triphosphates, which are inserted into the newly synthesized DNA upon cytokinesis and terminate its subsequent synthesis. It is the dividing cells that die, rather than the resting cells, in which DNA is not synthesized and ganciclovir or acyclovir is not inserted [14]. The gene *HSVtk* has been successfully used for the experimental therapy of numerous types of tumors in animals. A number of systems comprising this gene have been undergoing clinical trials [13, 15, 16]. The use of the *FCY1* gene is based on the absence of its product, cytosine desaminase, in mammal cells and on its ability to convert 5-fluorocytosine, which is not toxic to humans, into a known cytostatic, 5-fluorouracil [17, 18]. After the incorporation of cytosine desaminase into tumor cells and its specific expression in these cells, the introduction of fluorocytosine

sine into a patient's organism results in its intracellular conversion into fluorouracil, which reduces the toxic effect that fluorouracil has on normal cells.

The specificity of the vector to tissue of this type can be specified either by delivering it exactly into the tissue or by creating conditions for the specific expression of the transgene in the specified tissue. Due to its simplicity, the latter method has been used more frequently. With this aim, promoters and enhancers that act specifically in the tumors of the given tissue are used in the construction of vectors [19, 20]. In the case of malignant melanoma, promoters and enhancers of the genes that are involved in melanin biosynthesis are used. The fact that transgene expression is ensured only in tumor cells, and not in normal cells, is an advantage of the promoters and other regulatory elements that are strictly specific to tumors of this type. However, their non-universality and the inevitable increase in the cost of drugs based on the promoters connected with this fact is a significant disadvantage of such approaches. A variant which offers a potential compromise consists in the use of more universal tumor-specific promoters capable of acting in a wide range of tumors, but not in normal cells. Although this approach slightly increases the risk of affecting normal tissues, it is considered to be more economically viable, since the same constructs can be used for the therapy of a wide range of tumors. An additional factor that supports promoters having a broader action spectrum is connected with the poorly studied specificity of gene expression in metastases of the given tumor. There is no strict guarantee that a narrow-specific promoter that acts well in a primary tumor will retain this ability in all its metastases. The use of universal promoters reduces the probability of promoter inactivation in metastases.

This review describes the structure and properties of promoters that are specific to melanoma cells and those that are active for a wide range of tumors but are still used in the gene therapy of melanoma.

PROMOTERS THAT ARE SPECIFICALLY ACTIVE IN MELANOCYTES

The most well-studied promoter modules that control the specific expression of the therapeutic gene in melanoma cells, with recent widespread application, are promoters of the tyrosinase gene (*TYR*) or the gene encoding the melanoma inhibitory activity (*MIA*), sometimes combined with distal elements of other promoters and/or the enhancers [21, 22].

Tyrosinase gene promoter

Tyrosinase (TYR) is one of the key enzymes required for the synthesis of pigment melanin, which is formed only in melanocytes and in retinal pigment epithelium. The

TYR gene is expressed only in the specified cells and in many (but not in all) human melanomas and serves as a good marker of melanocyte differentiation [23]. It has been shown that the 5'-region with respect to the transcription start site (TSS) determines the specificity of tyrosinase gene expression [24, 25]. It was demonstrated by the deletion analysis that the minimal promoter of the human tyrosinase gene is likely to be located in coordinates -209/+51 with respect to TSS [26] (*Fig. A*). A 115 bp fragment is enough for a tissue-specific activity of the human *TYR* promoter [24]. This promoter fragment contains three positive regulatory elements: the conservative element that is typical for melanocyte-specific promoters – M-box (-104/-37 from the TSS), linked with nine nucleotides that are known as CR1; the Sp1-site (-45/-37 from the TSS); and the evolutionarily conservative element CR2 consisting of the E-box motif and the octamer element (-14/+1 from the TSS) overlapping with it [24]. It is significant that the octamer element in the *TYR* promoter is degenerate in many mammals, including mice [27]. The E-box contains the CANNTG motif, which binds bHLH family transcription factors (basic-helix-loop-helix). This motif was detected in *TYR* gene promoters in various animal species. A similar motif can be found within the M-box and the enhancer region of the tyrosinase gene [27]. Melanocyte-specific expression of the tyrosinase gene is activated upon the binding of the product of the *MITF* gene to the promoter region, including the M-box and the E-box starting region [24].

Promoters of the human and mouse tyrosinase genes are characterized by a high degree of identity of the nucleotide sequence [25]. However, a functional comparison of the promoters of these genes for a human and a mouse has demonstrated that the human *TYR* promoter has a lower efficacy and specificity of expression in melanocytes in comparison with the mouse *Tyr* promoter [25]. It has been assumed that an enhancer plays a significant role in the activity of the human *TYR* promoter. The human *TYR* enhancer, termed tyrosinase distal element (TDE), is located at positions -2014/-1810 and contains the E-box [25]. The binding of two MITF transcription factors to the E-boxes found within both the promoter and enhancer is significant for the specific activity of the human tyrosinase gene [21].

A 200 bp enhancer identical to the human *TYR* enhancer was also found in the 5'-region of the mouse tyrosinase gene; however, only the promoter is essential for manifesting the specific activity of the mouse gene [26, 28].

Promoter of the gene encoding melanoma inhibitory activity (*MIA*)

The gene encoding the melanoma inhibitory activity (*MIA*) is expressed predominately in melanoma or

chondrosarcoma cells, in certain adenocarcinomas and chondrocytes; however, it is inactive in normal melanocytes [29–31]. The MIA protein, the secreted inhibitor of cell growth, prevents the attachment of melanoma cells to the extracellular matrix, thus promoting invasion and metastasizing [32–34]. As opposed to the *TYR* gene promoter, the activity of the human *MIA* gene promoter correlates with melanoma progression [35]. It has been known that the 1.4 kb-long region flanking the 5'-fragment of the *MIA* gene with respect to the transcription starting site provides the specificity of expression of this gene only in melanoma cells, not in melanocytes [36]. By means of deletion analysis it has been demonstrated that the minimal promoter of the human *MIA* gene consists of 212 bp (positions -211/+1) and of 230 bp (-229/+1), in the case of the mouse *MIA* gene, as is shown in *Fig. B*. The elements of the promoters of this gene for humans and mice, which are responsible for the specificity of expression in melanoma cells, are located at positions -212/-170 and -230/-130, respectively [36, 37]. The structure and size of the human and mouse *MIA* promoters are conservative and contain identical elements, which can differ only in their position [38]. Thus, both *MIA* promoters contain no TATA-box and/or CAAT-sequence near the transcription start site. Site Sp1 is conservative and is located at position -108/-103 in the human *MIA* promoter, and at 106/-101, in the mouse promoter. *MIA* promoters contain multiple E-boxes with bHLH-binding sites [36] (*Fig. B*). The binding site of the NF- κ B transcription factor is also highly conservative in human and mouse genes; in addition, it is located at different positions (-207/-198 and -819/-811, respectively) [36]. Deletion or mutation of this site results in a considerable decrease in human *MIA* promoter activity in melanoma cell lines [36]. Human and mouse *MIA* promoters also comprise such widespread elements as the binding sites α -INF-2, C/EBP, GATA-1, GM-CSF, NF-IL6, NF- κ B, TCF-2, etc. It is of interest that the activity of the *MIA* promoter may be dependent on the NF- κ B factor, which controls the expression of the genes encoding the immune response, apoptosis, and cell cycle [36]. At the time of writing, nothing was yet known about the enhancer elements of the *MIA* gene.

Promoter of the melanocortin receptor gene

The melanocortin 1 receptor (receptor MC1R) is expressed predominately in melanocytes and melanomas [39, 40]. MC1R is a transmembrane G-protein-coupled receptor of the α -melanocyte-stimulating hormone (α -MSH). High expression of the *MC1R* gene is also typical of the cell lines originating from primary and metastatic melanomas [41]. Minor amounts of these receptors are found in other tissues and cells; e.g., in testicles,

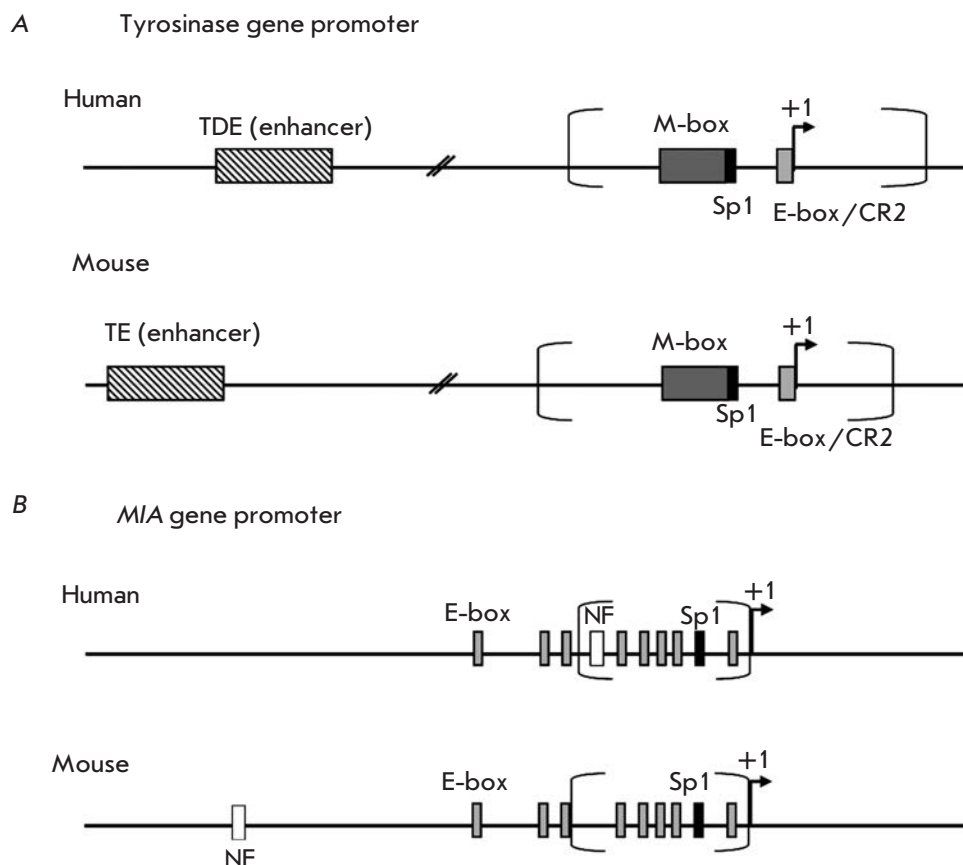
ovary, adrenal glands, keratinocytes, dendrite cells, and activated monocytes [41, 42]. The 3.2 kb-long fragment located in the 5'-region with respect to the TSS of the *MC1R* gene contains several Sp1-binding motifs, consensus sequences of the AP-1 and AP-2 sites, and several E-boxes. The *MC1R* gene promoter contains no TATA- or CAAT-sequences near the TSS [43, 44]. Melanocyte-specific expression of *MC1R*, similar to that of the tyrosinase gene, is activated upon binding of the MITF transcription factor to the E-box [45–48]. It has been shown that 150 bp located above the ATG codon of the *MC1R* gene are sufficient in order to initiate the melanocyte-specific transcription [49]. This minimal promoter can be considered as one of the possible candidates for the transcriptional control of transgene expression in melanoma cells.

The use of heterologous regulatory elements to enhance melanoma promoters

The use of *cis*-regulatory elements based on various combinations of the tyrosinase gene promoter and additional heterologous enhancers, which control transcription for specific transgene expression in melanoma, has been described in a number of studies [21, 22, 26]. It is apparent that the *TYR* promoter ensures high activity and specificity of the human *TYR* gene only in the presence of the enhancer element [25]. The construct consisting of the human *TYR* promoter (209 bp) and two or more sequentially attached human *TYR* enhancers (200 bp each) exhibit the highest specific effect upon transfection of melanoma cell lines [26]. The dimer of the mouse tyrosinase gene enhancer linked with the mouse gene promoter also enhances the activity and specificity of the mouse gene [26]. Similar constructs were used when constructing the conditionally replicating adenoviruses (CRAds), where the promoter of the adenoviral *E1A* gene was substituted for the promoter hTy2E/P that is specifically active in melanomas and consists of the dimer of the human tyrosinase gene enhancer and the core promoter of this human gene [50]. The resulting adenoviruses manifested a pronounced oncolytic effect on melanoma cell lines. The cytotoxic effect of these constructs was also comparable in terms of the level of CRAd action with the strong nonspecific cytomegalovirus (CMV) promoter. Meanwhile, a strong decrease in the cytotoxic effect of the adenovirus on normal fibroblasts and keratinocytes was observed [50]. Thus, the use of the specific promoter in the *E1A* region of the adenovirus genome made it possible to attain a selective effect on melanoma cells. The binding of several enhancers of the mouse tyrosinase gene had an even stronger effect on the activity and specificity of the human *TYR* promoter. Thus, when constructing oncolytic adenoviral vectors, the TETP promoter con-

Schematic presentation of the *tyrosinase* and melanoma inhibitory activity (*MIA*) promoters.

A – scheme of *tyrosinase* promoter, B – scheme of *MIA* promoter. The rectangle with diagonal hatching indicates an enhancer, open rectangle indicates the binding site of the transcription factor NF- κ B, dark-gray rectangle – the M-box, light-gray rectangle – the E-box, black rectangle – the binding site of the Sp1 factor, a loci corresponding to the minimal promoter is given in parentheses. The arrow shows the transcription start site.



struct was used. It contained the core human tyrosinase promoter (TP) and a tandem consisting of four mouse tyrosinase gene enhancers (tyrosinase enhancer – TE) [51]. The use of this promoter to control the expression of the luciferase reporter gene enhanced the activity of the latter in melanoma cells by several orders of magnitude in comparison with the activity in non-melanoma cells [51]. The replacement of mouse enhancers by human enhancer sequences in these constructs resulted in only a 2–3-fold increase in reporter gene activity [51]. The same promoter (TETP) was used to control the expression of suicide genes that were delivered to melanoma cells by bacteria *Listeria monocytogenes* [52]. It was demonstrated earlier that avirulent listeria strains can penetrate into solid tumor cells and provide replication of the delivered plasmids in them [53–55]. Upon bacterial delivery of plasmids, in which the TETP promoter controls the suicide gene of purine nucleoside phosphorylase (PNP) or the chimeric gene of cytosine desaminase and phosphoryl transferase (FCU1) of yeasts, the transgene is specifically expressed in B16 melanoma cells, but not in kidney COS-1 fibroblasts. If a nonspecific CMV promoter is used, the suicide genes are expressed in both cell lines [52].

The Tyrex2 promoter that contains the human *TYR* core promoter and the tandem that consists of two

mouse tyrosinase gene enhancers may serve as another example of using heterologous regulatory elements in order to enhance the *TYR* promoter [56]. When constructing the adenoviral vector, this promoter was used to control the activity of the *PNP* suicide gene, which can convert prodrug 6-methylpurine deoxyribonucleoside into a highly toxic purine-base 6-methylpurine [57]. After treating melanoma cells with adenovirus Tyrex2-PNP and introducing the prodrug, approximately 90% of the cells died. In nonmelanoma cell lines, there was a cytotoxic effect only when the nonspecific constitutive CMV promoter was used [56].

The reporter gene of chloramphenicol acetyltransferase (CAT) and therapeutic genes *HSVtk* and *DT-A* (diphtheria toxin A-chain) were used to compare the activity of the mouse *Tyr* gene promoters and human *MIA* gene promoters and their combinations with one or several enhancers of the mouse tyrosinase gene [22]. Promoters of genes encoding *Tyr*, *MIA*, and various combinations of them with one or several enhancers of the mouse tyrosinase gene provided a specific expression of both the CAT reporter gene and therapeutic genes *HSVtk* and *DT-A* in melanoma cell lines. It was demonstrated that the binding of several enhancers of the tyrosinase gene to the *MIA* promoter considerably enhances the specific activity of the *MIA* promoter in melanoma

cell lines; the effect of mouse enhancers is stronger by an order of magnitude in comparison with that from human *TYR* enhancers, similar to the case of using the tyrosinase gene promoter. The strongest effect in both cases was observed when using constructs containing three or four mouse enhancers simultaneously [22].

The recombinant adeno-associated vector, in which the suicide gene is placed under the *MIA* promoter linked to the tandem consisting of four enhancer elements of the mouse tyrosinase gene, was described in [58]. The constructs with a full-size *MIA* promoter (1386 bp) and the minimal *MIA* promoter (493 bp) that is sufficient for maintaining the specific transcription in melanoma cells have been studied (*Fig. B*). It was shown that the constructs containing only *MIA* promoters have a low transcriptional activity only in melanoma cell lines [58]. The transcriptional potential of a construct with tyrosinase gene enhancers and the minimal *MIA* promoter was somewhat lower than that of the construction with the full-size promoter. The inhibition effect of melanoma cell growth with the use of *MIA* promoters with four tyrosinase gene enhancers is only slightly lower to the effect of the construct with the CMV-promoter; however, the latter does not provide the selectivity of transgene expression [58].

The given results demonstrate that the use of various combinations of melanoma-specific promoters and enhancers provides a high level of transgene expression in melanoma cells and can resolve the specificity problem for the gene therapy of the specified disease [50, 52, 56]. The *MIA* gene promoter is of special interest, since this gene, as opposed to the *TYR* gene, is expressed only in malignant melanoma cells but not in other cells of the melanocyte lineage. Thus, the regulatory elements of this gene may combine both tissue-specific and tumor-specific properties. However, the *MIA* gene promoter has still not been adequately studied as a candidate for the gene therapy of melanoma; almost nothing is known about the potential of the *MC1R* gene promoter.

PROMOTERS SPECIFICALLY ACTIVE IN CELLS OF MELANOMA AND OTHER TUMORS

Another approach that makes it possible to specifically control transgene expression in melanoma cells is the use of promoters that are specific not only in melanoma, but in other tumor cells as well. The examples of such tumor-specific promoters (TSP) include promoters of the genes *TERT*, *Cox-2*, *CXCR4*, and *BIRC5*, for which overexpression of the genes controlled by them in numerous tumor types and the absence or a minimal expression in the normal tissues is typical.

The *TERT* gene encodes the catalytic subunit of human telomerase. This gene is active during the embryonic development and in tumor cells (in approximately

85% of all cases), whereas the expression of *TERT* is suppressed in the overwhelming majority of normal cells in the organism [59]. The level of *TERT* expression is increased for superficial spreading melanoma [60], which is believed to prevent the cells from entering apoptosis.

Cyclooxygenase 2 (*Cox-2*) is the inducible isoform of *Cox-1*, which cannot be detected in most normal tissues, as opposed to *Cox-1* [61]. Expression of the *Cox-2* gene is closely associated with cancerogenesis and the progression of certain types of intestinal neoplasias and tumors of epithelial origin [62, 63]. The *Cox-2* gene is expressed at a high level in melanoma cells and is not expressed in nevus and in the normal epithelium of the gene [64].

The expression of the α -chemokine CDF-1 receptor – *CXCR4* gene is typical for breast cancer cells and virtually cannot be detected in the normal breast epithelium [65]. Overexpression of the *CXCR3* and *CXCR4* receptors was demonstrated in melanoma cells as well. It is assumed that receptors play a significant role upon melanoma invasion by modulating cell mobility, proliferation, and survival [66].

Survivin encoded by the *BIRC5* gene belongs to the group of apoptosis-inhibitory proteins; it plays an important role in the growth and progression of tumors of various types [67]. *BIRC5* is expressed in embryonic and fetal tissues [68], many types of neoplasias, including melanoma [69–71], and cannot be detected in differentiated adult tissues [72].

Tumor-specific promoters can be used within the conditionally replicating adenoviruses (CRAds) that were described above to achieve the oncolytic effect. Thus, the *TERT* promoter was used instead of the *E1A* gene promoter for transcriptional control of adenovirus replication. Moreover, this construct contained the apoptin gene under the strong constitutive CMV promoter [73]. Apoptin is a viral protein which specifically induces the apoptosis of cancer cells [74]. Thus, a system is constructed possessing “double” tumor-specificity, which is determined by the *TERT* promoter (activated in tumor cells) and apoptin (which has a selective effect on tumor cells). When cells were infected with Ad-*TERT*-Apoptin viruses, the growth of melanoma cells (line A375 and B16) was suppressed, resulting in apoptosis, whereas the normal epidermal melanocytes were protected from this effect [73]. Moreover, the reduction of lung metastases upon intratumoral and systemic administration of the Ad-*TERT*-Apoptin construct was demonstrated on a model of mouse metastatic melanoma. When using this system, a higher mouse survival rate was also observed [73].

The potential benefits of using other tumor-specific promoters in melanoma therapy were assessed by determining the activity of the luciferase reporter gene, when it is transcriptionally controlled by promoters

of the *Cox-2*, *CXCR4*, and *BIRC5* genes. Recombinant adenoviruses containing one of the TSP promoters and the luciferase gene controlled by them, instead of the E1 region, were used as a vector [75]. The luciferase activity was measured in four melanoma cell lines (Mel-624, A375M, SK-MEL-28 и MeWo) and in normal epithelial melanocytes (HEM) [75]. The *CXCR4* gene promoter had no required specificity; its activity in the normal melanocytes was even higher than in melanoma cells [75]. Earlier, the transcriptional activity of the *Cox-2* promoter that was inactive in primary melanocytes had been revealed in melanoma cell lines [76]. However, the activity of the *Cox-2* gene promoter varies considerably depending on the cell line type [75]. The highest specific activity was demonstrated by the survivin gene promoter. Moreover, its activity in the normal melanocytes was considerably lower than it was in melanoma cells [75]. It has been recently shown that upon using the survivin gene promoter to control the expression of the iodide symporter (*NIS*) gene, the cells of the melanoma line A375 acquire the ability to uptake radioactive iodine-131, which has a negative effect on their survival [77]. Meanwhile, normal fibroblasts of human tooth pulp transfected by the same construct neither absorb iodine nor die. Thus, the survivin promoter was the optimal one for melanoma therapy among the tumor-specific promoters under comparison.

The activity of most tumor-specific promoters is lower than that of constitutive strong promoters, such as the SV40 and CMV promoters [75, 78, 79]. The activity of even relatively strong tumor-specific promoters varies considerably depending on the type of cancer cells. In different tumor cell lines, the activity of the survivin gene promoter varies from 0.3 to 16% of the activity of the CMV promoter [80–82], while the efficacy of the performance of the *TERT* promoter may differ by up to 20 fold [83].

The use of promoters that have a certain tissue-specific activity allows one to solve a number of problems associated with the nonspecific toxicity of the delivery vector. Thus, adenoviral vectors have considerable restrictions caused by the low efficacy of the transduction of melanoma cells, due to the low concentration or absence of the coxsackievirus and adenovirus receptors (CAR) that mediate cell transduction on melanoma cells [84]. The introduction of high doses of adenoviruses had a negative effect on the organism in general. Constructs of AdRGD adenoviruses that possess tropism towards α_v -integrins and transduce melanoma cells more efficiently as compared with the standard adenoviruses have been created [85]. Nevertheless, the systemic introduction of such adenoviral constructs resulted in nonspecific transduction and death of normal cells. The problem was solved by using specific promot-

ers. AdRGD adenoviruses containing the *HSVtk* suicide gene under the transcriptional control of the tumor-specific promoter *TERT* or melanoma-specific promoter Tyrex2, instead of the standard nonspecific CMV promoter, turned out to be promising for melanoma therapy [86]. A decrease in the size of mice tumors was observed upon intratumoral introduction of AdRGD-*TERT*-*HSVtk* or AdRGD-Tyrex2-*HSVtk*, after subsequent administration of ganciclovir. The same effect is achieved by the introduction of low doses of nonspecific AdRGD-CMV-*HSVtk*; however, in this case increasing the dose of the vector resulted in weight loss and hepatotoxicity in the mice [86]. On the other hand, even an intravenous introduction of high doses of the AdRGD-*TERT*-*HSVtk* or AdRGD-Tyrex2-*HSVtk* vector does not cause toxic damage to the liver. Thus, the suppression of the nonspecific cytotoxicity of adenoviruses in normal nontumor cells is achieved via the use of specific promoters [86].

The size of the promoter plays a significant role in the design of efficient gene therapy agents, since many vectors are characterized by their limited capacity. Thus, it has been demonstrated that in retroviral vectors containing long promoter modules, the viral titer typically decreases when the size of the promoter introduced is increased [87]. However, a large number of short promoters are either very weak or lose their tissue specificity; therefore, the possibility of constructing short and specific promoters that would possess sufficient transcriptional potential is a considerable task. Construction of synthetic and/or double (chimeric) promoters may become a method that could allow to overcome these limitations.

CONSTRUCTION AND OPTIMIZATION OF SYNTHETIC AND DOUBLE PROMOTERS POSSESSING TISSUE-SPECIFIC ACTIVITY

The controlling elements of the known promoters that have been characterized are used to construct *de novo* specific promoter modules. For instance, artificial promoters based on the elements of the promoters of the human tyrosinase and α -fetoprotein (AFP1) genes possessing strong and specific expression in melanoma cell lines were constructed [88]. As previously mentioned, the tyrosinase promoter contains the M-box, the conservative element that is common to melanocyte-specific promoters [89]. This element was used in combination with the elements from the 5'-region of the *AFP1* promoter – the GRE element, which is specific for the cell cycle and the AP1-binding element. Several efficient melanocyte-specific promoters were obtained upon different combinations of one or several copies of fragments of the tyrosinase and α -fetoprotein promoters – the M-box, AP1 and GRE elements. These pro-

motors were selectively active in the B16 melanoma line, but not in the HeLa cell line [88]. The length of the artificial constructs was not more than 300 bp; the promoter consisting of three GRE, three AP1 elements, and two M-boxes was the most efficient one. It was ascertained that if the number of regulatory elements of the promoter in the chimeric construct is higher than eight units, a loss in promoter specificity is observed [88]. It seems that the activity of synthetic promoters is dependent both upon the number of regulatory elements and upon the vector. The optimal number of regulatory elements has to be selected in each case. For example, it was shown in the above-mentioned study by Rothfels *et al.* [22] that it is sufficient to bind four copies of the enhancers of the mouse tyrosinase gene in order to increase the activity of both the *MIA* and *TYR* promoters.

Another approach to constructing specific promoters consists in the construction of chimeric or double promoters.

As previously mentioned, most tumor-specific promoters show lower activity in comparison with constitutive strong promoters, such as the promoters of the SV40 and CMV viruses. One of the approaches that help to resolve the problems related to the efficacy of tumor-specific promoters is the use of hybrid double promoters: (i) one of them being tumor-specific, while the second is a strong nonspecific promoter; (ii) each promoter being tumor-specific. The double promoters described exhibit a higher activity in tumors of a certain type in comparison with natural promoters.

The chimeric promoter CMV-hTERT is an example of the first construct [90]. The chimeric construct was obtained on the basis of the promoter of the human telomerase reverse transcriptase (hTERT) gene and the minimal CMV promoter, which is characterized by a higher activity in comparison with the nonmodified *hTERT* promoter, while it retains tumor specificity.

Double tumor-specific promoters have also been described [91, 92]. In order to increase the efficacy of expression of therapeutic genes in small lung cancer cell (SCLC), a chimeric double promoter based on promoters of the *hASH1* and *EZH2* genes with a high level of expression in SCLC cells was obtained. The activity of the double chimeric promoter was higher than the activities of the corresponding single promoters by up to 1–8 fold, depending on the cell line of SCLC [92].

In another study, a high level of expression of apoptosis activator *tBid* in breast cancer cells was achieved via the use of a hybrid promoter consisting of promoters of the human survivin gene and the gene encoding glycoprotein mucin; its expression increased in breast cancer cells [91]. Thus, the use of double promoters permits one to provide a high level of expression of the

therapeutic gene in tumor cells, retaining specificity towards cancer. The use of double tumor-specific promoters facilitates the construction of more universal gene therapeutic constructs: i.e., constructs that provide the expression of the therapeutic gene in many types of cancer cells. For instance, a vector bearing two *DT-A* gene fragments controlled by the promoters of the *IGF2-P4* and *H19* genes was constructed [93]. The introduction of this vector to cells of several lines of urinary bladder cancer ensured gene expression in all lines, whereas the *DT-A* gene controlled by one of the promoters, *IGF2-P4* or *H19*, exhibited activity not in all the lines of tumor cells that were used.

No systems of double promoters containing melanoma-specific promoters have been described yet. However, the construction of systems based on melanoma-specific promoters, such as promoters of the *MIA* and *TYR* genes, could provide a universal, highly efficient, and specific expression of the therapeutic gene in melanoma cells.

CONCLUSION

Melanoma treatment is associated with a number of difficulties, including the high resistance of melanoma cells and early metastasizing, which determine the unfavourable prognosis. The necessity to affect the metastatic loci disseminated over the entire organism requires the systemic administration of antimelanoma agents, which involves a certain risk that other cells of the organism can be affected. Gene therapy, which has known rapid development, offers new methods that allow to increase the specificity of the effect on melanoma cells whilst simultaneously decreasing the probability of damaging healthy cells. The use of melanoma-specific promoters makes it possible to specifically affect melanoma cells. These methods have recently gone into the stage of development and are permanently being improved to find the most efficient solutions, starting with the selection of optimal regulatory elements, the designing of constructs based on these elements, and ending with the search for new vectors, with both natural viruses or artificially constructed systems for packing the genetic material being used as such vectors [94, 95]. One can hope that a simple and efficient system for the elimination of melanomas and its metastases will be designed. ●

This work was supported by The Presidential grant for Scientific Schools (5638.2010.4); the Program of the Presidium of the Russian Academy of Sciences “Molecular and Cellular Biology,” and the Federal Target Program (Government Contract № 16.512.12.2002).

REFERENCES

1. Atallah E., Flaherty L. // *Curr. Treat. Options Oncol.* 2005. V. 6. P. 185–193.
2. Bhatia S., Tykodi S.S., Thompson J.A. // *Oncology (Williston Park)*. 2009. V. 23. P. 488–496.
3. Ganesan P., Bakhshi S. // *Natl. Med. J. India*. 2010. V. 23. P. 21–27.
4. Ko J.M., Fisher D.E. // *J. Pathol.* 2011. V. 223. P. 241–250.
5. Nishizaki M., Fujiwara T., Tanida T., Hizuta A., Nishimori H., Tokino T., Nakamura Y., Bouvet M., Roth J.A., Tanaka N. // *Clin. Cancer Res.* 1999. V. 5. P. 1015–1023.
6. Seth P. // *Cancer Biol. Ther.* 2005. V. 4. P. 512–517.
7. Takeuchi M., Shichinohe T., Senmaru N., Miyamoto M., Fujita H., Takimoto M., Kondo S., Katoh H., Kuzumaki N. // *Gene Ther.* 2000. V. 7. P. 518–526.
8. Denny W.A. // *J. Biomed. Biotechnol.* 2003. V. 2003. P. 48–70.
9. Dudek A.Z. // *Transl. Res.* 2010. V. 156. P. 136–146.
10. Springer C.J., Niculescu-Duvaz I. // *J. Clin. Invest.* 2000. V. 105. P. 1161–1167.
11. Mullen C.A., Coale M.M., Lowe R., Blaese R.M. // *Cancer Res.* 1994. V. 54. P. 1503–1506.
12. Sverdlov E. // *Molecular Genetics, Microbiology and Virology*. 2009. V. 24. P. 93–113.
13. Yamamoto S., Yamano T., Tanaka M., Hoon D.S., Takao S., Morishita R., Aikou T., Kaneda Y. // *Cancer Gene Ther.* 2003. V. 10. P. 179–186.
14. Ezzeddine Z.D., Martuza R.L., Platika D., Short M.P., Malick A., Choi B., Breakefield X.O. // *New Biol.* 1991. V. 3. P. 608–614.
15. Ambade A.V., Joshi G.V., Mulherkar R. // *Indian. J. Med. Res.* 2010. V. 132. P. 415–422.
16. Li S., Tokuyama T., Yamamoto J., Koide M., Yokota N., Namba H. // *Oncology*. 2005. V. 69. P. 503–508.
17. Erbs P., Regulier E., Kintz J., Leroy P., Poitevin Y., Exinger F., Jund R., Mehtali M. // *Cancer Res.* 2000. V. 60. P. 3813–3822.
18. Graepler F., Lemken M.L., Wybranietz W.A., Schmidt U., Smirnow I., Gross C.D., Spiegel M., Schenk A., Graf H., Lauer U.A., et al. // *World J. Gastroenterol.* 2005. V. 11. P. 6910–6919.
19. Robson T., Hirst D.G. // *J. Biomed. Biotechnol.* 2003. V. 2003. P. 110–137.
20. Saukkonen K., Hemminki A. // *Expert. Opin. Biol. Ther.* 2004. V. 4. P. 683–696.
21. Lillehammer T., Tveito S., Engesaeter B.O., Fodstad O., Maelandsmo G.M., Engebraaten O. // *Cancer Gene Ther.* 2005. V. 12. P. 864–872.
22. Rothfels H., Paschen A., Schadendorf D. // *Exp. Dermatol.* 2003. V. 12. P. 799–810.
23. Hearing V.J., Tsukamoto K. // *FASEB J.* 1991. V. 5. P. 2902–2909.
24. Bentley N.J., Eisen T., Goding C.R. // *Mol. Cell Biol.* 1994. V. 14. P. 7996–8006.
25. Shibata K., Muraosa Y., Tomita Y., Tagami H., Shibahara S. // *J. Biol. Chem.* 1992. V. 267. P. 20584–20588.
26. Siders W.M., Halloran P.J., Fenton R.G. // *Cancer Res.* 1996. V. 56. P. 5638–5646.
27. Sato S., Tanaka M., Miura H., Ikeo K., Gojobori T., Takeuchi T., Yamamoto H. // *J. Investig. Dermatol. Symp. Proc.* 2001. V. 6. P. 10–18.
28. Ganss R., Montoliu L., Monaghan A.P., Schutz G. // *EMBO J.* 1994. V. 13. P. 3083–3093.
29. Bosserhoff A.K., Moser M., Hein R., Landthaler M., Buettner R. // *J. Pathol.* 1999. V. 187. P. 446–454.
30. Dietz U.H., Sandell L.J. // *J. Biol. Chem.* 1996. V. 271. P. 3311–3316.
31. Perez R.P., Zhang P., Bosserhoff A.K., Buettner R., Abuhadid M. // *Hum Pathol.* 2000. V. 31. P. 1381–1388.
32. Blesch A., Bosserhoff A.K., Apfel R., Behl C., Hessdoerfer B., Schmitt A., Jachimczak P., Lottspeich F., Buettner R., Bogdahn U. // *Cancer Res.* 1994. V. 54. P. 5695–5701.
33. Bosserhoff A.K., Echtenacher B., Hein R., Buettner R. // *Melanoma Res.* 2001. V. 11. P. 417–421.
34. Winklmeier A., Contreras-Shannon V., Arndt S., Melle C., Bosserhoff A.K. // *Cancer Sci.* 2009. V. 100. P. 261–268.
35. Bosserhoff A.K., Kaufmann M., Kaluza B., Bartke I., Zirngibl H., Hein R., Stolz W., Buettner R. // *Cancer Res.* 1997. V. 57. P. 3149–3153.
36. Bosserhoff A.K., Hein R., Bogdahn U., Buettner R. // *J. Biol. Chem.* 1996. V. 271. P. 490–495.
37. Golob M., Buettner R., Bosserhoff A.K. // *J. Invest. Dermatol.* 2000. V. 115. P. 42–47.
38. Bosserhoff A.K., Kondo S., Moser M., Dietz U.H., Copeland N.G., Gilbert D.J., Jenkins N.A., Buettner R., Sandell L.J. // *Dev. Dyn.* 1997. V. 208. P. 516–525.
39. Roberts D.W., Newton R.A., Beaumont K.A., Helen Leonard J., Sturm R.A. // *Pigment Cell Res.* 2006. V. 19. P. 76–89.
40. Schwahn D.J., Xu W., Herrin A.B., Bales E.S., Medrano E.E. // *Pigment Cell Res.* 2001. V. 14. P. 32–39.
41. Salazar-Onfray F., Lopez M., Lundqvist A., Aguirre A., Escobar A., Serrano A., Korenblit C., Petersson M., Chhajlani V., Larsson O., et al. // *Br. J. Cancer.* 2002. V. 87. P. 414–422.
42. Thornwall M., Dimitriou A., Xu X., Larsson E., Chhajlani V. // *Horm. Res.* 1997. V. 48. P. 215–218.
43. Moro O., Ideta R., Ifuku O. // *Biochem. Biophys. Res. Commun.* 1999. V. 262. P. 452–460.
44. Rouzaud F., Hearing V.J. // *Peptides*. 2005. V. 26. P. 1858–1870.
45. Aoki H., Moro O. // *Life Sci.* 2002. V. 71. P. 2171–2179.
46. Smith A.G., Box N.F., Marks L.H., Chen W., Smit D.J., Wyeth J.R., Huttley G.A., Eastel S., Sturm R.A. // *Gene*. 2001. V. 281. P. 81–94.
47. Tachibana M. // *Pigment Cell Res.* 2000. V. 13. P. 230–240.
48. Yasumoto K., Yokoyama K., Takahashi K., Tomita Y., Shibahara S. // *J. Biol. Chem.* 1997. V. 272. P. 503–509.
49. Miccadei S., Pascucci B., Picardo M., Natali P.G., Civitareale D. // *J. Exp. Clin. Cancer Res.* 2008. V. 27. P. 71.
50. Nettelbeck D.M., Rivera A.A., Balague C., Alemany R., Curiel D.T. // *Cancer Res.* 2002. V. 62. P. 4663–4670.
51. Peter I., Graf C., Dummer R., Schaffner W., Greber U.F., Hemmi S. // *Gene Ther.* 2003. V. 10. P. 530–539.
52. Stritzker J., Pilgrim S., Szalay A.A., Goebel W. // *BMC Cancer*. 2008. V. 8. P. 94.
53. Huang B., Zhao J., Shen S., Li H., He K.L., Shen G.X., Mayer L., Unkeless J., Li D., Yuan Y., et al. // *Cancer Res.* 2007. V. 67. P. 4346–4352.
54. Riedel C.U., Monk I.R., Casey P.G., Morrissey D., O'Sullivan G.C., Tangney M., Hill C., Gahan C.G. // *Appl. Environ. Microbiol.* 2007. V. 73. P. 3091–3094.
55. Yu Y.A., Shabahang S., Timiryasova T.M., Zhang Q., Beltz R., Gentschev I., Goebel W., Szalay A.A. // *Nat. Biotechnol.* 2004. V. 22. P. 313–320.
56. McCart J.A., Wang Z.H., Xu H., Hu Y., Park B., Alexander H.R., Bartlett D.L. // *Mol. Ther.* 2002. V. 6. P. 471–480.
57. Sorscher E.J., Peng S., Bebok Z., Allan P.W., Bennett L.L., Jr., Parker W.B. // *Gene Ther.* 1994. V. 1. P. 233–238.

REVIEWS

58. Schoensiegel F., Paschen A., Sieger S., Eskerski H., Mier W., Rothfels H., Kleinschmidt J., Schadendorf D., Haberkorn U. // *Cancer Gene Ther.* 2004. V. 11. P. 408–418.
59. Cong Y.S., Wright W.E., Shay J.W. // *Microbiol. Mol. Biol. Rev.* 2002. V. 66. P. 407–425, table of contents.
60. Slater M., Scolyer R.A., Gidley-Baird A., Thompson J.F., Barden J.A. // *Melanoma Res.* 2003. V. 13. P. 137–145.
61. Dubois R.N., Abramson S.B., Crofford L., Gupta R.A., Simon L.S., van De Putte L.B., Lipsky P.E. // *FASEB J.* 1998. V. 12. P. 1063–1073.
62. Ristimaki A., Honkanen N., Jankala H., Sipponen P., Harkonen M. // *Cancer Res.* 1997. V. 57. P. 1276–1280.
63. Williams C., Shattuck-Brandt R.L., DuBois R.N. // *Ann. N.-Y. Acad. Sci.* 1999. V. 889. P. 72–83.
64. Denkert C., Kobel M., Berger S., Siegert A., Leclere A., Trefzer U., Hauptmann S. // *Cancer Res.* 2001. V. 61. P. 303–308.
65. Muller A., Homey B., Soto H., Ge N., Catron D., Buchanan M.E., McClanahan T., Murphy E., Yuan W., Wagner S.N., et al. // *Nature.* 2001. V. 410. P. 50–56.
66. Robledo M.M., Bartolome R.A., Longo N., Rodriguez-Frade J.M., Mellado M., Longo I., van Muijen G.N., Sanchez-Mateos P., Teixido J. // *J. Biol. Chem.* 2001. V. 276. P. 45098–45105.
67. Altieri D.C. // *Prog. Cell Cycle Res.* 2003. V. 5. P. 447–452.
68. Adida C., Crotty P.L., McGrath J., Berrebi D., Diebold J., Altieri D.C. // *Am. J. Pathol.* 1998. V. 152. P. 43–49.
69. Chiodino C., Cesinaro A.M., Ottani D., Fantini F., Giannetti A., Trentini G.P., Pincelli C. // *J. Invest. Dermatol.* 1999. V. 113. P. 415–418.
70. Sarela A.I., Verbeke C.S., Ramsdale J., Davies C.L., Markham A.F., Guillou P.J. // *Br. J. Cancer.* 2002. V. 86. P. 886–892.
71. Tanaka K., Iwamoto S., Gon G., Nohara T., Iwamoto M., Tanigawa N. // *Clin. Cancer Res.* 2000. V. 6. P. 127–134.
72. Bao R., Connolly D.C., Murphy M., Green J., Weinstein J.K., Pisarcik D.A., Hamilton T.C. // *J. Natl. Cancer Inst.* 2002. V. 94. P. 522–528.
73. Li X., Liu Y., Wen Z., Li C., Lu H., Tian M., Jin K., Sun L., Gao P., Yang E., et al. // *Mol. Cancer.* 2010. V. 9. P. 10.
74. Rohn J.L., Noteborn M.H. // *Apoptosis.* 2004. V. 9. P. 315–322.
75. Lu B., Makhija S.K., Nettelbeck D.M., Rivera A.A., Wang M., Komarova S., Zhou F., Yamamoto M., Haisma H.J., Alvarez R.D., et al. // *Gene Ther.* 2005. V. 12. P. 330–338.
76. Nettelbeck D.M., Rivera A.A., Davydova J., Dieckmann D., Yamamoto M., Curiel D.T. // *Melanoma Res.* 2003. V. 13. P. 287–292.
77. Huang R., Zhao Z., Ma X., Li S., Gong R., Kuang A. // *Cancer Gene Ther.* 2010. V. 18. P. 144–152.
78. Rein D.T., Breidenbach M., Nettelbeck D.M., Kawakami Y., Siegal G.P., Huh W.K., Wang M., Hemminki A., Bauerschmitz G.J., Yamamoto M., et al. // *J. Gene Med.* 2004. V. 6. P. 1281–1289.
79. van Houdt W.J., Haviv Y.S., Lu B., Wang M., Rivera A.A., Ulasov I.V., Lamfers M.L., Rein D., Lesniak M.S., Siegal G.P., et al. // *J. Neurosurg.* 2006. V. 104. P. 583–592.
80. Chen J.S., Liu J.C., Shen L., Rau K.M., Kuo H.P., Li Y.M., Shi D., Lee Y.C., Chang K.J., Hung M.C. // *Cancer Gene Ther.* 2004. V. 11. P. 740–747.
81. Konopka K., Spain C., Yen A., Overlid N., Gebremedhin S., Duzgunes N. // *Cell Mol. Biol. Lett.* 2009. V. 14. P. 70–89.
82. Zhu Z.B., Makhija S.K., Lu B., Wang M., Kaliberova L., Liu B., Rivera A.A., Nettelbeck D.M., Mahasreshti P.J., Leath C.A., et al. // *Cancer Gene Ther.* 2004. V. 11. P. 256–262.
83. Gu J., Fang B. // *Cancer Biol Ther.* 2003. V. 2. P. S64–70.
84. Hemmi S., Geertsens R., Mezzacasa A., Peter I., Dummer R. // *Hum. Gene Ther.* 1998. V. 9. P. 2363–2373.
85. Okada Y., Okada N., Nakagawa S., Mizuguchi H., Kanehira M., Nishino N., Takahashi K., Mizuno N., Hayakawa T., Mayumi T. // *Cancer Lett.* 2002. V. 177. P. 57–63.
86. Okada Y., Okada N., Mizuguchi H., Hayakawa T., Nakagawa S., Mayumi T. // *Cancer Gene Ther.* 2005. V. 12. P. 608–616.
87. Diaz R.M., Eisen T., Hart I.R., Vile R.G. // *J. Virol.* 1998. V. 72. P. 789–795.
88. Martinelli R., De Simone V. // *FEBS Lett.* 2005. V. 579. P. 153–156.
89. Lowings P., Yavuzer U., Goding C.R. // *Mol. Cell Biol.* 1992. V. 12. P. 3653–3662.
90. Davis J.J., Wang L., Dong F., Zhang L., Guo W., Teraishi F., Xu K., Ji L., Fang B. // *Cancer Gene Ther.* 2006. V. 13. P. 720–723.
91. Farokhimanesh S., Rahbarizadeh F., Rasaei M.J., Kamali A., Mashkani B. // *Biotechnol. Prog.* 2010. V. 26. P. 505–511.
92. Poulsen T.T., Pedersen N., Juel H., Poulsen H.S. // *Cancer Gene Ther.* 2008. V. 15. P. 563–575.
93. Amit D., Hochberg A. // *J. Transl. Med.* 2010. V. 8. P. 134.
94. Fernandez C.A., Rice K.G. // *Mol. Pharm.* 2009. V. 6. P. 1277–1289.
95. Yao H., Ng S.S., Tucker W.O., Tsang Y.K., Man K., Wang X.M., Chow B.K., Kung H.F., Tang G.P., Lin M.C. // *Biomaterials.* 2009. V. 30. P. 5793–5803.

Posttranslational Modifications of Ribosomal Proteins in *Escherichia coli*

M. V. Nesterchuk*, P. V. Sergiev, O. A. Dontsova

Belozersky Institute of Physico-Chemical Biology, Lomonosov Moscow State University

Faculty of Chemistry, Lomonosov Moscow State University

*E-mail: nesterchuk.mihail@gmail.com

Received 14.02.2011

ABSTRACT A number of ribosomal proteins in *Escherichia coli* undergo posttranslational modifications. Six ribosomal proteins are methylated (S11, L3, L11, L7/L12, L16, and L33), three proteins are acetylated (S5, S18, and L7), and protein S12 is methylthiolated. Extra amino acid residues are added to protein S6. C-terminal amino acid residues are partially removed from protein L31. The functional significance of these modifications has remained unclear. These modifications are not vital to the cells, and it is likely that they have regulatory functions. This paper reviews all the known posttranslational modifications of ribosomal proteins in *Escherichia coli*. Certain enzymes responsible for the modifications and mechanisms of enzymatic reactions are also discussed.

KEYWORDS ribosomal proteins; posttranslational modification; *Escherichia coli*

ABBREVIATIONS RNA – ribonucleic acid; rRNA – ribosomal RNA; mRNA – messenger RNA; tRNA – transfer RNA; IF2 – initiation factor 2; EF-Tu – elongation factor Tu; EF-G – elongation factor G; RF3 – release factor 3; GTP – guanosine-5'-triphosphate

INTRODUCTION

Ribosome is a sophisticated molecular machine that is responsible for the correct translation of genetic information from the mRNA nucleotide sequence into the amino acid sequence of the synthesized protein. A ribosome is a complex of ribosomal RNAs (rRNAs) and proteins consisting of two unequal parts (the large and the small subunits). The small subunit of *Escherichia coli* ribosomes consists of 16S rRNAs and 22 proteins (denoted as S1–S22); the large subunit consists of 5S and 23S rRNAs and 34 different proteins (L1–L36). Both rRNAs and ribosomal proteins undergo enzymatic modification in the cell. The N-terminal methionine residue is cleaved in more than half of ribosomal proteins. Six proteins are methylated (S11, L3, L11, L7/L12, L16, and L33), three proteins are acetylated (S5, S18, and L7), the S12 protein is methylthiolated, additional amino acid residues are added to the S6 protein, and the L31 protein undergoes partial proteolysis (L31) (Table 1). The nature of certain modifications of the ribosomal proteins of *E. coli* has yet to be determined [1].

Most genes encoding the enzymes that perform posttranslational modification have been identified. Nonetheless, the functional role of these modifications remains poorly studied. The central role of the ribosome in the mechanism of realization of the genetic information in the cell permits to assume that modified ribosomal

proteins can be significant in a number of mechanisms of the regulation of gene expression.

PROCESSING OF THE N-TERMINUS OF RIBOSOMAL PROTEINS

Removal of the N-terminal methionine residue by methionine aminopeptidase (MAP) is the most common type of posttranslational modifications in proteins. The terminal methionine is cleaved in 37 *E. coli* ribosomal proteins out of 57 (Table 2).

This modification is most frequently found in proteins in which the amino acid following methionine has the short side chain [2]. Large side chains impede the penetration of a protein into the active site of methionine aminopeptidase. If the second residue in a protein molecule is alanine (21 case) or leucine, proline, or glycine, the N-terminal residue is always cleaved. If the first residue is followed by lysine, isoleucine, glutamine, arginine, aspartic acid, tyrosine, glutamic acid, phenylalanine, or valine, as it is observed in 20 ribosomal proteins, the N-terminal methionine residue is always retained in the protein molecule. When position 2 is occupied by serine, in four cases out of five, the methionine residue is retained. It should be noted that methionine residues are cleaved only from a certain portion of protein L33 molecules; some chains (no more than 25%) remain with the N-terminal methylated methionine. It is possible that this is associated with the competi-

Table 1. Modifications of *E. coli* ribosomal proteins

Protein	Modification position	Modification	Modifying enzyme
S5	N-terminal amino group	Acetylation	RimJ
S6	C-terminus	Insertion of additional glutaminic acid residues	RimK
S11	N-terminal amino group	Methylation, formation of the isopeptide bond	Not determined
		Formation of isoaspartate residue	Not determined
S12	Asp88	Methylthiolation	RimO
S18	N-terminal amino group	Acetylation	RimI
L3	Gln150	Methylation	PrmB
L7/L12	Lys81	Methylation	Not determined
L11	Ala1, Lys3, Lys39	Methylation	PrmA
L12	N-terminal amino group	Acetylation	RimL
L16	N-terminal amino group	Methylation	Not determined
L31	C-terminus	Removal of amino acid residues	Not determined
L33	N-terminal amino group	Methylation	Not determined

tion between N-terminal methylation and methionine cleaving [3].

PROCESSING OF THE C-TERMINUS OF PROTEIN L31

The C-terminus amino acid sequence of the ribosomal protein L31 (...RFNK) determined chemically in [4] differs from the one predicted on the basis of the nucleotide sequence of the gene of this protein (...RFNKRFPNIPGSK). A conclusion was made that protein L31 undergoes C-terminal processing (there may be a specific protease removing the RFNIPGSK fragment). These data were subsequently refuted; the primary structure of L31 was shown to agree with the genomic structure [5]. However, a mass spectrometry analysis of ribosomal proteins detects two peaks for L31: at 7871.1 Da, corresponding to the complete sequence of L31 predicted on the basis of the genomic sequence and that at 6971.1 Da, corresponding to the L31 fragment without the C-terminus region ...RFNIPGSK [1]. Protein L31 molecules are apparently only partially processed.

L31 is a component of a bacterial ribosome that has not been studied adequately. L31 is known to form a ribonucleoprotein complex with the rRNA proteins L5, L18, L25, and 5S. It is located at the vertex of the central protuberance in immediate proximity to the site of the subunit contact. It is probable that the posttranslational modification serves the purpose of protein activation or has a regulatory role. However, there is no data on the function of the site-specific proteolysis of L31 or on its possible mechanism.

It is of interest that the *E. coli* genome contains two genes of protein L31 with a similar, but not identical, sequence [6]. Protein L31 that is present in cells under “regular” laboratory conditions in which culturing

is performed contains the “zinc ribbon” motif. When there is a deficiency in zinc ions, the expression of another variant of L31 without the “zinc ribbon” is activated by the transcriptional regulator Zur. This switching likely facilitates economy of zinc ions in the cell. A similar mechanism has been described for ribosomal protein L36 [7].

METHYLATION OF RIBOSOMAL PROTEINS

Methylation is one of the most common types of post-translational protein modifications to which various prokaryotic and eukaryotic proteins are subjected. Methylation is performed by special enzymes (methyltransferases), which use S-adenosylmethionine as a methyl group donor. Five classes of methyltransferases differing in structure and substrate specificity exist.

The methylation of ribosomal proteins usually occurs at the side amino group of lysine or arginine; methylation of N-terminal amino groups is also common. Six ribosomal proteins are methylated in *E. coli* cells (Table 1) [8]. Methyltransferases that are specific to two proteins (L11 and L3) (PrmA and PrmB, respectively) have been identified; the genes encoding them have been found. Very little data exist about other modifications.

Certain methylated ribosomal proteins play a significant role in the functioning of ribosome: L7/L12 and L11 interact with the translation factors, and L3 participates in ribosome assembly. However, regardless of the fact that the functions of these ribosomal proteins have been studied appreciably well, the biological significance of their methylation is yet to be satisfactorily elucidated. Mutations in the genes encoding the corresponding methyltransferases do not result in noticeable phenotypical changes. The methylation apparently regulates the intra- and intermolecular interactions in

Table 2. Posttranslational removal of the N-terminal methionine residue in *E. coli* ribosomal proteins [1]

Protein	Removal of Met	The second residue following Met
S1	?	Thr
S2	+	Ala
S3	+	Gly
S4	+	Ala
S5	+	Ala
S6	–	Arg
S7	+	Pro
S8	+	Ser
S9	+	Ala
S10	–	Gln
S11	+	Ala
S12	+	Ala
S13	+	Ala
S14	+	Ala
S15	+	Ser
S16	–	Val
S17	+	Thr
S18	+	Ala
S19	+	Pro
S20	+	Ala
S21	+	Pro
S22	–	Lys
L1	+	Ala
L2	+	Ala
L3	–	Ile
L4	–	Glu
L5	+	Ala
L6	+	Ser
L7	+	Ser
L9	–	Gln
L10	+	Ala
L11	+	Ala
L12	+	Ser
L13	–	Lys
L14	–	Ile
L15	–	Arg
L16	–	Leu
L17	–	Arg
L18	–	Asp
L19	–	Ser
L20	+	Ala
L21	–	Tyr
L22	–	Glu
L23	–	Ile
L24	+	Ala
L25	–	Phe
L26	+	Ala
L27	+	Ala
L28	+	Ser
L29	–	Lys
L30	+	Ala
L31	–	Lys
L32	+	Ala
L33	+	Ala
L34	–	Lys
L35	+	Pro
L36	–	Lys

a protein or impacts its affinity to RNA, thus influencing various cell processes: translation regulation, its accuracy, RNA processing, and ribosome assembly.

Protein L11 Methylation

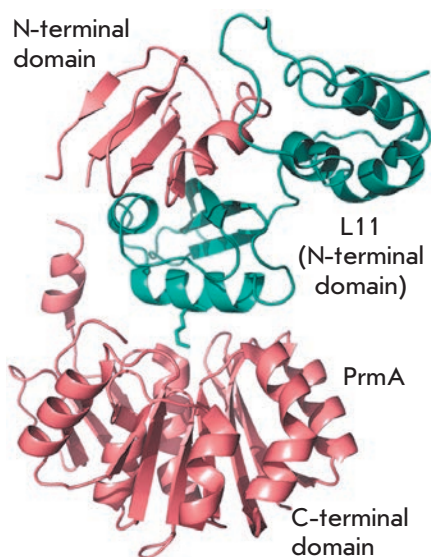
Ribosomal protein L11 is the most strongly methylated protein of the bacterial translation apparatus [9]. It contains three methylated amino acid residues: the N-terminal alanine residue is trimethylated at the α -amino group, the 3rd and 39th lysine residues are trimethylated at ϵ -amino groups. Thus, a total of nine methyl groups are posttranslationally bound to the protein [10]. The methylation is performed by a single enzyme, PrmA (protein modification), which has been isolated and characterized [11]. It was ascertained that this protein has a mass of 31 kDa and uses S-adenosyl-methionine as a methyl group donor and preferentially modifies the unbound protein L11. The latter fact attests to the fact that methylation precedes the insertion of a protein into the ribosome [11].

The mutant *E. coli* strain containing no methyl groups in protein L11 was obtained. The position of the *prmA* gene encoding methyltransferase PrmA was determined using this strain [12].

This enzyme has a unique substrate specificity, which enables the modification of several amino groups of the protein which belong to different amino acid residues and are located at different sites with respect to the peptide backbone (α - and ϵ -amino groups). To do so, either the enzyme has to be bound to a substrate in several different orientations, or the system of flexible substrate positioning has to be used for the multiple modifications. This system facilitates the reorientation of the substrate with respect to the permanent binding site. The PrmA structure and the mechanism of its interaction with the substrate has been the subject of thorough study [13, 14].

Methyltransferase PrmA consists of two domains connected by a flexible linker (*Fig. 1*). A large catalytic C-terminal domain is a typical example of class I methyltransferases. Seven-stranded β -sheet is flanked on both sides by α -helices. A small additional three-stranded β -sheet acts as an interlink between the C-terminal domain and the linker interdomain α -helix. The small N-terminal domain consists of a four-stranded β -sheet flanked by an interdomain linker α -helix, on one side, and by an N-terminal α -helix, on the other side. The N-terminal domain PrmA is unique; it is capable of recognizing and binding protein L11 (*Fig. 1*) [13]. It was ascertained using bioinformatics methods that the structure of the N-terminal domain PrmA is reminiscent of the V-domain of the EF-G factor, which is located in close proximity to protein L11 upon binding with the ribosome [15].

Fig. 1. The PrmA–L11 complex structure. PrmA and L11 are colored in salmon and cyan. The Lys39 side chain is shown in a stick representation [13].



The binding surface between the N-terminal domain PrmA and protein L11 is partially overlapped by the binding surface of L11 and 23S rRNA. Therefore, PrmA modifies L11 only in the unbound state, prior to its insertion into the ribosome. This fact is confirmed by the data obtained earlier on *in vitro* methylation [11]. The binding of the N-terminal domain PrmA to L11 is highly specific and is stabilized by a number of hydrogen bonds, whereas the catalytic C-terminal domain does not possess any specificity; its interaction with the substrate is stabilized only by the local hydrophobic interaction (the side chain of the modified lysine residue enters the active site via the tunnel formed by hydrophobic amino acid residues, which interact with the hydrophobic part of the side lysine radical). Due to the flexibility of the interdomain linker, the catalytic domain can change its position with respect to the N-terminal domain bound to L11 and methylate all the amino groups that are available to it (Fig. 2).

In the structure of a catalytic domain, there is a special hydrophobic pocket for the binding of S-adenosylmethionine; this pocket is open. This means that the exchange between S-adenosylhomocysteine (the reaction product) and S-adenosylmethionine is possible without disturbance of the enzyme–substrate complex. The active site of PrmA contains no atoms that could impede the rotation of the methylated amino group, which allows the enzyme that are bound to the substrate to trimethylate it. To methylate the amino group, it is necessary that the catalytic centre contain a basic amino acid residue that can accept a proton from the nitrogen atom. His104 located in the active site opposite the cofactor binding site apparently acts as such a residue.

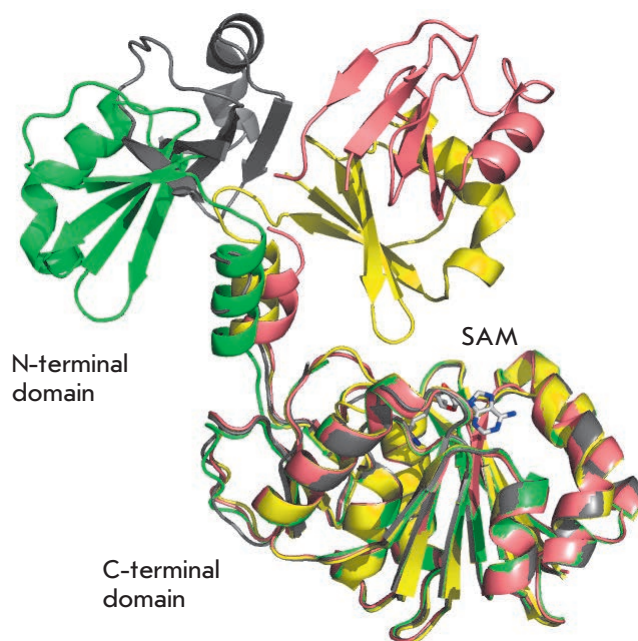


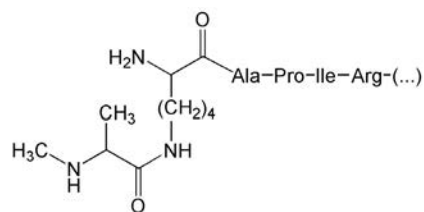
Fig. 2. Superposition of four different conformations of PrmA. Apo-enzyme structures are colored in green and grey. The SAM-bound form of PrmA is colored in yellow. The structure of PrmA in the complex with L11 is colored in salmon [13].

Thus, the methylation performed by enzyme PrmA is a rare example of simultaneous specific recognition of the target and multiple modifications of substrate due to the spatial separation of the binding site and the catalytic center, as well as their mutual mobility. A single methyltransferase molecule is capable of sequentially introducing nine methyl groups into protein L11, without the dissociation of the enzyme–substrate complex.

Protein L11 is a conservative component of the large subunit of the bacterial ribosome and is an active participant of the interaction between the ribosome and the factors of translation initiation, elongation, and termination. It consists of two domains connected by a flexible linker: the C-terminal domain binding 23S rRNA and the N-terminal domain interacting with the translation factors [13]. The N-terminal domain is the target of antibiotic thiostrepton, which inhibits EF-G–ribosome binding (resistance towards thiostrepton is ensured by a number of mutations in the N-terminal domain of protein L11) [16]. It was revealed via cryo-electron microscopy that the N-terminal domain of L11 is in direct contact with the EF-G [15] and EF-Tu factors [17].

All amino acid residues trimethylated with PrmA are located in the N-terminal domain. This arrangement of the modified residues near the site of contact

Fig. 3. Structure of the N-terminal amino acid residue of S11, which is methylated and forms isopeptide linkage [25].



with the translation factors may point to the functional significance of methylation. The PrmA structure is conservative in all bacteria, which may also attest to its contribution to L11 functions. Nevertheless, the function of modification carried out by PrmA has not, as yet, been ascertained. In addition to being viable, the strain with a mutation of the *prmA* gene does not differ noticeably from the wild-type strain (the same growth rate and the same behavior under stress conditions) [18, 19]. This means that multiple methylation of L11 is not necessary for the normal functioning of the ribosome. Meanwhile, it may have an effect both on the rate and accuracy of such stages of ribosome functioning as decoding and translocation, which can be detected only using a very accurate kinetic *in vitro* analysis or by the *in vivo* introduction of specific mutations into protein L11 or other components of the translation apparatus [13].

Methylation of Protein L3

One methyl group is posttranslationally added to ribosomal protein L3 [20]. The methylation takes place at the amide group of the 150th glutamine residue [21]. Modification is performed by specific methyltransferase PrmB. Its gene has been identified [12]. PrmB is the first described methyltransferase with an amide nitrogen atom acting as its target.

The absence of methylation in protein L3 in the strain containing a mutation in the *prmB* gene is combined with cold sensitivity. The growth rate of mutant cells at 22°C is considerably lower than that in wild-type cells [22, 23]. This is due to the fact that at low temperatures ribosome assembly in mutant cells is inefficient; the structure and stability of the resulting intermediate ribonucleoprotein complexes differ from that of the corresponding intermediates in the wild-type strain. Nevertheless, the mutant ribosomes that are completely formed at a reduced temperature do not differ from the wild-type ribosomes in terms of their stability. No difference in the translation rate or its accuracy was observed neither *in vivo* nor *in vitro* [22].

In vitro studies of the activity of the PrmB enzyme demonstrated that protein L3, in the unbound state, does not undergo methylation. Neither does methyltransferase methylate, the completely assembled ribosome.

The highest activity is observed in the partially assembled ribosome and in the presence of RNA (of any type, not necessarily ribosomal) in the reaction mixture [22].

Protein L3 is bound to the 3'-terminal site of 23S rRNA at the very first stage of structure folding and, along with L24, is the initiator of the entire process of ribosome assembly [24].

A conclusion can be made from the aforementioned that PrmB *in vivo* methylates L3 by binding to the ribosome at one of the intermediate stages of its folding; hence, it is likely to have a certain effect on the correctness of its packing. Thus, the PrmB enzyme can be referred to ribosome assembly factors.

Protein L3 has a globular domain located on the ribosome surface and a long tail that is deeply submerged inside. The modified 150th glutamine residue is located inside the ribosome near the tunnel or the growing polypeptide chain. It forms contacts with the nucleotide residues G2032, C2055, and A2572, which are located in the 3'-terminal region of 23S rRNA. This residue apparently contributes to the formation and maintenance of the correct rRNA conformation.

Methylation of Protein S11 and Formation of the Isopeptide Bond

In ribosomal protein S11, the N-terminal amino group belonging to the alanine residue undergoes methylation. In addition to methylation, the formation of an isopeptide bond is observed. Only one *E. coli* protein, S11, is susceptible to this transformation. During this process, the peptide bond between the first and second residues (alanine and lysine) in the S11 molecule is destroyed (*Fig. 3*) [25].

It was reported [26] that the isoaspartate residue was detected in the protein S11; there is 0.5 mol of isoaspartate per 1 mol of the protein. It was demonstrated that only S11 has such a modification in the logarithmic growth phase.

Neither the enzymes that perform the aforementioned modifications nor the functional role of the modifications have been ascertained.

Protein S11 is located in immediate proximity to mRNA and tRNA in the E-site. Its N-terminus protruding on the ribosome surface cannot be seen in the crystal structure and probably has no fixed orientation. It is unlikely that the modified residue contributes to the maintenance of the ribosome structure. The methylated N-terminus of S11 probably interacts with tRNA and facilitates its escape from the E-site.

Methylation of Protein L7/L12

Ribosomal protein L7/L12 is monomethylated at the ϵ -amino group of the 81st lysine residue. The degree of

methylation strongly depends on temperature. At 37°C, almost no modification is observed (less than 0.1 methyl groups per protein molecule). The number of groups introduced increases abruptly with decreasing temperature and is equal to 0.6 monomethyl-lysine residues per protein molecule [27]. The enzyme performing this reaction has not been identified.

The protein L7/L12 is located in the ribosome as a tetramer representing a rod-shaped appendix, the so-called “L7/L12 stalk”. Each chain in a tetramer consists of two domains: the N-terminal domain, which is bound to protein L10, and the C-terminal domain. The domains are connected by a flexible linker, which makes it possible for the C-terminal domains to change their orientation with respect to the large subunit. Thus, L7/L12 is the only ribosomal protein that does not have direct contact with rRNA; it is bound to it via the complex with protein L10. This complex plays a significant role in the translation process; it participates in the binding between the translation factors (IF2, EF-Tu, EF-G, and RF3) and the ribosome [28]. The methylated residues are located in the C-terminal domain, and it is possible that they contribute to the interaction with the translation factors.

Methylation of Proteins L16 and L33

N-terminal amino groups are methylated in the ribosomal proteins L16 and L33. In L16, the first methionine residue is methylated [29]. In L33, some polypeptide chains start with the monomethylated methionine (no more than 25%), whereas some chains start with monomethylated alanine [30]. Such heterogeneity is probably associated with the competition between the processes of methylation and N-terminal methionine cleavage [30]. The assumption of a possible reduction of N-formylmethionine to N-methylmethionine has been refuted [3].

The methyltransferases performing the modification of proteins L16 and L33 have not been identified.

Another modification type has been detected in protein L16. Based on the amino acid sequence, the molecular weight of protein L16 is supposed to be 15281.3 Da. However, there is no peak in the mass spectrum of this protein that would correspond to this weight, although, there is a peak corresponding to 15326.2 Da, which is higher by 44.9 Da. The methyl group at the N-terminus of the protein increases its weight only by 14 Da. This entails that the molecule L16 should contain at least one more posttranslational modification. Hypothetically, Arg81 undergoes hydroxylation. However, in this case the modified protein should be lighter than the value observed by mass spectroscopy: 14.9 Da [1]. Another methylation or hydroxylation may take place. The more explicit data concerning the nature and lo-

calization of the unknown modification were obtained from the mass spectra of the products of tryptic cleavage of protein L16.

Proteins L16 and L33 are located near the central protuberance on the opposite sides from it. Their N-terminal residues are exposed to the ribosome surface and are not in direct contact with rRNA and the proteins.

ACETYLATION OF RIBOSOMAL PROTEINS

N^α-acetylation of proteins is catalysed by N^α-acetyltransferases, which transfer the acetyl group from acetylcoenzyme A to the N-terminal amino group of the protein. In eukaryotes, this modification of proteins is widespread: 80–90% of cytoplasmic proteins in mammals and 50% in yeasts are acetylated at the N-terminal amino acid residue [31]. In prokaryotes, this modification is rarely realized. Only four *E. coli* proteins are known to undergo this process: the EF-Tu factor and the ribosomal proteins S5, S18, and L7. The genes which encode the enzymes that perform the modification of the ribosomal proteins S5, S18, and L7 were determined: *rimJ*, *rimI*, and *rimL*, respectively. Each of the mentioned transferases specifically modifies only one protein (as opposed to eukaryotes, in which these enzymes are less specific). Despite their similar functions, the structures of these enzymes are very different. The similarity between sequences *RimI* (148 residues), *RimJ* (194 residues), and *RimL* (178 residues) is 19 and 20%, respectively; while that between *RimJ* and *RimL* is 23% (although *RimI* and *RimJ* are alanine acetyltransferases, whereas *RimL* is serine acetyltransferase). It is likely that these proteins have no common ancestor and evolved independently from each other [32].

Eukaryotic N^α-acetyltransferases typically consist of two or three different subunits; they cotranslationally modify the substrate, whereas the prokaryotic enzymes are most frequently monomeric or in the form of homodimers (e.g., *RimL*) and acetylate substrate posttranslationally [33].

Acetylation of Protein S5

Ribosomal protein S5 is acetylated at the α-amino group of the first alanine residue [34]. The acetylation is performed by a specific enzyme, *RimJ* (ribosomal modification) [35]. The *rimJ* gene encoding this enzyme has been identified and sequenced [36].

The substrate specificity of *RimJ* has been ascertained. Poot *et al.* [37] investigated an *E. coli* strain containing the mutation in the central pseudoknot in 16S rRNA (C18A). This mutation leads to the disturbance of the assembly of the 30S subunit, deterioration of binding between it and proteins S1, S2, S18, and S21

and, therefore, to the reduction in translation efficacy. Moreover, the mutation results in a decrease in the proportion of acetylated molecules S5; i.e., the activity of RimJ decreases. This is apparently connected with the fact that S5 is located in immediate proximity to the central pseudoknot, in which the mutations can change the site of landing of S5 on the 30S subunit; therefore, RimJ cannot be bound to the substrate. It should be noted that non-acetylated S5 has not been found in the assembled 70S mutant ribosomes. The binding between the mutant 30S subunit and 50S apparently stabilizes the functionally active conformation of the 30S subunit. Having this conformation, the 30S subunit becomes the RimJ substrate. It was earlier demonstrated that the mutation in protein S4 also results in lower efficacy of acetylation of S5 [38]. These data attest to the fact that acetylation of S5 is performed on an assembled ribosome.

The function of RimJ is associated not only with the modification of protein S5, but also with other stages of biogenesis of the small ribosomal subunit [39]. In the *E. coli* strain with mutation in the gene of protein S5 (the 28th glycine residue is substituted for aspartic acid), the assembly of ribosomes is disturbed, translation accuracy is reduced, and cold sensitivity is observed. The superexpression of RimJ in this strain completely recovers all the translational defects. This

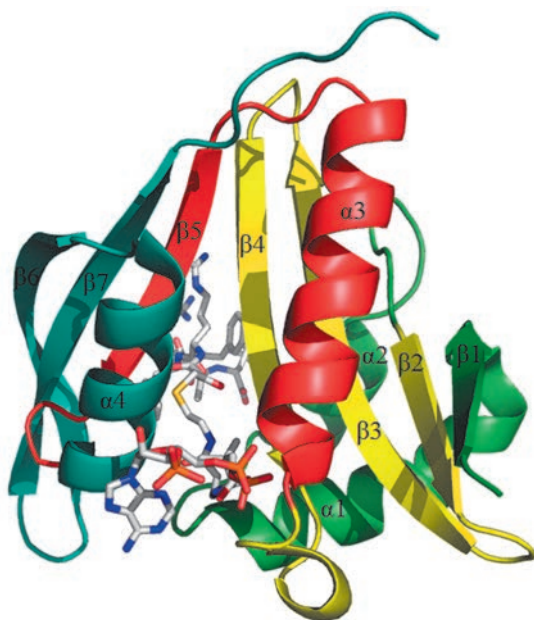


Fig. 4. Structure of the RimI-bisubstrate complex. Bisubstrate is shown as sticks. From the N-terminus, secondary structural elements are colored green (b1, a1, a2), yellow (b2–b4), red (a3, b5), and blue (a4, b6) [32].

entails that, regardless of the acetyltransferase activity, RimJ contributes to the formation of the correct ribosome structure. It can be proven by the fact that RimJ is bound to subunit 30S at early stages of its assembly [39]. The functions of RimJ as a factor of ribosome and acetyltransferase assembly can be combined and performed simultaneously or sequentially.

Protein S5 is located on the side of the small subunit that is opposite to the decoding centre. The N-terminal residues protrude over the ribosome surface and cannot be seen in the crystal structure. Therefore, the α -amino group of the first residue of protein S5 within a ribosome is accessible for acetylation, which agrees with the results of study [37].

Protein RimJ performs functions that are not directly connected with the acetylation of S5. It has been demonstrated that RimJ is a repressor of the pap operon responsible for pilus biosynthesis in the pathogenic *E. coli* strain causing pyelonephritis. RimJ regulates the transcription of this operon depending on environmental conditions (temperature, the presence of nutrients). The mechanism of this regulation and how it is connected to the acetyltransferase function of RimJ have not been ascertained [40].

Acetylation of Protein S18

In a similar fashion to S5 and L12, protein S18 undergoes N-terminal acetylation (at the alanine residue) [41]. The modification is performed by the specific acetyltransferase encoded by the *rimI* gene [36].

Acetylation of S18 does not belong to the modifications that are vital to a cell. The cells with mutations in the *rimI* gene are not only viable, but they also do not phenotypically differ from wild-type cells [42].

The 3D structure of RimI from *Salmonella typhimurium* (the primary structure being absolutely identical to RimI from *E. coli*) has been determined [32]. The enzyme has a mixed $\alpha\beta$ -structure, with the central seven-stranded β -sheet flanked by four α -helices (Fig. 4). The central sheet has a predominately antiparallel structure, with the exception of the parallel 4th and 5th strands. The order of β -strands in the sheet is linear, with the exception of strand $\beta 7$ that is located between $\beta 5$ and $\beta 6$. The sheet has a V-shaped structure, where strands $\beta 1$ – $\beta 4$ form one shoulder, while strands $\beta 5$ – $\beta 7$ form the other shoulder. It is assumed that the acetyltransferase center is located in the V-shaped broadening between the $\beta 4$ - and $\beta 5$ -strands.

Based on the data on the 3D structure of the complex of enzyme with substrate and coenzyme (acetyl coenzyme A), a mechanism of acetyltransferase reaction was proposed (Fig. 5).

The N-terminal nitrogen atom in S18 nucleophilically attacks the carbonyl carbon atom of acetyl coenzyme A,

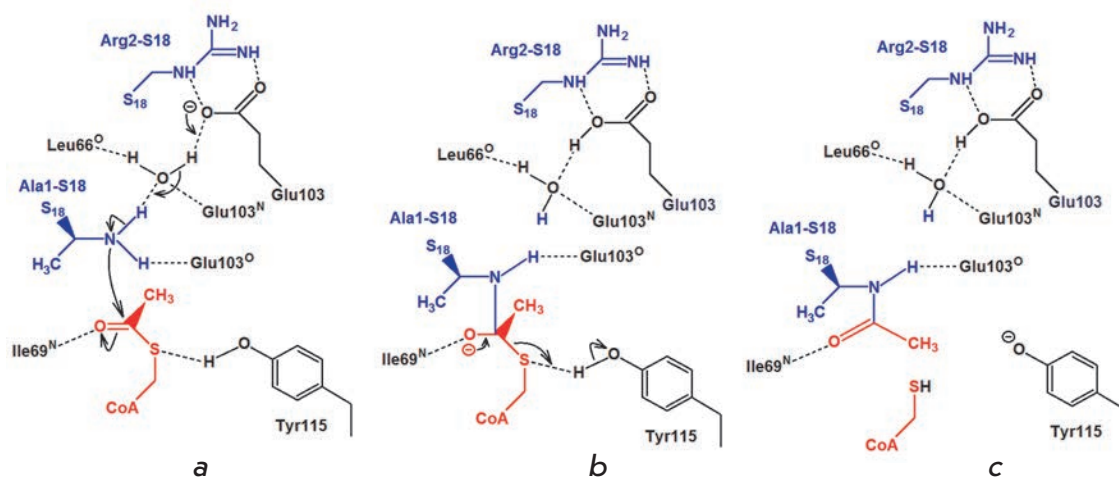


Fig. 5. The proposed mechanism of the reaction catalyzed by RimL. (i) Nucleophilic attack on the carbonyl carbon of Ac-CoA; (ii) collapse of the tetrahedral intermediate; (iii) product complex [32].

with the Glu103 residue acting as a proton acceptor (Fig. 5a). This results in the formation of a tetrahedral intermediate (Fig. 5b). Tyr115 acts as a proton donor upon decomposition of the intermediate (Fig. 5c).

Despite the fact that the mechanism of S18 acetylation has been ascertained, the function of acetylation and the stage at which it takes place have not as yet been elucidated. Protein S18 is located in the central domain of the small ribosomal subunit near proteins S11 and S6. The interaction between S18 and S6 is so strong that a stable heterodimer is formed [43]. S18 is located near the E-site. The first 15 N-terminal residues in S18 cannot be seen in the crystal structure of the ribosome; therefore, it is most likely that they do not have a fixed 3D position. They are probably located near the site of mRNA landing on the small subunit. In this case, the N-terminal acetylation can have an effect on the translation initiation process.

Acetylation of Protein L12

Ribosomal protein L12 exists in two different forms: the non-acetylated (L12) and acetylated (so-called L7) forms [44]. Due to the identity of the amino acid sequences, this protein is called L7/L12.

Acetylation of the α -N-atom of Ser1 in protein L12 is performed by the specific enzyme RimL and results in the formation of L7 [45]. RimL is capable of *in vitro* acetylation of the two unbound proteins L12 [46] and L12 within the ribosome [33]. Apparently, *in vivo* modification of L12 can also take place at any stage of ribosome biogenesis. As opposed to the totally modified S5 and S18, L12 is only partially acetylated. The L7/L12 ratio varies depending on the phase and rate of cell growth. In the middle of the logarithmic phase, the proportion of L12 attains 85%; then, the L7 content gradually increases to 75–80% in the stationary phase [47]. When the cells grow in a minimum medium, all of

the protein is converted into the L7 form.

The modification of L12 was shown to enhance the strength of the complex formed by the L7/L12 tetramer and protein L10 [48]. These authors account that by the fact that acetylation stabilizes the N-terminal α -helices of L7 (are denoted as α 1 in Fig. 6) and fix the position of the N-terminal residue in space, thus making the structure more compact and stronger.

Nevertheless, the strain with a mutation in the *rimL* gene, in which the entire protein L12 is present in deacetylated form, has no noticeable phenotypic distinctions from the wild-type strain. In particular, there is no difference in the cell growth rate at 25, 37, or 42°C [46]. Therefore, the modification is insignificant for ribosome functioning; the question as to its possible function remains open.

The substrate specificity of RimL and nature of the N-terminal amino acid residue of the substrate was studied in [33]. According to the data published, in N ^{α} -acetylated proteins these residues typically are represented by serine, alanine, or methionine. Thus, it is serine for L12 from *E. coli* and alanine for L12 from *Pseudomonas aeruginosa* and *Bacillus subtilis* and S18 and S5 from *E. coli*. The assumption that RimL is not specific towards the N-terminal residue has been experimentally confirmed. RimL efficiently acetylates *in vitro* the mutant L12, with Ser1 replaced by Ala1 [33].

In the case of eukaryotic N ^{α} -acetyltransferases, the second amino acid residue of the N ^{α} -acetylated protein has an effect on the modification of the first protein. If the second residue is aspartate or glutamate, modification occurs efficiently. In order to investigate the effect of the second amino acid residue on the activity of RimL, the mutant L12 was obtained, with Ile2 replaced by Asp2. It turned out that RimL acetylates this mutant protein much less efficiently in comparison

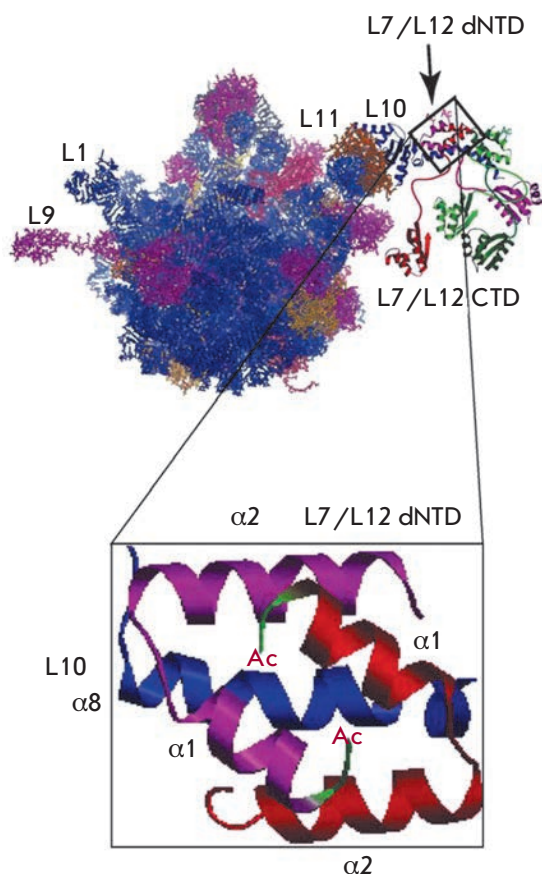


Fig. 6. A hypothetical model of *E. coli* ribosomes with the ribosomal stalk complex attached. L10 is shown in blue; L7/L12 dimers, in red/magenta and light/dark green. The detailed view of the interaction of the L7/L12 NTD dimer with a segment of the $\alpha 8$ helix of L10 illustrates the hypothesis that N-terminal acetylation results in stronger binding of the L7 NTD dimer onto the $\alpha 8$ helix of L10 [48].

with the native L12. This, again, emphasizes the difference between prokaryotic N^α-acetyltransferases and eukaryotic ones [33].

The crystal structure of RimL was obtained from *Salmonella typhimurium* (the similarity between the primary structure and the RimL from *E. coli* is 83%). RimL is a homodimer that is capable of binding two molecules of acetyl coenzyme A and modifying dimeric L12 [49].

METHYLTHIOLATION OF PROTEIN S12

The primary structure of ribosomal protein S12 of *E. coli* was determined chemically; however, its 88th amino acid residue could not be identified [50]. The subsequent sequencing of the gene encoding S12 demonstrated that aspartic acid is located at this position [51]. Only 20 years later was it shown mass spectrometrical-

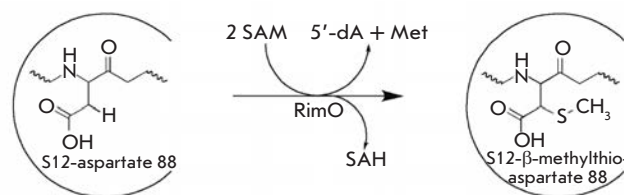


Fig. 7. Reaction catalysed by RimO. The methylthiolation of aspartyl 88 of protein S12.

ly that the molecular weight of S12 is equal to 13652 Da (which is bigger than that predicted on the basis of the nucleotide sequence by 46.1 Da) [1]. Further study of this phenomenon demonstrated that this discrepancy is conditioned by the presence of the methylthioether group ($-\text{SCH}_3$) (Fig. 7) at the β -carbon atom of Asp88 [52]. Later, the *rimO* gene encoding methylthiotransferase that performs this posttranslational modification was found [53].

This reaction is an example of the enzymatic formation of the C–S bond from C–H, which is relatively rare in nature. These reactions occur via a radical mechanism using S-adenosylmethionine as a coenzyme [54].

S12 is the conservative element of ribosome; the Asp88 residue was found in all known S12 homologues: in bacteria, archaeobacteria and eukaryotes (although the modification is not always observed). Asp88 is located near the functional centers of the ribosome. The attempts to obtaining *E. coli* cells with a mutation of this amino acid were unsuccessful. All these facts point to the significance of Asp88 in the functioning of ribosome.

All the methylthiotransferases that had been known before RimO posttranscriptionally modify RNA; RimO is the first studied enzyme in this family, with a protein as its target. In addition to RimO, only one methylthiotransferase was detected in *E. coli*: MiaB modifying tRNA. The amino acid sequences of these two proteins are characterized by a close similarity [53]. In particular, they both contain the CxxxCxxC motif, which is canonical for the entire methylthiotransferase family.

The methylthiolation of protein S12 was carried out via a radical mechanism (Fig. 8). At the first stage, the C–S bond in S-adenosylmethionine is broken, yielding an unbound methionine and a 5'-deoxyadenosyl radical. Then, this radical takes away a hydrogen atom from the β -carbon atom of Asp88. Next, a thioether is formed, which undergoes methylation at the final stage. Thus, two molecules of S-adenosylmethionine are required to modify a single molecule of protein S12 [55].

At the final stage, the RimO enzyme also takes part in the methylation. This means that RimO is methyl-

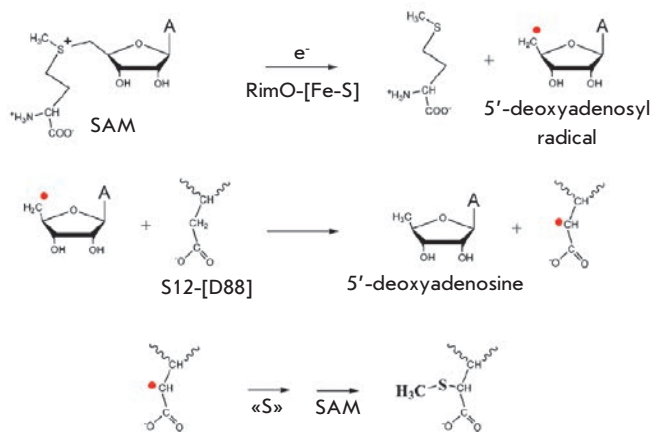


Fig. 8. Mechanism of the reaction catalysed by RimO [55].

transferase, although no conservative S-adenosylmethionine-binding motifs that are typical of enzymes of this class have been detected in it [56].

It was ascertained through spectroscopic studies that there are two [4Fe-4S] clusters in the structure of RimO (Fig. 9). The first cluster is coordinated by the residues Cys150, Cys154, and Cys157 (the conservative CxxxCxxC motif); the second is coordinated by the residues Cys17, Cys53, and Cys82. It is assumed that the first cluster participates in the formation of the 5'-deoxyadenosyl radical, whereas the second one serves as the source of sulphur atoms for thioether formation [56].

RimO contains the so-called TRAM domain, which serves for RNA binding in MiaB [53]. This could be an indication that RimO modifies protein S12 within the ribosome. It has indeed been confirmed experimentally that RimO *in vivo* methylthiolates residue Asp88 of protein S12, which is a component of the small subunit [57]. It was ascertained earlier that the recombinant RimO from *E. coli* and *Thermatoga maritima* can modify *in vitro* the synthetic peptide substrate imitating a loop containing residue Asp88; however, the efficacy of the modification is very low [58].

It was recently demonstrated that in addition to RimO, the conservative protein YcaO also participates in the modification of protein S12; the function of YcaO remained unknown. Knockout of the *ycaO* gene results in the almost complete suppression of the methylthiolating activity of RimO. Moreover, the transcriptome analysis of strains with the deletion of the *rimO* and *ycaO* genes points to the overlapping of transcriptional phenotypes, which attests to the functional similarity between RimO and YcaO. Protein YcaO is bound to the small subunit and probably functions as a chaperon by facilitating the formation of the enzyme-substrate complex [57].

It should be mentioned that after the methylthiolation of the aspartic acid residue, a new chiral centre (β -carbon atom) emerges; however, its configuration has not yet been ascertained.

Protein S12 consists of a globular domain located near the A-site in the decoding centre and a long rod-shaped tail, which fixates the protein on the small subunit. S12 is the only protein located on the contact surface between the large and small subunits. The modified residue is located near the decoding centre; however, it forms direct contacts neither with mRNA nor tRNA. It is submerged into a pocket formed by two loops: the first loop is formed from the nucleotides 522–528 of 16S rRNA, the second loop is formed from the amino acid residues 44–51 of S12.

The function of S12 modification has not been elucidated yet. It is known that mutations in the neighboring residues (Lys87, Ley89, Pro90, Gly91, and Arg93) lead to the emergence of resistance to streptomycin or streptomycin dependence [53]. It is also known that protein S12 participates in the spontaneous translocation of the ribosome (independent of EF-G and GTP), whereas the mutation in the neighboring 87th amino acid residue violates this function [59]. Nevertheless, in case of mutation in the *rimO* gene, none of these phenotypical changes take place. The only difference between this mutant and the wild-type strain consists in a slightly reduced growth rate [53].

MODIFICATION OF PROTEIN S6

Ribosomal protein S6 has a unique type of posttranslational modification. From two to six glutaminic acid residues (...ADDAEAGDSEE(E)₀₋₄) are located on its C-terminus [60, 61]. Only the first two (...ADDAEAGDSEE) are encoded in the gene (*rpsF*) [62]; the rest of the residues are added posttranslationally. The modification occurs in a stepwise fashion; glutaminic acid residues being added one by one [63].

The mutant strain was obtained; it contained only two glutaminic acid residues and demonstrated no heterogeneity of the C-terminus of protein S6. Using this

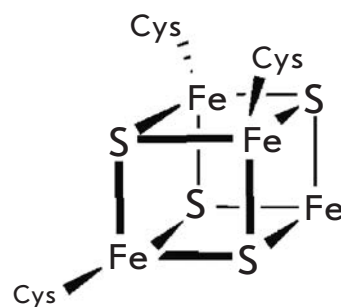


Fig. 9. The [4Fe-4S] cluster coordinated by cysteine residues in the structure of RimO [56].

strain, the *rimK* gene that is responsible for this modification was detected [64]. This gene encodes an enzyme with a molecular weight of 31.5 kDa, which recognizes the protein S6 and adds more residues on its C-terminus. In the case of the mutation in the *rpsF* gene, resulting in substitution of the penultimate residue of glutamic acid by lysine, no posttranslational modification of protein S6 was observed [64]. This means that RimK recognizes the C-terminal region of wild-type protein S6. In some mutant strains, RimK adds more than four glutamic acid residues to S6; however, the reasons for this have not been elucidated [65].

It was ascertained that under conditions when ribosome assembly does not occur (in cells irradiated with ultraviolet light), S6 does not undergo modification [66]. The RNA-binding motif was found in RimK using bioinformatics methods [67]. These data may point to the fact that modification occurs during or after the insertion of protein S6 into the ribosome.

Protein S6 is located in the central domain of the small ribosomal subunit. By interacting with the proteins S18, S8, and S15, it protects 16S rRNA against attacks by endonucleases. The C-terminal amino acid residues of S6 protrude outside and are not seen in the crystal structure.

S6 is the most acidic protein of the 30S subunit ($pI = 4.8$), the posttranslational modification enhancing its acidity to a larger extent. The function of this modification has yet to be elucidated; however, it is the first known case of posttranslational addition of amino acid residues. ●

This work was supported by the Russian Foundation for Basic Research (project no. 10-04-01345-a), the Federal Program "Personnel" NK29P P800, grant HFSP RGY 0088/2008, and the Program of Moscow State University PNR 5.13.

REFERENCES

1. Arnold R.J., Reilly J.P. // *Anal. Biochem.* 1999. V. 269. P. 105–112.
2. Ben-Bassat A., Bauer K., Chang S.Y., Myambo K., Boosman A., Chang S. // *J. Bacteriol.* 1987. V. 169. P. 751–757.
3. Chang F.N., Budzilowicz C. // *J. Bacteriol.* 1977. V. 131. P. 105–110.
4. Brosius J. // *Biochemistry.* 1977. V. 17. P. 501–508.
5. Eistetter A.J., Butler P.D., Traut R.R., Fanning T.G. // *FEMS Microbiol. Lett.* 1999. V. 180. P. 345–349.
6. Makarova K.S., Ponomarev V.A., Koonin E.V. // *Genome Biol.* 2001. V. 2. Research 0033.
7. Gabriel S.E., Helmann J.D. // *J. Bacteriol.* 2009. V. 191. P. 6116–6122.
8. Polevoda B., Sherman F. // *Mol. Microbiol.* 2007. V. 65. P. 590–606.
9. Chang C.N., Chang N. // *Biochemistry.* 1975. V. 14. P. 468–477.
10. Dognin M.J., Wittmann-Liebold B. // *Eur. J. Biochem.* 1980. V. 112. P. 131–151.
11. Chang F.N., Cohen L.B., Navickas I.J., Chang C.N. // *Biochemistry.* 1975. V. 14. P. 4994–4998.
12. Colson C., Lhoest J., Urlings C. // *Mol. Gen. Genet.* 1979. V. 169. P. 245–250.
13. Demirci H., Gregory S.T., Dahlberg A.E., Jøgl G. // *EMBO J.* 2007. V. 26. P. 567–577.
14. Demirci H., Gregory S.T., Dahlberg A.E., Jøgl G. // *Structure.* 2008. V. 16. P. 1059–1066.
15. Agrawal R.K., Linde J., Sengupta J., Nierhaus K.H., Frank J. // *J. Mol. Biol.* 2001. V. 311. P. 777–787.
16. Cameron D.M., Thompson J., March P.E., Dahlberg A.E. // *J. Mol. Biol.* 2002. V. 319. P. 27–35.
17. Valle M., Zavialov A., Li W., Stagg S.M., Sengupta J., Nielsen R.C., Nissen P., Harvey S.C., Ehrenberg M., Frank J. // *Nat. Struct. Biol.* 2003. V. 10. P. 899–906.
18. Vanet A., Plumbbridge J.A., Guerin M.F., Alix J.H. // *Mol. Microbiol.* 1994. V. 14. P. 947–958.
19. Colson C., Smith H.O. // *Mol. Gen. Genet.* 1977. V. 154. P. 167–173.
20. Lhoest J., Colson C. // *Mol. Gen. Genet.* 1977. V. 154. P. 175–180.
21. Muranova T.A., Muranov A.V., Markova L.F., Ovchinnikov Y.A. // *FEBS Lett.* 1978. V. 96. P. 301–305.
22. Lhoest J., Colson C. // *Eur. J. Biochem.* 1981. V. 121. P. 33–37.
23. Heurgue-Hamard V., Champ S., Engstrom A., Ehrenberg M., Buckingham R.H. // *EMBO J.* 2002. V. 21. P. 769–778.
24. Kaczanowska M., Ryden-Aulin M. // *Microbiol. Mol. Biol. Rev.* 2007. V. 71. P. 477–494.
25. Chen R., Chen-Schmeisser U. // *Proc. Natl. Acad. Sci. USA.* 1977. V. 74. P. 4905–4908.
26. David C.L., Keener J., Aswad D.W. // *J. Bacteriol.* 1999. V. 181. P. 2872–2877.
27. Chang F.N. // *J. Bacteriol.* 1978. V. 135. P. 1165–1166.
28. Gudkov A.T. // *FEBS Lett.* 1997. V. 407. P. 253–256.
29. Brosius J., Chen R. // *FEBS Lett.* 1976. V. 68. P. 105–109.
30. Chang C.N., Schwartz M., Chang F.N. // *Biochem. Biophys. Res. Commun.* 1976. V. 73. P. 233–239.
31. Polevoda B., Sherman F. // *Genome Biol.* 2002. V. 3. Review 0006.
32. Vetting M.W., Bareich D.C., Yu M., Blanchard J.S. // *Protein. Sci.* 2008. V. 17. P. 1781–1790.
33. Miao L., Fang H., Li Y., Chen H. // *Biochem. Biophys. Res. Commun.* 2007. V. 357. P. 641–647.
34. Wittmann-Liebold B., Greuer B. // *FEBS Lett.* 1978. V. 95. P. 91–98.
35. Janda I., Kitakawa M., Isono K. // *Mol. Gen. Genet.* 1985. V. 201. P. 433–436.
36. Yoshikawa A., Isono S., Sheback A., Isono K. // *Mol. Gen. Genet.* 1987. V. 209. P. 481–488.
37. Poot R.A., Jeeninga R.E., Pleij C.W., van Duin J. // *FEBS Lett.* 1997. V. 401. P. 175–179.
38. Cumberlidge A.G., Isono K. // *J. Mol. Biol.* 1979. V. 131. P. 169–189.
39. Roy-Chaudhuri B., Kirthi N., Kelley T., Culver G.M. // *Mol. Microbiol.* 2008. V. 68. P. 1547–1559.
40. White-Ziegler C.A., Black A.M., Eliades S.H., Young S., Porter K. // *J. Bacteriol.* 2002. V. 184. P. 4334–4342.

REVIEWS

41. Yaguchi M. // *FEBS Lett.* 1975. V. 59. P. 217–220.
42. Isono K., Isono S. // *Mol. Gen. Genet.* 1980. V. 177. P. 645–651.
43. Recht M.I., Williamson J.R. // *J. Mol. Biol.* 2001. V. 313. P. 35–48.
44. Terhorst C., Moller W., Laursen R., Wittmann-Liebold B. // *Eur. J. Biochem.* 1973. V. 34. P. 138–152.
45. Tanaka S., Matsushita Y., Yoshikawa A., Isono K. // *Mol. Gen. Genet.* 1989. V. 217. P. 289–293.
46. Isono S., Isono K. // *Mol. Gen. Genet.* 1981. V. 183. P. 473–477.
47. Ramagopal S., Subramanian A.R. // *Proc. Natl. Acad. Sci. USA.* 1974. V. 71. P. 2136–2140.
48. Gordiyenko Y., Deroo S., Zhou M., Videler H., Robinson C.V. // *J. Mol. Biol.* 2008. V. 380. P. 404–414.
49. Vetting M.W., de Carvalho L.P., Roderick S.L., Blanchard J.S. // *J. Biol. Chem.* 2005. V. 280. P. 22108–22114.
50. Funatsu G., Yaguchi M., Wittmann-Liebold B. // *FEBS Lett.* 1977. V. 73. P. 12–17.
51. Post L.E., Nomura M. // *J. Biol. Chem.* 1980. V. 255. P. 4660–4666.
52. Kowalak J.A., Walsh K.A. // *Protein. Sci.* 1996. V. 5. P. 1625–1632.
53. Anton B.P., Saleh L., Benner J.S., Raleigh E.A., Kasif S., Roberts R.J. // *Proc. Natl. Acad. Sci. USA.* 2008. V. 105. P. 1826–1831.
54. Booker S.J., Cicchillo R.M., Grove T.L. // *Curr. Opin. Chem. Biol.* 2007. V. 11. P. 543–552.
55. Fontecave M., Mulliez E., Atta M. // *Chem. Biol.* 2008. V. 15. P. 209–210.
56. Lee K.H., Saleh L., Anton B.P., Madinger C.L., Benner J.S., Iwig D.F., Roberts R.J., Krebs C., Booker S.J. // *Biochemistry.* 2009. V. 48. P. 10162–10174.
57. Strader M.B., Costantino N., Elkins C.A., Chen C.Y., Patel I., Makusky A.J., Choy J.S., Court D.L., Markey S.P., Kowalak J.A. // *Mol. Cell. Proteomics.* 2011. V. 10. M110.005199.
58. Arragain S., Garcia-Serres R., Blondin G., Douki T., Clemancey M., Latour J.M., Forouhar F., Neely H., Montelione G.T., Hunt J.F., et al. // *J. Biol. Chem.* 2010. V. 285. № 8. P. 5792–5801.
59. Asatryan L.S., Spirin A.S. // *Mol. Gen. Genet.* 1975. V. 138. P. 315–321.
60. Hitz H., Schafer D., Wittmann-Liebold B. // *FEBS Lett.* 1975. V. 56. P. 259–262.
61. Hitz H., Schäfer D., Wittmann-Liebold B. // *Eur. J. Biochem.* 1977. V. 75. P. 497–512.
62. Schnier J., Kitakawa M., Isono K. // *Mol. Gen. Genet.* 1986. V. 204. P. 126–132.
63. Reeh S., Pedersen S. // *Mol. Gen. Genet.* 1979. V. 173. P. 183–187.
64. Kang W.K., Icho T., Isono S., Kitakawa M., Isono K. // *Mol. Gen. Genet.* 1989. V. 217. P. 281–288.
65. Kade B., Dabbs E.R., Wittmann-Liebold B. // *FEBS Lett.* 1980. V. 121. P. 313–316.
66. Kitakawa M., Blumenthal L., Isono K. // *Mol. Gen. Genet.* 1980. V. 180. P. 343–349.
67. Koonin E.V., Bork P., Sander C. // *Nucl. Acids Res.* 1994. V. 22. P. 2166–2167.

Gold Nanoparticles in Biology and Medicine: Recent Advances and Prospects

L. A. Dykman¹, N. G. Khlebtsov^{1,2*}

¹Institute of Biochemistry and Physiology of Plants and Microorganisms, Russian Academy of Sciences

²Saratov State University

*E-mail: khlebtsov@ibppm.sgu.ru

Received 21.02.2011

ABSTRACT Functionalized gold nanoparticles with controlled geometrical and optical properties are the subject of intensive studies and biomedical applications, including genomics, biosensorics, immunoassays, clinical chemistry, laser phototherapy of cancer cells and tumors, the targeted delivery of drugs, DNA and antigens, optical bioimaging and the monitoring of cells and tissues with the use of state-of-the-art detection systems. This work will provide an overview of the recent advances and current challenges facing the biomedical application of gold nanoparticles of various sizes, shapes, and structures. The review is focused on the application of gold nanoparticle conjugates in biomedical diagnostics and analytics, photothermal and photodynamic therapies, as a carrier for delivering target molecules, and on the immunological and toxicological properties. Keeping in mind the huge volume and high speed of the data update rate, 2/3 of our reference list (certainly restricted to 250 Refs.) includes publications encompassing the past 5 years.

KEYWORDS gold nanoparticles; plasmon resonance; biosensors; biomedical diagnostics; photothermal and photodynamic therapy; targeted drug delivery; nanotoxicology

ABBREVIATIONS GNP – gold nanoparticles; PR – plasmon resonance; PPTT – plasmonic photothermal therapy; PEG – polyethyleneglycol; SEM – scanning electron microscopy; TEM – transmission electron microscopy; PDT – photodynamic therapy; TNF – tumor necrosis factor; CTAB – cetyltrimethylammonium bromide; SPIA – sol particle immunoassay

CONTENTS

Introduction

1. Gold nanoparticles in diagnostics
 - 1.1. Visualization and bioimaging methods
 - 1.2. Analytic methods for diagnostics
 - 1.2.1. Homophase methods
 - 1.2.2. Dot-immunoassay
 - 1.2.3. Immune chromatography
 - 1.2.4. Plasmon resonance biosensors
 2. Gold nanoparticles in therapy
 - 2.1. Photothermal therapy using gold nanoparticles
 - 2.2. Photodynamic therapy using gold nanoparticles
 - 2.3. Use of gold nanoparticles as therapeutic agents
 3. Gold nanoparticles as drug carriers
 4. Immunological properties of gold nanoparticles
 5. Biodistribution and toxicity of gold nanoparticles
- Conclusion

INTRODUCTION

Gold is one of the first metals to have been discovered; the history of its study and application spans at least several thousand years. The first data on colloidal gold

can be found in treatises by Chinese, Arabian, and Indian scientists, who managed to obtain colloidal gold as early as in the V–IV centuries BC. They utilized it for medicinal purposes (Chinese “golden solution” and Indian “liquid gold”), amongst other uses. In Europe during the Middle Ages, colloidal gold was studied and used in alchemist laboratories. Paracelsus wrote about the therapeutic properties of gold quintessence — “*quinta essentia auri*,” which he obtained via the reduction of gold chloride by vegetable extracts in alcohols or oils. He used the “potable gold” for the treatment of a number of mental diseases and syphilis. His contemporary, Giovanni Andrea, used “*aurum potabile*” as a therapy for patients with leprosy, plague, epilepsy, and diarrhea. In 1583, the alchemist David de Planis-Campy, who served as doctor to Louis XIII of France, recommended his “longevity elixir,” a colloidal solution of gold in water. The first book on colloidal gold preserved to our days was published in 1618 by the philosopher and doctor of medicine Francisco Antonii [1]. It contains data on how to obtain colloidal gold and its application in medicine, including practical advice.

Despite its centuries-old history, the “revolution in immunochemistry” associated with the use of gold nanoparticles (GNP) in biological studies occurred only in 1971, when the British researchers Faulk and Taylor [2] described a method of antibody conjugation with colloidal gold for direct electron microscopy visualization of the surface antigens of salmonellae. The study was initiated using biospecific markers – colloidal gold conjugated with immunoglobulins and other molecules – in different spheres of biology and medicine. Over the past 40 years, there have been many studies devoted to the application of functionalized nanoparticles – conjugates with recognizing biomacromolecules (antibodies, lectins, enzymes, aptamers, etc.) – in biochemistry, microbiology, immunology, cytology, plant physiology, morphology, etc.

The range of GNP use in modern medical and biology studies is extremely wide. In particular, it comprises genomics, biosensorics, immunoanalysis, clinical chemistry, detection and photothermolysis of microorganisms and cancer cells; the targeted delivery of drugs, DNA and antigens; optical bioimaging and the monitoring of cells and tissues using modern registration systems. It has been argued that gold nanoparticles could be used in almost all medical applications: diagnostics, therapy, prevention, and hygiene. A wealth of information on how to obtain and use colloidal gold in biology and medicine, as well as how it functions, can be found in books and reviews [3–8]. The broad range of applications for GNP is based on their unique physical and chemical properties. In particular, the optical properties of GNP are determined by their plasmon resonance, which is associated with the collective excitation of conduction electrons and localized in the broad region, from the visible to the infrared (IR) region, depending on the particle size, shape, and structure [9].

Taking into account the large volume of data published and the high speed at which they are updated, our review aimed to generalize the results obtained over the past several years in the most promising directions in the use of GNP in modern medical and biological studies.

1. GOLD NANOPARTICLES IN DIAGNOSTICS

1.1. Visualization and bioimaging

Gold nanoparticles have been in active use in the identification of chemical and biological agents. Electron microscopy (predominantly, transmission electron microscopy — TEM) has historically remained the predominant means to detect biospecific interactions using colloidal gold particles (due to their high electron density). It is not by happenstance that the first three-volume publication about the application of colloidal gold [10] was chiefly devoted to TEM using GMP. The use

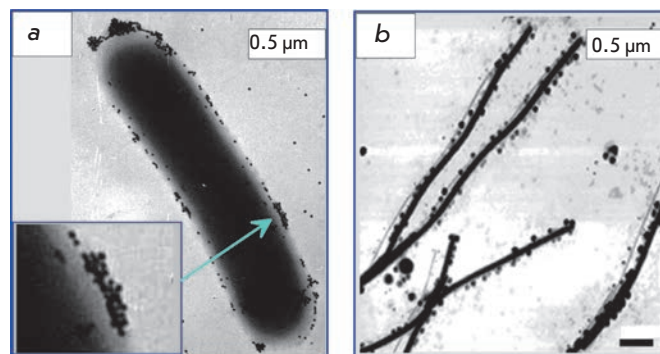


Fig. 1. TEM image of a *Listeria monocytogenes* cell (a) and AFM image of a tobacco mosaic virus labeled by colloidal gold nanoparticles conjugated with the corresponding antibodies. (b). Adapted from Refs. [11] (a) and [12] (b).

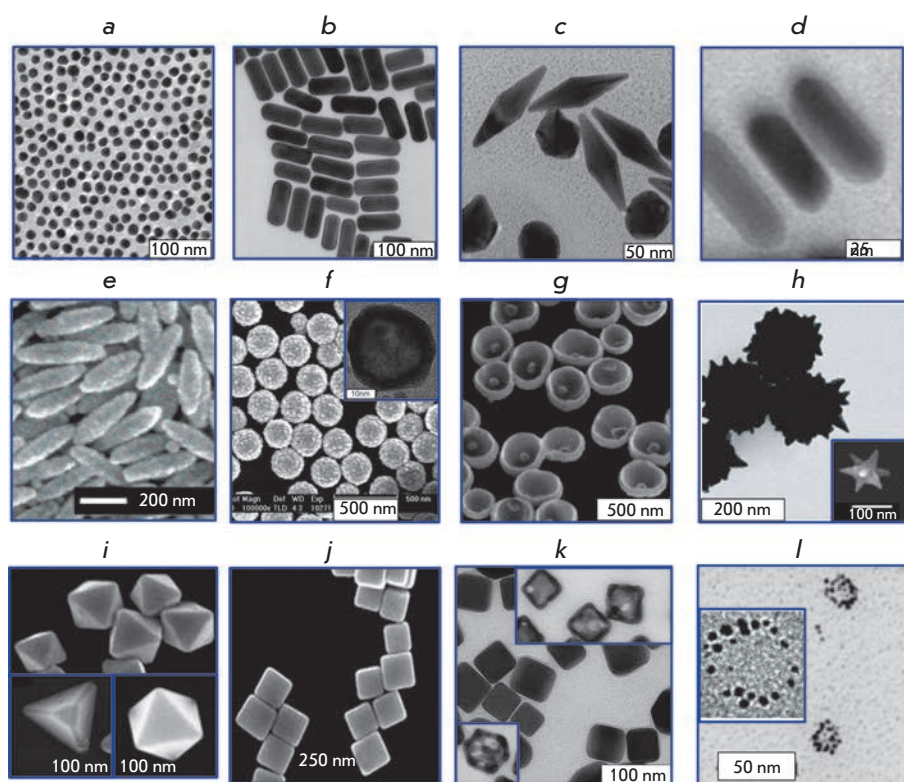
of high-resolution instruments (high-resolution transmission electron microscope – HRTEM) and systems of digital recording and the processing of images are examples of the modern application of electron microscopy equipment. The main practical use of immune electron spectroscopy in modern medico-biological studies is for the identification of causative agents of infectious diseases and their surface antigens [11] (Fig. 1A). Scanning probe microscopy [12] (Fig. 1B), scanning electron microscopy [13], and fluorescence microscopy [14] are frequently used for the same purpose.

In addition to the conventional colloidal gold with quasi-spherical particles (nanospheres), non-spherical particles, such as nanorods, nanoshells, nanocages, nanostars, and other types of particles (this group of particles were named “plasmon resonance particles of noble metals”) have recently been used [8] (Fig. 2).

The visualization methods with the use of GNP and optical microscopy [27], in particular, confocal laser microscopy, have gained increasing popularity in medical and biological research. Confocal microscopy is a method for the detection of micro-objects using an optical system, which permits the registering of light radiation only from the objects located in its focal plane; therefore, the scanning of samples along their height can be performed, and their 3D images can be obtained by superposition of scanograms. The use of GNP and antibody–GNP conjugates allows for real-time detection of the penetration of gold into living cells (e.g., cancer cells) at the level of a single particle and even for the estimation of their amount [28].

The methods for obtaining confocal images include fluorescence detection (confocal fluorescence microscopy) or resonance elastic or two-photon (multiphoton) light scattering by plasmon nanoparticles (resonance scattering confocal microscopy or two-photon lumines-

Fig. 2. Various types of gold plasmon-resonance nanoparticles: 16-nm nanospheres (a) [8], nanorods (b) [15], bipyramids (c) [16], gold nanorods with silver coating (d) [17], "nanorice" – Fe_2O_3 nanorods covered by a gold nanoshell (e) [18], gold nanoshells onto silica cores, SiO_2/Au (f) [19] (the inset shows a hollow gold nanoshell [20]), nanobowls with a gold seed on the bottom (g) [21], "spiky nanoshells" with SiO_2/Au cores [22] (the inset shows a "nanostar" particle [23]) (h), tetrahedra, octahedra, and cubooctahedra (i) [24], nanocubes (j) [24], silver nanocubes and gold-silver nanocages obtained with silver cube templates (insets) (k) [25], nanonecklaces [26] (l). The figures were adapted from the cited works. The figures are reproduced by permission from The Royal Society of Chemistry (<http://dx.doi.org/10.1039/b711490g>, <http://dx.doi.org/10.1039/c0cs00018c>), The PCCP Owner Societies (<http://dx.doi.org/10.1039/b925102b>) and The American Chemical Society.



cence confocal microscopy). These techniques are based on detecting micro-objects using an optical microscope in which the object's luminescence is excited due to the simultaneous absorption of two (or more) photons; the energy of each of them being lower than that required for fluorescence excitation. The major advantage of this method is that the strong decrease in the background signal results in the contrast being enhanced. The use of two-photon luminescence of gold nanoparticles allows to visualize (amongst other objects) oncomarkers on the surface or inside a cell [29, 30]. *Figure 3A* provides an example of combined bioimaging of a malignant cell using adsorption, fluorescence, and luminescence plasmon resonance labels.

Dark-field microscopy based on light scattering by microscopic objects (resonance scattering dark-field microscopy), including objects with a size less than the resolution limit of a light microscope, remains one of the most popular methods in bio-imaging using GNP (*Figs. 3B, C*). Upon dark-field microscopy, only the light scattered by an object under lateral illumination can reach the lens (similar to the Tyndall effect); therefore, the scattering object shines brightly against the dark background. Gold nanoparticles offer more possibilities for the detection of biospecific interactions using dark-field spectroscopy in comparison with fluores-

cence labels [8], since the scattering cross-section of a particle is higher than the fluorescence cross-section of one molecule by 3–5 orders of magnitude. This principle was applied by American researchers at the El-Sayed laboratory [31] in a new method for a simple and reliable diagnostics of oncologic diseases with the use of GNP. The method is based on the preferential binding of GNPs conjugated with antibodies specific to tumor antigens to the surface of cancerous cells, as compared with binding to healthy cells. Thus, resonance scattering dark-field microscopy can be used to map a tumor with an accuracy of up to several cells (*Figs. 3B, C*). In subsequent studies, gold nanorods [32], nanoshells [33], nanostars [34], and nanocages [35] were used with the same purpose.

Nanocages belong to a relatively new family of nanoparticles fabricated by galvanic replacement on silver nanocube templates. In this reaction, three silver atoms are replaced by a single gold atom, resulting in the gradual formation of various porous alloy structures of gold and silver, which are called nanoboxes and nanocages [35]. In the formation process of these particles, the plasmon resonance shifts from 430–440 nm for cubes to 700–900 nm for nanocages.

The use of nonspherical and/or heterogeneous particles, as well as self-assembling particle monolayers

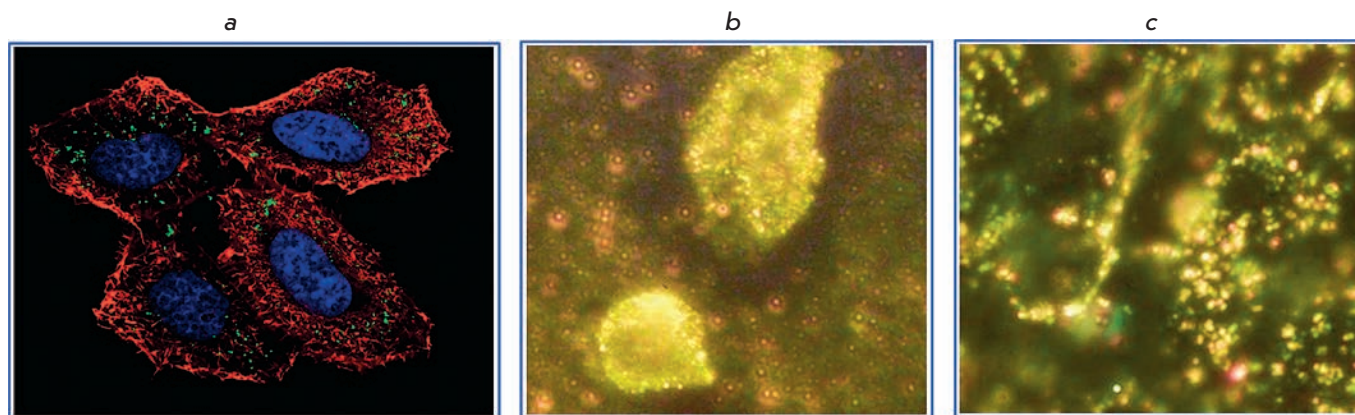


Fig. 3. a - Confocal image of HeLa cells in the presence of gold nanoparticles. The nucleus was stained with a Hoechst 33258 reagent (in blue), whereas the actin cytoskeleton was stained with an Alexa Fluor 488 labeled falloidine (in red), and gold nanoparticles (in green) were detected by two-photon luminescence [30]. A dark-field microscopic image of cancer (b) and healthy (c) cells with gold nanoparticles conjugated with antibodies to EGRF [31]. Adapted from the cited works by permission from The American Chemical Society.

or island films, opens up new opportunities to enhance sensitivity in detecting biomolecular binding on or near the surface of nanostructures. The principle of amplification of the biomolecular binding signal is based on inducing strong local electromagnetic fields near particles with sharp regions on their surface or in the narrow (on the order of nanometer or less) gaps between two nanoparticles. It stipulates enhanced sensitivity of plasmon resonance to the local dielectric environment and a high scattering intensity in comparison with spheres of the same volume. Therefore, these nanostructures can be considered as having significant potential for application for biomedical diagnostics purposes using dark-field microscopy [36].

Gold nanoparticles are used in resonance scattering dark-field microscopy for the detection of microbial cells and their metabolites [37], the bio-imaging of tumor cells [38], and for the detection of receptors on their surface [39], and for the study of endocytosis [40]. In most biomedical applications, the efficacy of labeling cells with conjugates is assessed at the qualitative level. The method of quantitative assessment of the efficacy of cell labelling with gold nanoparticles that was used for labelling pig embryo kidney cells with gold nanoshell conjugates is one of the few exceptions [41].

In addition to the aforementioned methods used to detect biospecific interactions using different variants of optical microscopy and GNP, other modern methods for detecting and bio-imaging have recently been in active development; these methods can be combined under the general name “biophotonic methods” [9]. Biophotonics combines all studies associated with the interaction between light and biological cells and tissues. Biophotonic methods include optical coherence tomog-

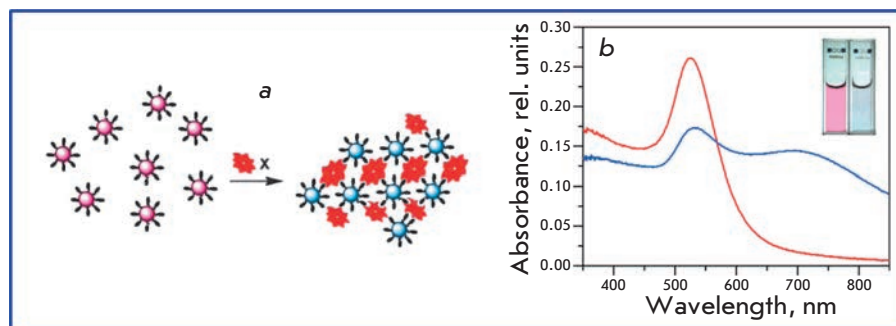
raphy [42], X-ray and magneto-resonance tomography [43, 44], photoacoustic microscopy [45] and tomography [46], fluorescence correlation microscopy [47], etc. Gold nanoparticles of various sizes and shapes are also successfully used in these methods. We believe that biophotonic methods with the use of gold non-spherical nanoparticles may prove to be of considerable promise for *in vivo* bioimaging [48]. Moreover, the significance of a new class of GNP conjugates with recognized constructions based on the barnase–barstar module [49] should be noted.

1.2. Analytic methods for diagnostics

1.2.1. Homophase methods. Beginning in the 1980s, conjugates of colloidal gold and recognizing biomacromolecules began to be used in various analytic methods of clinical diagnostics. In 1980, J. Leuvering *et al.* [50] proposed a new method that was called sol particle immunoassay (SPIA). This method is based on two principles: 1) the color and absorption spectrum of a sol vary little upon biopolymer adsorption on individual particles [51]; 2) when particles approach a distance that is less than one-tenth of their diameter, the sol’s red color changes into purpuric; the absorption spectrum broadens and shifts into the red region [51]. These changes in the absorption spectrum can be easily detected either spectrophotometrically or visually (*Fig. 4*, [52]).

An optimized version of this method (using larger gold particles and monoclonal antibodies to various sites of an antigen) was applied to detect chorionic gonadotropin in the urine of pregnant women [53]. On the basis of these elaborations, Chefaro Company (Netherlands) launched the Discretest™ kit for early out-of-hospital diagnosis of pregnancy. Kits for immune colorimetric

Fig. 4. Sol-particle immunoassay: a scheme of conjugate aggregation caused by binding to target molecules (a) and corresponding changes in the sol color and absorbance spectra (b). Adapted from Ref. [52] by permission from The American Chemical Society.



determination of the rheumatoid factor and streptolysin are produced by PLIVA Lachema Company (Czech Republic).

This method was subsequently used for performing immunoassay of the antigens of schistosomes and rubella viruses and for the quantitative determination of immunoglobulins (refs. in [5]), for determining thrombin (using aptamers) [54] and glucose [55], for the direct detection of cancer cells [56] and leptospira cells in urine [57], and for determining markers of Alzheimer's disease [58] and protease activity [59]. The simultaneous use of conjugates of gold nanorods and nanospheres with antibodies for detecting tumor antigens was described in [60]. The data on the determination of the hepatitis B virus in blood using gold nanorods conjugated with specific antibodies were published in [61].

The implementation of all versions of the SPA method proved to be relatively simple but at the same time both highly sensitive and specific. However, in a number of cases, despite the evident complementarity of a pair, no aggregation took place; the solution's color and the absorption spectra either did not change or changed to an insignificant degree. The model of formation of the second protein layer on gold particles without a loss in the aggregate stability of the sol was suggested in [62]. The changes in spectra caused by adsorption of biopolymers on the surface of gold nanoparticles are relatively small. However, even such negligible changes in absorption spectra resulting from the change in the biopolymer layer structure (or, equivalently, in its average refractive index) near the GNP surface can be recorded and used for a quantitative analysis in biological applications [63].

Various optical methods, including different versions of IR Fourier [64] and UV-vis beam absorption or deflection spectroscopy (see refs. in [5]), hyper-Rayleigh [65], differential static [51], and dynamic [60] light scattering, as well as surface-enhanced Raman scattering [66], have been used to enhance the sensitivity of the analytical homophase reaction.

A new version of the SPIA method was proposed by C. Mirkin *et al.* [67] for the colorimetric detection

of DNA. Currently, the colorimetric determination of DNA involves two strategies: (1) the use of GNP conjugated with thiol-modified single-stranded DNA [67–71] and (2) the use of nonmodified GNP [72, 73]. The first strategy is based on the aggregation of conjugates of 10–30 nm GNP with thiol-modified single-stranded DNA probes upon introduction of target polynucleotides into the system. In this case, probes of two types are used, which are complementary to two terminal regions of the targets. Hybridization of targets and probes results in the formation of GNP aggregates, which is accompanied by changes in the absorption spectrum of the solution and can be easily detected visually, photometrically [74], or via dynamic-light scattering [71]. Within the framework of the first strategy proposed by Maeda *et al.* [75], the diagnostic system based on the aggregation of GNP modified by probes of one type upon introduction of DNA targets into the solution under conditions of high ionic strength was used. Meanwhile, Baptista *et al.* [70] elaborated a method based on the enhanced stability of conjugates upon the introduction of complementary targets even under conditions of high ionic strength (2 M NaCl), and the aggregation of noncomplementary targets was observed. The apparent contradictions between the two approaches were ascribed [76] to the difference in the surface functionalization density.

The second strategy [72] is based on the fact that the single-stranded DNA protects unmodified GNP against aggregation upon high ionic strength, while the formation of duplexes upon hybridization cannot stabilize the system. This approach was used to determine the hepatitis C virus [77]. Xia *et al.* [78] recently described a new variant of the second strategy in which single-stranded DNA, unmodified GNP, and cationic polyelectrolyte are used. The same approach turned out to be suitable for determining a wide range of targets, including peptides, amino acids, pesticides, antibiotics, and heavy metals. Contrary to the procedures with usual GNP, He *et al.* [73] proposed a method for determining HIV-1 U5 viral DNA using nanorods stabilized by cetyltrimethylammonium bromide (CTAB) and the light scat-

Table 1. The sensitivity limits of the immunodot/blot methods on nitrocellulose filters using various labels (according to [89])

Label	Sensitivity limit, pg of protein/fraction
¹²⁵ I	5
Horseradish peroxidase	10
Alkaline phosphatase	1
Colloidal gold	1
Colloidal gold + silver	0.1
Fluorescein isothiocyanate (FITC)	1000

tering method with a detection limit of about 100 pM. In the optimized version where absorption spectroscopy is used [79], the detection limit was reduced to 0.1 pM. It has been recently demonstrated that positively charged GNP coated with CTAB can be used for the detection of DNA targets in combination with spectroscopy and dynamic scattering methods [15].

The enumerated versions of the method of sol particle aggregation due to the hybridization reaction were used to determine the DNA of micobacteria [70], staphylococci [80], streptococci [81], and chlamydiae [82] in clinical samples.

The ability of gold particles to aggregate upon interaction with proteins inducing colour change in the solution served as the basis for the quantitative method of colorimetric determination of proteins [83]. A new version of the SPIA method using microtitration plates, an ELISA reader, and colloidal gold-trypsin conjugates was proposed for the detection of proteins [84].

1.2.2. Dot immunoassay. At the early stages of the development of immunoassays, preference was given to liquid phase techniques, in which the bound antibodies were deposited or the unbound antigen was removed using dextran-coated activated coal. The solid-phase techniques have recently been the most widely used (first used in radioimmunoassay of proteins), since they provide the possibility to considerably simplify the analysis procedure and reduce the background signal. The most widespread solid-phase carriers are polystyrene plates and nitrocellulose membranes.

Radioactive isotopes (¹²⁵I, ¹⁴C, ³H) and enzymes (peroxidase, alkaline phosphatase, etc.) are widely used as a label in membrane tests (dot and blot analyses). In 1984, four studies were independently published [85–88] in which colloidal gold was used as a label for solid-phase immunoanalysis. The use of GNP conjugates in solid-phase analysis is based on the fact that the intense red coloration of a gold-containing marker allows one to determine visually the results of a reaction that was car-

ried out on a solid carrier. “Immuno-gold techniques” in dot blot assay are superior to the other types of assays (e.g., immunoenzyme assay) in sensitivity (Table 1, [89]), simplicity, speed, and cost. The GNP size after the corresponding immunochemical reaction can be increased using the reaction of amplification with silver [90] or gold salts (autometallography) [91], which considerably broadens the limits of application of this method. The optimized version of solid-phase assay using the Quantity One densitometry system (Bio-Rad, USA) provided a linear range of detection from 1 pM to 1 μM [92] with a limit of 100 aM and its decrease to 100 zM by silver amplification. It should be kept in mind that this record decrease in the detection limit due to silver amplification was attained using the sensitive densitometry system (Quantity One). The modern instrument methods, such as photothermal deflection of a probe laser beam induced by heating of the local environment near the absorbing particles by heating laser pulses (LISNA [93]), also ensure a very broad detection range: from several orders of magnitude to several isolated particles per blot.

When carrying out specific staining, the membrane with the material applied on it is incubated in a solution containing antibodies (or other biospecific probes) labelled with colloidal gold [94]. Immunoglobulins, Fab- and scFv- antibody fragments, protein A, lectins, enzymes, avidin or anti-biotin antibodies upon the study of biotin conjugated samples, aptamers, and other recognizing molecules are used as probes when carrying out “gold” dot or blot assay. Several labels can be simultaneously used as well (e.g., colloidal gold and peroxidase or alkaline phosphatase) to reveal different antigens on a membrane.

Colloidal gold in membrane tests was used to diagnose parasitic, virus, and fungus diseases; tuberculosis, melioidosis, syphilis, brucellosis, shigellosis, and coli-infections; to determine blood groups and pregnancy at an early stage, for dot blot hybridization, and for revealing the diphtheritic toxin, diagnostics of myocardial infarction, and hepatitis B (see refs. in [5]).

Immunodot assay is one of the simplest methods for determining the antigens immobilized on membranes; in some cases, this method allows one to estimate their quantitative content. Most frequently, immunodot assay is used to study soluble antigens [95]. However, few studies have been published in which corpuscular antigens (whole bacterial cells) were studied by dot assay with enzyme labels [96]. The procedure of dot assay in whole bacterial cells with visualization of the reaction products using colloidal gold conjugates as biospecific markers (“cell-gold immunoblotting”) was first used for serotyping soil nitrogen-fixating microorganisms of the *Azospirillum* genus [97]. This method was subsequently

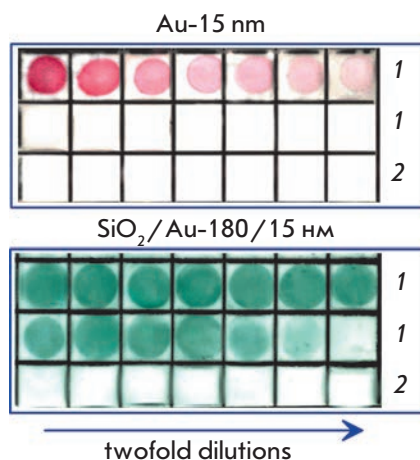


Fig. 5. Dot immunoassays of a normal rabbit serum (1) by using 15-nm GNPs and silica/gold nanoshells (180-nm-core diameter and 15-nm gold shell) conjugated to sheep's antirabbit antibodies. The IgG quantity equals 1 μg for the first (upper left) square and is decreased by twofold dilution (left to right). The bottom rows (2) correspond to a negative control (10 μg BSA in each square). Adapted from Ref. [100].

used for express diagnostics of enteric infections [98].

The results of applying gold nanoshells as biospecific labels for dot assay were first presented in paper [99], where three types of gold nanoshells with diameters of the silicate nucleus of 100, 140, and 180 nm and gold shell thickness of approximately 15 nm were studied. Normal rabbit serum (target molecules) and sheep antirabbit immunoglobulins (recognizing molecules) were used as a biospecific pair. When using the standard protocol of the dot assay on a nitrocellulose membrane with 15-nm colloidal gold nanoparticles as labels, the minimum detectable amount of rabbit IgG was equal to 15 ng. The replacement of the colloidal gold conjugates for nanoshells enhanced the assay sensitivity to 0.2 ng in the case of gold nanoshells of 180/15 nm, and to 0.4 ng in the case of gold nanoparticles of 100/15 and 140/15 nm type (*Fig. 5*). Such a noticeable increase in the sensitivity of the dot assay with nanoshells, in comparison with colloidal gold, was explained by the differing optical properties of the particles [100].

The use of GNP seems to have a high potential for analyzing large arrays of antigens in micromatrices (immuno-chips) [101], which permits the simultaneous determination of the analyzed compound in 384 samples at a concentration of 60–70 ng/l or (taking into account the microliter amounts of the sample and the immunogold marker) with a detection limit of less than 1 pg.

1.2.3. Immunochromatography. Approximately 10 years ago, several foreign companies launched immunochromatographic test systems for instrument-free diagnostics. Due to the high specificity and sensitivity of the immunoassay, these tests found wide application in determining narcotic agents, toxins, early diagnostics of pregnancy, and screening of extremely dangerous and urogenital infections. New methods for the diagnostics of tuberculosis, helicobacteriosis, staphylococcus infection, hepatitis B, prostatitis, determining pregnancy at the early stages, pesticides, aflatoxin, diethylstilbestrol and cephalixin in the environment, and DNA hybridization have been elaborated (see refs. in [5]).

Immunochromatographic assay [102] is based on eluent motion along the membrane (lateral diffusion), resulting in the formation of specific immune complexes that are detected as stained bands on different membrane regions. Enzymes, stained latexes, and quantum dots [102] are used as labels in these systems; however, in the overwhelming majority of cases, gold nanoparticles are used [103].

The sample under investigation migrates along the test strip due to capillary forces. If a sample contains the desired compound or immunologically close ones when the sample passes through the absorbing device, a reaction with specific antibodies labelled with colloidal gold occurs, accompanied by the formation of an antigen–antibody complex. The colloidal preparation is involved in the reaction of competitive binding with the antigen immobilized in the test zone (haptene conjugated with a protein carrier is usually used for immobilization in the detection of low-molecular-weight compounds). If the concentration of antigens in the sample is higher than the threshold level, the conjugate has no vacant valences for interacting in the test zone; the stained band corresponding to complex formation is not observed. If the sample does not contain the desired compound, or its concentration is lower than the threshold level, antigen immobilized in the test zone of the strip reacts with antibodies on the surface of colloidal gold, which results in the formation of a stained band.

As the liquid front moves further, gold particles with immobilized antibodies, which did not react with the antigen in the test zone of the strip, are bound to antispesific antibodies in the control zone of the test strip. The emergence of a stained band in the control zone attests to the validity of the testing procedure and the diagnostic activity of the components of the system. The negative testing result, the emergence of two stained bands (in the test zone and the control zone), points to the fact that the sample contains no antigen or its concentration is lower in comparison with the threshold level. The positive testing result, the emergence of a

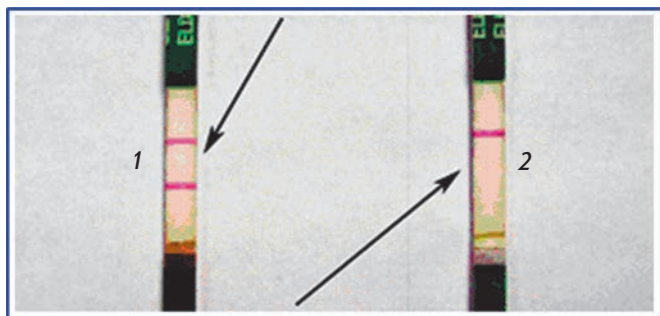


Fig. 6. Positive (1) and negative (2) results of an immunochromatographic assay.

single stained band in the control zone attests to the fact that antigen concentration is higher than the threshold concentration (*Fig. 6*).

The study of these test systems has demonstrated their high stability, the reproducibility of the results, and correlation with alternative methods. Densitometric characterization of the degree of heterogeneity of the samples stands at 5–8%, which enables one to visually assess the results of the analysis with an appreciably reliable accuracy. These tests are very simple and convenient to use.

1.2.4. Plasmon resonance biosensors. Over the past years, gold and silver nanoparticles and their composites have found broad application as efficient optical detectors of biospecific interactions [104]. In particular, the resonance optical properties of nanometer-sized metal particles have found successful application in the design of so-called biochips and biosensors. There are many types of sensors, *viz.* colorimetric, refractometric, electrochemical, piezoelectric, and certain others [102, 105, 106]. These devices are of great interest in biology (determination of nucleic acids, proteins, and metabolites); medicine (drug screening, analysis of antibodies and antigens, diagnostics of infectious diseases); and chemistry (environmental express monitoring, quantitative analysis of solutions and dispersed systems).

The study of the biospecific interactions in such systems, where GNP are represented by ordered structures (self-assembling thin films) [107] or within polymer matrices [108], has been developing for over a decade. In this case, the amplification of the optical signal from the conjugate due to the strengthening of the exciting local field in an aggregate that was formed from gold nanoclusters is used. New unique technologies are currently being used for the design of biosensor devices, including monolayer self-assembly of metal particles (see [109] and refs therein), nanolithography [110], vacuum evaporation [111], etc. It is of funda-

mental significance to note that particle size and shape [112], interparticle distance [113], and the optical properties of the local environment [114] have a considerable effect on the optical response obtained from nanoparticles or their aggregates (in particular, the ordered ones), which provides the possibility of controlling the sensor's "tuning." These properties of metal clusters served as the basis for the design of new promising plasmon resonance biosensor systems (SPR-biosensors) based on the conversion of biospecific interactions into an optical signal. The theory behind the designing process and variants of practical application of such systems were considered in reviews [115–119].

Sensor sensitivity, stability, and selectivity directly depend on the characteristics of the optical registration system. BIAcore™ is the most popular sensor system of this kind [120]. The measurement principle in planar, prismatic, or mirror biosensors is analogous to the principle used in the method of frustrated total internal reflection, which has been conventionally used to measure the thickness and the refractive index of ultrathin organic films on metal (reflecting) surfaces [105]. Plasmon resonance excitation in a planar gold layer occurs when polarized light falls onto the surface at a certain angle. The electromagnetic fields running along the boundary of the surface and localized in its proximity due to the exponential decrease in the amplitude perpendicular to the dielectric with a typical attenuation distance of up to 200 nm are excited on the metal/dielectric interface (the effect of total internal reflection, *Fig. 7*). The index of refraction at a certain angle and at a certain wavelength depends on the dielectric properties of the thin layer on the interface, which are determined in the final analysis by the concentration of target molecules in the layer.

Various types of biosensors using GNP have been developed for immunodiagnostics of tick-borne encephalitis [121], human papilloma [122] and immunodeficiency-associated [123] viruses, Alzheimer's disease [124], the determination of phosphororganic compounds

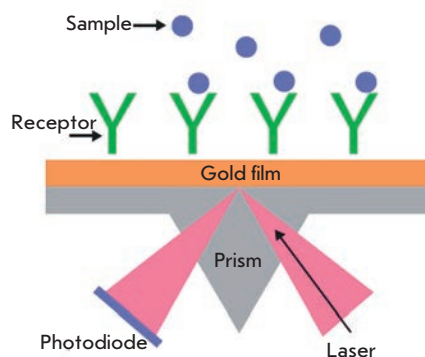


Fig. 7. Scheme for detection of target molecules with a BIAcore™ device based on a total internal reflection prism covered by a thin gold layer. Adapted from Ref. [106].

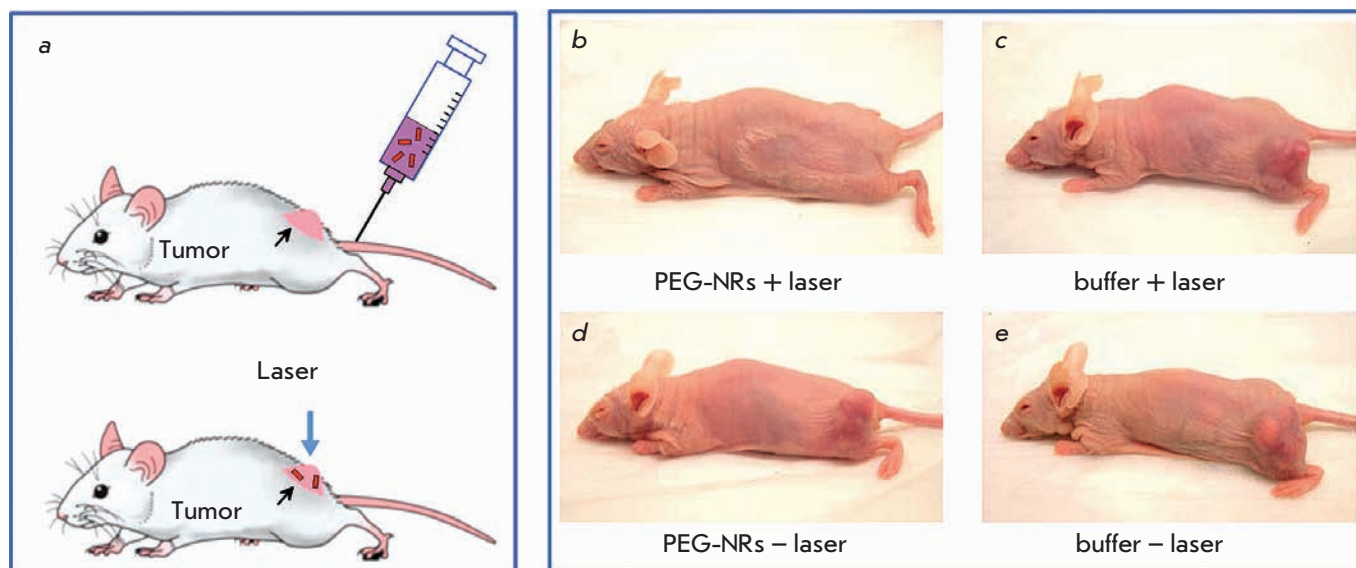


Fig. 8. Scheme (left) and photothermal therapy of tumor-burdened mice (2-3 weeks after injection of MDA-MB-435 human cancer cells into opposite flanks). Laser irradiation (a, b, 810 nm, 2 Wt/cm², 5 min) were performed 72 h after injection of PEG-coated gold nanorods (NR) (a, c, 20 mg Au/kg) or saline buffer (b, d). It can be seen that the irradiation without particles (control b), as well as the injection of nanorods or saline without irradiation (controls c and d), had no destructive effect, whereas the nanoparticle and laser treatment completely destroyed tumor. Adapted from Ref. [145] by permission of the Publisher.

and pesticides [125], antibiotics [126], allergens [127], cytokines [128], hydrocarbons [129], immunoglobulins [130], for detecting tumor [131] and bacterial [132] cells, and for determining the activity of cerebral cells [133].

GNP-based biosensors are applied not only in immunoanalysis [134], but also for the detection of nucleotide sequences [67, 119]. A record sensitivity was achieved for these sensors in pioneer studies [135, 136] in the zepto-molar range based on the recording spectra of resonant scattering from individual particles. This opened the door for the registration of intermolecular interactions at the level of individual molecules [137].

2. GOLD NANOPARTICLES IN THERAPY

2.1. Photothermal therapy using gold nanoparticles

Photothermal cell damage is a promising direction in both tumor therapy [138] and the therapy of infectious diseases, which has been intensively developing. The essence of this technique is as follows: gold nanoparticles reach their absorption maximum in the visible or near-infrared region and become hot when irradiated at the corresponding light wavelength. If they are located inside or around the target cells (which can be achieved by conjugation of gold particles with antibodies or other molecules), these cells die.

Thermal exposure has been used in tumor therapy since the 18th century. To do that, both local heating (using microwave, ultrasound, and radio radiation) and

hyperthermia of the entire organism [139] (heating to 41–47°C for 1 h) [139] were applied. Upon local heating to 70°C, the duration of the procedure can be reduced to 3–4 min. Local and general hyperthermia result in irreversible cell damage caused by the disruption of the cell's membrane permeability and protein denaturation. Healthy tissues are also clearly damaged in this process. All this imposes considerable restrictions on the application of this method.

The revolution in cancer thermotherapy was triggered by the use of laser radiation, which made controlled and directed damaging of tumor tissues possible [140]. The combination of laser radiation with fiber-optic waveguides gave excellent results and was named interstitial laser hyperthermia [141]. The disadvantages of laser therapy include the low selectivity associated with the necessity of using powerful lasers for the efficient stimulation of tumor cell death.

In 2003, GNP were applied for the first time as agents for photothermal therapy [142, 143]; it was latter proposed to refer to this kind of therapy as plasmonic photothermal therapy (PPTT) [139]. A new method for selective damaging of target cells, which is based on the use of 20–30 nm gold nanospheres radiated by 20 ns laser pulses (532 nm) in order to create local warming-up, was described in [144]. The sandwich technology consisting in labeling T-lymphocytes with GNP conjugates was used for the pulse phototherapy in the model

experiment. The use of GNP for the photothermal therapy of chemotherapy-resistant types of cancers seems to be the most promising direction. As opposed to photosensitizers (see below), GNP appear unique because the cells retain their optical properties under certain conditions for a significant amount of time. Successive irradiations with several laser pulses allows to control cell inactivation using a method that is not traumatic, while the use of the nanoparticles, properties to simultaneously scatter and absorb radiation makes PPTT possible using optical tomography [33].

Figure 8 represents an example of the successful therapy of induced tumors in mice [145]. Further development of PPTT and its introduction in clinical practice will depend on how successful scientists will be in solving a host of problems, the most significant ones being 1) selecting nanoparticles with the optimal optic properties; 2) increasing the contrast of nanoparticle accumulation in a tumor and decreasing overall potential toxicity; and 3) elaborating methods for delivering optical radiation to the targets and searching for alternative irradiation sources, which would combine high permeation ability with the possibility of GNP heating.

The first requirement is determined by the coincidence of the spectral position of the maximum of the plasmon absorption resonance and the biotissue transparency window in the near-infrared region (700–900 nm). The summarizing theoretical analysis of the photothermal efficiency of GNP depending on their size, shape, structure, and degree of aggregation has been published [113]. It was shown that although gold nanospheres are inefficient in the near-infrared range, their aggregates can be very efficient at appreciably small interatomic distances (below 10% of their diameter). Such clusters form both on a cell's surface and inside cells [146]. Data on the amplification of PPTT due to clusterization were obtained [147, 148]. In particular, it was ascertained [147] that small aggregates consisting of 30 nm particles enable the destruction of cancer cells at an intensity lower than that in the particle-free control by a factor of 20.

The parameters of gold nanoshells and nanorods that are optimal for PPTT were determined [113, 149]. Today, a number of studies have been published in which the application of gold nanorods [32, 150], nanoshells [142, 151], and a relatively new class of particles – gold-silver nanocages [152, 153] – for PPTT is described. The results of a comparison of the efficiency of heating nanorods, nanoshells, and nanocages are provided in [25, 154].

Three fundamental things should be kept in mind in connection with the optimization of the parameters of a particle. First, intrinsic absorption is not the only pa-

rameter determining the efficiency of PPTT [155]. The rapid heating of nanoparticles or clusters results in the formation of vapor bubbles [156], which can cause cavitation cell damage upon irradiation with visible [148] or near-infrared light [157]. The efficiency in the formation of vapor bubbles considerably improves upon the formation of nanoparticle clusters [143, 146]. It is possible that it is this effect, instead of the enhanced absorption, that determines the larger extent of cell damage, other conditions being equal [155]. Finally, irradiation of nanoparticles by high-intensity resonance nanosecond IR pulses may result in the destruction of particles as early as after the first pulse (e.g., see [158, 159] and refs. therein). In a series of studies, Lapotko *et al.* (see [160] and refs. therein) focussed their attention on the fact that the heating of GNP and their destruction may result in an abrupt decrease in the photothermal efficacy of “cold” particles tuned to the laser wavelength. The use of femtosecond pulses does not solve this problem because of the low energy supplied; therefore, it is necessary to accurately control the retention of nanoparticles' properties for the selected irradiation mode.

We shall now turn our attention to the second issue connected with the problem of targeted delivery of nanoparticles into the tumor. This issue has two significant aspects: increasing the contrast in the desired biotarget and decreasing the side effects conditioned by the accumulation of GNP in other organs, primarily in the liver and spleen (see below). Two delivery strategies are typically used. The first strategy is based on GNP conjugation with PEG, and the second one is based on GNP conjugation with antibodies to certain marker proteins of tumor cells. PEG is used to enhance the bioavailability and stability of nanoparticles, resulting in the increase in time of their circulation in blood flow. Citrate-coated gold nanospheres and CTAB-coated nanorods and nanoshells are characterized by low stability in buffer saline solutions. Upon conjugation of nanoparticles with PEG, their stability increases considerably, preventing salt-induced aggregation.

PEGylated nanoparticles are preferentially accumulated *in vivo* due to the enhanced permeability of tumor vessels [161] and are retained in it due to the reduced lymphatic drainage. Moreover, PEGylated nanoparticles possess lower availability for the immune system (stealth technologies). This delivery method is called passive delivery, as opposed to the active method, in which antibodies are used [162] (*Fig. 9*). The active delivery method is more reliable and efficient. Antibodies to tumor markers are used in it. Most frequently, the epidermal growth factor receptor (EGFR) and its varieties (e.g., Her2) [152, 163], and the tumor necrosis factor, (TNF) [164] serve as such markers. The use of GNP conjugated with antibodies simultaneously for diagnostics

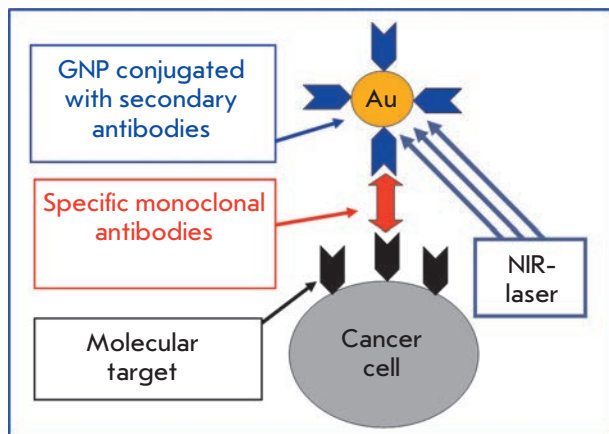


Fig. 9. Scheme of the plasmon photothermal therapy with an active delivery of GNPs to cancer cells. Reproduced from Ref. [8] by permission of Elsevier.

and photothermal therapy (the so-called theranostics methods) seems to be the most promising [165]. In addition to antibodies, folic acid, ligand of numerous folate receptors of tumor cells [150], and hormones [166] can be used for active delivery.

The question of the efficacy of targeted delivery of nanoparticles into the tumor has recently resurfaced as the subject of investigation and discussion [167]. In experiments with liposomes labeled with anti-Her2-antibodies [168] and GNP labeled with transferrine [169], it was shown that functionalization improves the penetration of nanoparticles into cells; however, the contrast of particle accumulation in the tumor does not improved considerably. The biodistribution and localization of gold nanorods labeled with three types of probe molecules, including the (1) scFv-fragment of EGFR antibodies; the (2) N-terminal fragment of the peptide recognizing the urokinase plasminogen activator receptor (uPAR); and the (3) cyclic RGD-peptide recognizing the $\alpha_v\beta_3$ -integrin receptor have been studied [167]. It appears that all three types of ligands fail to significantly improve the contrast of particle accumulation in cell models and in the tumor upon intravenous administration, but they do have a considerable effect on extracellular distribution and intracellular localization. Therefore, a conclusion can be made that in the case of PPTT, the direct introduction of particles into the tumor can be more efficient than intravenous administration.

The last important question associated with modern PPTT has to do with the efficient delivery of radiation to the biotarget. Since the absorption of tissue chromophores in the visible region is lower by two

orders of magnitude than it is in the infrared region [138], the use of IR radiation dramatically reduces the nontarget thermal dose and increases the deep tissue penetration of the radiation. Nevertheless, the penetration depth typically does not exceed 5–10 mm [142, 170]; therefore, it is necessary to search for alternative solutions. The first approach consists in using impulse (nanoseconds) modes of radiation instead of continuous ones, which allow to increase the intensity of the irradiation without additional side effects. The second approach consists in using fibre-optic devices for endoscopic delivery of the radiation or delivery inside the tissue. The advantages and drawbacks of this approach are evident. Finally, radiation with deeper penetration, such as radio radiation [171], can be used for hyperthermia.

GNP conjugated with antibiotics and antibodies have also been used as photothermal agents to inflict selective damage to protozoa and bacteria [172, 173]. The data on some questions related to the use of PPTT can be found in books and reviews [139, 170, 174, 175]. The thorough review [138] warrants special attention.

2.2. Photodynamic therapy using gold particles

The photodynamic method [176] is applied in the therapy of oncological diseases, certain dermal or infectious diseases, and is based on the use of light-sensitive agents – photosensitizers (including dyes) and, typically, visible light of a certain wavelength. Most frequently, the sensitizers is introduced into the organism intravenously; it may also be administered applicatively or perorally. The agents for photodynamic therapy (PDT) can selectively accumulate in the tumor or other target tissues (cells). The affected tissues are radiated with laser light with a wavelength corresponding to the absorption maximum of the dye. In addition to the usual heat release due to absorption [6], the second mechanism is also significant. It is associated with the photochemical generation of singlet oxygen and the formation of highly active radicals inducing necrosis and apoptosis of tumor cells. PDT results in tumor malnutrition and death due to the damage inflicted on its microvessels. The major drawback of PDT is that the photosensitizers remain in the organism for a long period of time; as a result, the patient's tissues remain highly sensitive to light. On the other hand, the use of dyes for the selective heating of tissues [6] is characterized by low efficacy due to the small absorption cross-section of chromophores.

It is well-known [177] that metal nanoparticles are efficient fluorescence quenching agents. However, it has been recently demonstrated [178] that the fluorescence intensity can be amplified by a plasmon particle, by locating molecules at optimum distance from the

metal. Theoretically, this idea can be used to enhance the efficacy of PDT.

In a number of studies, the proposed method allowed to deliver drugs in polyelectrolyte capsules on GNP that disintegrate under laser radiation and deliver the therapeutic agent to the targets [179, 180] or to use nanoparticles surrounded by a layer of polymer nanogel [181, 182]. Moreover, photoactive agents [183] and peptides facilitating the intracellular penetration [184] are used within conjugates. It has recently been proposed [185] to use composite nanoparticles that, in addition to gold nanoshells, comprise magnetic particles, photodynamic dye, PEG, and antibodies. Finally, according to the data [186], nanoparticles conjugated with photodynamic dyes can have a synergetic antimicrobial effect.

Thus, gold nanostructures with plasmon resonance show promise for the selective PPTT of oncological and other diseases. However, it is clear that a number of questions require further study, such as: stability, biocompatibility, chemical interaction between nanoparticle conjugates in physiological environments, blood circulation time, penetration into the tumor, interaction with the immune system, excretion of nanoparticles, etc. We expect that the success in the initial stages in the use of nanoparticles for selective PPTT will be broadened to the clinical stage [138], provided that the optimal technical parameters are studied further.

2.3. The use of gold nanoparticles as therapeutic agents

Gold nanoparticles are increasingly actively being used not only in diagnostics and cell photothermolysis experiments, but also for therapeutic purposes. In 1997, the successful application of colloidal gold in a patient with rheumatoid arthritis was first reported [187]. In 2008, a vast array of data on the ten-year-long clinical trials of the preparation Aurasol® for peroral administration upon severe forms of rheumatoid arthritis was published [188]. The positive results achieved upon intra-articular introduction of colloidal gold into rats with collagen-induced arthritis were described [189]. The authors attribute the positive effect to an increase in anti-angiogenic activity due to the binding between GNP and the vascular endothelial growth factor and, therefore, the decrease in macrophage infiltration and inflammation. Similar results were obtained upon subcutaneous introduction of gold nanoparticles into rats with collagen- and pristan-induced arthritis [190].

Researchers from Maryland University used a colloidal gold vector to deliver the TNF to solid tumors in mice [191, 192]. Upon intravenous injection, GNP conjugated with TNF rapidly accumulates in tumor cells and is not detected in cells of the liver, spleen, and other healthy organs. Accumulation of GNP in the tu-

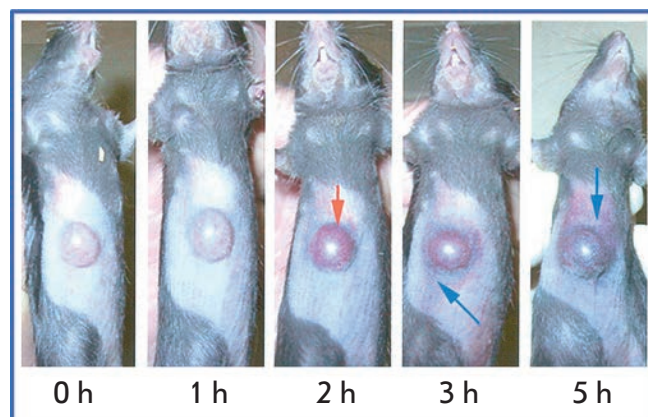


Fig. 10. Accumulation of the GNP-TNF conjugates in mice tumors over 5 h after injection. A MC-38 tumor-burdened C57/BL6 mouse was intravenously injected with 15 μg of the GNP-TNF conjugates. The ventral surface of the animal was photographed at the indicated times, showing the color changes of the tumor over 5 hr. Red arrows show tumor uptake in the conjugates; blue arrows show accumulation of the conjugates in the tissues surrounding the tumor. Adapted from Ref. [191] by permission of The American Association for Cancer Research.

mor is attested by the change in the color of the tumor; the tumor acquires a bright red/purple color (the color typical of colloidal gold and its aggregates), which coincides with the maximum of tumor-specific activity of the TNF (Fig. 10). The colloidal gold-TNF vector had lower toxicity and a higher efficacy in reducing tumor size in comparison with the native TNF, since maximum antitumor reaction was attained by using lower doses of the drug. The preparation for intravenous administration based on a GNP-TNF conjugate named AurImmune™ has already passed the second stage of clinical trials.

The antiangiogenic properties of GNP [193] were observed *in vitro* and *in vivo*. It turned out that GNP interact with heparin-binding glycoproteins – vascular permeability factors, growth factors of cardiac endothelium and fibroblasts. These agents mediate angiogenesis, including that in tumor tissues; therefore, GNPs inhibit their activity. Since intensive angiogenesis (the process of formation of new blood vessels in organs or tissues) is considered as one of the main tumor growth factors, the existence of antiangiogenic properties in GNPs could make them promising for tumor therapy. It was also demonstrated by the same researchers that gold nanoparticles enhance the apoptosis of the chronic lymphocytic leukemia cells that are stable to programmed death [194] and suppress the proliferation of multiple myeloma cells [195].

3. GOLD NANOPARTICLES AS DRUG CARRIERS

The targeted delivery of drugs is one of the most promising and actively developing directions in the medicinal use of GNPs [196, 197]. Antitumor agents and antibiotics are the most popular objects of target delivery.

The options of using GNP conjugated with the following antitumor agents were proposed: paclitaxel [192], methotrexate [198], daunorubicine [199], hem-cytabin [200], 6-mercaptapurine [201], dodecylcysteine [202], sulfonamide [203], 5-fluorouracil [204], platinum complexes [205], kahalalide [206], tamoxifen [207], herceptin [208], doxorubicin [209], prospidin [210], etc. The conjugation was carried out either by simple physical adsorption of the drugs onto GNPs or via the use of alkanethiol linkers. The effect of conjugates was assessed both (chiefly) on *in vitro* models, using tumor cell cultures, and *in vivo*, in mice with induced tumors of different natures and localizations (Lewis lung carcinoma, pancreatic adenocarcinoma, etc.). In addition to the active substance, target molecules (e.g., cetuximab) providing better anchoring and penetration of the complex into the target cells were used to design the delivery system. It was also proposed to use multimodal delivery systems, when a gold nanoparticle is loaded with several therapeutic agents (both hydrophilic and hydrophobic) and auxiliary agents, such as target molecules, dyes for photodynamic therapy, etc. [211]. Most researchers note high the efficacy of antitumor agents conjugated with gold nanoparticles.

Antibiotics and other antibacterial agents are also considered as objects that can be delivered by gold nanoparticles. The possibility of producing a stable complex of vancomycin and colloidal gold and the efficacy of such a complex against various enteropathogenic strains of *Escherichia coli*, *Enterococcus faecium*, *Enterococcus faecalis* (including vancomycin-resistant strains) have also been demonstrated [212]. Similar results were obtained in [213]: a complex of ciprofloxacin with gold nanoshells showed high antibacterial activity towards *E. coli*. The anti-leukemia drug 5-fluorouracil, conjugated with colloidal gold, has a noticeable antibacterial and antifungal effect against *Micrococcus luteus*, *Staphylococcus aureus*, *Pseudomonas aeruginosa*, *E. coli*, *Aspergillus fumigates*, and *A. niger* [214]. It should be noted that in all of the listed cases, the complexes of drugs with gold nanoparticles were stable, which could be attested by the optical spectra of conjugates.

On the contrary, stable complexes with gold nanoparticles could not be obtained for such antibiotics as ampicillin, streptomycin, kanamycin, hentamycin, neomycin, ciprofloxacin, gatifloxacin, and norfloxacin, which are active against *E. coli*, *M. luteus*, *S. aureus*, and *P. aeruginosa* [215–217]. Nevertheless, their ac-

tivity when mixed with colloidal gold was higher by 12–40% than that of the antibiotic when used alone, depending on the antibiotic. On the basis of these data, the authors arrived at the conclusion that the antibacterial activity of antibiotics was enhanced by GNPs. However, the issue of the mechanisms underlying the possible boosting of the antibacterial effect of drugs has remained unsolved. It has been proved experimentally [218] that unbound gentamicin and a mixture of it with gold nanoparticles do not considerably differ in terms of their antimicrobial activity in tests on both dense and liquid nutrient media. It is speculated that stable conjugates of nanoparticles coated with antibiotic molecules are required to enhance the antibacterial activity. Thus, it was proposed to use the antibiotic cefaclor directly in the synthesis of GNPs. As a result, a stable conjugate was obtained. It was characterized by high antibacterial activity against *E. coli* and *S. aureus*.

There has been much less data on other drugs conjugated with gold nanoparticles. However, the high anti-oxidant activity of the tocoferol complex with gold nanoparticles should be noted, along with [220] the variants of its potential use that were proposed. Data has been published [22] indicating that, due to high local concentration, GNPs conjugated with the drug TAK-799 manifested a more pronounced activity against the human immunodeficiency virus, as compared with the drug itself. The procedure of per oral and intranasal introduction of insulin conjugated with colloidal gold was elaborated on rat models of diabetes mellitus. A decrease in blood sugar levels comparable with the effect of a subcutaneous introduction of insulin was reliably demonstrated [222]. Finally, the therapeutic effect of the antirheumatic drug etanercept conjugated with gold nanorods has been described [223].

In the end of this section, we would like to mention gene therapy, which seems to be the ideal strategy concerning genetics, as well as acquired, diseases [224]. Gene therapy implies an approach based on the introduction of genetic structures into cells and the organism for therapeutic purposes [225]. The desired effect was achieved either due to the expression of the inserted gene or by partial or complete suppression of the function of the damaged or overexpressed gene. Attempts to adjust the structure and function of the ill-functioning (affected) gene were recently made. In this case, gold nanoparticles can act as an efficient agent for delivering the genetic material into the cytoplasm and cell nucleus [226].

4. IMMUNOLOGIC PROPERTIES OF GOLD NANOPARTICLES

Since the 1920s, researchers have shown keen interest in the immunological properties of colloidal metals

(gold, in particular). This has been associated mainly with the physicochemical (non-specific) immunity theory proposed by J. Bordet, which postulates that immunogenicity and antigenic specificity depend predominately on the physicochemical properties of the compounds and, first and foremost, on their colloidal state. L.A. Zilber was successful in his attempts to obtain agglutinating sera from colloidal gold [227]. Moreover, it was shown in a number of studies that the introduction of a rigorous antigen, together with colloidal metals, stimulates the production of antibodies. Furthermore, it was found that certain haptens adsorbed on colloidal particles can cause the formation of antibodies. In one of the best early reviews [228], a trove of data on the effect of colloidal gold on nonspecific immune reactions was provided [228]. In particular, it was noted that, 2 h after 5 ml of colloidal gold is introduced intravenously into rabbits, the leukocyte content in 1 ml of blood considerably increases (from 9900 to 19800) against a negligible decrease in mononuclear forms (from 5200 to 4900) and a considerable increase in polynuclear forms (from 4700 to 14900). It should be noted that such effects have not been observed upon the introduction of other colloidal metals. Unfortunately, with the development of immunology and the negation of many postulates in Bordet's theory, interest towards the immunological properties of colloids has abated. However, the data on the amplification of the immune response to antigens adsorbed on colloidal particles has been used in the design of various adjuvants.

It is known that antibody synthesis is induced by agents that have an appreciably developed structure (immunogenicity). They include proteins, polysaccharides, and certain synthetic polymers. On the contrary, a considerable share of biologically active compounds (vitamins, hormones, antibiotics, narcotics, etc.) have a relatively low molecular weight and, therefore, cause a low immune response. In order to overcome this limitation in the standard methods used to produce antibodies *in vivo*, such agents (haptens) are chemically bound to high-molecular-weight carriers (most frequently, to proteins), making it possible to produce specific antisera. However, such antisera usually contain accompanying antibodies to the antigenic structures of the carrier [229].

In 1986, in a pioneering study by Japanese researchers [230], information on a successful attempt at producing antibodies to glutamic acid using colloidal gold particles as a carrier was published. A number of studies were subsequently published, in which this method was applied and developed in order to produce antibodies to the following haptens and rigorous antigens: amino acids, the platelet-activating factor, quinolinic acid, biotin, recombinant peptides, lysophosphatide acid, en-

dostatin, peptides of viral capsid of B and C hepatitis, influenza, murrain, α -amidated peptides, actin, antibiotics, azobenzene, A β -peptide, clenbuterol, surface *Yersinia* antigens, transmissible gastroenteritis virus, and tuberculin (see review [231] and refs. therein). In all of the works listed, hapten was directly conjugated with colloidal gold particles and mixed with Freund's complete adjuvant to immunize animals. As a result, sera with a high titre were obtained. The sera required no further purification to remove ballast antibodies.

In 1993, it was suggested that hapten (gamma-aminobutyric acid) be bound to the carrier protein before its conjugation with colloidal gold [232]. The proposition was supported in the studies devoted to the production of antibodies to a number of peptides, amino acids, phenyl- β -D-thioglucuronide, and diminazene (see [231 and refs. therein]). The antibodies obtained through this procedure were characterized by both a high specificity to antigens and a higher titre ("extremely high, according to [232]") –from 1 : 250000 to 1 : 1000000, in comparison with those produced using a routine method. The ImmunoSolution company currently offers antibodies to a number of neurotransmitters and amino acids. These antibodies are produced according to the procedure in [232].

In 1996, the possibility of using colloidal gold particles in the antiviral vaccine as the carriers of protein antigen of the capsid of the tick-borne encephalitis virus was first demonstrated [233]. Despite the fact that the vaccine contained no adjuvants, the experimental vaccine had better protective properties as compared with its commercial analogues.

A significant number of studies devoted to the use of GNP in designing DNA vaccines with gene constructions encoding proteins, to which antibodies had to be produced, have been published. In the case of efficient gene expression, these proteins serve as antigens for the development of the immune response. Colloidal gold particles are the most popular examples of nanoparticles–DNA carriers [234].

The technology used to produce antibodies against various antigens using colloidal gold as a carrier and adjuvant was described in [233, 235]. In this case, antigens are adsorbed directly at the surface of gold nanoparticles without using any binding agents. It was ascertained that the immunization of animals with an antigen conjugated with colloidal gold (both using Freund's complete adjuvant and without it) results in the obtainment of specific antibodies with a high titre to a wide range of antigens without ballast antibodies. Gold nanoparticles can stimulate antibody synthesis in rabbits, rats, and mice if a lower dose of the antigen is used in comparison with the amount that is required when using a number of conventional adjuvants (Table 2).

Table 2. Indices of antibody titres during immunization of rabbits with yersiniose antigen (according to [235])

Preparation	First immunization	Second immunization	Reimmunization
Colloidal gold + antigen (1 mg)	1:32	1:256	1:10240
Freund's complete adjuvant + antigen (100 mg)	1:32	1:256	1:10240
Physiological solution + antigen (100 mg)	1:32	1:256	1:512

Gold nanoparticles used as antigen carriers were shown to stimulate the phagocytic activity of macrophages and affect the functioning of lymphocytes, which probably is responsible for their immune-modulating effect. Moreover, gold nanoparticles and their conjugates with low- and high-molecular-weight antigens stimulate the respiratory activity of the cells of the reticulo-endothelial system and the activity of the mitochondrial enzymes of macrophages [236], which may be one of the causal factors behind the adjuvant properties of colloidal gold. The fact that gold nanoparticles act both as a carrier and an adjuvant (i.e., represent haptens to T-cells) should be considered as the most interesting side of the manifestation of the immune properties of colloidal gold. In particular, gold nanoparticles conjugated with antigens affect T-cell activation: a tenfold increase in the proliferation, as opposed to that upon the addition of a native antigen, was detected. This provides evidence in support of the fact that it is fundamentally possible to act directly on T-cells with the subsequent activation of macrophages and destruction of a pathogen.

However, none of the studies contains data on the mechanisms that underline these properties of gold particles. We consider the discussion in [232] on the preferable macrophage response to corpuscular antigens, as opposed to the soluble ones, to be undoubtedly reasonable. The researchers who study the mechanisms of action of DNA vaccines and use gold nanoparticles to deliver genetic material into the cell also confirm this fact [234]. The role of Kupfer cells and Langerhans cells in the formation of the immune response was revealed in these studies. The effect of dendrite cells on the formation of the immune response upon the introduction of an antigen conjugated with gold nanoparticles was discussed in [237]. Moreover, it was noted that when using nanoparticles in medical practice, one should make sure that there are no lipopolysaccharides on their surface. The recent studies [238, 239] were devoted to the interaction between the cells of the immune system and gold nanoparticles.

The penetration of peptide-conjugated GNP into macrophage cytoplasm resulting in their activation was shown by electron microscopy [240]. It was ascertained that after the conjugates interact with the TLR-4 receptors of macrophages, the nanoparticles penetrate into the cell, which is accompanied by the secretion of inflammatory cytokines – TNF, interleukin-1 β and interleukin-6—and the inhibition of macrophage proliferation. Upon the introduction of GNP, the amount of macrophages decreases, while their size increases [241]. The level of interleukin-1 and interleukin-6 and TNF also increases. Another (noninflammatory) mechanism of penetration of gold nanoparticles into macrophages – by interaction with scavenger receptors—is not improbable [242]. The effect on nonconjugated colloidal gold on immune-competent cells *in vivo* was studied [243]. It was shown that the introduction of GNP into mice results in an increase in the proliferation of lymphocytes and normal killers and an increase in interleukin-2 production.

We believe that the detection of adjuvant properties in GNP creates favorable conditions for the development of a new generation of vaccines.

5. BIODISTRIBUTION AND TOXICITY OF GOLD NANOPARTICLES

All the facts mentioned above are proof that GNP have recently been actively used in different spheres of nanomedicine for diagnostic and therapeutic purposes. Moreover, they are being introduced parenterally into the organism of animals and humans with increasing frequency. The acute questions concerning their biodistribution, blood stream circulation, pharmacokinetics and removal from the organism, as well as possible toxicity at the level of the entire organism or at the level of cyto- and genotoxicity, emerged almost at the same time when GNP started to be used in medicine. It should be noted that data on the biodistribution and toxicity of GNP at the time of writing remained scarce and inconsistent.

It was demonstrated by the analysis of published data that the burst in activity regarding investigations

into the biodistribution and toxicity of GNP took place during the past 3–4 years [7, 244–248]. Since numerous research groups started their projects independently, there is a vast dispersion in the experimental design, including the size and shape of particles, functionalization methods, types of animals, doses and methods of particle introduction, etc. As a result, there has been serious discrepancies in the data and conclusions on the level and kinetics of biodistribution for toxicity estimations, as well. Yet, certain tentative conclusions can still be made.

Firstly, the organs of the reticuloendothelial system serve as the main target for the accumulation of 10–100 nm GNP; biodistribution homogeneity decreasing with decreasing size. The rapid reduction in particle concentration in blood and their prolonged retention in the organism is associated with the functioning of the hepatobiliary system. Since it takes 3 to 4 months for the accumulated particles to be excreted from the liver and spleen, the question of the doses and possible inflammatory processes is of paramount importance.

Secondly, the available data allows for the reasonable assumption that the effect of nanoparticle penetration via the hematoencephalic barrier depends critically on their size; 5–20 nm being the upper limit. Thirdly, gold nanoparticles 1–2 nm in diameter could be more toxic due to the possibility of irreversible binding to the biopolymers in cells. Also, numerous experiments on cell cultures have revealed no observable toxicity in colloidal particles with a size of 3–100 nm, provided that the threshold dose does not exceed a value of the order of 10^{12} particles/ml.

Data on *in vivo* experiments is scarce and somewhat inconsistent. It can only be assumed that there is no observable toxicity upon the short-term (approximately one week long) introduction of GNP at a daily dose lower than 0.5 mg/kg.

Recent data underscore the interest generated by and intensity of studies in the sphere of nanotoxicology, whose number has exploded. *Figure 11* shows the general scheme of a study of the biodistribution and toxicity of nanoparticles, which can be used for planning experiments [248]. For a better insight into the problems of the biodistribution and toxicity of GNP, we recommend reviews [244–248].

CONCLUSIONS

Thanks to the rapid development in technologies for the chemical synthesis of GNP over the past decade, a great variety of particles with different sizes, shapes, structures, and optical properties are now available to contemporary researchers. Moreover, the question of the simulation of nanoparticles that would possess the desired physical (optical, thermal, etc.) properties, with

subsequent development of the procedures for synthesizing the simulated structures, is now on the agenda.

In terms of applications in medicine, the development of efficient technologies for the functionalization of GNP with different classes of molecules providing stabilization *in vivo* and directed interaction with biological targets is of significance. Today, thiolated derivatives of PEG and other molecules are considered to be the best stabilizing agents. In particular, PEG-coated particles can remain in the blood flow for a longer time and are less susceptible to attacks from the cell components of the immune system.

It is now widely accepted that GNP conjugates are excellent labels for solving the problems of bioimaging, which can be implemented using various optical technologies, including resonance scattering dark-field microscopy, confocal laser microscopy, different variants of two-photon luminescence of GNP, optical coherence tomography, acoustic tomography, etc.

GNP conjugates have found application in analytic studies that can be based both on modern instrumental methods (surface-enhanced Raman spectroscopy, LISNA, IR Fourier spectroscopy, etc.) and on the use of simple solid-phase or homophase procedures (dot analysis, immunochromatography). Two examples can be given as illustrations: (1) the prostate-specific antigen can be determined using GNP conjugated with antibodies with a sensitivity that is higher than that in the conventional immunoenzyme assay by a factor of 1,000,000 [249]; (2) the strict dependence of color on interparticle distances allows visual detection of mutant DNAs in the so-called “Northwestern spot test” [68]. Along with the examples of clinical diagnostics of cancer, Alzheimer’s disease, HIV, hepatitis, tuberculosis, diabetes mellitus, and other diseases, new diagnostic applications for GNP should be expected.

Plasmon photothermal laser therapy of cancer using GNP was first described in 2003 and recently moved into the stage of clinical approval. The actual clinical success of this technology will depend on how quickly several urgent problems can be solved: (1) developing efficient methods for the delivery of radiation to tumors inside the organism using fibre-optic technologies or nonoptical heating methods; (2) elaborating methods for delivering conjugates to tumors, enhancing the contrast and uniformity of accumulation; and (3) developing methods for controlling the *in situ* photothermolysis process.

Targeted delivery of DNA, antigens, and drugs using GNP is one of the most promising directions in biomedicine. In particular, the studies performed by Jiang *et al.* of the University of Toronto [250] have revealed the size-dependent possibility of herceptin conjugated GNP into tumor cells with a much higher efficacy in

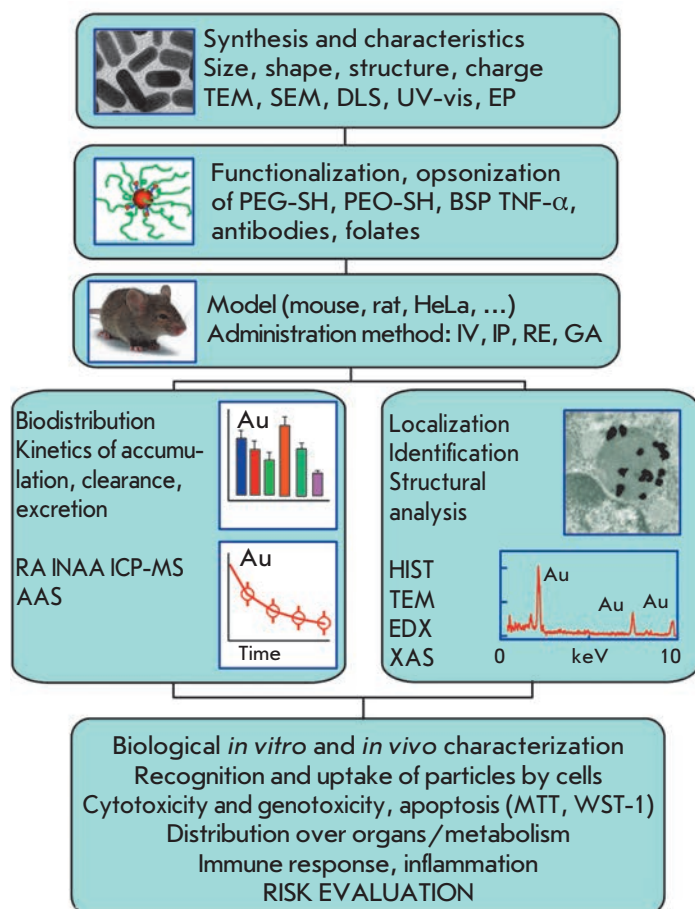


Fig. 11. Scheme of biodistribution and nanotoxicology experiments. The first step is the fabrication of desired particles and the characterization of their size, shape, structure, charge by transmission or scanning electron microscopy (TEM, SEM), dynamic light scattering (DLS), UV-vis spectroscopy at the ensemble (suspension) and single-particle levels, electrophoresis, and other methods. The second step includes the functionalization of the particle surface with appropriate ligands, including thiolated PEG or poly(ethylene oxide) (PEO) molecules, tumor necrosis factor (TNF- α), antibodies, and folates, as well as opsonization with blood serum proteins (BSP, like albumin etc.). Conjugates are administered to models in accordance with the experimental design, i.e., by using selected doses and routes of exposure, including intravenous (IV), intraperitoneal (IP), respiratory (RE), or gastrointestinal (GA). The biodistribution into organs and the kinetics of accumulation/clearance are determined according to a selected time-dependent scheme of tissue sampling. Samples are analyzed by radioactive analysis (RA), instrumental neutron activation analysis (INAA), inductively coupled plasma-mass spectrometry (ICP-MS), and atomic absorption spectroscopy (AAS). Particles and related structures also can be identified at the tissue (histological, HIST) and cellular levels by electron microscopy (SEM, TEM), energy dispersive X-ray spectroscopy (EDX), and X-ray absorption spectroscopy (XAS). The final step is the integration of data for the biological characterization of GNP effects and the evaluation of possible risks through the use of cellular-level information (cellular recognition and penetration, cytotoxicity, genotoxicity, and apoptosis/necrosis; MTT and WST-1 assays) and at the whole organism level (organ distribution, accumulation and clearance/excretion, degradation and metabolism, immunogenicity, and inflammation). Reproduced from Ref. [248] (<http://dx.doi.org/10.1039/c0cs00018c>) by permission from The Royal Society of Chemistry.

comparison with that of the pure preparation. The recent critical revision of the PPTT concept based on the intravenous-targeted delivery of GNP conjugated with molecular probes to tumor receptors [167] points to the necessity to continue studies in this direction. In view of the data in [167], it seems quite reasonable to use the “non-targeted” PEG-coated gold nanoshells of the SiO₂/Au type with a nucleus diameter of 120 nm and thickness of the gold layer of 15–20 nm as a universal marker for PPTT and bioimaging [25, 41]. It should be emphasized that N. Halas, J. West, *et al.* of Rice University (United States) started clinical trials of these particles for PPTT in 2010.

Finally, there is a necessity to continue and broaden studies of the biodistribution and the toxicity of GNP. First of all, a coordinated program is required, which would reveal the correlations between particle parameters (size, shape, functionalization with various molec-

ular probes), experimental parameters (model, doses, method, and administration scheme, observation duration; organs, cells, subcellular structures under study, etc.), and the observed biological effects. Coordinated efforts in the introduction of standards for the particles and methods used for the testing of nanomaterial toxicity are also required. ●

This work was partially supported by grants from the RAS Presidium’s Program “Fundamental Sciences for Medicine” (direction “Biophotonics”), the Russian Foundation for Basic Research, the Ministry of Education and Science of the Russian Federation (Contracts № 2.1.1/2950, 14.740.11.260, and 02.740.11.0484), and a grant from the Government of the Russian Federation for state support of research carried out by leading scientists in Russian educational institutions of higher professional education.

REFERENCES

1. Antonii F. *Panacea Aurea-Auro Potabile*. Hamburg: Ex Bibliopolio Frobeniano, 1618. 250 p.
2. Faulk W.P., Taylor G.M. // *Immunochemistry*. 1971. V. 8. P. 1081–1083.
3. Dykman L.A., Bogatyrev V.A., Shehegolev S.Yu., Khlebtsov N.G. *Zolotyie nanochastitsy: sintez, svoystva, biomeditsinskoe primenenie (Gold Nanoparticles: Synthesis, Properties, and Biomedical Applications)*. Moscow: Nauka, 2008. 319 p.
4. *Gold Nanoparticles: Properties, Characterization and Fabrication* / Ed. P.E. Chow. N. Y.: Nova Science Publisher, 2010. 343 p.
5. Dykman L.A., Bogatyrev V.A. // *Russ. Chem. Rev.* 2007. V. 76. P. 181–194.
6. Wilson R. // *Chem. Soc. Rev.* 2008. V. 37. P. 2028–2045.
7. Boisselier E., Astruc D. // *Chem. Soc. Rev.* 2009. V. 38. P. 1759–1782.
8. Khlebtsov N.G., Dykman L.A. // *J. Quant. Spectrosc. Radiat. Transfer*. 2010. V. 111. P. 1–35.
9. Khlebtsov N.G. // *Quantum Electron.* 2008. V. 38. P. 504–529.
10. *Colloidal Gold: Principles, Methods, and Applications* / Ed. M.A. Hayat. San Diego: Acad. Press, 1989. V. 1. 538 p.; V. 2. 484 p.; 1990. V. 3. 421 p.
11. Bunin V.D., Ignatov O.V., Gulii O.I., et al. // *Biophysics*. 2005. V. 50. P. 299–302.
12. Drygin Yu.F., Blintsov A.N., Osipov A.P., et al. // *Biochemistry (Moscow)*. 2009. V. 74. P. 986–983.
13. Naja G., Hrapovic S., Male K., Bouvrette P., Luong J.H.T. // *Microsc. Res. Tech.* 2008. V. 71. P. 742–748.
14. Phillips R.L., Miranda O.R., You C.C., Rotello V.M., Bunz U.H. // *Angew. Chem. Int. Ed.* 2008. V. 47. P. 2590–2594.
15. Pylaev T.E., Khanadeev V.A., Khlebtsov B.N., et al. // *Colloid J.* 2011. V. 73. № 2. P. 1–12.
16. Liu M., Guyot-Sionnest P. // *J. Phys. Chem. B.* 2005. V. 109. P. 22192–22200.
17. Khlebtsov B., Khanadeev V., Khlebtsov N. // *Phys. Chem. Chem. Phys.* 2010. V. 12. P. 3210–3218.
18. Wang H., Brandl D.W., Le F., Nordlander P., Halas N.J. // *Nano Lett.* 2006. V. 6. P. 827–832.
19. Khlebtsov B.N., Khanadeev V.A., Ye J., Mackowski D.W., Borghs G., Khlebtsov N.G. // *Phys. Rev. B.* 2008. V. 77. P. 035440-1–035440-14.
20. Schwartzberg A.M., Olson T.Y., Talley C.E., Zhang J.Z. // *J. Phys. Chem. B.* 2006. V. 110. P. 19935–19944.
21. Ye J., van Dorpe P., van Roy W., Borghs G., Maes G. // *Langmuir*. 2009. V. 25. P. 1822–1827.
22. Sanchez-Gaytan B.L., Park S.-J. // *Langmuir*. 2010. V. 26. P. 19170–19174.
23. Nehl C.L., Liao H., Hafner J.H. // *Nano Lett.* 2006. V. 6. P. 683–688.
24. Grzelczak M., Pérez-Juste J., Mulvaney P., Liz-Marzán L.-M. // *Chem Soc. Rev.* 2008. V. 37. P. 1783–1791.
25. Khlebtsov B.N., Khanadeev V.A., Maksimova I.L., Terentyuk G.S., Khlebtsov N.G. // *Nanotechnologies in Russia*. 2010. V. 5. P. 454–468.
26. Ramakrishna G., Dai Q., Zou J., Huo Q., Goodson Th. // *J. Am. Chem. Soc.* 2007. V. 129. P. 1848–1849.
27. Wang G., Stender A.S., Sun W., Fang N. // *Analyst*. 2010. V. 135. P. 215–221.
28. Klein S., Petersen S., Taylor U., Rath D., Barcikowski S. // *J. Biomed. Opt.* 2010. V. 15. P. 036015.
29. Durr N.J., Larson T., Smith D.K., Korgel B.A., Sokolov K., Ben-Yakar A. // *Nano Lett.* 2007. V. 7. P. 941–945.
30. Maiorano G., Sabella S., Sorce B., Brunetti V., Malvindi M.A., Cingolani R., Pompa P.P. // *ACS Nano*. 2010. V. 4. P. 7481–7491.
31. El-Sayed I.H., Huang X.H., El-Sayed M.A. // *Nano Lett.* 2005. V. 5. P. 829–834.
32. Huang X., El-Sayed I.H., Qian W., El-Sayed M.A. // *J. Am. Chem. Soc.* 2006. V. 128. P. 2115–2120.
33. Loo C., Hirsch L., Lee M., Chang E., West J., Halas N., Drezek R. // *Opt. Lett.* 2005. V. 30. P. 1012–1014.
34. Aaron J., de la Rosa E., Travis K., Harrison N., Burt J., José-Yakamán M., Sokolov K. // *Opt. Express*. 2008. V. 16. P. 2153–2167.
35. Au L., Zhang Q., Cobley C.M., Gidding M., Schwartz A.G., Chen J., Xia Y. // *ACS Nano*. 2010. V. 4. P. 35–42.
36. Schultz D.A. // *Curr. Opin. Biotechnol.* 2003. V. 14. P. 13–22.
37. York J., Spetzler D., Hornung T., Ishmukhametov R., Martin J., Frasch W.D. // *J. Bioenerg. Biomembr.* 2007. V. 39. P. 435–439.
38. Hu R., Yong K.T., Roy I., Ding H., He S., Prasad P.N. // *J. Phys. Chem. C.* 2009. V. 113. P. 2676–2684.
39. Bickford L., Chang J., Fu K., Sun J., Hu Y., Gobin A., Yu T.K., Drezek R. // *Nanobiotechnology*. 2008. V. 4. P. 1–8.
40. Wang S.-H., Lee C.-W., Chiou A., Wei P.-K. // *J. Nanobiotechnology*. 2010. V. 8. <http://www.jnanobiotechnology.com/content/8/1/33>.
41. Khanadeev V.A., Khlebtsov B.N., Staroverov S.A., Vid-yasheva I.V., Skaptsov A.A., Ilineva E.S., Bogatyrev V.A., Dykman L.A., Khlebtsov N.G. // *J. Biophotonics*. 2011. V. 4. P. 74–83.
42. Zagaynova E.V., Shirmanova M.V., Kirillin M.Yu., Khlebtsov B.N., Orlova A.G., Balalaeva I.V., Sirotkina M.A., Bugrova M.L., Agrba P.D., Kamensky V.A. // *Phys. Med. Biol.* 2008. V. 53. P. 4995–5009.
43. Kim D., Park S., Lee J.H., Jeong Y.Y., Jon S. // *J. Am. Chem. Soc.* 2007. V. 129. P. 7661–7665.
44. Patra C.R., Jing Y., Xu Y.-H., Bhattacharya R., Mukhopadhyay D., Glockner J.F., Wang J.-P., Mukherjee P. // *Cancer Nano*. 2010. V. 1. P. 13–18.
45. Zharov V., Galanzha E., Shashkov E., Khlebtsov N., Tuchin V. // *Opt. Lett.* 2006. V. 31. P. 3623–3625.
46. Li C., Wang L.V. // *Phys. Med. Biol.* 2009. V. 54. P. R59–R97.
47. Chen J., Irudayaraj J. // *ACS Nano*. 2009. V. 3. P. 4071–4079.
48. Hutter E., Boridy S., Labrecque S., Lalancette-Hébert M., Kriz J., Winnik F.M., Maysinger D. // *ACS Nano*. 2010. V. 4. P. 2595–2606.
49. Deyev S.M., Lebedenko E.N. // *Acta Naturae*. 2009. V. 1. № 1. P. 32–50.
50. Leuvering J.H.W., Thal P.J.H.M., van der Waart M., Schuurs A.H.W.M. // *J. Immunoassay*. 1980. V. 1. P. 77–91.
51. Khlebtsov N.G., Melnikov A.G., Dykman L.A., Bogatyrev V.A. // *Photopolarimetry in Remote Sensing* / Eds G. Videen, Ya.S. Yatskiv, M.I. Mishchenko. Dordrecht: Kluwer Acad. Publ., 2004. P. 265–308.
52. Wu S.H., Wu Y.S., Chen C.H. // *Anal. Chem.* 2008. V. 80. P. 6560–6566.
53. Leuvering J.H.W., Coverde B.C., Thal P.J.H.M., Schuurs A.H.W.M. // *J. Immunol. Meth.* 1983. V. 60. P. 9–23.
54. Pavlov V., Xiao Y., Shlyahovsky B., Willner I. // *J. Am. Chem. Soc.* 2004. V. 126. P. 11768–11769.
55. Aslan K., Lakowicz J.R., Geddes C.D. // *Anal. Biochem.* 2004. V. 330. P. 145–155.

REVIEWS

56. Medley C.D., Smith J.E., Tang Z., Wu Y., Bamrungsap S., Tan W. // *Anal. Chem.* 2008. V. 80. P. 1067–1072.
57. Chirathaworn C., Chantaramalai T., Sereemasun A., Kongthong N., Suwancharoen D. // *Comp. Immunol. Microbiol. Infect. Dis.* 2011. V. 34. P. 31–34.
58. Neely A., Perry C., Varisli B., Singh A.K., Arbnesi T., Senapati D., Kalluri J.R., Ray P.C. // *ACS Nano.* 2009. V. 3. P. 2834–2840.
59. Guarise C., Pasquato L., De Filippis V., Scrimin P. // *Proc. Natl. Acad. Sci. USA.* 2006. V. 103. P. 3978–3982.
60. Liu X., Dai Q., Austin L., Coutts J., Knowles G., Zou J., Chen H., Huo Q. // *J. Am. Chem. Soc.* 2008. V. 130. P. 2780–2782.
61. Wang X., Li Y., Wang H., Fu Q., Peng J., Wang Y., Du J., Zhou Y., Zhan L. // *Biosens. Bioelectron.* 2010. V. 26. P. 404–410.
62. Khlebtsov N.G., Bogatyrev V.A., Khlebtsov B.N., Dykman L.A., Englebienne P. // *Colloid J.* 2003. V. 65. P. 622–635.
63. Englebienne P. // *Analyst.* 1998. V. 123. P. 1599–1603.
64. Kamnev A.A., Dykman L.A., Tarantilis P.A., Polissiou M.G. // *Biosci. Reports.* 2002. V. 22. P. 541–547.
65. Russier-Antoine I., Huang J., Benichou E., Bachelier G., Jonin C., Brevet P.F. // *Chem. Phys. Lett.* 2008. V. 450. P. 345–349.
66. Lin C.-C., Yang Y.-M., Chen Y.-F., Yang T.-S., Chang H.-C. // *Biosens. Bioelectron.* 2008. V. 24. P. 178–183.
67. Mirkin C.A., Letsinger R.L., Mucic R.C., Storhoff J.J. // *Nature.* 1996. V. 382. P. 607–609.
68. Elghanian R., Storhoff J.J., Mucic R.C., Letsinger R.L., Mirkin C.A. // *Science.* 1997. V. 277. P. 1078–1081.
69. Sato K., Onoguchi M., Sato Y., Hosokawa K., Maeda M. // *Anal. Biochem.* 2006. V. 350. P. 162–164.
70. Baptista P., Koziol-Montewka M., Paluch-Oles J., Doria G., Franco R. // *Clin. Chem.* 2006. V. 52. P. 1433–1434.
71. Dai Q., Liu X., Coutts J., Austin L., Huo Q. // *J. Am. Chem. Soc.* 2008. V. 130. P. 8138–8139.
72. Li H.X., Rothberg L. // *Proc. Natl. Acad. Sci. USA.* 2004. V. 101. P. 14036–14039.
73. He W., Huang C.Z., Li Y.F., Xie J.P., Yang R.G., Zhou P.F., Wang J. // *Anal. Chem.* 2008. V. 80. P. 8424–8430.
74. Storhoff J.J., Elghanian R., Mucic R.C., Mirkin C.A., Letsinger R.L. // *J. Am. Chem. Soc.* 1998. V. 120. P. 1959–1964.
75. Sato K., Hosokawa K., Maeda M. // *J. Am. Chem. Soc.* 2003. V. 125. P. 8102–8103.
76. Song J., Li Z., Cheng Y., Liu Ch. // *Chem. Commun. (Camb.)* 2010. № 46. P. 5548–5550.
77. Shawky S.M., Bald D., Azzazy H.M.E. // *Clin. Biochem.* 2010. V. 43. P. 1163–1168.
78. Xia F., Zuo X., Yang R., Xiao Y., Kang D., Vallée-Bélisle A., Gong X., Yuen J.D., Hsu B.B., Heeger A.J., Plaxco K.W. // *Proc. Natl. Acad. Sci. USA.* 2010. V. 107. P. 10837–10841.
79. Ma Z., Tian L., Wang T., Wang C. // *Anal. Chim. Acta.* 2010. V. 673. P. 179–184.
80. Storhoff J.J., Marla S.S., Bao P., Hagenow S., Mehta H., Lucas A., Garimella V., Patno T., Buckingham W., Cork W., Müller U.R. // *Biosens. Bioelectron.* 2004. V. 19. P. 875–883.
81. Storhoff J.J., Lucas A.D., Garimella V., Bao Y.P., Müller U.R. // *Nat. Biotechnol.* 2004. V. 22. P. 883–887.
82. Parab H.J., Jung C., Lee J.H., Park H.G. // *Biosens. Bioelectron.* 2010. V. 26. P. 667–673.
83. Stoschek C.M. // *Anal. Biochem.* 1987. V. 160. P. 301–305.
84. Dykman L.A., Bogatyrev V.A., Khlebtsov B.N., Khlebtsov N.G. // *Anal. Biochem.* 2005. V. 341. P. 16–21.
85. Brada D., Roth J. // *Anal. Biochem.* 1984. V. 142. P. 79–83.
86. Moeremans M., Daneles G., van Dijk A., Langanger G., De Mey J. // *J. Immunol. Meth.* 1984. V. 74. P. 353–360.
87. Surek B., Latzko E. // *Biochem. Biophys. Res. Commun.* 1984. V. 121. P. 284–289.
88. Hsu Y.-H. // *Anal. Biochem.* 1984. V. 142. P. 221–225.
89. Danscher G. // *Histochemistry.* 1981. V. 71. P. 81–88.
90. Ma Z., Sui S.-F. // *Angew. Chem. Int. Ed.* 2002. V. 41. P. 2176–2179.
91. Hou S.-Y., Chen H.-K., Cheng H.-C., Huang C.-Y. // *Anal. Chem.* 2007. V. 79. P. 980–985.
92. Blab G.A., Cognet L., Berciaud S., Alexandre I., Husar D., Remacle J., Lounis B. // *Biophys. J.* 2006. V. 90. P. L13–L15.
93. Bio-Rad Labs Bulletin 1310. Western blotting detection systems: how do you choose? 1987. P. 3.
94. Dykman L.A., Bogatyrev V.A. // *Biochemistry (Moscow).* 1997. V. 62. P. 350–356.
95. Starodub N.F., Artyukh V.P., Nazarenko V.I., Kolomiets L.I. // *Ukr. Biokhim. Zh.* 1987. V. 59. P. 108–120.
96. Fenoll A., Jado I., Vicioso D., Casal J. // *J. Clin. Microbiol.* 1997. V. 35. P. 764–766.
97. Bogatyrev V.A., Dykman L.A., Matora L.Yu., Schwartsburd B.I. // *FEMS Microbiol. Lett.* 1992. V. 96. P. 115–118.
98. Dykman L.A., Bogatyrev V.A. // *FEMS Immunol. Med. Microbiol.* 2000. V. 27. P. 135–137.
99. Khlebtsov B.N., Dykman L.A., Bogatyrev V.A., Zharov V., Khlebtsov N.G. // *Nanoscale Res. Lett.* 2007. V. 2. P. 6–11.
100. Khlebtsov B.N., Khanadeev V.A., Bogatyrev V.A., Dykman L.A., Khlebtsov N.G. // *Nanotechnologies in Russia.* 2008. V. 3. P. 442–455.
101. Han A., Dufva M., Belleville E., Christensen C.B.V. // *Lab. Chip.* 2003. V. 3. P. 329–332.
102. Biokhimicheskie metody analiza (Biochemical analysis methods) / Ed. Dzantiev B.B. Moscow: Nauka, 2010. 391 p.
103. Cho J.-H., Paek S.-H. // *Biotechnol. Bioengineer.* 2001. V. 75. P. 725–732.
104. Schalkhammer Th. // *Chem. Monthly.* 1998. V. 129. P. 1067–1092.
105. *Biosensors and Biodetection* / Eds A. Rasooly, K.E. Herold. N.-Y.: Humana Press, 2009. V. 1. 454 p.; V. 2. 470 p.
106. Li Y., Schluesener H.J., Xu S. // *Gold Bull.* 2010. V. 43. P. 29–41.
107. Musick M.D., Keating C.D., Lyon L.A., Botsko S.L., Peña D.J., Holliday W.D., McEvoy T.M., Richardson J.N., Natan M.J. // *Chem. Mater.* 2000. V. 12. P. 2869–2881.
108. Shipway A.N., Katz E., Willner I. // *ChemPhysChem.* 2000. V. 1. P. 18–52.
109. Nath N., Chilkoti A. // *J. Fluorescence.* 2004. V. 14. P. 377–389.
110. Haynes C.L., van Duyne R.P. // *J. Phys. Chem. B.* 2001. V. 105. P. 5599–5611.
111. Lyon L.A., Musick M.D., Natan M.J. // *Anal. Chem.* 1998. V. 70. P. 5177–5183.
112. Miller M.M., Lazarides A.A. // *J. Phys. Chem. B.* 2005. V. 109. P. 21556–21565.
113. Khlebtsov B.N., Melnikov A.G., Zharov V.P., Khlebtsov N.G. // *Nanotechnology.* 2006. V. 17. P. 1437–1445.
114. Templeton A.C., Pietron J.J., Murray R.W., Mulvaney P. // *J. Phys. Chem. B.* 2000. V. 104. P. 564–570.
115. Stewart M.E., Anderton C.R., Thompson L.B., Maria J., Gray S.K., Rogers J.A., Nuzzo R.G. // *Chem. Rev.* 2008. V. 108. P. 494–521.
116. Sepúlveda B., Angelomé P.C., Lechuga L.M., Liz-Marzán L.M. // *Nano Today.* 2009. V. 4. P. 244–251.
117. Daghestani H.N., Day B.W. // *Sensors.* 2010. V. 10. P. 9630–9646.

118. Abbas A., Linman M.J., Cheng Q. // *Biosens. Bioelectron.* 2011. V. 26. P. 1815–1824.
119. Peng H.-I., Miller B.L. // *Analyst.* 2011. V. 136. P. 436–447.
120. Jason-Moller L., Murphy M., Bruno J. // *Curr. Protoc. Protein Sci.* 2006. Ch. 19. Unit 19.13.
121. Brainina K., Kozitsina A., Beikin J. // *Anal. Bioanal. Chem.* 2003. V. 376. P. 481–485.
122. Baek T.J., Park P.Y., Han K.N., Kwon H.T., Seong G.H. // *Anal. Bioanal. Chem.* 2008. V. 390. P. 1373–1378.
123. Mahmoud K.A., Luong J.H. // *Anal. Chem.* 2008. V. 80. P. 7056–7062.
124. Haes A.J., Chang L., Klein W.L., van Duyne R.P. // *J. Am. Chem. Soc.* 2005. V. 127. P. 2264–2271.
125. Simonian A.L., Good T.A., Wang S.-S., Wild J.R. // *Anal. Chim. Acta.* 2005. V. 534. P. 69–77.
126. Boghaert E.R., Khandke K.M., Sridharan L., Dougher M., DiJoseph J.F., Kunz A., Hamann P.R., Moran J., Chaudhary I., Damle N.K. // *Cancer Chemother. Pharmacol.* 2008. V. 61. P. 1027–1035.
127. Maier I., Morgan M.R., Lindner W., Pittner F. // *Anal. Chem.* 2008. V. 80. P. 2694–2703.
128. Huang T., Nallathamby P.D., Xu X.H. // *J. Am. Chem. Soc.* 2008. V. 130. P. 17095–17105.
129. Aslan K., Zhang J., Lakowicz J.R., Geddes C.D. // *J. Fluoresc.* 2004. V. 14. P. 391–400.
130. Wang L., Jia X., Zhou Y., Xie Q., Yao S. // *Microchim. Acta.* 2010. V. 168. P. 245–251.
131. de la Escosura-Muñiz A., Sánchez-Espinel C., Díaz-Freitas B., González-Fernández A., Maltez-da Costa M., Merkoçi A. // *Anal. Chem.* 2009. V. 81. P. 10268–10274.
132. Eum N.-S., Yeom S.-H., Kwon D.-H., Kim H.-R., Kang S.-W. // *Sens. Actuator B Chem.* 2010. V. 143. P. 784–788.
133. Zhang J., Atay T., Nurmikko A.V. // *Nano Lett.* 2009. V. 9. P. 519–524.
134. Adamczyk M., Moore J.A., Yu Z. // *Methods.* 2000. V. 20. P. 319–328.
135. Raschke G., Kowarik S., Franzl T., Sönnichsen C., Klar T.A., Feldmann J., Nichtl A., Kürzinger K. // *Nano Lett.* 2003. V. 3. P. 935–942.
136. McFarland A.D., van Duyne R.P. // *Nano Lett.* 2003. V. 3. P. 1057–1062.
137. Mayer K.M., Hao F., Lee S., Nordlander P., Hafner J.H. // *Nanotechnology.* 2010. V. 21. P. 255503.
138. Kennedy L.C., Bickford L.R., Lewinski N.A., Coughlin A.J., Hu Y., Day E.S., West J.L., Drezek R.A. // *Small.* 2011. V. 7. P. 169–183.
139. Huang X., Jain P.K., El-Sayed I.H., El-Sayed M.A. // *Lasers Med. Sci.* 2008. V. 23. P. 217–228.
140. Minton J.P., Carlton D.M., Dearman J.R., McKnight W.B., Ketcham A.S. // *Surg. Gynaecol. Obstet.* 1965. V. 121. P. 538–544.
141. Masters A., Bown S.G. // *Br. J. Cancer.* 1992. V. 8. P. 242–249.
142. Hirsch L.R., Stafford R.J., Bankson J.A., Sershen S.R., Price R.E., Hazle J.D., Halas N.J., West J.L. // *Proc. Natl. Acad. Sci. USA.* 2003. V. 100. P. 13549–13554.
143. Zharov V.P., Galitovsky V., Viegas M. // *Appl. Phys. Lett.* 2003. V. 83. P. 4897–4899.
144. Pitsillides C.M., Joe E.K., Wei X., Anderson R.R., Lin C.P. // *Biophys. J.* 2003. V. 84. P. 4023–4032.
145. von Maltzahn G., Park J.-H., Agrawal A., Bandaru N.K., Das S.K., Sailor M.J., Bhatia S.N. // *Cancer Res.* 2009. V. 69. P. 3892–3900.
146. Lapotko D., Lukianova-Hleb E., Oraevsky A. // *Nanomedicine.* 2007. V. 2. P. 241–253.
147. Huang X., Qian W., El-Sayed I.H., El-Sayed M.A. // *Lasers Surg. Med.* 2007. V. 39. P. 747–753.
148. Lapotko D., Lukianova E., Potapnev M., Aleinikova O., Oraevsky A. // *Cancer Lett.* 2005. V. 239. P. 36–45.
149. Harris N., Ford M.J., Cortie M.B. // *J. Phys. Chem. B.* 2006. V. 110. P. 10701–10707.
150. Huff T.B., Tong L., Zhao Y., Hansen M.N., Cheng J.X., Wei A. // *Nanomedicine.* 2007. V. 2. P. 125–132.
151. Loo C., Lowery A., Halas N.J., West J.L., Drezek R. // *Nano Lett.* 2005. V. 5. P. 709–711.
152. Hu M., Petrova H., Chen J., McLellan J.M., Siekkinen A.R., Marquez M., Li X., Xia Y., Hartland G.V. // *J. Phys. Chem. B.* 2006. V. 110. P. 1520–1524.
153. Chen J., Wang D., Xi J., Au L., Siekkinen A., Warsen A., Li Z.-Y., Zhang H., Xia Y., Li X. // *Nano Lett.* 2007. V. 7. P. 1318–1322.
154. Terentyuk G.S., Maslyakova G.N., Suleymanova L.V., Khlebtsov N.G., Khlebtsov B.N., Akchurin G.G., Maksimova I.L., Tuchin V.V. // *J. Biomed. Opt.* 2009. V. 14. P. 021016.
155. Lapotko D. // *Nanomedicine.* 2009. V. 4. P. 253–256.
156. Hleb E., Hu Y., Drezek R., Hafner J., Lapotko D. // *Nanomedicine.* 2008. V. 3. P. 797–812.
157. Zharov V.P., Galitovskaya E.N., Johnson C., Kelly T. // *Lasers Surg. Med.* 2005. V. 37. P. 219–226.
158. Akchurin G., Khlebtsov B., Akchurin G., Tuchin V., Zharov V., Khlebtsov N. // *Nanotechnology.* 2008. V. 19. P. 015701.
159. Hleb E.Y., Lapotko D.O. // *Nanotechnology.* 2008. V. 19. P. 355702.
160. Lukianova-Hleb E.Y., Anderson L.J.E., Lee S., Hafner J.H., Lapotko D.O. // *Phys. Chem. Chem. Phys.* 2010. V. 12. P. 12237–12244.
161. Jain R.K., Booth M.F. // *J. Clin. Invest.* 2003. V. 112. P. 1134–1136.
162. Nie S.M. // *Nanomedicine.* 2010. V. 5. P. 523–528.
163. El-Sayed I.H., Huang X., El-Sayed M.A. // *Cancer Lett.* 2006. V. 239. P. 129–135.
164. Visaria R.K., Griffin R.J., Williams B.W., Ebbini E.S., Paciotti G.F., Song C.W., Bischof J.C. // *Mol. Cancer Ther.* 2006. V. 5. P. 1014–1020.
165. Larson T.A., Bankson J., Aaron J., Sokolov K. // *Nanotechnology.* 2007. V. 18. P. 325101.
166. Lu W., Xiong C., Zhang G., Huang Q., Zhang R., Zhang J.Z., Li C. // *Clin. Cancer Res.* 2009. V. 15. P. 876–886.
167. Huang X., Peng X., Wang Y., Wang Y., Shin D.M., El-Sayed M.A., Nie S. // *ACS Nano.* 2011. V. 4. P. 5887–5896.
168. Kirpotin D.B., Drummond D.C., Shao Y., Shalaby M.R., Hong K., Nielsen U.B., Marks J.D., Benz C.C., Park J.W. // *Cancer Res.* 2006. V. 66. P. 6732–6740.
169. Choi C.H.J., Alabi C.A., Webster P., Davis M.E. // *Proc. Natl. Acad. Sci. USA.* 2010. V. 107. P. 1235–1240.
170. *Handbook of Photonics for Biomedical Science* / Ed. V.V. Tuchin. Boca Raton: CRC Press, 2009. 868 p.
171. Hainfeld J.F., Slatkin D.N., Smilowitz H.M. // *Phys. Med. Biol.* 2004. V. 49. P. N309–N315.
172. Pissuwan D., Valenzuela S.M., Miller C.M., Cortie M.B. // *Nano Lett.* 2007. V. 7. P. 3808–3812.
173. Zharov V.P., Mercer K.E., Galitovskaya E.N., Smeltzery M.S. // *Biophys. J.* 2006. V. 90. P. 619–627.
174. Pissuwan D., Valenzuela S.M., Cortie M.B. // *Trends Biotech.* 2006. V. 24. P. 62–67.
175. *Cancer Nanotechnology. Methods and Protocols* / Eds S.R. Grobmyer, B.M. Moudgil. N.-Y.: Humana Press, 2010. 396 p.
176. Wilson B.C. // *Handbook of Photonics for Biomedical*

- Science / Ed. V.V. Tuchin. Boca Raton: CRC Press, 2010. P. 649–686.
177. Lakowicz J.R., Ray K., Chowdhury M., Szmanski H., Fu Y., Zhang J., Nowaczyk K. // *Analyst*. 2008. V. 133. P. 1308–1346.
178. Bardhan R., Grady N.K., Cole J.R., Joshi A., Halas N.J. // *ACS Nano*. 2009. V. 3. P. 744–752.
179. Sershen S.R., Westcott S.L., Halas N.J., West J.L. // *J. Biomed. Mater. Res*. 2000. V. 51. P. 293–298.
180. Radt B., Smith T.A., Caruso F. // *Adv. Mater*. 2004. V. 16. P. 2184–2189.
181. Shiotani A., Mori T., Niidome T., Niidome Y., Katayama Y. // *Langmuir*. 2007. V. 23. P. 4012–4018.
182. Nakamura T., Tamura A., Murotani H., Oishi M., Jinji Y., Matsuishi K., Nagasaki Y. // *Nanoscale*. 2010. V. 2. P. 739–746.
183. Thomas K.G., Kamat P.V. // *Acc. Chem. Res*. 2003. V. 36. P. 888–898.
184. Liu S.Y., Liang Z.S., Gao F., Luo S.F., Lu G.Q. // *J. Mater. Sci. Mater. Med*. 2010. V. 21. P. 665–674.
185. Bardhan R., Chen W., Bartels M., Perez-Torres C., Botero M.F., McAninch R.W., Contreras A., Schiff R., Pautler R.G., Halas N.J., Joshi A. // *Nano Lett*. 2010. V. 10. P. 4920–4928.
186. Kuo W.-S., Chang C.-N., Chang Y.-T., Yang M.-H., Chien Y.-H., Chen S.-J., Yeh C.-S. // *Angew. Chem. Int. Ed*. 2010. V. 49. P. 2711–2715.
187. Abraham G.E., Himmel P.B. // *J. Nutr. Med*. 1997. V. 7. P. 295–305.
188. Abraham G.E. // *Orig. Intern*. 2008. V. 15. P. 132–158.
189. Tsai C.Y., Shiao A.L., Chen S.Y., Chen Y.H., Cheng P.C., Chang M.Y., Chen D.H., Chou C.H., Wang C.R., Wu C.L. // *Arthritis Rheum*. 2007. V. 56. P. 544–554.
190. Brown C.L., Whitehouse M.W., Tiekink E.R.T., Bushell G.R. // *Inflammopharmacology*. 2008. V. 16. P. 133–137.
191. Paciotti G.F., Myer L., Weinreich D., Goia D., Pavel N., McLaughlin R.E., Tamarkin L. // *Drug Deliv*. 2004. V. 11. P. 169–183.
192. Paciotti G.F., Kingston D.G.I., Tamarkin L. // *Drug Dev. Res*. 2006. V. 67. P. 47–54.
193. Mukherjee P., Bhattacharya R., Wang P., Wang L., Basu S., Nagy J.A., Atala A., Mukhopadhyay D., Soker S. // *Clin. Cancer Res*. 2005. V. 11. P. 3530–3534.
194. Mukherjee P., Bhattacharya R., Bone N., Lee Y.K., Patra C.R., Wang S., Lu L., Secretro C., Banerjee P.C., Yaszemski M.J., Kay N.E., Mukhopadhyay D. // *J. Nanobiotechnology*. 2007. V. 5. <http://www.jnanobiotechnology.com/content/5/1/4>
195. Bhattacharya R., Patra C.R., Verma R., Kumar S., Greipp P.R., Mukherjee P. // *Adv. Mater*. 2007. V. 19. P. 711–716.
196. Duncan B., Kim C., Rotello V.M. // *J. Control. Release*. 2010. V. 148. P. 122–127.
197. Pissuwan D., Niidome T., Cortie M.B. // *J. Control. Release*. 2011. V. 149. P. 65–71.
198. Chen Y.H., Tsai C.Y., Huang P.Y., Chang M.Y., Cheng P.C., Chou C.H., Chen D.H., Wang C.R., Shiao A.L., Wu C.L. // *Mol. Pharm*. 2007. V. 4. P. 713–722.
199. Li J., Wang X., Wang C., Chen B., Dai Y., Zhang R., Song M., Lv G., Fu D. // *ChemMedChem*. 2007. V. 2. P. 374–378.
200. Patra C.R., Bhattacharya R., Wang E., Katarya A., Lau J.S., Dutta S., Mudders M., Wang S., Buhrow S.A., Safgren S.L., Yaszemski M.J., Reid J.M., Ames M.M., Mukherjee P., Mukhopadhyay D. // *Cancer Res*. 2008. V. 68. P. 1970–1978.
201. Podsiadlo P., Sinani V.A., Bahng J.H., Kam N.W., Lee J., Kotov N.A. // *Langmuir*. 2008. V. 24. P. 568–574.
202. Azzam E.M.S., Morsy S.M.I. // *J. Surf. Deterg*. 2008. V. 11. P. 195–199.
203. Stiti M., Cecchi A., Rami M., Abdaoui M., Barragan-Montero V., Scozzafava A., Guari Y., Winum J.Y., Supuran C.T. // *J. Am. Chem. Soc*. 2008. V. 130. P. 16130–16131.
204. Agasti S.S., Chompoosor A., You C.C., Ghosh P., Kim C.K., Rotello V.M. // *J. Am. Chem. Soc*. 2009. V. 131. P. 5728–5729.
205. Dhar S., Daniel W.L., Giljohann D.A., Mirkin C.A., Lip-pard S.J. // *J. Am. Chem. Soc*. 2009. V. 131. P. 14652–14653.
206. Hosta L., Pla-Roca M., Arbiol J., López-Iglesias C., Samitier J., Cruz L.J., Kogan M.J., Albericio F. // *Bioconjug. Chem*. 2009. V. 20. P. 138–146.
207. Dreaden E.C., Mwakwari S.C., Sodji Q.H., Oyelere A.K., El-Sayed M.A. // *Bioconjug. Chem*. 2009. V. 20. P. 2247–2253.
208. Eghtedari M., Liopo A.V., Copland J.A., Oraevsky A.A., Motamedi M. // *Nano Lett*. 2009. V. 9. P. 287–291.
209. Asadishad B., Vossoughi M., Alemzadeh I. // *Ind. Eng. Chem. Res*. 2010. V. 49. P. 1958–1963.
210. Staroverov S.A., Gasina O.A., Kladiev A.A., Bogatyrev V.A. // *Rossiyski bioterapevticheski zhurnal*. 2010. V. 9. P. 22–23.
211. Kim C.-K., Ghosh P., Rotello V.M. // *Nanoscale*. 2009. V. 1. P. 61–67.
212. Gu H., Ho P.L., Tong E., Wang L., Xu B. // *Nano Lett*. 2003. V. 3. P. 1261–1263.
213. Rosemary M.J., MacLaren I., Pradeep T. // *Langmuir*. 2006. V. 22. P. 10125–10129.
214. Selvaraj V., Alagar M. // *Int. J. Pharm*. 2007. V. 337. P. 275–281.
215. Saha B., Bhattacharya J., Mukherjee A., Ghosh A.K., Santra C.R., Dasgupta A.K., Karmakar P. // *Nanoscale Res. Lett*. 2007. V. 2. P. 614–622.
216. Grace A.N., Pandian K. // *Colloids Surf. A: Physico-chem. Eng. Aspects*. 2007. V. 297. P. 63–70.
217. Grace A.N., Pandian K. // *J. Bionanosci*. 2007. V. 1. P. 96–105.
218. Burygin G.L., Khlebtsov B.N., Shantrokha A.N., Dykman L.A., Bogatyrev V.A., Khlebtsov N.G. // *Nanoscale Res. Lett*. 2009. V. 4. P. 794–801.
219. Rai A., Prabhune A., Perry C.C. // *J. Mater. Chem*. 2010. V. 20. P. 6789–6798.
220. Nie Z., Liu K.J., Zhong C.J., Wang L.F., Yang Y., Tian Q., Liu Y. // *Free Radic. Biol. Med*. 2007. V. 43. P. 1243–1254.
221. Bowman M.C., Ballard T.E., Ackerson C.J., Feldheim D.L., Margolis D.M., Melander C. // *J. Am. Chem. Soc*. 2008. V. 130. P. 6896–6897.
222. Joshi H.M., Bhumkar D.R., Joshi K., Pokharkar V., Sas-try M. // *Langmuir*. 2006. V. 22. P. 300–305.
223. Chamberland D.L., Agarwal A., Kotov N., Fowlkes J.B., Carson P.L., Wang X. // *Nanotechnology*. 2008. V. 19. P. 095101.
224. Miller A.D. // *Nature*. 1992. V. 357. P. 455–460.
225. Zelenin A.V. // *Herald of the RAS*. 2001. V. 71. P. 215–222.
226. Patel P.C., Giljohann D.A., Daniel W.L., Zheng D., Pri-godich A.E., Mirkin C.A. // *Bioconjug. Chem*. 2010. V. 21. P. 2250–2256.
227. Zilber L.A., Friese W.W. // *Zh. Eksp. Biol*. 1929. V. 11. P. 128–135.
228. Pacheco G. // *Mem. Inst. Oswaldo Cruz*. 1925. V. 18. P. 119–149.
229. Kovalev I.E., Polevaya O.Yu. *Biokhimicheskie osnovy immuniteta k nizkomolekulyarnim khimicheskim soed-ineniyam (Biochemical Foundations of Immunity to Low-*

REVIEWS

- molecular Chemical Compounds). Moscow: Nauka, 1985. 304 p.
230. Shiosaka S., Kiyama H., Wanaka A., Tohyama M. // *Brain Res.* 1986. V. 382. P. 399–403.
231. Dykman L.A., Staroverov S.A., Bogatyrev V.A., Shchyogolev S.Yu. // *Nanotechnologies in Russia.* 2010. V. 5. P. 748–761.
232. Pow D.V., Crook D.K. // *J. Neurosci. Meth.* 1993. V. 48. P. 51–63.
233. Demenev V.A., Shchinova M.A., Ivanov L.I., Vorob'eva R.N., Zdanovskaya N.I., Nebaykina N.V. // *Vopr. Virusol.* 1996. V. 41. P. 107–110. (in Russian)
234. Zhao Z., Wakita T., Yasui K. // *J. Virol.* 2003. V. 77. P. 4248–4260.
235. Dykman L.A., Staroverov S.A., Bogatyrev V.A., Shchyogolev S.Yu. *Gold nanoparticles as an antigen carrier and an adjuvant.* New York: Nova Science Publishers, 2010. 54 p.
236. Staroverov S.A., Aksinenko N.M., Gabalov K.P., Vasilenko O.A., Vidyasheva I.V., Shchyogolev S.Yu., Dykman L.A. // *Gold Bull.* 2009. V. 42. P. 153–156.
237. Vallhov H., Qin J., Johansson S.M., Ahlborg N., Muhammed M.A., Scheynius A., Gabrielsson S. // *Nano Lett.* 2006. V. 6. P. 1682–1686.
238. Villiers C.L., Freitas H., Couderc R., Villiers M.-B., Marche P.N. // *J. Nanopart. Res.* 2010. V. 12. P. 55–60.
239. Zolnik B.S., González-Fernández A., Sadrieh N., Dobrovolskaia M.A. // *Endocrinology.* 2010. V. 151. P. 458–465.
240. Bastús N.G., Sánchez-Tilló E., Pujals S., Farrera C., Kogan M.J., Giralt E., Celada A., Lloberas J., Puntès V. // *Mol. Immunol.* 2009. V. 46. P. 743–748.
241. Yen H.J., Hsu S.H., Tsai C.L. // *Small.* 2009. V. 5. P. 1553–1561.
242. Dobrovolskaia M.A., McNeil S.E. // *Nat. Nanotechnol.* 2007. V. 2. P. 469–478.
243. Lou H., Tian Y., Gao J.-Q., Deng S.-Y., Li J.-L. // *J. Foshan Univ.* 2007. V. 25. P. 24–27.
244. Lewinski N., Colvin V., Drezek R. // *Small.* 2008. V. 4. P. 26–49.
245. Alkilany A.M., Murphy C.J. // *J. Nanopart. Res.* 2010. V. 12. P. 2313–2333.
246. Fadeel B., Garcia-Bennett A.E. // *Adv. Drug Deliv. Rev.* 2010. V. 62. P. 362–374.
247. Johnston H.J., Hutchison G., Christensen F.M., Peters S., Hankin S., Stone V. // *Crit. Rev. Toxicol.* 2010. V. 40. P. 328–346.
248. Khlebtsov N.G., Dykman L.A. // *Chem. Soc. Rev.* 2011. V. 40. P. 1647–1671.
249. Nam J.M., Thaxton C.S., Mirkin C.A. // *Science.* 2003. V. 301. P. 1884–1886.
250. Jiang W., Kim B.Y.S., Rutka J.T., Chan W.C.W. // *Nat. Nanotechnol.* 2008. V. 3. P. 145–150.

Characteristics of Populations of the Russian Federation over the Panel of Fifteen Loci Used for DNA Identification and in Forensic Medical Examination

V. A. Stepanov^{1,6*}, O. P. Balanovsky^{2,5}, A. V. Melnikov³, A. Yu. Lash-Zavada³, V. N. Khar'kov^{1,6}, T. V. Tyazhelova², V. L. Akhmetova⁴, O. V. Zhukova², Yu. V. Shneider², I. N. Shil'nikova², S. A. Borinskaya², A. V. Marusin¹, M. G. Spiridonova¹, K. V. Simonova¹, I. Yu. Khitrinskaya¹, M. O. Radzhabov⁷, A. G. Romanov⁵, O. V. Shtygasheva⁸, S. M. Koshel'⁹, E. V. Balanovskaya⁵, A. V. Rybakova³, E. K. Khusnutdinova⁴, V. P. Puzyrev¹, N. K. Yankovsky²

¹ Institute for Medical Genetics, Russian Academy of Medical Sciences

² Vavilov Institute of General Genetics, Russian Academy of Sciences

³ Forensic Centre, Ministry of Interior of Russian Federation

⁴ Institute of Biochemistry and Genetics, Ufa Research Centre, Russian Academy of Sciences

⁵ Research Centre for Medical Genetics, Russian Academy of Sciences

⁶ Genome Diagnostics, Ltd.

⁷ Dagestan State University

⁸ Katanov Khakas State University

⁹ Geography Faculty, Lomonosov Moscow State University

*E-mail: vadim.stepanov@medgenetics.ru

Received 05.03.2011

ABSTRACT Seventeen population groups within the Russian Federation were characterized for the first time using a panel of 15 genetic markers that are used for DNA identification and in forensic medical examinations. The degree of polymorphism and population diversity of microsatellite loci within the Power Plex system (Promega) in Russian populations; the distribution of alleles and genotypes within the populations of six cities and 11 ethnic groups of the Russian Federation; the levels of intra- and interpopulation genetic differentiation of population; genetic relations between populations; and the identification and forensic medical characteristics of the system of markers under study were determined. Significant differences were revealed between the Russian populations and the U.S. reference base that was used recently in the forensic medical examination of the RF. A database of the allelic frequencies of 15 microsatellite loci that are used for DNA identification and forensic medical examination was created; the database has the potential of becoming the reference for performing forensic medical examinations in Russia. The spatial organization of genetic diversity over the panel of the STR markers that are used for DNA identification was revealed. It represents the general regularities of geographical clusterization of human populations over various types of genetic markers. The necessity to take into account a population's genetic structure during forensic medical examinations and DNA identification of criminal suspects was substantiated.

KEYWORDS microsatellites; short tandem repeats; allelic frequencies; forensic medical examination; DNA identification; population of Russia; reference database; genetic diversity; gene geography

ABBREVIATIONS MI RF – Ministry of Interior of the Russian Federation; PCR – polymerase chain reaction; He – expected heterozygosity; AMOVA – Analysis of molecular variance; CODIS – combined DNA index system; EDNAP – the European DNA Profiling Group; ENFSI – European Network of Forensic Science Institutes; ESS – European Standard Set; MP – matching probability; PD – power of discrimination; PE – power of exclusion; PI – paternity index; SNP – single nucleotide polymorphism; STR – short tandem repeats; UPGMA – unweighted pair group method with arithmetic mean

INTRODUCTION

Molecular genetic analysis methods are now widely applied in the identification of the biological samples of individuals: victims of crimes, disasters, and acts of

terrorism, criminals, and contingent of special divisions of armies or law enforcement. A genetic DNA analysis in forensic medical examinations has two stages. At the first stage, the DNA characteristics of the samples col-

lected at the locus delicti are determined. At the second stage, they are matched with the DNA collected from the suspects or relatives of the victims. If there is no match of the genotypes, that points to the fact that the samples examined do not belong to the individual in question (taking into account the exclusion probability). When genotypes match, the probability of their random matching, i.e., the probability that other individuals may have the same genotypes, is also taken into account.

The probability of a random match is calculated on the basis of data on the occurrence frequencies of the alleles (and genotypes) of the analyzed panel of genetic markers in reference populations. In order to create such reference databases, population samples collected with allowance for the population genetic structure of certain ethno-territorial groups are used. Allelic frequencies in various populations and groups have been published and presented in databases. These reference databases serve as a legally valid basis for forensic medical conclusions in interpreting the results of genotype comparisons.

The reliability and efficiency of DNA identification depends on two key factors: on the choice of the locus panel and the choice of the reference population.

Selection of the loci panel. The genetic markers that are used for forensic medical expertise should be highly polymorphic and should possess a high resolution capacity. Multiallelic (mostly consisting of 8–10 alleles) unlinked microsatellite markers – STR (Short Tandem Repeats) loci are considered to be the most efficient ones. However, different panels of these STR markers are used in different regions.

In Europe, Interpol uses two standards of loci sets – ENFSI (the European Network of Forensic Science Institutes) and EDNAP (the European DNA Profiling Group), consisting of seven STR loci each. In 2005, an agreement on the unification of the loci systems used in Europe was signed. The ENFSI proposed six more markers as candidates to be included into the European standard set (ESS) [1]. In 2009, the ENFSI added five out of six candidate markers to its standard, thus broadening the European Standard panel ESS to 12 STR: *TH01*, *vWA*, *D18S51*, *D8S1179*, *D3S1358*, *FGA*, *D21S11*, *D1S1656*, *D2S441*, *D10S1248*, *D12S391* и *D22S1405*. In 2010, the standard was approved by the European Union.

Starting in 1994, the CODIS (Combined DNA Index System) system has been in use in the United States, its full format comprising 13 loci (*D7S820*, *D13S317*, *CSF1PO*, *TPOX*, *D16S539*, *TH01*, *vWA*, *D5S818*, *D18S51*, *D8S1179*, *D3S1358*, *FGA*, *D21S1*). The CODIS and ENFSI systems have seven markers in common from the EDNAP/ENFSI primary standard.

In all the aforementioned systems (with the exception of the polymorphic autosomal STR loci,) another locus (amelogenin) is used, the size of its PCR fragments being different on the X and Y chromosomes, which allows for the determination of the sex of an individual by analyzing the DNA of a biological sample.

When creating these systems, among the several tens of STR loci that had been tested, the most highly polymorphic ones within the majority of the examined populations were selected. For the convenience of genetic typing, the PowerPlex 16 system was designed, enabling the simultaneous amplification of 16 polymorphic loci in a single test tube, which considerably simplifies the analysis and reduces its cost. In addition to the amelogenin locus and the 13 loci from the CODIS system, this kit also comprises two highly polymorphic and easily readable pentanucleotide markers (*PentaD* and *PentaE*) [2].

On December 3, 2008, the Federal Law of the Russian Federation On State Genomic Registration in the Russian Federation was adopted. The law provides for the creation of the Federal database of genomic information under the Ministry of the Interior of the Russian Federation. Order of the Ministry of the Interior of the RF no. 70 dated February 10, 2006, is the official statutory act regulating the gene typing procedures for DNA identification; in the edition dated May 21, 2008, it establishes a set consisting of 12 STR markers and the amelogenin locus, which is totally identical to the American CODIS standard, as a mandatory set.

Selection of the reference population. In order to reliably compare genotypes in each case, the choice of the reference population should depend on the group that the individual who has left biological marks belongs to. In actual practice, the reference population is usually selected among the populations represented in the criminal databases which were studied using this panel of STR markers.

The less the reference population represents the gene pool of a tested group, the more individuals within this group have alleles that are not in the reference database, which results in a considerable decrease in the discrimination capacity of the method. There are correlations between the number (percentage) of individuals who have alleles that are not in the reference population and the genetic distance between the reference population and the population under analysis [3].

The use of an inadequate reference group may result in a decrease in the total identification probability by several orders of magnitude. The situation can be improved by introducing corrections based on the maximum degree of genetic differences between subpopulations within a reference population (e.g., an ethnic group). In order to introduce such a correction, it is

necessary to have information on the genetic differentiation between populations (F_{st}) with respect to the loci used for each specific group within each specific territory. This correction permits the replacement of alleles and genotypes that are unknown for the reference population by their calculated frequencies, with allowance made for the differentiation degree F_{st} [4]. It is assumed that these calculated frequencies take into account the maximally possible differences between the unknown and reference populations.

Even if the group of an individual to whom the biological sample belongs is unknown, it can be identified with a certain probability, provided that there are population databases. Thus, when identifying the victims of the World Trade Centre terrorism act in New York, if the remains belonged to an unknown group, the probability was calculated using all four major American groups as reference points; the most conservative estimate was used as the final one [5]. After four years, 1,594 remains have been identified out of 2,749; 850 of those were identified only on the basis of data of a DNA analysis [5].

The criminal databases and criteria of comparison were developed with allowance for the genetic characteristics of ethno-territorial groups (e.g., see [4]) and are published in accordance with specific rules [6].

In the United States and Europe, a large mass of population has been characterized with respect to the loci used in forensic medical examinations. In other regions, several tens of population groups have been known to have been studied on the basis of panels of ENFSI, EDNAP, and CODIS genetic markers [7–14].

Data on the distribution of individual genetic markers from these panels in Russian populations has remained fragmentary [15–18]. In terms of interpretability of the data, Russia stands out upon DNA identification by its diverse mix of nationalities and vast geographical expanse. The considerable differences in the range of individual features of the genomes that are typical of various ethnic groups, in particular, the spatially remote ones, have been well known. Numerous population genetic studies of the Russian population performed using various systems of genetic markers, including mtDNA, the Y chromosome, and autosomal markers, have demonstrated that the range of interpopulation variability for different ethnic and territorial groups of the RF exceeds considerably the variability of the entire population of Europe [19–22]. However, because of the absence of systematic information on the RF population in terms of the marker panels that are commonly accepted in the world, the data on the frequencies of genetic characteristics in the population of the U.S. and Europe are used in practice for DNA identification in the RF, although whether

these data can be applied to the RF population has not been assessed.

In this context, our work was aimed at determining the allelic frequencies of 15 autosomal STR loci from the PowerPlex 16 system in six urban population groups and 11 ethnic groups in the RF. A solution to this problem will allow to characterize the genetic variability of the Russian population using this system of markers and will lay the basis for the creation of our own reference population for DNA identification and forensic medical examinations in Russia.

EXPERIMENTAL

Populations

Seventeen population groups with a total of 1,156 people representing different geographical regions of Russia (European part of the RF, the North Caucasus, the Volga–Ural region, Siberia) and belonging to different linguistic groups and different anthropological types were examined.

Six samplings represent the Russian urban population: Moscow ($N = 60$), Belgorod ($N = 50$), Orel ($N = 51$), Orenburg ($N = 50$), Yaroslavl ($N = 50$), and Tomsk ($N = 185$). Eleven samplings represent a wide range of the Russian population and neighboring countries: Komi ($N = 50$), Mari ($N = 52$), Khakas ($N = 92$), Bashkir ($N = 70$), Tatar ($N = 61$), Chuvash ($N = 53$), Dargins ($N = 48$), Avars ($N = 50$), Lezgins ($N = 50$), Ukrainians ($N = 138$), and Belorussians ($N = 46$).

Molecular biology techniques

The amplification of 15 STR loci and the sex marker (amelogenin gene) was carried out in the multiplex PCR format (one multiplex per all 16 loci) on Applied Biosystems and Biometra gradient amplifiers under the conditions that were recommended by the manufacturer of the commercial PowerPlex system (Promega). Fluorescently labeled PCR fragments were separated by capillary gel electrophoresis on an ABIPrism 3130 and an ABIPrism 310 genetic analyzer (Applied Biosystems). The genotypes were read using Gene Mapper software (Applied Biosystems). The quality of gene typing was controlled using the standard set of alleles of all 16 microsatellites (“ladder”) supplied within the PowerPlex 16 system; the “ladder” were loaded in each gene typing cycle (in each run).

Methods of statistical analysis of the results

The data were analyzed using the modern statistical approaches employed in population genetics and forensic medicine. Correspondence of the observed genotype distributions to the Hardy–Weinberg equilibrium was estimated by the exact test of Guo and Thomp-

son [23] implemented using the Arlequin and GenePop software. The genetic diversity of populations and the genetic variability of 15 STR were analyzed using the Arlequin software [24].

The genetic differentiation of the populations was analyzed by a calculation of pairwise F_{st} values and by an analysis of molecular variance (AMOVA), using the matrix of root-mean-square discrepancies in repeat numbers of R_{st} . The dendrogram illustrating the genetic relationships between the populations was constructed using the unweighed pair group method with the arithmetic mean (UPGMA) in PHYLIP software.

The variability of the studied loci in the population of North Eurasia was analyzed using the database on the frequencies of microsatellite markers in 51 populations that we compiled (the total sampling volume was 8,700 individuals). The database comprised both our own results presented in this paper and the data from earlier studies [25–39], including data on the populations of 12 countries (Belorussia, Bosnia, Greece, China, Macedonia, Mongolia, Pakistan, Poland, Russia, Slovakia, Sweden, and the Czech Republic). The database contains information on 17 loci (*D3S1358*, *TH01*, *D21S11*, *D18S51*, *D13S317*, *D7S820*, *D16S539*, *CSF1PO*, *vWA*, *D8S1179*, *TPOX*, *FGA*, *D5S818*, *PentaD*, *PentaE*, *D2S1338*, and *D19S433*). However, since five markers (*D5S818*, *PentaD*, *PentaE*, *D2S1338*, and *D19S433*) had not been studied in a number of populations, the remaining 12 loci were used in the analysis.

The analysis of this vast massif was carried out using both statistical and cartographic gene-geographic. The statistical analysis consisted of the calculation of genetic distances according to Nei [40] using the DJgenetic software designed by Yu.A. Seregin and E.V. Balanovskaya. The Statistica 6.0 program (StatSoft. Inc., 2001) [41] was used to visualize the resulting genetic distance matrix on a multidimensional scaling diagram.

Heterozygosity with respect to each locus was calculated, and the averaged (over 12 loci) values of heterozygosity were obtained in each population. These values were mapped using GeneGeo software that was developed by a number of authors for several years. The calculation of interpolated heterozygosity values was performed on the basis of the data in reference points (immediately in the populations under study) to a uniform grid consisting of 335,661 nodes (881×381); the 301,681 nodes remaining after the water area were eliminated. Interpolation was performed using the generalized Shepard's method. The cube of the weighting function was employed; i.e., the contribution of each point into the calculated value in a certain node was in reverse proportion to the cube of the distance between the reference point and the node; the reference points

at a distance of more than 3,000 km were not taken into account.

The discrimination potential of the system, which consisted of 15 microsatellites, was estimated using standard medical forensic indices that included the matching probability (MP), power of discrimination (PD), power of exclusion (PE), and paternity index (PI) [42].

RESULTS AND DISCUSSION

Genetic variability of 15 STR PowerPlex 16

In addition to 15 unlinked autosomal STR markers, the PowerPlex 16 system, which is intended for determining an individual's genetic profile, comprises the marker of the amelogenin gene, which is located on X and Y chromosomes and is required for sex determination. *Figure 1* shows an example of the multiplex gene typing of amelogenin and 15 satellites from the PowerPlex 16 system in one of the samples. Only the panel of microsatellite markers (15 STR) was used to perform the analysis in this study.

The results of a study of the genetic variability of these 15 STR in Russia and neighboring countries are listed in *Table 1*. The average level of intra-population genetic diversity (expected heterozygosity, H_e) of 15 STR in the populations under study was 0.796; the most variable loci ($H_e > 0.85$) – *D21S11*, *D18S51*, *PentaE*, and *FGA* – have more than 15 alleles. The highest number of alleles was found in loci *FGA* (20), *PentaE* (18), and *D18S51* (18).

Pentanucleotide microsatellites *PentaE* are characterized by the highest dispersion of the repeat number (the 18-repeat difference between the shortest and the longest alleles) and *PentaD* (17-repeat dispersion). The least polymorphic marker ($H_e = 0.612$), *TPOX*, has eight alleles. The expected heterozygosity of the remaining 10 microsatellites of the PowerPlex 16 system varies within the range $0.74 < H_e < 0.82$, the number of alleles detected varying from 8 to 12.

Distribution of alleles and genotypes over populations

In the populations consisting of 255 genotype distributions (15 loci in 17 samplings) that were studied, the deviation from the Hardy–Weinberg equilibrium (HWE) ($p < 0.05$) was detected only in 21 of them. The accumulation of deviations from the Hardy–Weinberg equilibrium was detected only in the Tomsk population (five loci out of 15). However, when introducing the Bonferroni correction for comparison multiplicity, the actual significance level for the kit consisting of 15 tests per population is equal to 0.0035; therefore, with allowance for the Bonferroni correction, only one deviation from the Hardy–Weinberg equilibrium (*FGA* locus in

Fig. 1. Multiplex genotyping of 15 microsatellites and the amelogenin locus (AMEL) in the PowerPlex 16 System by capillary electrophoresis.

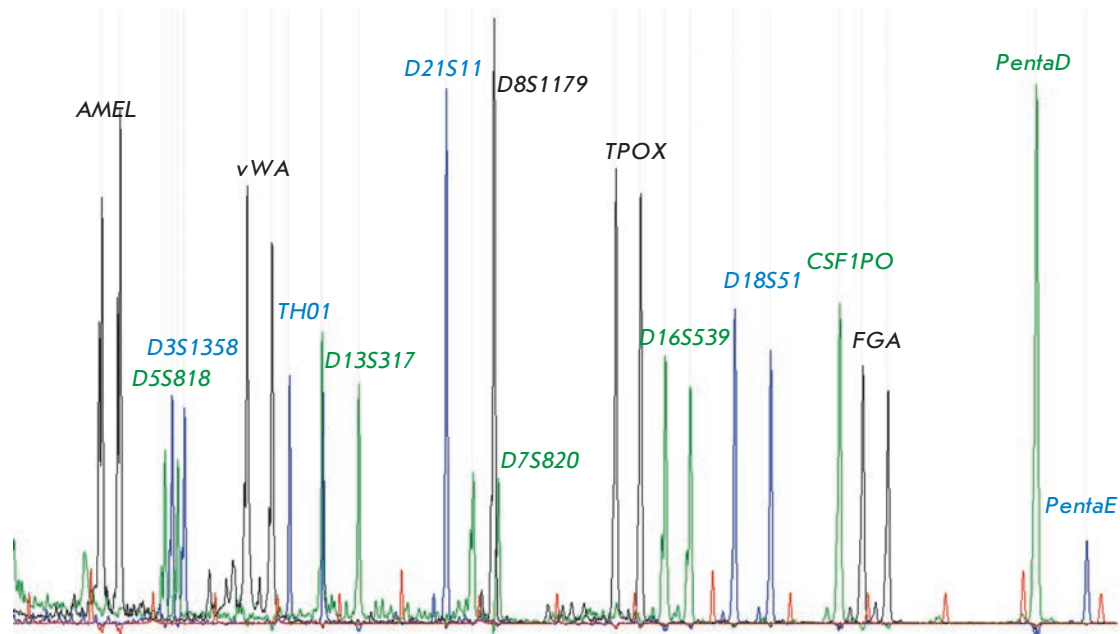


Table 1. Genetic variability of 15 STR from the PowerPlex 16 system

Locus	Expected heterozygosity	Average expected heterozygosity per population	Number of alleles	Average number of alleles per population	Dispersion of repeat numbers	Average dispersion of repeat numbers per population
<i>D3S1358</i>	0.77543	0.76634	8	5.647	7	4.765
<i>TH01</i>	0.78141	0.76693	8	5.588	6	3.588
<i>D21S11</i>	0.84974	0.84229	17	10.588	9	6.353
<i>D18S51</i>	0.87419	0.86735	18	11.882	16	11.118
<i>PentaE</i>	0.91497	0.90474	18	15.176	18	16.118
<i>D5S818</i>	0.73859	0.73546	9	6.529	8	5.941
<i>D13S317</i>	0.79676	0.78925	10	7.176	9	6.176
<i>D7S820</i>	0.80174	0.79478	12	7.471	10	6.471
<i>D16S539</i>	0.78966	0.78064	9	7.000	7	5.941
<i>CSF1PO</i>	0.73503	0.73035	8	5.882	7	5.059
<i>PentaD</i>	0.82446	0.82034	13	8.588	17	8.588
<i>vWA</i>	0.79355	0.79053	10	7.176	9	6.235
<i>D8S1179</i>	0.79676	0.79044	11	8.471	10	7.647
<i>TPOX</i>	0.61227	0.60398	8	5.294	7	4.412
<i>FGA</i>	0.85811	0.85062	20	10.941	13	8.882
Average per locus	0.79618	0.78893	11.933	8.227	10.200	7.153

the Tomsk population) turned out to be statistically significant.

An example of allele distribution in populations (*D7S820* locus in six Russian cities) is shown in *Fig. 2*. The genetic variability indices of 17 populations over 15 microsatellites are summarized in *Table 2*. All 17 populations have close degrees of genetic diversity (the average heterozygosity fluctuating within 0.771–0.803). The highest degree of genetic variability was revealed in the populations of Lezgins, Ukrainians, and Tomsk

residents; the lowest degree was revealed in the Mari, Khakas, and Orel residents.

Gene geography of genetic diversity of PowerPlex 16 markers in North Eurasia

The heterozygosity of 12 loci (*D3S1358*, *TH01*, *D21S11*, *D18S51*, *D13S317*, *D7S820*, *D16S539*, *CSF1PO*, *vWA*, *D8S1179*, *TPOX*, and *FGA*) was calculated in 51 populations of Russia and neighboring countries using both our data and the results obtained by other authors rep-

Table 2. Genetic variability (expected heterozygosity) of 17 studied populations with respect to 15 STR from the PowerPlex 16 system

Locus	Belgorod	Orel	Orenburg	Yaroslavl	Belorussians	Ukrainians	Komi	Mari	Tomsk	Khakas	Moscow	Dargins	Lezgins	Avars	Bashkir	Tatar	Chuvash
<i>D3S1358</i>	0.79434	0.77946	0.77232	0.75394	0.73459	0.79831	0.76929	0.78771	0.78909	0.68603	0.79342	0.77325	0.79535	0.77616	0.72816	0.72917	0.76712
<i>TH01</i>	0.76465	0.76024	0.78586	0.76707	0.78094	0.77249	0.74990	0.72087	0.78202	0.74157	0.75644	0.79518	0.74040	0.78384	0.78479	0.77686	0.77466
<i>D21S11</i>	0.83960	0.83460	0.85556	0.86465	0.86742	0.86777	0.85354	0.84055	0.85443	0.81528	0.85224	0.83224	0.86465	0.82020	0.79486	0.81222	0.84906
<i>D18S51</i>	0.87859	0.86469	0.87859	0.87071	0.86359	0.86551	0.87091	0.84839	0.87784	0.81938	0.88683	0.87149	0.86101	0.87273	0.86608	0.87847	0.87008
<i>PentaE</i>	0.90626	0.90390	0.90081	0.89778	0.89489	0.89926	0.90586	0.90497	0.91035	0.93258	0.90168	0.90548	0.91172	0.84869	0.92415	0.91695	0.91518
<i>D5S818</i>	0.73737	0.72898	0.73172	0.74404	0.74439	0.72419	0.73980	0.75243	0.75267	0.75956	0.71346	0.75022	0.76283	0.74465	0.69681	0.70383	0.71590
<i>D13S317</i>	0.76808	0.79616	0.80889	0.79434	0.81510	0.78100	0.78828	0.80284	0.80313	0.81332	0.77184	0.69825	0.77354	0.79960	0.79589	0.82834	0.77862
<i>D7S820</i>	0.81657	0.77985	0.75838	0.78101	0.78882	0.80208	0.80727	0.77072	0.80964	0.80928	0.79636	0.79232	0.81071	0.77273	0.81470	0.79230	0.80845
<i>D16S539</i>	0.70889	0.76471	0.76626	0.77455	0.77520	0.75109	0.76485	0.77857	0.76974	0.79615	0.77691	0.82456	0.79091	0.80444	0.81048	0.80734	0.80629
<i>CSF1PO</i>	0.73838	0.70938	0.75636	0.72970	0.73865	0.74740	0.76141	0.70874	0.73273	0.74584	0.71527	0.69737	0.67495	0.73172	0.72528	0.70440	0.73836
<i>PentaD</i>	0.82202	0.82392	0.81111	0.80869	0.83516	0.82482	0.81192	0.79593	0.83174	0.81682	0.81597	0.80855	0.85010	0.80000	0.82713	0.84677	0.81509
<i>vWA</i>	0.81212	0.77888	0.81960	0.80909	0.79312	0.80398	0.81818	0.76176	0.77623	0.76734	0.81653	0.75504	0.82525	0.81111	0.76053	0.75559	0.77466
<i>D8S1179</i>	0.74889	0.80606	0.79919	0.81899	0.80029	0.79702	0.81333	0.74571	0.79657	0.74964	0.79566	0.79298	0.79333	0.76545	0.81357	0.81358	0.78724
<i>TPOX</i>	0.64646	0.54533	0.61818	0.59879	0.55638	0.63578	0.60061	0.52502	0.62928	0.61469	0.59608	0.65175	0.74727	0.57354	0.60113	0.58231	0.54501
<i>FGA</i>	0.86586	0.81965	0.85131	0.85778	0.86168	0.85447	0.85960	0.82207	0.85388	0.83904	0.87171	0.80899	0.84909	0.84727	0.86701	0.87170	0.85948
Average per locus	0.78987	0.77972	0.79428	0.79141	0.79001	0.79501	0.79432	0.77109	0.79796	0.78043	0.79069	0.78385	0.80341	0.78347	0.78737	0.79199	0.78701

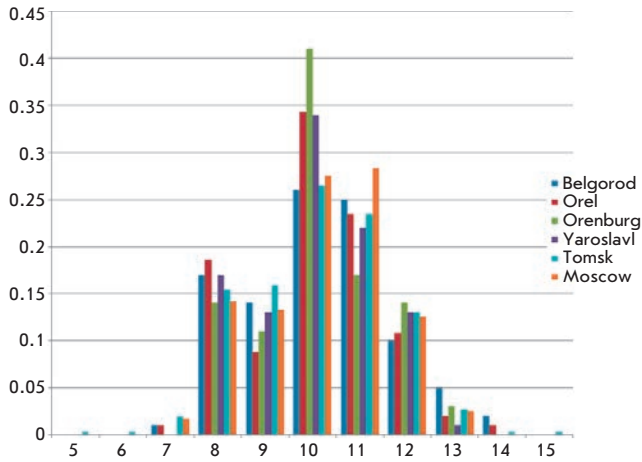


Fig. 2. Allelic distribution of the D7S20 locus in populations of six Russian cities. The X axis shows the alleles (repeat numbers), the Y axis shows the allelic frequencies (fractions of one).

resented in the database compiled by us (Fig. 3). Although all the markers contained in the PowerPlex 16 panel were selected on the basis of the maximum intra-population variability (including heterozygosity), the populations in different Russian regions differ in terms of their heterozygosity level. The map demonstrates that the maximum heterozygosity (above 79%) is observed in the populations of Western and Central Europe and in the neighboring western regions of NIS countries. The heterozygosity level decreases gradually when moving eastwards. Thus, in the European part of Russia and the Trans-Urals, it is equal to 78%; in Central Asia and Altai, approximately 77%; in the Baikal region, less than 77%. This regularity of gradual decrease in heterozygosity across the entire Eurasian continent (from the Atlantic to the Pacific coast) can be clearly traced to an appreciable degree, although separate populations may fall out of the general trend (e.g., heterozygosity in the Kostroma population abruptly decreases). In the deep south, an increase in heterozygosity to maximum values exemplified by the Pakistani population was observed.

The longitude tendency towards decreasing heterozygosity (from the west to the east of North Eurasia) that was first described in the markers of the “criminal panel” has been well-known on the basis of the con-

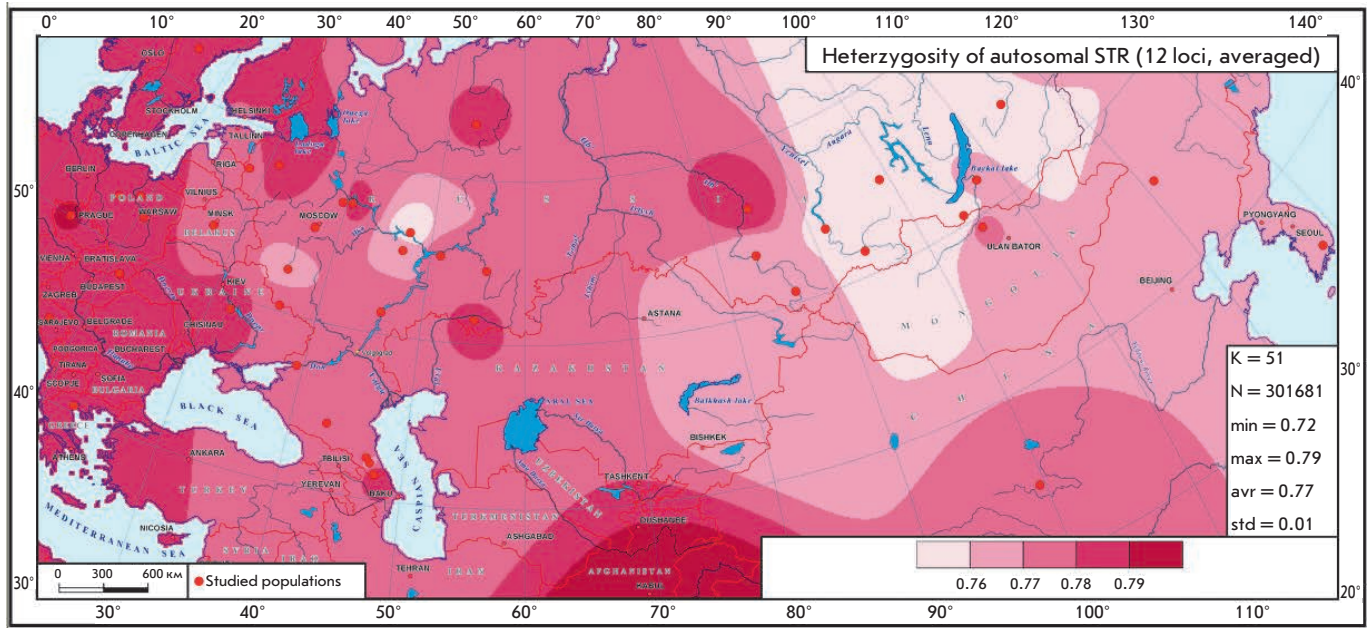


Fig. 3. Map of average heterozygosity for 12 autosomal microsatellites (*D3S1358*, *TH01*, *D21S11*, *D18S51*, *D13S317*, *D7S820*, *D16S539*, *CSF1PO*, *VWA*, *D8S1179*, *TPOX*, and *FGA*). The color saturation level corresponds to the level of average heterozygosity (exact delimiter values are indicated on the map scale). Populations are depicted by red dots. In the legend window, the following parameters are indicated: the number of reference points (K); the number of the map grid nodes (N); minimum (min), maximum (max) and average (aver) heterozygosity values, and the standard deviation (std).

ventional gene-geographic studies of the population of the USSR. Heterozygosity maps of the conventional (immunobiochemical) markers are given in [43], which also demonstrate a decrease in variability from the European part towards Siberia. The reason for the decrease in heterozygosity can be accounted for by the more intense genetic drift in the relatively small and isolated Siberian populations; whereas the effect of genetic drift in the East, and particularly in the Western part of Europe, is levelled by intense population migrations.

Genetic differentiation of populations

The analysis of the genetic differences between populations was performed by the molecular variance method (AMOVA) with account for the variation in allelic frequencies, and the dispersion of tandem repeat numbers revealed significant genetic variations between the groups of populations studied. All Russian populations, the Ukrainians, Belorussians, and Komis are characterized by a community of the gene pool with respect to the studied markers and the absence of a significant inter-population differentiation (F_{st} values compared pairwise are not higher than 0.25%). Meanwhile, the group of Slavic populations significantly differs from most of the other populations. Populations of the Volga-Ural region (the Tatars and Chuvash), as well as the Mari, have no significant genetic difference between each other; however, they differ from other ethnic groups. Two other groups that are characterized by significant differences from all the other groups are the populations from the North Caucasus (Dargins, Avars, and Lezgins), the Bashkirs, and the Khakas.

The total level of genetic differentiation of the pool consisting of 17 populations turned out to be relatively high ($F_{st} = 0.0267$, or 2.67%) and highly significant ($p > 0.00001$).

Meanwhile, the analysis inside the massif consisting of six Russian urban populations, in spite of the considerable territorial sparseness of the cities that represent the center of the European section of Russia (Moscow), its south (Belgorod, Orel), north (Yaroslavl), the Urals (Orenburg), and Siberia (Tomsk) revealed the total absence of inter-population differences between 15 microsatellites in these populations in terms of frequencies and molecular dispersion. The F_{st} value in six Russian urban populations was equal to 0.00095 ($p = 0.6187$).

Within the context of using and studying 15 STR to perform DNA identification, these data point to the possibility of using the sum frequencies over Russian megapolises when carrying out a medical forensic expertise of the urban (predominantly Russian) population. In addition, these data indicate the necessity for accounting for data on the frequencies of the “identi-

fication” markers in other ethnic groups of the Russian Federation to perform calculations in these populations.

The comparison of the frequencies of 15 STR in an aggregate sampling of the populations of Russian cities with the frequencies in Caucasian Americans supplied by Promega company [2] as the reference frequencies for the PowerPlex 16 system by an analysis of the molecular dispersion for each locus revealed reliable differences in frequencies in 12 out of the 15 microsatellite loci (Table 3).

Genetic relationships between populations: phylogenetic analysis

The tree of genetic inter-population relationships was constructed based on the matrix of pairwise genetic distances between populations with respect to the combination of the 15 STR loci obtained by AMOVA and with account for the differences in allelic frequencies and the dispersion of the tandem repeat number. The dendrogram constructed by the unweighed pair-group method with an arithmetic mean (UPGMA) in PHYLIP software is shown in Fig. 4.

The arrangement of populations on the dendrogram completely coincides with the revealed pattern of genetic differentiation in the Russian population over the DNA markers that are used for medical forensic expertise. The populations studied are grouped into four clusters, each of these clusters being characterized by a community of the gene pool of populations inside the cluster and significant differences (and large genetic

Table 3. Comparison of 15 STR frequencies for each locus in Russian urban populations and in Caucasian Americans

Locus	F_{st}	p
D3S1358	0.00169	0.02444+-0.00383
TH01	0.00238	0.00782+-0.00343
D21S11	0.00113	0.04008+-0.00603
D18S51	0.00380	0.00000+-0.00000
PentaE	0.00181	0.00196+-0.00136
D5S818	0.00091	0.13001+-0.01025
D13S317	0.00638	0.00000+-0.00000
D7S820	0.00436	0.00000+-0.00000
D16S539	0.00132	0.05963+-0.00636
CSF1PO	0.00205	0.02835+-0.00465
PentaD	0.00460	0.00000+-0.00000
vWA	0.00154	0.02639+-0.00540
D8S1179	0.00256	0.00391+-0.00185
TPOX	0.00438	0.00489+-0.00203
FGA	0.00095	0.06256+-0.00769

distances) from the populations belonging to other clusters.

The most distant cluster is formed by the Khakas and Bashkir populations, the ones with the highest proportion of the mongoloid race component. The rest of the populations are much closer to each other than they are to the Bashkirs or Khakas; however, they can also be clearly divided into three separate groups – Slavic populations (all of the Russian megapolises that were studied, Ukrainians, Belorussians) and Komis; populations of the Volga-Ural region (Chuvash, Tatar, Mari); and North Caucasus populations (Dargins and Avars). The location of the Lezgin population in a cluster with the Turk-lingual and the Uralian-lingual populations of the Volga-Ural region is a surprise. This is likely associated with random effects due to the small number of samplings.

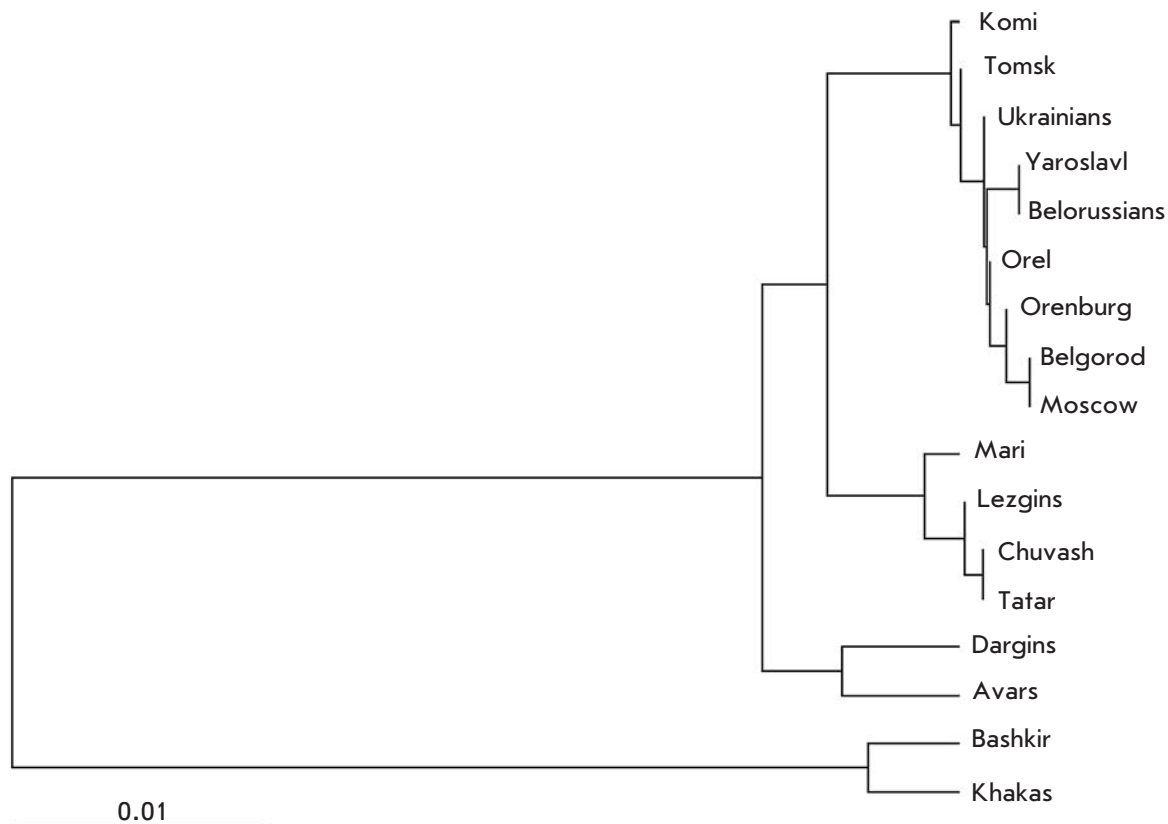
Genetic relationships between populations: multidimensional scaling

The location of the populations in the space within the first two dimensions of multidimensional scaling is shown in *Fig. 5*. The spatial distribution of a population represents the degree of similarity between the individual gene pools in the best way. It can be seen that all European populations are concentrated in the left-hand

side of the plot. The proximity of populations in the European cluster points to the unity of the gene pool of the populations studied (the Swedes, the Greeks, the Poles, the Slovaks, a number of East Slavic populations, and the Komi). Two more clusters are located in direct proximity: the population of the Volga-Ural region and the North Caucasus population. It is noteworthy that, as opposed to a phylogenetic analysis, the multidimensional scaling places the Lezgins into a cluster together with the Dargins and Avars. The Asian populations are located in the right-hand side of the plot. Here, the largest and vastest (i.e. genetically diverse) cluster was formed by the South Siberian and Central Asian populations. The populations of the extreme northwest of Siberia (the Koryak and Chukchi) stand apart and form their own cluster. Finally, the East Asian populations (the Chinese and Koreans) also form a separate cluster. It is interesting that the population of Russians who have been living in China for several generations [35] cannot be genetically differentiated from the native populations of East Asia.

A conclusion can be reasonably drawn that the panel consisting of the 12 autosomal microsatellite loci that are used in the practical activity of medical forensic experts also happens to be highly informative for fundamental studies into the gene pool. Firstly, this fact

Fig. 4. Dendrogram of the genetic distances between populations.



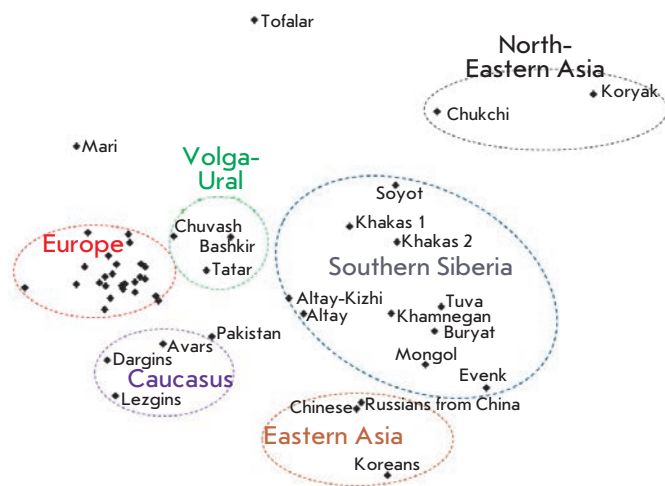


Fig. 5. Location of the first two dimensions of the multidimensional scaling of the genetic distance matrix for 51 populations (17 populations from this paper and 34 populations from earlier published data). The European cluster includes the following populations: Swedes, Greeks, Komis, Czechs, Slovaks (2 samples), Polish (3 samples), Ukrainians, Belorussians, Russians from Belgorod (2 samples), Orel (2 samples), Yaroslavl, Kostroma, Novgorod, Pskov, Mineralnye Vody, Rostov-on-Don, Saratov, Orenburg, and Tomsk.

is attested to by the consistency between the genetic clusterization of populations with respect to the markers set and the geographic (and linguistic) grouping of the same populations. Secondly, the distribution of populations within the plot space repeats their spatial distribution on the geographical map (e.g., the Koryaks and Chukchis are located in the top-right corner of the plot and in the top-right corner of the geographical map of Russia). Thirdly, the relative dimensions of the clusters correlate well with the concepts that were earlier formulated in science (e.g., decreasing heterozygosity when moving eastwards, the pronounced heterozygosity of the Siberian cluster). Let us specify that high interpopulation variability in Siberia agrees well with the low interpopulation variability (heterozygosity) of these populations (*Fig. 3*), since both features typically result from genetic drift, its intensity being higher in small and isolated Siberian populations. Another significant conclusion consists in the contrast between the homogeneity of European populations (such geographically distant from each other populations as the Swedes, Greeks, and Russians are almost indiscernible in the plot) and heterogeneity of the other regions studied. The populations of the Caucasus, Volga-Ural region, Southern Siberia, Northeastern Siberia, and East Asia have drastically different allelic frequencies.

In addition, Siberian populations differ considerably between each other.

This fact is likely to be of great practical significance, since it becomes clear in which geographic range the databases concerning the frequencies of the markers used in medical forensic expertise can be employed. Thus, the use of separate databases for native populations of the Caucasus, the Volga-Ural region, and Siberia can be recommended when calculating the probability of a random match during the identification of a person. For Siberia, an even more detailed zoning may be required. The data on the allelic frequencies in Russian populations that are presented in our study may serve as one of the most important sources of information in the compilation of these databases.

Identification potential of 15 STR in populations of Russia and neighboring countries

To assess the possibility of using the marker system under study for DNA identification in medical forensic expertise, the standard population statistic indices characterizing the identification potential of the marker system were determined. These indices include the matching probability (MP), the power of discrimination (PD), the power of exclusion (PE), and the paternity index (PI). The MP and PD indices are used in the DNA identification of a person, whereas the PE and PI indices are calculated when determining paternity. The values of these indices in certain populations, as well as those in Caucasian Americans, are listed in *Table 4*.

In general, all the populations studied had very high values of the discrimination potential of the PowerPlex 16 system. The matching probability of genotypes with respect to 15 STR markers for a total sampling of the Russian urban population was equal to 1 out of 281 000 000 000 000 000 (1 out of 281 quadrillion) individuals. In other populations, this index is slightly lower, but it still considerably exceeds all reasonable thresholds for DNA identification.

It should also be noted that the paternity indices in all populations are higher than the values set by the statutory acts prevailing on the territory of the Russian Federation by several orders of magnitude. Thus, the following levels of evidence of the expert investigation was ascertained in Section 7 of the Instruction for Organization and Production of Expert Investigations in the Bureau of Medical Forensic Expertise approved by Order of the Ministry of Healthcare of the Russian Federation no. 161 dated March 24, 2003: The Bayesian probability of paternity is at least 0.9990, and the paternity index (PI) is at least 1,000 for a case of complete trio mother-child-putative father; and the Bayesian probability is at least 0.9975, and the PI is at least 400 for a duet child-putative father.

Table 4. Identification parameters of 15 STR in certain populations

Population	Probability of genotype matching (MP)	MP recalculated for 1 out of...	Power of exclusion (PE)	Paternity index (PI)
Belgorod	1.66×10^{-16}	6.33×10^{15}	0.999998	742717
Orel	2.53×10^{-16}	3.95×10^{15}	0.9999992	1003109
Orenburg	1.06×10^{-16}	9.36×10^{15}	0.9999991	1065170
Yaroslavl	2.46×10^{-16}	4.04×10^{15}	0.9999997	3378695
Tomsk	3.44×10^{-18}	2.81×10^{17}	0.9999990	880293
Russians, in total	3.19×10^{-18}	3.12×10^{17}	0.9999989	834233
Belorussians	9.11×10^{-17}	1.08×10^{16}	0.999997	284297
Ukrainians	6.34×10^{-18}	1.56×10^{17}	0.9999995	1834277
Komi	5.60×10^{-17}	1.73×10^{16}	0.999998	451441
Mari	3.28×10^{-16}	3.04×10^{15}	0.99998	46918
Khakas	7.42×10^{-17}	1.37×10^{16}	0.99991	192783
Caucasian Americans		1.83×10^{17}	0.9999994	1520000

The resulting indices of informativeness of the 15 STR for DNA identification in a medical forensic expertise for the Russian and Ukrainian populations either exceed those of U.S. Caucasian Americans or are very close to them (the reference data provided by Promega company). In other ethnic groups of Russia, these indices are somewhat lower either due to the smaller volume of the samplings or due to the features of their population-genetic structure, but in any case they remain very highly informative.

RusDNAid DNA Identification Database

Primary data on the allelic frequencies of 15 microsatellite loci from the PowerPlex 16 system in 17 populations within Russia and neighboring countries are represented in the RusDNAid database designed by us. The database is hosted online on the websites of the Institute of Medical Genetics, Siberian Branch of the Russian Academy of Medical Sciences (<http://www.medgenetics.ru/web-resources/pp16-rus/>) and the Vavilov Institute of General Genetics, Russian Academy of Sciences (www.vigg.ru/info/data_bases/human/DNAid). The frequencies mentioned can be used as reference frequencies (for the corresponding population or ethnic group) in order to calculate identification probabilities for a genetic expertise, including the identification of a person, establishment of paternity, etc. Moreover, these data can be used in comparative population genetic studies.

CONCLUSIONS

Estimates of the genetic variability of microsatellite loci, which are used for DNA identifications that com-

ply with the international standards for such studies, were obtained for the first time in this study for the population of Russia and neighboring countries. The informativeness and resolution capacity of the full panel of STR loci was first estimated, and the reference allelic frequencies for Russian urban populations, certain ethnic groups of the Russian Federation, and neighboring countries were obtained.

The identification indices of the systems used for DNA identification based on the CODIS international standard comprising 13 STR loci, or its extended version consisting of 15 STR, that make up the PowerPlex 16 system (the reference allelic frequencies and indices of the identification capacity of gene typing systems) were estimated for most of the populations of European countries, the USA, Japan, and a number of other countries. These reference databases underlie the performance of the national services of medical forensic expertise. In Russia, until recently, there was no reference database on the locus contained in the standard identification panels. The results of the present study allow to fill this gap and offer a possibility to align the standards of personality typing with international practice.

The spatial organization of genetic diversity, which was revealed by a gene-geographic method, phylogenetic analysis and multidimensional scaling on the basis of the panel of STR markers used for DNA identification, demonstrates the general regularity of the geographic clusterization of human populations on the basis of different types of genetic markers, from the conventional protein polymorphism to full-genomic SNP sets (e.g., see [22]); it shows a considerable tenden-

cy within the gene pool of the Russian population and neighboring countries towards subdivision and the necessity to account for a population's genetic structure when performing medical forensic investigations and the DNA identification of persons in criminal cases. ●

The authors are grateful to Promega company for providing the PowerPlex 16 systems. This work was supported by the Russian Foundation for Basic Research (grants № 07-04-01749, 09-04-00143, 10-04-01603, 10-06-00451, and 11-04-01867),

the Federal Special-Purpose Program "Research and Developments on Priority Directions of the Development of the Science and Technology Complex of Russia for 2007–2011" (Government contract № 16.512.11.2033), the Federal Special-Purpose Program Scientific and Educational Specialists of Innovation Russia" (Government contracts № P321 and 02.740.11.0284), and the Program of Fundamental Research of the RAS Presidium "Molecular and Cell Biology".

REFERENCES

- Gill P., Fereday L., Morling N., Schneider P.M. // *Forensic Sci. Int.* 2006. V. 156. P. 242–244.
- www.promega.com
- Rowold D.J., Herrera R.J. // *Forensic Sci. Int.* 2005. V. 151. P. 59–69.
- Human Identification: The use of DNA markers / Ed. B. Weir. London: Kluwer Acad. Publ., 1995.
- Biesecker L.G., Bailey-Wilson J.E., Ballantyne J. // *Science.* 2005. V. 310. P. 1122–1123.
- Lincoln P., Carracedo A. // *Forensic Sci. Int.* 2000. V. 110. P. 3–5.
- Budowle B., Shea B., Niezgodna S., Chakraborty R. // *J. Forensic Sci.* 2001. V. 46. P. 453–489.
- Lessig R., Willuweit S., Krawczak M. // *Leg. Med. (Tokyo).* 2003. V. 5 Suppl 1. P. 160–163.
- Budowle B., Moretti T.R., Baumstark A.L., Defenbaugh D.A., Keys K.M. // *J. Forensic Sci.* 1999. V. 44. P. 1277–1286.
- Borys S., Vanstone H., Carmody G., Fournery R. // *J. Forensic Sci.* 2000. V. 45. P. 945–946.
- Kuperschmid T., Calicchio T., Budowle B. // *J. Forensic Sci.* 1999. V. 44. P. 392–395.
- Gehrig C., Hochmeister M., Borer U.V., Dirnhofer R., Budowle B. // *J. Forensic Sci.* 1999. V. 44. P. 1035–1038.
- Borys S., Iwamoto R., Miyakoshi J., Carmody G., Fournery R. // *J. Forensic Sci.* 1999. V. 44. P. 1319.
- Bhoopat T., Leaungsiyakul T., Steger H.F. // *Leg. Med. (Tokyo).* 2006. V. 8. P. 198–200.
- Zhivotovsky L.A., Akhmetova V.L., Fedorova S.A., Zhirkova V.V., Khusnutdinova E.K. // *Forensic Sci. Int. Genet.* 2009. V. 3. P. E111–116.
- Malyarchuk A.B., Wozniak M., Czarny J., Derevenko M.B., Grzybowski T., Miscicka-Sliwka D. // *Mol. Biol. (Moscow).* 2007. V. 41. № 1. P. 1–4.
- Shorokhova D.A., Stepanov V.A., Udovenko Y.D., Novoselov V.P., Puzyrev V.P. // *Mol. Biol. (Moscow).* 2005. V. 39. № 6. P. 845–850.
- Stepanov V.A., Melnikov A.V., Lash-Zavada A.Y., Kharkov V.N., Borinskaya S.A., Tyazhelova T.V., Zhukova O.V., Schneider Y.V., Shil'nikova I.N., Puzyrev V.P., Rybakova A.A., Yankovsky N.K. // *Leg. Med.* 2010. V. 12. № 5. P. 256–258.
- Stepanov V.A. *Etnogenomika naselenia Severnoi Evrazii (Ethnogenomics of North Eurasian Population)*. Tomsk: Pechatnaya Manufactura, 2002. 244 p.
- Balanovska E.V., Balanovsky O.P. *Russkiy genofond na russkoy ravnine (Russian Gene Pool on the Russian Plain)*. Moscow: Luch, 2007. 416 p.
- Khusnutdinova E.K. *Molekulyarnaya genetika narodov Volgo-Uralskogo regiona (Molecular Genetics of the Volga-Ural Populations)*. Ufa: Gilem, 1999. 238 p.
- Stepanov V.A. // *Acta Naturae.* 2010. V. 2. № 4 (7). C. 15–30.
- Guo S., Thompson E. // *Biometrics.* 1992. V. 48. P. 361–372.
- Excoffier L., Laval G., Schneider S. // *Evolutionary Bioinformatics Online.* 2005. V. 1. P. 47–50.
- Konjhodžić R., Kubat M., Škavić J. // *Int. J. Leg. Med.* 2004. V. 118. P. 119–121.
- Jakovski Z., Nikolova K., Furac I., Masic M., Janeska B., Kubat M. // *Int. J. Leg. Med.* 2006. V. 120. P. 53–55.
- Liao G., Liu T., Ying B., Sun L., Zou Y., Wang Z., Fan H., Wen F. // *J. Forensic Sci.* 2008. V. 53. № 1. P. 252–253.
- Jacewicz R., Jedrzejczyk M., Ludwikowska M., Berent J. // *Forensic Sci. Int. Genet.* 2008. V. 2. № 1. P. 1–3.
- Kovatsi L., Parsons T.J., Just R.S., Irwin J.A. // *Forensic Sci. Int.* 2006. V. 159. P. 61–63.
- Montelius K., Karlsson A.O., Holmlund G. // *Forensic Sci. Int. Genet.* 2008. V. 2. № 3. P. 49–52.
- Piatek J., Jacewicz R., Ossowski A., Parafiniuk M., Berent J. // *Forensic Sci. Int. Genet.* 2008. V. 2. № 3. P. 41–43.
- Rebała K., Wysocka J., Kapińska E., Cybulska L., Mikulich A.I., Tsybovsky I.S., Szczerkowska Z. // *Forensic Sci. Int.* 2007. V. 173. № 2–3. P. 235–237.
- Soták M., Petrejčíková E., Bernasovská J., Bernasovský I., Sivicová A., Boronová I., Svicková P., Bôžiková A., Gabriková D. // *Forensic Sci. Int. Genet.* 2008. V. 3. № 1. P. 21–25.
- Szczerkowska Z., Kapińska E., Wysocka J., Cybulska L. // *Forensic Sci. Int.* 2004. V. 11. № 144(1). P. 69–71.
- Zhu B.F., Yang G., Shen C.M., Qin H.X., Fan S.L., Deng L.B., Chen F., Chen L.P., Wang H.D., Wang Z.Y., Lucas R., Lian Z.M. // *Mol. Biol. Rep.* 2010. V. 37. P. 3889–3895.
- Zhivotovsky L.A., Malyarchuk B.A., Derenko M.V., Wozniak M., Grzybowski T. // *Forensic Sci. Int. Genet.* 2009. V. 3. № 4. P. 111–116.
- Simková H., Faltus V., Marvan R., Pexa T., Stenzl V., Brouček J., Horínek A., Mazura I., Zvárová J. // *Forensic Sci. Int. Genet.* 2009. V. 4. № 1. P. 15–17.
- Soták M., Petrejčíková E., Bôžiková A., Bernasovská J., Bernasovský I., Svičková A., Boroňová I., Svičková P., Gabriková D., Mačeková S., Carnogorská J., Rębała K., Vlček D. // *Forensic Sci. Int. Genet.* 2010. V. 5. P. e53–62.
- Rakha A., Yu B., Hadi S., Sheng-Bin L. // *Leg. Med.* 2009. V. 11. № 6. P. 305–307.
- Nei M. *Molecular Population Genetics and Evolution*. Amsterdam: North-Holland Publ. Co., 1975. 290 p.
- StatSoft, Inc. 2001. STATISTICA (data analysis software system), version 6. www.statsoft.com.
- Powerstats Version 1.2, Promega Corporation.
- Rychkov Y.G., Balanovska E.V. // *Genetika.* 1992. V.28. P. 52–75.

N-Terminal Moiety of Antimicrobial Peptide Ltc1-K Increases its Toxicity for Eukaryotic Cells

O. V. Samsonova^{1,2}, K. S. Kudryashova¹, A. V. Feofanov^{1,2*}

¹Biological Faculty, Lomonosov Moscow State University

²Shemyakin and Ovchinnikov Institute of Bioorganic Chemistry, Russian Academy of Sciences

*E-mail: avfeofanov@yandex.ru

Received 11.02.2011

ABSTRACT The antimicrobial peptide Ltc1-K and its derivatives without one, two, then three N-terminal amino acid residues were studied based on the hypothesis (backed by some experimental data) that the hydrophobic N-terminal moiety of linear cationic antimicrobial peptides defines their haemolytic activity. It was discovered that the excision of three N-terminal amino acid residues considerably decreases the peptide's toxicity for eukaryotic cells and simultaneously increases the selectivity of antibacterial activity for some bacteria species. Studies performed with the model membrane systems and human erythrocytes revealed that the main reason for the observed effect is a multifold decrease in the peptide's affinity to an eukaryotic cellular membrane enriched with zwitterionic phospholipids.

KEYWORDS antimicrobial peptides; laticin; haemolytic activity; circular dichroism; fluorescent confocal microscopy

ABBREVIATIONS AMP – antimicrobial peptides; LSCM – laser scanning confocal microscopy; CD – circular dichroism; NMR – nuclear magnetic resonance; LML – large monolamellar liposomes; DOPC – 1,2-dioleoyl-sn-glycero-3-phosphocholine; LMPC – 1-myristoyl-2-hydroxy-sn-glycero-3-phosphocholine; CF – carboxyfluorescein; FD70 and FD500 – fluorescein-labelled dextrans of 70 kDa and 500 kDa, respectively; EC_{50} – peptide concentration required for 50% haemolysis or cell death; MIC – minimal inhibitory concentration; K_d – dissociation constant

INTRODUCTION

Antimicrobial peptides (AMP) are natural substances that vary in structure and biological functions. They possess in common the capability of inhibiting the vital activity of pathogenic microorganisms. Endogenous AMPs are considered to be one of the key factors (and simultaneously an evolutionarily ancient one) of the innate immunity of multicellular organisms, which enables them to be regarded as prototypes for a new generation of antibiotics [1–3]. The search for new AMPs and the detailed study of the existing ones is stimulated by the development of resistance to conventional antibiotics in microorganisms and by the capability of many AMPs to overcome this resistance.

A new group of AMPs consisting of seven short cationic linear peptides – laticins – have recently been isolated from the poison of the Central Asian spider *Lachesana tarabaevi* and characterized [4]. Laticins Ltc1, Ltc2, and Ltc5, which are similar to a number of other AMPs, along with moderate haemolytic activity, display high antibacterial activity [4]. AMPs are regarded as an alternative to existing antibiotics: therefore, their cytotoxicity with respect to human cells is unde-

sirable. The structural determinants of the cytotoxicity of AMPs have been revealed both from the research and practical perspectives. One of such structural elements was identified in linear α -helix AMPs [5]. It was ascertained that the hydrophobic N-terminal fragment enhances the haemolytic activity of these peptides, based on the structural and functional analysis of a large number of α -helix AMPs. Using the example of laticins Ltc2a and Ltc5, it was demonstrated that the activity of AMPs with respect to eukaryotic cells can be reduced via the removal of their N-terminal fragment or via point amino acid replacements that decrease their hydrophobic potential [5].

We follow this direction and present the results of an investigation into the properties of AMP Ltc1-K (Table 1), which corresponds to the non-processed form of laticin Ltc1 with an additional lysine residue on the C-terminus. In terms of haemolytic activity and bactericidal effect with respect to *Escherichia coli* and *Bacillus subtilis*, Ltc1-K does not differ from mature Ltc1 [6]. It was demonstrated by NMR that when Ltc1-K binds to sodium dodecylsulfate micelles (the simplest membrane-imitating model), the N-terminal fragment

Table 1. Amino acid sequences of Ltc1-K and its derivatives

Peptide	Amino acid sequence
Ltc1-K	SMWSGMWRRKLLKLRNALKKKLGKEK
(-1)Ltc1-K	MWSGMWRRKLLKLRNALKKKLGKEK
(-2)Ltc1-K	WSGMWRRKLLKLRNALKKKLGKEK
(-3)Ltc1-K	SGMWRRKLLKLRNALKKKLGKEK

of the α -helix peptide is embedded into the hydrophobic region of a micelle [7]. Taking into account the NMR data [7] and structural and functional analysis [5], we assumed that the N-terminal fragment enhances the binding of Ltc1-K to the membranes consisting of zwitterionic lipids and determines the cytotoxic activity of a peptide. Three Ltc1-K analogues shortened from the N-terminus by one, two, and then three amino acid residues (*Table 1*) were synthesized in order to verify this hypothesis. The comparative analysis of their structures, activity, and features of haemolytic action was performed.

EXPERIMENTAL

Reagents

The following reagents were used in this study: 1,2-dioleoyl-*sn*-glycero-3-phosphocholine (DOPC) and 1-myristoyl-2-hydroxy-*sn*-glycero-3-phosphocholine (LMPC) (Avanti Polar Lipids, United States); Mueller – Hinton broth, carboxyfluorescein (CF), fluorescein-labelled dextrans with molecular weight 70 and 500 kDa (FD70 and FD500), fluorescent dyes FM1-43, propidium iodide, and Hoechst 33342 (Sigma Aldrich, United States); culture medium Roswell Park Memorial Institute 1640 (RPMI-1640) purchased from PanEco (Russia); and heparin (Sintez, Russia). The remaining reagents were of special purity grade.

The peptides (*Table 1*) were synthesized by solid phase synthesis in the Peptide Synthesis Laboratory of the Institute of Bioorganic Chemistry of the Russian Academy of Sciences (Moscow) (team leader N.S. Egorova) and characterized by HPLC and mass spectrometry (MALDI-MS) as described earlier [4, 6]. Peptide concentrations in aqueous solutions were determined on the basis of UV absorption using a SF-256 spectrophotometer (LOMO, Russia) and the molar extinction coefficients $5500 \text{ M}^{-1}\text{cm}^{-1}$ for (-3)Ltc1-K and $11000 \text{ M}^{-1}\text{cm}^{-1}$ for Ltc1-K, (-1)Ltc1-K, and (-2)Ltc1-K at a wavelength of 280 nm.

Recording and analysis of the circular dichroism (CD) spectra

The CD spectra of the peptides were recorded in a phosphate buffered saline (110 mM NaCl, 50 mM NaH_2PO_4 ,

pH 7.4) and in LMPC micelles (30 mM with respect to lipid) in a phosphate-buffered saline at a peptide concentration of $40 \mu\text{M}$, using a Jasco J-810 spectropolarimeter (Jasco, Japan). In order to attain an equilibrium distribution of the peptide over the micelles, LMPC-containing samples were pre-incubated for 30 min at a temperature of 25°C . The spectra were recorded within a range from 190 to 250 nm with a 0.2 nm increment (the slit spectral width being 1 nm). A sample was placed into a cell with a detachable window (Hellma, Germany) with an optical path length of 0.01 cm. The secondary structures of the peptides were calculated on the basis of the CD spectra using CONTILL software [8]. The calculation results were averaged on the basis of two independent experiments.

Preparation of erythrocyte suspension

The donor's capillary blood (100–150 μl) was mixed with a RPMI-1640 medium containing heparin (10 u/ml). The cells were precipitated by centrifugation for 2 min at 300 g; the precipitate was re-suspended in a heparin-free medium until a final erythrocyte concentration of $2 \times 10^7 \text{ CFU/ml}$ was attained. All experiments were carried out during 2–3 h after blood sampling.

Analysis of haemolytic activity

The erythrocyte suspension was mixed at an equivalent ratio with a peptide that was preliminarily diluted by RPMI-1640 to the desired concentration, in order to ascertain the haemolytic activity of peptides; the mixture was then incubated for 1 h (37°C) under constant stirring (140 rpm). Fetal bovine serum (8%) was either added or not added to the mixture. The cells were then precipitated by centrifugation (1200 g, 5 min), and supernatant was taken. The haemoglobin release from erythrocytes was estimated on the basis of the optical density of supernatant at a wavelength of 414 nm, measured on a photometric plate reader Uniplan (PICON Russia). The haemolysis degree was calculated using the following formula:

$$\text{HC}_{\%} = (\text{OD}_e - \text{OD}_0) / (\text{OD}_{100} - \text{OD}_0) \times 100\%, \quad (1)$$

where OD_e , OD_0 , and OD_{100} are the optical densities (414 nm) of supernatants obtained from the sample under study, from the control cells and the totally lysed cells, respectively. For total lysis of erythrocytes, the RPMI-1640 medium was substituted for deionised water. The results of two independent experiments, with measurements repeated thrice in each of them, were averaged. The equivalent amount of a peptide-free medium was added to the control cells. The concentration dependence of haemolysis was approximated by the

sigmoid dependence equation; the peptide concentration that caused a 50% release of haemoglobin from erythrocytes (HC_{50}) was determined.

Analysis of cytotoxicity

Human erythromyeloid leukemia K562 cells were cultured (5% CO_2 , 37°C) in a RPMI-1640 medium with 8% fetal bovine serum and L-glutamine (2 mM). The cytotoxicity of peptides was determined as described earlier [9]. The cells were incubated for 3 h (5% CO_2 , 37°C) in a medium containing the peptides under study in serial dilutions (from 0.1 to 100 μM). Then, propidium iodide (10 μM) and Hoechst 33342 (10 μM) were introduced into the medium; after 10 min, the state of the cells was analyzed using an Axiovert 200M fluorescence microscope (Carl Zeiss, Germany). The cells stained only with Hoechst 33342 were considered to be living, whereas the cells stained with Hoechst 33342 and propidium iodide were regarded as dead. At least 500–1,000 cells were analyzed for each peptide concentration. The results of two independent experiments were averaged. The equivalent amount of the peptide-free medium was added to the control cells. The concentration dependence of cytotoxicity was approximated by the sigmoid curve, and the peptide concentration causing the death of 50% of cells (EC_{50}) was determined.

Analysis of antibacterial activity

Cells from *E. coli* C600, *Micrococcus luteus* Ac-2230 VKM, and *B. subtilis* B-501 VKM were cultured in a Mueller–Hinton broth (37°C). The anti-bacterial activity of the peptides was measured using the method of serial dilution in a liquid medium as described earlier [9]. The bacterial suspension (10^5 CFU/ml) was incubated in the Mueller–Hinton broth in the presence of serial dilutions of peptides for 24 h at 37°C. The absence of bacterial reproduction served as the criterion of peptide activity; the reproduction was detected by comparing the optical density (595 nm) of the bacterial culture in the presence of the peptide with that in the control using the photometric plate reader Uniplan (PICON Russia). The results of two independent experiments, the measurements being repeated thrice in each of them, were averaged. The equivalent amount of the peptide-free medium was added to the control cells. The activity was characterized by the minimum inhibitory concentration (MIC) value.

Preparation of large monolamellar liposomes (LML)

A weighed portion of DOPC was hydrated in a phosphate buffered saline solution (110 mM NaCl, 50 mM NaH_2PO_4 , pH 7.4) for 2 h at 25°C upon vigorous shaking. The suspension of multilamellar liposomes with DOPC at a concentration of 10 mM was obtained by the

freeze–thaw method in liquid nitrogen (10 cycles). An LML with a diameter of 100 nm was prepared by extrusion of the multilamellar liposome suspension through a polycarbonate filter with a 100-nm-pore diameter (Whatman, Great Britain) according to the recommendations of the manufacturer of the mini-extruder (Avanti Polar Lipids, United States).

Studying the interaction between peptides and DOPC liposomes

The level of binding to the lipid bilayer was assessed on the basis of the short-wavelength shift of the fluorescence spectrum of Trp residues within the peptides as the side chain of Trp transferred from the polar environment into a hydrophobic one. The fluorescence spectra were recorded on an LS 55 spectrofluorimeter (Perkin Elmer, Great Britain) at 25°C. Fluorescence was excited at 270 nm, and the emission spectrum was registered within a range from 300 to 500 nm with a measurement increment of 0.5 nm. In order to reduce the distortions of the spectra due to light scattering on liposomes, a quartz cell with a 10×2 mm cross-section was used when recording the fluorescence of a thin layer of the sample (2 mm).

The samples contained 2 μM of peptide and 0.1–0.5 mM of DOPC in the form of LML in the phosphate buffered saline. The recorded spectra were analyzed in LabSpec2.0 software (Dilor, France). The mathematical procedure of representing the experimental spectrum as a sum of two spectra (a peptide in the aqueous environment and a peptide totally bound to lipids) was used with the corresponding weight coefficients in order to calculate the ratio between the bound and unbound forms of the peptide. The suspension of zwitterionic LMPC micelles (20 mM lipid) was used to measure the spectrum of the peptide that was completely bound to the lipids. The complete binding of peptides to the LMPC micelles was confirmed by the CD method based on the dependence of formation of the α -helix conformation of peptides on micelle concentration.

The dissociation constant (K_d) was determined according to the earlier described procedure [10], based on the data averaged in two independent experiments, using the following formula:

$$C_M/L = 1/K_d \times C_{buf}, \quad (2)$$

where C_{buf} is the concentration of the unbound peptide in the solution and C_M/L is the concentration of the membrane-bound peptide reduced to lipid concentration.

It should be noted that at a DOPC concentration higher than 1 mM, the intensity of the fluorescence recorded decreases due to light scattering, which results

in the underestimation of the C_M and C_{buf} values under determination. However, this fact has no effect on the calculated ratio C_M/C_{buf} , which is used to determine K_d .

Microscopic studies

When studying the peptide-induced morphological changes in erythrocytes in the RPMI-1640 medium, equal volumes of the erythrocyte solution (6×10^6 CFU/ml) and peptide solution were mixed, ensuring equi-effective concentrations of Ltc1-K and (-3)Ltc1-K (the final concentration in the sample was $4 \mu\text{M}$ Ltc1-K or $30 \mu\text{M}$ (-3)Ltc1-K); CF ($20 \mu\text{M}$) was also added. The sample was placed into a 12-well chamber flexiPERM (Perbio, Belgium) with a 0.17-mm-thick glass bottom, centrifugated for 1 min at 250 rpm to deposit the cells onto the glass, and transferred under a microscope for analysis.

The erythrocytes, at a concentration of 10^7 CFU/ml, were incubated in the presence of equi-effective concentrations of Ltc1-K ($2 \mu\text{M}$) or (-3)Ltc1-K ($15 \mu\text{M}$) in the RPMI-1640 medium for 20 min at 37°C in order to obtain ghosts. Membrane permeability markers (CF, FD70 or FD500) at a concentration of $20 \mu\text{M}$ and FM1-43 ($0.9 \mu\text{M}$) staining the plasma membrane were then added. The incubation of the samples was continued for an additional 1 h at 37°C . The samples were then analyzed analytically.

An LSM 510 Meta laser scanning confocal microscope (Carl Zeiss, Germany) with a C-Apochromat $63\times/1.2$ W objective was utilized. The measurements were performed with a lateral resolution of $0.3 \mu\text{M}$ and an axial resolution of $0.6 \mu\text{M}$. The fluorophores were excited by an Ar⁺ laser with wavelengths of 458 nm (FM1-43) and 488 nm (CF, FD70, and FD500). The fluorescence was recorded by isolating the desired spectral range using a band-pass filter at 505–550 nm (CF, FD70, and FD500) and a long-wave barrier filter with the boundary set at 585 nm (FM1-43). The transmitted light images of cells were recorded simultaneously with the fluorescence images.

When studying the dynamics of the processes, 100 repeated measurements were performed with an increment of 2 s.

The images were processed using the ImageJ software (National Institute of Health, United States). The extent of influx (A) of the membrane permeability markers (CF, FD70, FD500) inside an erythrocyte (%) was calculated using the following formula:

$$A = (F_{in} - F_0)/(F_{out} - F_0) \times 100, \quad (3)$$

where F_{in} is the average fluorescence intensity inside the ghost, F_{out} is the average fluorescence intensity of

the medium around the cells, and F_0 is the background signal inside the intact erythrocytes. The extent of influx was averaged with respect to 100–150 cells.

RESULTS AND DISCUSSION

Biological activities of peptides

The abilities of laticin Ltc1-K and its derivatives (Table 1) to lyse erythrocytes and human erythromyeloid leukemia cells and inhibit *in vitro* bacterial growth (Table 2) were compared in order to assess the effect of the N-terminal fragment on haemolytic, cytotoxic, and antibacterial activities.

The excision of one to three N-terminal amino acid residues had no effect on the capability of the peptides to inhibit the growth of the gram-positive bacteria *B. subtilis*. The activity with respect to gram-negative *E. coli* and gram-positive *M. luteus* decreased considerably only for (-3)Ltc1-K. No interrelation between the change in the range of activity of Ltc1-K upon excision of the N-terminal fragment and the morphological or tinctorial properties of the bacteria was established: the activity decreased not only with respect to gram-negative *E. coli* bacilli, but also for gram-positive cocci *M. luteus*, which have no lipopolysaccharide core. Meanwhile, the sensitivity of the gram-positive bacilli *B. subtilis* remained at the same level. It can be assumed that the decrease in activity observed is to a large extent associated with the features of interaction between the peptides and the plasma membrane of certain types of bacteria.

Peptide-mediated permeabilization of the bacterial membrane is considered to be the most probable mechanism of antibacterial effect of Ltc1-K and its analogues, as well as that of other cationic AMPs. The data on the ability of the peptides studied to induce defects in the erythrocyte membrane indirectly attest to this fact. Permeabilization of the bacterial membrane can occur either by formation of toroidal lipid-peptide pores or by the so-called “carpet” mechanism, which causes detergent-like damage to the membrane [11]. In the former case, the excision of the hydrophobic N-terminal fragment is more likely to reduce the ability of the peptide to weave into the hydrophobic membrane region and initiate the formation of lipid-peptide pores. In the latter case, the excision of the N-terminal fragment will have a smaller effect on the efficacy of membrane damage. In both cases, the initial binding of a peptide to the membrane is determined by electrostatic interactions between the cationic amino acid residues and anionic lipids, in which the bacterial membrane is enriched. In addition, the excision of the N-terminal fragment of Ltc1-K does not affect the electrostatic interactions.

Table 2. Characteristics of interaction of Ltc1-K and its derivatives with erythrocytes, K562 cells, bacteria and DOPC-liposomes

Peptide	Eukaryotic cells		Bacteria			DOPC-liposomes
	Erythrocytes HC ₅₀ , μM	K562 EC ₅₀ , μM	<i>E. coli</i> MIC, μM	<i>B. subtilis</i> MIC, μM	<i>M. luteus</i> MIC, μM	K _d , mM
Ltc1-K	1.1 ± 0.1	7.1 ± 0.4	1.3 ± 0.3	0.7 ± 0.2	1.1 ± 0.3	1.4 ± 0.5
(-1)Ltc1-K	0.8 ± 0.1	4.9 ± 0.2	2.6 ± 0.6	0.7 ± 0.2	2.7 ± 0.6	1.4 ± 0.7
(-2)Ltc1-K	1.3 ± 0.1	11 ± 1	2.6 ± 0.6	0.7 ± 0.2	2.9 ± 0.6	1.7 ± 0.6
(-3)Ltc1-K	8.0 ± 2.0	39 ± 5	6.5 ± 1.6	0.7 ± 0.2	5.6 ± 0.9	15 ± 3

Note. HC₅₀ – peptide concentration resulting in haemolysis of 50% of erythrocytes. EC₅₀ – peptide concentration resulting in death of 50% of cells. MIC – the minimum inhibitory concentration inhibiting the growth of a microorganism in a liquid nutrient medium. K_d – dissociation constant of peptide complexes with DOPC-liposomes.

Specific mechanisms of defect formation in the membrane of different types of bacteria may depend on the composition and rigidity of the membrane. Hence, the activity of (-3)Ltc1-K with respect to *E. coli* and *M. luteus* (lower than that of Ltc1-K) may imply the permeabilization of the membrane of these bacteria via the mechanism of formation of toroidal lipid-peptide pores, whereas a detergent-like damage to the membrane should be assumed in the case of *B. subtilis*. The experimental verification of this hypothesis requires a specific long-term study and lies beyond the scope of the present article.

No considerable differences in the haemolytic activity of Ltc1-K, (-1)Ltc1-K, and (-2)Ltc1-K has been detected, whereas the activity of (-3)Ltc1-K decreased by a factor of 7 (Table 2). A similar regularity was revealed during the analysis of the cytotoxicity of peptides with respect to K562 cells (Table 2). Let us note that, for convenience, haemolysis of erythrocytes by the peptides was compared in a medium containing no serum; its presence (same as the presence of blood plasma) protects erythrocytes and reduces the haemolytic activity of peptides down to moderate values. Thus, in the presence of 8% of fetal bovine serum, the HC₅₀ values for Ltc1-K, (-1)Ltc1-K, and (-2)Ltc1-K are 28, 67, and 58 μM, respectively. Attempts at measuring HC₅₀ for (-3)Ltc1-K over the available concentration range were unsuccessful (Fig. 1).

By comparison, HC₅₀ of mellitin from the poison of *Apis mellifera*, which belongs to the highly active haemolytic peptides, in the presence of 8% of serum is 0.3 μM (the data are not given), whereas HC₅₀ of the earlier studied laticins Ltc2a and Ltc5 are 6 and 12 μM, respectively [5]. The cytotoxicity (EC₅₀) of Ltc2a and Ltc5 for K562 cells is 3 and 12 μM [5]. The haemolytic activity of Ltc1-K is noticeably less than that of

Ltc2a, Ltc5, and mellitin, but it is comparable with the activity of other laticins with respect to K562 cells. The excision of the N-terminal fragment is accompanied by a multifold decrease in the cytotoxicity and haemolytic activity of Ltc2a, Ltc5 [5], and Ltc1-K. Thus, the resulting data (Table 2) lend support to the earlier conclusions [5] that the haemolytic and cytotoxic activities of α-helix AMPs are enhanced by the hydrophobic potential of the N-terminal fragment. In the case of Ltc1-K, the considerable decrease in membrane-lytic

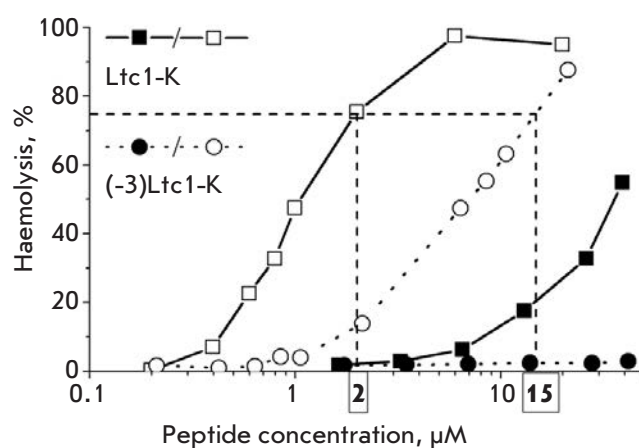


Fig. 1. Concentration dependence of the haemolytic effects of Ltc1-K and (-3)Ltc1-K. Open symbols correspond to erythrocyte treatment with peptides in a serum-free medium, closed symbols correspond to erythrocyte treatment with peptides in a medium complemented with a 8% fetal bovine serum. Each line is a best fit of the experimental data with a Hill function. Vertical dashed lines indicate the equi-effective Ltc1-K and (-3)Ltc1-K concentrations that were used in subsequent experiments.

activity is attained after the N-terminal hydrophobic residue Trp3 is removed.

The features of interaction of Ltc1-K and its derivatives with the erythrocytes and lipid systems (DOPC-liposomes, LMPC micelles) that simulate the membrane of eukaryotic cells were studied in order to establish the reasons for the reduction in toxicity.

Comparative analysis of peptide affinity to DOPC-liposomes

Assuming that the toxicity with respect to eukaryotic cells depends on the peptide affinity towards the zwitterionic lipids dominant within the plasma membrane, we measured the dissociation constants (K_d) of the complexes of Ltc1-K and its derivatives with DOPC-liposomes.

The results of the analysis of peptide binding to liposomes are represented in *Fig. 2*. As can be seen, the selected mathematical model adequately describes the resulting binding isotherms. The K_d values for the peptides Ltc1-K, (-1)Ltc1-K, and (-2)Ltc1-K determined on the basis of isotherms are equal, whereas the K_d value of (-3)Ltc1-K increases by a factor of 10 (*Table 2*), pointing to a considerable reduction in the affinity of (-3)Ltc1-K towards the lipid bilayer.

The estimation of the thermodynamic contribution, $\Delta G_{N\text{-term}}^0$, of the N-terminal peptide fragment to the binding with membrane, performed using the formula

$$\Delta G_{N\text{-term}}^0 \sim RT \ln (K_{d(\text{Ltc1-K})} / K_{d((-3)\text{Ltc1-K}}), \quad (4)$$

demonstrates that the free energies of interaction with the bilayer in Ltc1-K and (-3)Ltc1-K differ by 1.4 kcal/mol; i.e., the change in the free energy of interaction is ~20%. The major contribution to the free energy of interaction between the N-terminal fragment and the lipids is made by the Trp3 residue; this interaction seems to be of mostly hydrophobic character. The fact that the value $\Delta G_{N\text{-term}}^0$ is close to -1.95 kcal/mol (the value predicted by the White-Whimley method based on the empirical scale of hydrophobicity of amino acid residues [12]) lends support to this hypothesis.

Thus, the excision of the N-terminal fragment in Ltc1-K results in an abrupt decrease both in the haemolytic activity and cytotoxicity, and the K_d value, supporting the fact that peptide affinity towards the zwitterionic membrane is indeed of great significance for the development of the haemolysis and cytotoxic effects.

Effect of the N-terminal fragment of Ltc1-K on the secondary structure of peptide in peptide-lipid complexes

Peptide conformation is another factor that may have an effect on the activity of peptides. We compared the

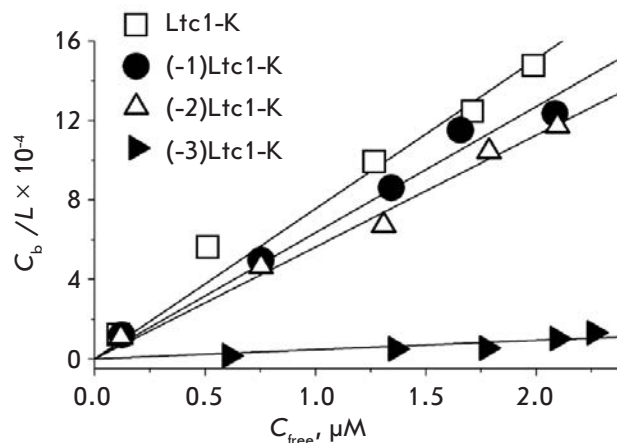


Fig. 2. Association isotherms for the binding of Ltc1-K, (-1)Ltc1-K, (-2)Ltc1-K, and (-3)Ltc1-K to DOPC-LML. Solid lines are a least squares approximation of experimental data with a linear function defined by equation (2).

secondary structure of Ltc1-K and its derivatives by analyzing the CD spectra of peptides in the phosphate buffered solution and in the lipid system – micelles of zwitterionic LMPC, which is used for simulating the surface of the eukaryotic cell membrane [13]. LMPC forms a 3D hydrophobic phase that is comparable in terms of its diameter with the thickness of the hydrophobic region of the biological membrane [14]. Moreover, LMPC does not have its own spectrum in the CD region of polypeptides and is characterized by a low level of light scattering at a high concentration of the phospholipid component, which provides the possibility to attain a high excess of lipid as compared with the peptide and ensures complete binding of peptide to micelles.

We found out that all the peptides under study in the buffer have a predominately disordered structure (*Fig. 3*) with an equally low content of elements with α -helix conformations (*Table 3*). Peptides undergo considerable conformational changes (*Fig. 3*) when bound to zwitterionic micelles: the α -helix becomes the predominant structural element, with 15–17 amino acid residues involved in its formation (*Table 3*). The results obtained correlate with the data on the high potential of helix formation in Ltc1-K in 50% of trifluoroethanol [6] and correspond to the general notion of the typical structural changes accompanying the interaction between linear cationic AMP and the lipid bilayer. Many AMPs have a disordered structure in water and form an amphipatic α -helix upon binding with lipids (see reviews [14–16]).

Thus, the formation of the α -helix in complex with lipids, which is typical of Ltc1-K, as well as its size, is

Table 3. Contribution of the α -helix conformation to the structure of Ltc1-K and its derivatives, based on the data of CD spectroscopy

Peptide	Phosphate buffered saline		LMPC micelles	
	%*	a.a.r.**	%*	a.a.r.**
Ltc1-K	17	4	59	15
(-1)Ltc1-K	14	4	67	17
(-2)Ltc1-K	15	4	72	17
(-3)Ltc1-K	16	4	65	15

* The proportion of the α -helix in the molecule structure.

** The number of amino acid residues involved in the formation of the α -helix.

retained after the excision of one, two, or three N-terminal amino acid residues. The N-terminal of Ltc1-K is apparently a part of the region with the disordered structure, providing a gain in free energy during peptide binding with zwitterionic lipids due to its conformational mobility. This assumption is indirectly supported by the structure of Ltc1-K in complex with negatively charged sodium dodecyl sulphate micelles, determined by NMR [7]. The data obtained allow us to eliminate conformational rearrangement from the list of the possible reasons behind the lower cytotoxic and haemolytic activity of (-3)Ltc1-K in comparison with Ltc1-K.

Comparative analysis of interaction of Ltc1-K and (-3)Ltc1-K with erythrocytes

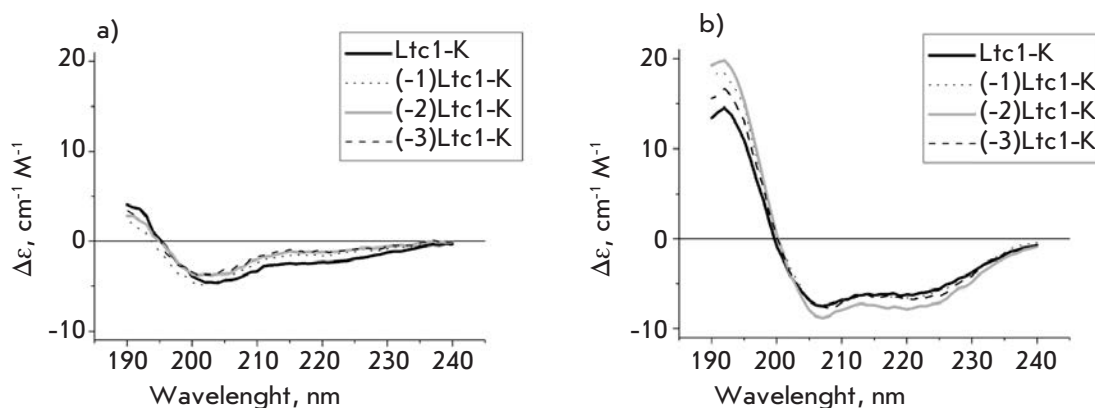
The search for the possible reasons that determine the differences in the activity of Ltc1-K and (-3)Ltc1-

K was taken further to the cell level. The features of haemolysis were compared at equi-effective concentrations of Ltc1-K and (-3)Ltc1-K (4 and 30 μ M, respectively), which were selected based on the concentration dependences of the haemolytic effect (*Fig. 1*). The difference in peptide concentration in the medium almost by a factor of 8 compensated for the differences between Ltc1-K and (-3)Ltc1-K in terms of affinity towards zwitterionic lipids (*Table 2*) and theoretically provided the same amount of Ltc1-K and (-3)Ltc1-K bound to the cell membrane.

The interactions between peptides and the erythrocyte membrane were analyzed in real time by LSCM with the synchronous registration of cell images in the transmitted light (in order to assess the erythrocyte morphology) and fluorescence images characterizing membrane permeability in terms of the penetration of CF into the cytoplasm (*Fig. 4*). The ability of LSCM to register fluorescence only from a thin layer near the focus of the objective and to eliminate the signals from the layers located above and below is critical in order to obtain contrast images of the distribution of CF around and inside the cells.

The exposure to Ltc1-K and (-3)Ltc1-K results in the equally complete release of haemoglobin from some erythrocytes and converting them into ghosts, whereas the proportion of lysed erythrocytes increases with a rising peptide concentration in the medium. The haemolysis process occurs very inhomogeneously: a number of erythrocytes are not subjected to any noticeable changes, whereas morphological changes emerge in some erythrocytes with a different delay after the peptide is introduced, which results in ghost formation. The differences in cell response are not connected with the local concentration gradients of the peptides introduced. The high inhomogeneity factor of peptide distribution in the medium was eliminated by means of thorough and rapid stirring of equal volumes of the peptide and cell suspensions. The exposure to Ltc1-K

Fig. 3. Circular dichroism (CD) spectra of Ltc1-K and its derivatives in phosphate buffered saline (a) and LMPS micelles (b).



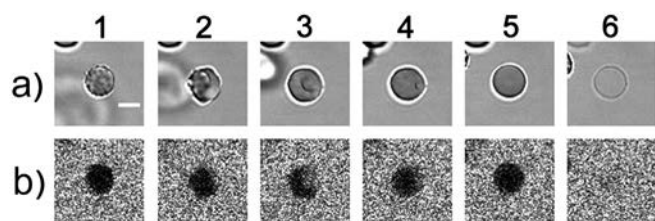


Fig. 4. A sequence of Ltc1-K-induced erythrocyte transformations: echinocyte (1), echinocyte-stomatocyte transition (2), stomatocyte (3), stomatocyte-spherocyte transition (4), spherocyte (5), ghost (6). Row (a) is the transmitted light images of a cell. Row (b) is the confocal fluorescence images showing the distribution of CF around and inside erythrocyte. The black area in the cell region indicates that an erythrocyte membrane is intact, and CF is unable to penetrate into cytoplasm. Bar is 5 μm .

and (-3)Ltc1-K results in an equal sequence of erythrocyte transformations (Figs. 4, 5): discocyte–echinocyte–stomatocyte–spherocyte–ghost. The lifetime of an echinocyte varies over a wide range (from several minutes to an hour) and is the limiting stage of haemolysis kinetics. The average duration of the stomatocyte stage is several minutes. Spherocyte is the shortest living state. It lasts no more than 10 s. No reliable differences in the duration of the separate stages of erythrocyte transformation under the action of both peptides were observed. The increase in peptide concentration in the medium primarily resulted in a decrease in the average lifetime of echinocytes.

Only at the stage when spherocyte was converted into the ghost did the erythrocyte membrane become permeable to the low-molecular-weight CF marker; a factor which is common to both peptides (Figs. 4–6). The influx of CF in cytoplasm and the beginning of haemoglobin release from a spherocyte (Fig. 6) are detected simultaneously. This implies the formation of large membrane defects without the indiscernible under our experimental conditions intermediate study of the formation of small lipid-peptide pores that would be permeable to CF (hydrodynamic diameter of the molecule of ~ 0.5 nm), but impermeable to haemoglobin (hydrodynamic diameter of 6.3 nm).

We found out that the membrane of the ghosts that remained under the action of Ltc1-K and (-3)Ltc1-K retains its permeability to CF, as opposed to the membrane of the ghosts emerging after osmotic haemolysis of erythrocytes caused by the replacement of the medium by distilled water (data not shown). Therefore, Ltc1-K and (-3)Ltc1-K form stable lipid-peptide pores in the erythrocyte membrane. The average size of these pores was estimated on the basis of the ability of fluorescein-labelled dextrans of various sizes to penetrate

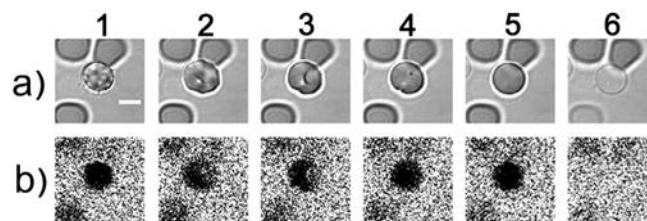


Fig. 5. A sequence of (-3)Ltc1-K-induced erythrocyte transformations: echinocyte (1), echinocyte-stomatocyte transition (2), stomatocyte (3), stomatocyte-spherocyte transition (4), spherocyte (5), ghost (6). Row (a) is the transmitted light images of a cell. Row (b) is the confocal fluorescence images showing the distribution of CF around and inside erythrocyte. The black area in the cell region indicates that an erythrocyte membrane is intact, and CF is unable to penetrate into the cytoplasm. Bar is 5 μm .

through the pores inside the ghosts. It was revealed that dextrans with a size of 40 kDa and lower can easily penetrate into the ghosts to rapidly balance the extra- and intracellular concentrations when added to the medium with lysed erythrocytes. Meanwhile, the diffusion of dextrans with a size of 70 and 500 kDa through pores into the ghosts is impeded (Figs. 7, 8). The extents of influx are approximately 70% and less than 40% for FD70 and FD500, respectively (Fig. 8). No reliable difference in the penetration of FD70 and FD500 into the ghosts formed under the action of Ltc1-K and (-3)Ltc1-K was detected (Fig. 8). Considering the hydrodynamic diameters of FD70 and FD500 (13 and 32 nm, respectively [17]), one may conclude that Ltc1-K and (-3)Ltc1-K form pores with a diameter of approximately 30 nm on the erythrocyte membrane.

Thus, the excision of the N-terminal fragment has no effect on the character, sequence, and duration of the stages of erythrocyte transformation or the features of formation of the pore size in the membrane in the haemolysis process. This attests to the fact that the mechanism and features of interaction of Ltc1-K and (-3)Ltc1-K with erythrocytes are equal.

The model of interaction of Ltc1-K and (-3)Ltc1-K with erythrocytes can be based on the coupled bilayer theory [18–21]. In this theory, an asymmetric plasma membrane is regarded as two protein-lipid layers that are capable of performing a relatively independent adaptive deformation without losing the contact between them. The coupled bilayer theory has frequently been used to interpret the formation of echinocytes and stomatocytes under the action of membrane-active agents, including AMPs [18, 22, 23]. According to this theory, echinocyte formation is conditioned by the accumulation of the actuating agent in the external layer of the membrane. The interactions with any agent,

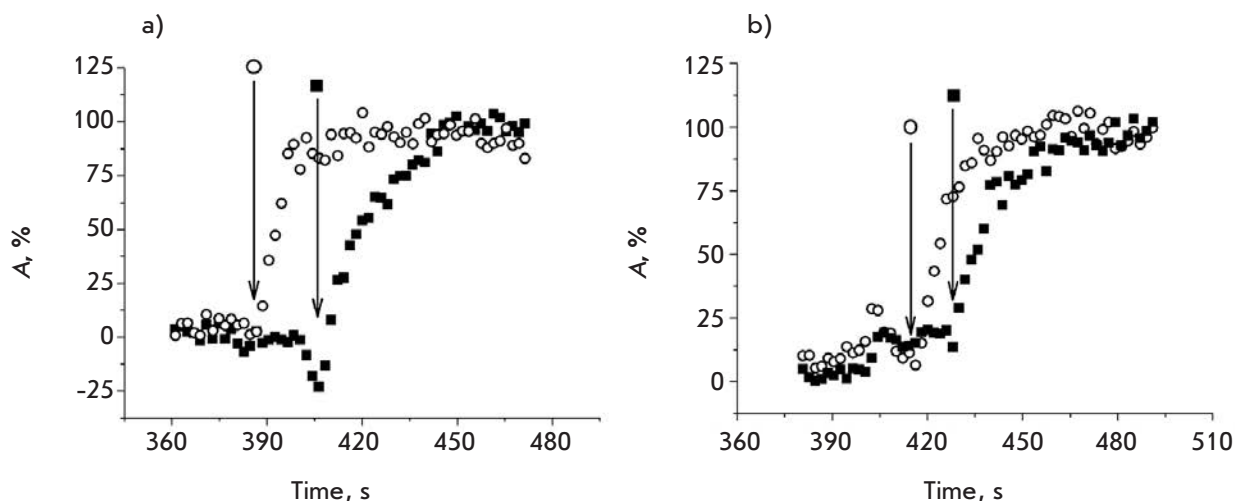
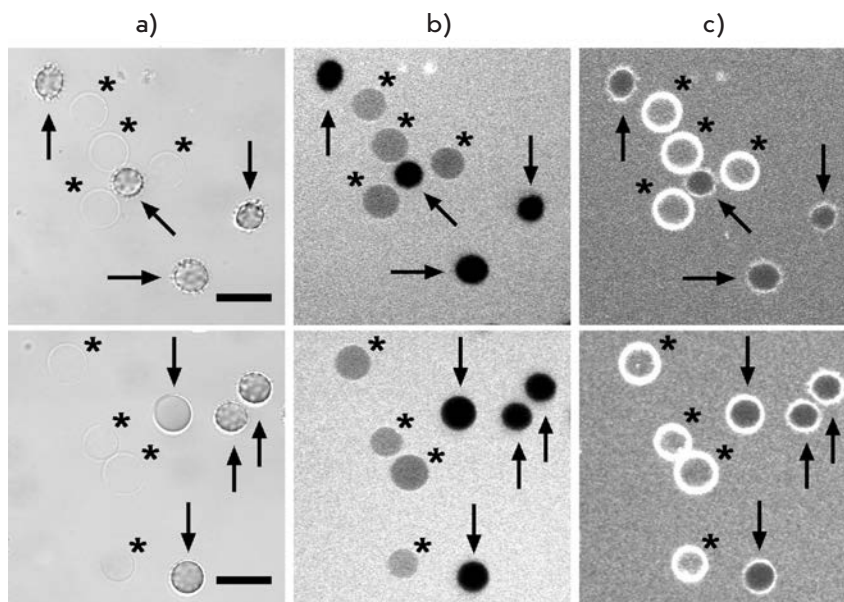


Fig. 6. Ltc1-K- (a) and (-3)Ltc1-K (b)-induced formation of membrane pores and influx of CF in erythrocytes. Typical examples are presented for two particular cells (○, ■). Abscissa is time after addition of the peptide and CF to cells. Ordinate is the extent of CF influx inside a cell (in percentages) as calculated with equation (3). Delay between peptide addition and beginning of haemolysis is the property of particular cells and is mainly defined by echinocyte-stage lifetime. A vertical arrow indicates the moment when haemoglobin release from the examined cell as recognized in transmitted light images of the cell begins.

Fig. 7. LSCM analysis of FD500 ability to penetrate through the ghost membrane pores produced by Ltc1-K (upper row) and (-3)Ltc1-K (lower row). FD500 and membrane marker FM1-43 were added to the erythrocytes pretreated with the peptide. Column (a) is the transmitted light images of the cells. Column (b) is the confocal fluorescent images showing the distribution of FD500 around and inside the cells. Column (c) is the confocal fluorescence images showing the distribution of FM1-43 at an erythrocyte membrane. Asterisks mark ghosts being restrictedly permeable to FD500. Arrows mark erythrocytes being impermeable to FD500. Bar – 10 μ m.



which stretch the external layer with respect to the internal layer, result in the formation of “spicules” – protrusions on the membrane, which are a characteristic feature of echinocytes. In turn, the formation of stomatocytes is induced by the accumulation of the agent in the internal layer and its deformation, which ends by the transformation of a discocyte into a spheroid with membrane cavity.

The interpretation of erythrocyte transformations under the action of Ltc1-K and (-3)Ltc1-K using the

coupled bilayer theory is complicated by the fact that the scenarios of the formation of echinocyte and stomatocyte are considered to be alternative. Assuming that the translocation of the agent from the external layer to the internal one is accompanied by echinocyte transformation into a discocyte, the interactions of Ltc1-K and (-3)Ltc1-K with erythrocytes can be explained as follows: the transition of a discocyte into an echinocyte is initiated by the initial adsorption of a peptide by the erythrocyte surface. The accumulation of a

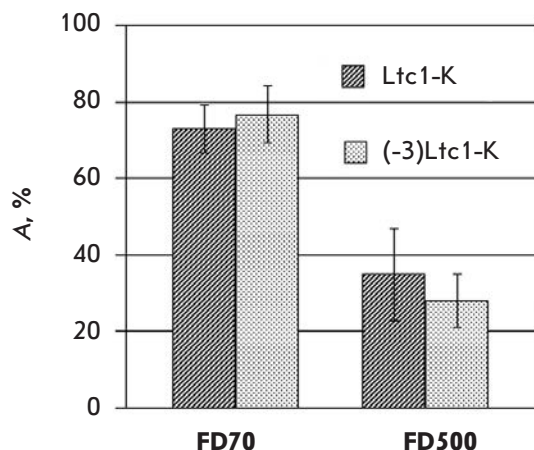


Fig. 8. Extent of influx (A) of the membrane permeability markers FD70 and FD500 into the ghosts formed as a result of Ltc1-K and (-3)Ltc1-K action on erythrocytes. Averaged data for 100-150 cells are presented.

peptide bound on the external side of the membrane results in the reorganization of lipid-peptide complexes and creates the conditions for peptide translocation to the internal surface of the plasma membrane, resulting in the transformation of an echinocyte into a stomatocyte. It should be emphasized that the hypothetical translocation of a peptide is not accompanied by the formation of structured defects in the bilayer, since the membranes of both the echinocyte and stomatocyte are impermeable to CF (Figs. 4, 5). The stomatocyte-spherocyte transition probably corresponds to a considerable accumulation of a cationic peptide in the internal membrane layer that is enriched in negatively charged phospholipids, and to the formation of a critical tension in both membrane layers. The process is terminated by the formation of lipid-peptide pores, which reduce the membrane tension and create the conditions for haemoglobin release and ghost formation.

This model of interactions of Ltc1-K and (-3)Ltc1-K with erythrocytes agrees with the lifetimes of the separate stages of erythrocyte transformation recorded in the experiment. Long erythrocyte lifetimes represent the continuous process of gradual accumulation of the peptide on the external side of the membrane. This process is accelerated with increasing peptide concentration in the medium. An increase in the amount of the peptide bound to the membrane to a critical level jumpwise increases the probability of peptide translocation to the internal layer of the membrane and considerably stabilizes the membrane, which is manifested in the acceleration of the subsequent processes resulting in haemolysis.

All the data obtained indicate that the binding of a peptide to the external layer of the erythrocyte membrane, with zwitterionic phospholipids dominated in its composition, and the accumulation of a critical amount of peptides on the membrane trigger the haemolysis process. The excision of the N-terminal fragment of Ltc1-K abruptly decreases the ability of the peptide to be bound to the membrane, thus protecting erythrocytes against haemolysis. An increase in the concentration of (-3)Ltc1-K in the medium compensates for the deficiency in bound peptide, all subsequent haemolysis stages with the participation of (-3)Ltc1-K occurring in the same manner as for the initial peptide Ltc1-K.

It can be assumed that the mechanism of the decrease in the toxicity of peptides that was proposed for a number of linear cationic AMPs and demonstrated by the example of laticins Ltc2a and Ltc5 by excising their N-terminal fragments [5] is similar to the mechanism ascertained for Ltc1-K. The N-terminal fragment seems to be responsible for the efficacy of peptide binding to the zwitterionic plasma membrane of eukaryotic cells when AMPs are organized according to the scheme “non-ordered hydrophobic N-terminal fragment + amphipatic α -helix.” Provided that the affinity of the N-terminal fragment of AMPs towards eukaryotic membranes is higher than that towards bacterial membranes, safety in the use of AMPs as an antibacterial agent can be improved by excising the N-terminal amino acids.

CONCLUSIONS

The excision of three N-terminal amino acid residues in Ltc1-K considerably reduces the haemolytic activity of AMPs, thus increasing the selectivity of its antibacterial action.

The major reason for the effect observed consists in a multifold decrease in peptide affinity towards the plasma membrane of eukaryotic cells enriched in zwitterionic phospholipids.

The haemolysis caused by the AMP of Ltc1-K and its derivative (-3)Ltc1-K is a sophisticated multistage process. The binding of peptides to the zwitterionic membrane of erythrocytes is accompanied by their transition into the α -helix conformation. By stabilizing the membrane, the bound peptides transform an erythrocyte from a discocyte into an echinocyte, followed by a transformation into a stomatocyte and a spherocyte. When the sufficient amount of peptide necessary to form pores accumulates on the membrane, spherocyte undergoes haemolysis, yielding stable lipid-peptide pores approximately 30 nm in diameter. The role of the N-terminal fragment of Ltc1-K consists in the enhancement of peptide binding to the erythrocyte membrane. The N-terminal fragment has no effect on the features

of the subsequent stages of peptide interaction with erythrocyte, which results in haemolysis. ●

This study was financially supported by the Program of the Presidium of the Russian Academy of Sciences “Molecular and Cell Biology” and a Carl Zeiss grant.

REFERENCES

1. Hancock R.E.W., Chapple S.D. // *Antimicrob. Agents Chemother.* 1999. V. 43. P. 1317–1323.
2. Finlay B.B., Hancock R.E.W. // *Nat. Rev. Microbiol.* 2004. V. 2. P. 497–504.
3. Jenssen H., Hamill P., Hancock R.E.W. // *Clin. Microbiol. Rev.* 2006. V. 19. P. 491–511.
4. Kozlov S.A., Vassilevski A.A., Feofanov A.V., Surovoy A.Y., Karpunin D.V., Grishin E.V. // *J. Biol. Chem.* 2006. V. 281. P. 20983–20992.
5. Polyansky A.A., Vassilevski A.A., Volynsky P.E., Vorontsova O.V., Samsonova O.V., Egorova N.S., Krylov N.A., Feofanov A.V., Arseniev A.S., Grishin E.V., et al. // *FEBS Lett.* 2009. V. 583. P. 2425–2428.
6. Vassilevski A. A., Kozlov S. A., Zhmak M. N., Kudelina I. A., Dubovskii P. V., Shatursky O. Ya., Arseniev A. S., Grishin E. V. // *Bioorg. Khim.* 2007. V. 33. P. 405–412.
7. Dubovskii P.V., Volynsky P.E., Polyansky A.A., Karpunin D.V., Chupin V.V., Efremov R.G., Arseniev A.S. // *Biochemistry.* 2008. V. 47. P. 3525–3533.
8. Provencher S.W., Glockner J. // *Biochemistry.* 1982. V. 20. P. 33–37.
9. Vassilevski A.A., Kozlov S.A., Samsonova O.V., Egorova N.S., Karpunin D.V., Pluzhnikov K.A., Feofanov A.V., Grishin E.V. // *Biochem. J.* 2008. V. 411. P. 687–696.
10. Seelig J. // *Biochim. Biophys. Acta.* 2004. V. 1666. P. 40–50.
11. Brogden K.A. // *Nat. Rev. Microbiol.* 2005. V. 3. P. 238–250.
12. White S.H., Whimley W.C. // *Annu. Rev. Biophys. Biomol. Struct.* 1999. V. 28. P. 319–365.
13. Yuan P., Fisher P.J., Prendergast F.G., Kemple M.D. // *Biophys. J.* 1996. V. 70. P. 2223–2238.
14. Strandberg E., Ulrich A. // *Concepts Magn. Reson. Part A. Bridg. Educ. Res.* 2004. V. 23. P. 89–120.
15. Fernandez D.I., Gehman J.D., Separovic F. // *Biochim. Biophys. Acta.* 2009. V. 1788. P. 1630–1638.
16. Dathe M., Wieprecht T. // *Biochim. Biophys. Acta.* 1999. V. 1462. P. 71–87.
17. Armstrong J.K., Wenby R.B., Meiselman H.J., Fisher T.C. // *Biophys. J.* 2004. V. 87. P. 4259–4270.
18. Sheetz M.P., Singer S.J.J. // *J. Cell Biol.* 1976. V. 70. P. 247–251.
19. Evans E.A. // *Biophys. J.* 1974. V. 14. P. 923–931.
20. Igljč A., Kralj-Igljč V., Hägerstrand H. // *Eur. Biophys. J.* 1998. V. 27. P. 335–339.
21. Lim G.H.W., Wortis M., Mukhopadhyay R. // *Proc. Natl. Acad. Sci. USA.* 2002. V. 99. P. 16766–16769.
22. Isomaa B., Hägerstrand H., Paatero G. // *Biochim. Biophys. Acta.* 1987. V. 899. P. 93–103.
23. Semrau S., Monster M.W., van der Knaap M., Florea B.I., Schmidt T., Overhand M. // *Biochim. Biophys. Acta.* 2010. V. 1798. P. 2033–2039.

Reconstruction of Purine Metabolism in *Bacillus subtilis* to Obtain the Strain Producer of AICAR: A New Drug with a Wide Range of Therapeutic Applications

K.V. Lobanov, L. Errais Lopes, N.V. Korol'kova, B.V. Tyaglov, A.V. Glazunov, R.S. Shakulov, A.S. Mironov*

State Research Institute for Genetics and Selection of Industrial Microorganisms

*E-mail: alexmir@genetika.ru

Received 24.02.2011

ABSTRACT AICAR is a natural compound, an analogue and precursor of adenosine. As activator of AMP-activated protein kinase (AMPK), AICAR has a broad therapeutic potential, since it normalizes the carbohydrate and lipid metabolism and inhibits the proliferation of tumor cells. The synthesis of AICAR in *Bacillus subtilis* cells is controlled by the enzymes of purine biosynthesis; their genes constituting purine operon (*pur*-operon). Reconstruction of purine metabolism in *B. subtilis* was performed to achieve overproduction of AICAR. For this purpose, the gene *purH*, which encodes formyltransferase/IMP-cyclohydrolase, an enzyme that controls the conversion of AICAR to IMP, was removed from the *B. subtilis* genome, ensuring the accumulation of AICAR. An insertion inactivating the gene *purR* that encodes the negative transcriptional regulator of the purine biosynthesis operon was introduced into the *B. subtilis* chromosome in order to boost the production of AICAR; the transcription attenuator located in the leader sequence of *pur*-operon was deleted. Furthermore, the expression integrative vector carrying a strong promoter of the *rpsF* gene encoding the ribosomal protein S6 was designed. The heterologous *Escherichia coli* gene *purF* encoding the first enzyme of the biosynthesis of purines with impaired allosteric regulation, as well as the modified *E. coli* gene *prs* responsible for the synthesis of the precursor of purines — phosphoribosyl pyrophosphate (PRPP) — was cloned into this vector under the control of the *rpsF* gene promoter. The modified *purF* and *prs* genes were inserted into the chromosome of the *B. subtilis* strain. *B. subtilis* strain obtained by these genetic manipulations accumulates 11–13 g/L of AICAR in the culture fluid.

KEYWORDS anticancer agent AICAR; purine metabolism; genome reconstruction; *Bacillus subtilis* strain - producer of AICAR

ABBREVIATIONS AICAR – 5-aminoimidazole-4-carboxamide ribofuranoside; AICAR-P – nucleotide AICAR phosphate; IMP – inosine monophosphate; AMP – adenosine monophosphate; AMPK – 5'-adenosine monophosphate-activated protein kinase; PRPP – phosphoribosyl pyrophosphate; GAR – 5'-phosphoribosyl glycineamide ribonucleotide; GMP – guanosine monophosphate; PCR – polymerase chain reaction; CF – culture fluid

INTRODUCTION

Despite the fact that the structural organization of the genes encoding the enzymes of purine nucleotide biosynthesis is quite versatile, the biochemistry of the process is conservative for different organisms: the formation of the purine cycle occurs on the basis of a riboso-5-phosphate (all intermediates are nucleotides) using a monocarbon component (formiate and/or N10-formyltetrahydrofolate) [1]. There is demand for monocarbon compounds at two stages of purine biosynthesis; therefore, the precursors – phosphoribosylglycineamide ribonucleoside (GAR) and 5-aminoimidazole-4-carboxamide ribonucleoside (AICAR-P) can be accumulated if there is a deficiency in these compounds. Among them, AICAR-P occupies a specific place, since

its formulation and subsequent cyclization crown the formation of the purine heterocycle that yields inosine monophosphate (IMP) (Fig. 1). The process of conversion of AICAR-P into IMP in prokaryotic cells is controlled by the gene *purH*, which encodes two domains with the activities of AICAR-P-formyltransferase and IMP cyclohydrolase [2, 3]. Further modifications of IMP yield AMP and GMP.

Despite the fact that the structure of purine heterocycle is incomplete, AICAR-P is a natural analogue of AMP, substituting it in certain enzymatic *in vitro* reactions. The possibility that AMP could be substituted in the reactions of activation of AMP-activated proteinkinase (AMPK) in mammals has been given a significant degree of attention over the past decade. AMPK is

the global regulator of the metabolic processes ensuring the energy status of the eukaryotic organism [4, 5]. For *in vivo* activation of AMPK, it is convenient to use a AICAR nucleoside, which can be rapidly phosphorylated in cells, yielding AICAR-P, an analogue of AMP. The emergence of AICAR-P imitates the accumulation of AMP and provokes the rearrangement of energy processes directed towards the overcoming of imaginary energetic stress. Due to their ability to activate AMPK, AICAR-based drugs have a broad therapeutic potential, since they normalize both the carbon [6] and lipid [7] metabolism. AICAR suppresses tumor cell growth by imitating the state of energetic stress [8]. The efficacy of AICAR in the prevention of type 2 diabetes mellitus has been demonstrated [9]. AICAR induces apoptosis; it is efficient upon chronic [10] and acute leukoses [11].

The present work was aimed at obtaining the strain producer of AICAR by directed reconstruction of purine metabolism in *B. subtilis* cells. The choice of *B. subtilis* was conditioned on the fact that genetic control and regulation of purine metabolism in these bacteria have been subjected to an appropriately thorough study. Furthermore, *Bacillus* strains have been in use for a significant length of time as producers of purine nucleosides and nucleotides, such as inosine and inosinic, as well as guanosinic, acids [12, 13].

Purine operon *B. subtilis*, *purEKBCSQLFMNHD* (hereafter referred to as *pur*-operon), encodes the enzymes of the synthesis of IMP, the most significant intermediate compound upon purine nucleotide biosynthesis (Fig. 1).

The group consisting of 12 linked genes that form the *pur*-operon is localized at the 55° region on the chromosome of *B. subtilis* (Fig. 2) [14]. Expression of the *pur*-operon of *B. subtilis* undergoes a double-negative regulation, by the protein-repressor PurR [15] and the transcription attenuator located in the leader sequence of *pur*-operon [16]. It was shown that PRPP acts as a low-molecular-weight effector of the PurR protein [15], whereas guanine serves as a modulator enhancing transcription termination prior to the first structural gene of the operon [17]. Later, it was revealed that a 5'-non-translatable sequence of mRNA has a sensory function with respect to the metabolite – guanine effector, and that it acts as the so-called riboswitch [18, 19], providing early termination of operon transcription [20, 21].

Thus, maximum *pur*-operon gene expression had to be made possible at the first stage of obtainment of the strain producer of AICAR by eliminating the negative regulation of the *pur*-operon under the action of the protein repressor PurR and the transcription attenuator in the leader sequence of the operon. The gene

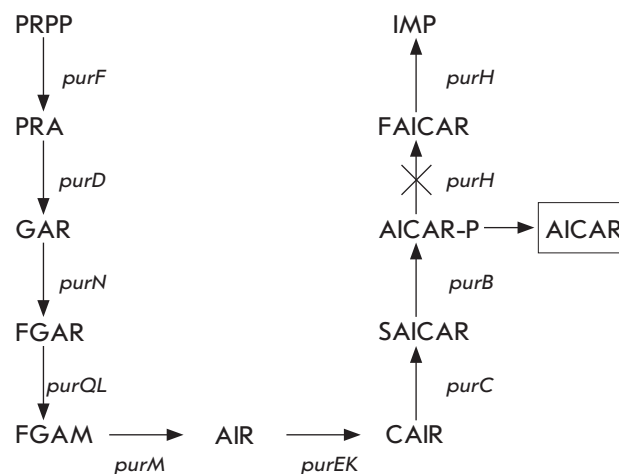


Fig. 1. De novo purine nucleotide biosynthesis in *B. subtilis*. Representative enzymatic steps of de novo purine biosynthesis are shown by the corresponding gene designations. Abbreviations: PRPP - 5'-phosphoribosyl-1-pyrophosphate, PRA - 5'-phosphoribosylamine, GAR - 5'-phosphoribosylglycineamide, FGAR - 5'-phosphoribosyl-N-formylglycineamide, FGAM - 5'-phosphoribosyl-N-formylglycinamide, AIR - 5'-phosphoribosyl-5-aminoimidazole, CAIR - 5'-phosphoribosyl-4-carboxy-5-aminoimidazole, SAICAR - 5'-phosphoribosyl-4 (N-succinocarboxamide)-5-aminoimidazole, AICAR-P - 5'-phosphoribosyl-4-carboxamide-5-aminoimidazole, FAICAR - 5-formamidoimidazole-4-carboxamide ribotide, IMP - inosine 5'-monophosphate, AICAR - 5-aminoimidazole-4-carboxamide 1-β-D-ribofuranoside.

purH encoding formyltransferase/IMP-cyclohydrolase, which participates in the synthesis of AICAR, was then deleted from the genome of the resulting strain. Inactivation of this enzyme is intended to ensure the intracellular accumulation of AICAR (Fig. 1). At the next stage, the pool of major precursors of *de novo* purine synthesis — PRPP — was to be increased. PRPP is synthesized from riboso-5-phosphate under the control of PRPP synthase encoded by the *prs* gene. This enzyme is susceptible to allosteric regulation with the participation of purine nucleotides. The structural and functional organization of PRPP synthase was studied more thoroughly in *E. coli* bacteria, in which a mutant variant of this enzyme, with eliminated allosteric regulation, was obtained [22]. Taking these data into account, site-directed mutagenesis of the *prs* gene of *E. coli* aimed at obtaining a mutant enzyme that would not be susceptible to retroinhibition by purine nucleotides was preformed with the purpose of its subsequent transfer into *B. subtilis* cells.

An additional impediment in the effort to boost AICAR production is the allosteric regulation of the first

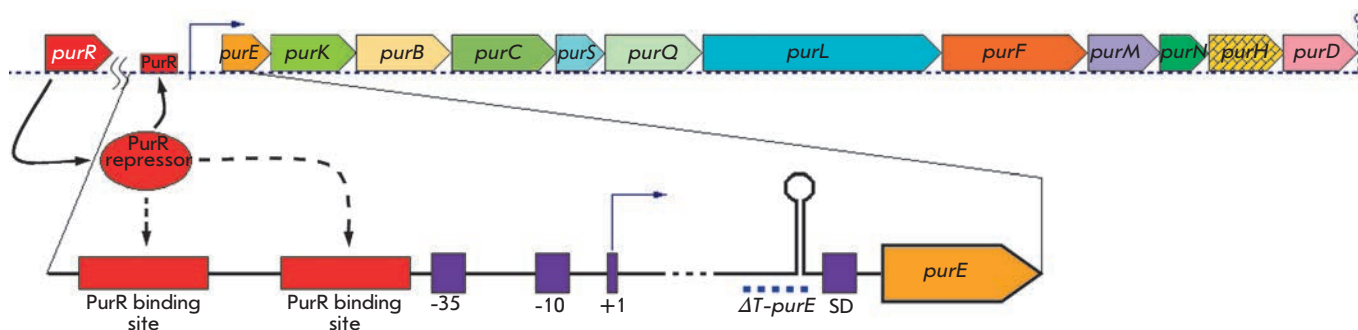


Fig. 2. Scheme of structural organization of the *B. subtilis* *pur*-operon and its regulation. Top: relative location of the 12 linked structural genes that constitute the *pur*-operon and unlinked *purR* gene, encoding a repressor of *pur*-operon. Bottom: the leader region of *pur*-operon, including binding sites for the repressor protein PurR, binding site for RNA polymerase (-35 ; -10), transcription start (+1), the terminator of transcription (hairpin structure) and the ribosome binding site (SD); the dotted line denotes deletion of the leader region of *pur*-operon (ΔT -*purE*).

enzyme of purine biosynthesis — glutamine-PRPP aminotransferase encoded by the *purF* gene [23]. It is well known that glutamine-PRPP aminotransferase from *E. coli*, as opposed to the enzyme from *B. subtilis*, is not susceptible to inactivation in the steady-state stage of bacterial growth [24]. Moreover, the mutant variant of this enzyme, which is resistant to inhibition by purine nucleotides, has been described for *E. coli* [25]. Therefore, in our case the decision was made to use the glutamine-PRPP aminotransferase from *E. coli* modified by site-directed mutagenesis with the aim of subsequently transferring it into *B. subtilis* cells. An integrative expression vector based on plasmid pDG268 was constructed comprising a strong promoter of the *rpsF* gene, which encodes the ribosomal protein S6, in order to ensure the optimal expression of the modified *prs* and *purF* genes of *E. coli* in *B. subtilis* cells. The final stage of the process comprised the integration of the resulting vector, containing clones of the *prs* and *purF* genes under the control of the *rpsF* gene promoter, into the chromosome of the AICAR-producing strain *B. subtilis*.

EXPERIMENTAL

Bacterial strains and plasmids

The bacterial strains and plasmids used in this study are listed in Table 1. The *B. subtilis* strain AM732 was obtained via the transformation of the Mu8u5u6 strain of chromosomal DNA isolated from the *B. subtilis* strain 168 with the selection of Pur⁺ transformants. Strain AM743 was obtained by the transformation of strain AM732 of chromosomal DNA isolated from *B. subtilis* strain LCC28 with the selection of transformants Neo^R in a neomycine-containing medium.

Media and culturing conditions

A LB medium [31], or the standard-minimal Spizizen's medium, with the required additives [26] was used as the nutrient medium to culture bacteria. Aminoacids were added in an amount of 50 $\mu\text{g}/\text{mL}$. Glucose (0.4%) was used as a source of carbon. The following antibiotics were added into the medium when necessary: ampicillin (Amp) – 100 $\mu\text{g}/\text{mL}$; chloramphenicol (Cm) – 10 $\mu\text{g}/\text{mL}$; erythromycin (Em) – 1 mg/mL; and neomycin (Neo) – 5 $\mu\text{g}/\text{mL}$. Methionine and leucine were added at a concentration of 50 $\mu\text{g}/\text{mL}$. Hypoxanthine, adenine, or guanine (20 $\mu\text{g}/\text{mL}$) was used as a purine source for purine auxotrophs. The DNA of *B. subtilis* was isolated according to the Saito-Miura procedure [32]; the transformation experiments were carried out in accordance with Anagnostopoulos and Spizizen's work [26].

Manipulations with plasmid DNA

The isolation of plasmid DNA, cloning, transformation into *E. coli* cells, and analysis of recombinant plasmids were performed using the standard methods [31].

Enzyme preparations

Restriction endonucleases, T4-DNA-ligase, and thermostable Taq DNA polymerase were purchased from Fermentas International Inc.

Polymerase chain reaction

The PCR was performed on a MyCycler thermal cycler (Bio-Rad Laboratories). The temperature mode was selected with due consideration of the length of the amplified fragment, as well as the length and composition of the primers used. The isolation and purification of the PCR products was carried out using a Silica Bead DNA Gel Extraction Kit (Fermentas International Inc.).

Table 1. Bacteria and plasmids used in the present study

Strain or plasmid	Description or genotype	Source or reference
<i>Bacillus subtilis</i>		
168	<i>trpC</i>	[26]
Mu8u5u6	<i>leu met purF</i>	[27]
LCC28	<i>purR::neo</i>	[28]
AM747	<i>trpC purH::(pMutin2purH'-lacZ) ΔT-purE</i>	[21]
AM732	<i>leu met</i>	This study
AM743	<i>leu met purR::neo</i>	- “ -
AM764	<i>leu met purR::neo ΔT-purE</i>	- “ -
AM778	<i>leu met purR::neo ΔT-purE ΔpurH</i>	- “ -
AM793	<i>leu met ΔpurH</i>	- “ -
AM811	<i>leu met purR::neo ΔT-purE ΔpurH amyE::[P_{rnsF}-pr_{sE}]</i>	- “ -
AM813	<i>leu met purR::neo ΔT-purE ΔpurH amyE::[P_{rnsF}-purF_E]</i>	- “ -
AM815	<i>leu met purR::neo ΔT-purE ΔT ΔpurH amyE::[P_{rnsF}-pr_{sE}-purF_E]</i>	- “ -
<i>E.coli</i>		
TG1	<i>thi supE hsdΔ5 Δ(lac-proAB)/F'tra Δ36 proAB⁽⁺⁾ lacI^(q) lacZ ΔM15</i>	VKPM
MG1655	prototroph	[29]
Plasmids:		
pDG268	Ap ^r (<i>E.coli</i>) Cm ^r (<i>B.subtilis</i>)	[18]
pNZT1	Em ^r	[30]
pLE1	as pDG268, but contains a promoter of <i>rpsF_E</i> gene	This study
pLE2	as pLE1, but contains a <i>pr_{sE}</i> gene	- “ -
pLE3	as pLE1, but contains a <i>purF_E</i> gene	- “ -
pLE4	as pLE1, but contains a <i>pr_{sE}</i> and <i>purF_E</i> genes	- “ -

Ap^r – ampicillin resistance, Em^r erythromycin resistance, Cm^r – chloramphenicol resistance.
VKPM Russian National Collection of Industrial Microorganisms

Site-directed mutagenesis

Site-directed mutagenesis was performed using specific oligonucleotide primers. The composition and characteristics of the primers are listed in Table 2. The presence of corresponding mutations was verified by sequencing according to Sanger [33].

Fermentation conditions

The ability of the strains obtained during the study to accumulate AICAR in culture liquid (CL) was assessed. The strain inoculum was cultivated at 37°C for 18 h on a LB broth. Then, 0.5 mL of the culture was added to each 20 x 200 mm vial with 4.5 mL of the fermentation medium and cultured at 37°C for 72 h on a rotary shaker. The fermentation medium had the following composition (%): soy flour – 3; nutrient yeast – 1; corn extract – 5; (NH₄)₂HPO₄ – 0.6; carbamide – 0.4; and sugar – 15, pH 7.0.

Determination of AICAR concentration in the culture liquid

The CL obtained during fermentation was centrifuged to remove the cells; the AICAR concentration was then

determined in the supernatant on Sorbfil plates (OOO Lenchrom, Saint Petersburg, Russia) by quantitative thin-layer chromatography. The composition of the eluting system designed was as follows: chloroform–methanol–water–25% aqueous solution of ammonia at a volume ratio of 5 : 3 : 1. Quantitative HPLC on a chromatograph (ALLIANCE, Separations Module Waters 2695, Photodiode Array detector Waters 2996) was employed as an alternative method.

RESULTS AND DISCUSSION

Enhancement of the expression of the *B. subtilis pur*-operon

In work [21] devoted to the study of *B. subtilis pur*-operon expression, it was demonstrated that an almost 20-fold enhancement of the expression of the *lacZ* reporter gene integrated into the *purH* gene, as compared with the expression in the wild-type strain when the *purR* gene that encodes the repressor protein of the operon is damaged, is achieved. After deletion of 94 n.p. of the wild-type strain, which captures the Rho-independent transcription attenuator (ΔT -*purE*)

Table 2. Primers used in this study

Name	Gene	Sequence*	Coordinates**	
			5'	3'
N1	<i>purN_B</i>	<u>ccccgcgggcggaacgattccat</u> (SacII)	+135	+154
N2	<i>purN_B</i>	<u>cgctgcagttcttttacgaaaggaacga</u> (PstI)	+652	+630
D1	<i>purD_B</i>	<u>cgctgcagcttcaaacattaaggggatgaaaa</u> (PstI)	-28	-5
D2	<i>purD_B</i>	<u>cgcggtaccttttctgcacatatgcc</u> (KpnI)	+410	+389
F1	<i>purF_E</i>	<u>cgcatcgataggaggtgcaaacagatgtcggtattgtcggtatc</u> (ClaI)	+1	+22
F2	<i>purF_E</i>	<u>cgcgctcagcgaaggcatcatcct</u> (EspI)	+1530	+1511
F3	<i>purF_E</i>	<u>gggctctggtCaaaaccgctat</u>	+968	+991
F4	<i>purF_E</i>	<u>atagcggttttGaacgaagccc</u>	+991	+968
F5	<i>purF_E</i>	<u>ggtattgatatgTGgagcggccacgg</u>	+1216	+1242
F6	<i>purF_E</i>	<u>ccgtggcgctcCAcatatacaatacc</u>	+1242	+1216
P1	<i>prs_B</i>	<u>cgcggatccaaggaggttctctcAtgcctgatatga</u> (BamHI)	-21	+3
P2	<i>prs_B</i>	<u>cccatcgatgccgggttcgattagtggtcga</u> (ClaI)	+949	+928
P3	<i>prs_B</i>	<u>ctgacagtggCctcgcacgctg</u>	+366	+377
P4	<i>prs_B</i>	<u>agcgtgcagaGcactgtcagc</u>	+377	+366
R1	<i>rpsF_B</i>	<u>cgcgaattcttgcggcgcggtat</u> (EcoRI)	-223	-205
R2	<i>rpsF_B</i>	<u>cgcggatccataatgggcaaggagcaat</u> (BamHI)	-31	-51

*The sequence of primers is given in the orientation 5'-3'. Uppercase bold letters indicate the nucleotide substitutions introduced in primers for site-directed mutagenesis. Recognition sites are underlined. Restriction enzymes are shown in parentheses.

**The coordinates of the 5'-and 3'-ends of the primers are relative to the start of translation of the corresponding genes. *B. subtilis* genes are marked with the symbol _(B); and *E. coli* - with the symbol _(E).

located in the leader region of the *pur*-operon (Fig. 2), the expression of the *lacZ* reporter gene increased approximately by a factor of 10. However, when combining both mutations, a pronounced synergic effect was observed; *lacZ* gene expression increased by a factor of more than 200. Taking these data into account, the experiments on the inactivation of the *purR* gene and deletion of the transcription attenuator (ΔT -*purE*) were performed at the first stage of construction of the AICAR-producing strain.

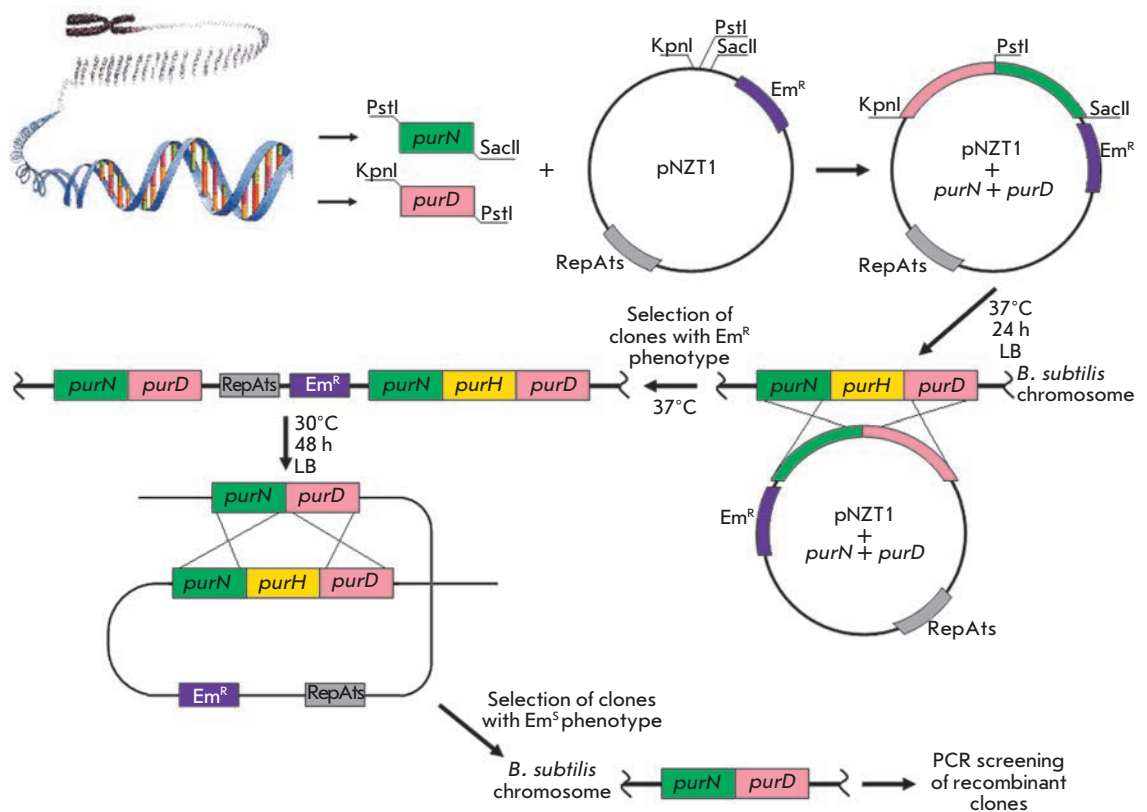
The AM732-Pur⁺ strain, a derivative of the earlier characterized Mu8u5u6 strain [21] (Table 1), was used as starting material. In order to transfer the *purR::neo* insertion, which completely inactivates the synthesis of the PurR repressor protein, into the genome of the AM732 strain, this strain was transformed by chromosomal DNA isolated from the LCC28 (*purR::neo*) strain, with the selection of recombinants that were resistant to neomycin (Neo^R). As a result, the AM743 *purR::neo* strain was selected for use in the subsequent work (Table 1). The deletion ΔT -*purE* in the genome of the AM743 *purR::neo* strain was obtained through the following scheme. First, the long-stretched deletion ΔL -*E* was obtained, completely overlapping the leader region of the *pur*-operon and partially overlapping the first structural gene *purE*, which resulted in the emer-

gence of auxotrophicity with respect to purines. How to achieve this deletion was thoroughly described in [21]. The deletion of the transcription attenuator ΔT -*purE* was transferred into the AM743 *purR::neo* ΔL -*E* strain by transforming DNA that was isolated from the AM747 strain (Table 1); Pur⁺ transformants were selected on the purine-free Spizizen's minimal medium. As a result, the AM764 strain was obtained. It contained the *purR::neo* insertion and deletion of the transcription attenuator ΔT -*purE* in the genome.

Obtaining the deletion of the *purH* gene in the *B. subtilis* chromosome

As follows from the schematic representation of purine biosynthesis (Fig. 1), for intracellular accumulation of AICAR, it is necessary to inactivate formyltransferase/IMP-cyclohydrolase encoded by the *purH* gene. The PurH gene deletion in the *B. subtilis* chromosome was achieved using the method described in [30] based on using a specially constructed pNZT1 plasmid, a derivative of the integrative vector pKS1 [34]. The pNZT1 plasmid contains the erythromycin (Em^R) resistance marker and a polylinker with multiple restriction sites for cloning the target fragments of chromosomal DNA. Of paramount importance is the fact that its replication is temperature-sensitive: at 30°C, the plasmid exists in

Fig. 3. A schematic representation of isolation of the *purH* gene deletion using the method described in [30].



an autonomous state. However, at 37°C the replication is blocked. As a result, if the plasmid has a chromosome fragment cloned into its structure, it is capable of integration into the chromosome by homologous recombination (Fig. 3). Since plasmid integration into the chromosome results from the single recombination act in the homology region between the cloned fragment and the chromosome, the integration site of the plasmid into the chromosome turns out to be flanked by homologous duplicated sequences. Culturing of these bacteria at 30°C (permissive, for pNZT1 plasmid replication) may result in its removal from the chromosome with capture of a copy of the flanked chromosome sequences, which allows for the replacement of the wild allele of any chromosome gene by the mutant gene cloned in the pNZT1 plasmid (Fig. 3).

This feature of the pNZT1 plasmid was used for the deletion of the *purH* gene. With this aim in mind, the PCR amplification of the chromosome fragments that flanked the *purH* gene was performed. A distal region (517 np) of the *purN* gene adjacent to the 5'-terminus of the *purH* gene was amplified using N1 and N2 primers, followed by cloning into pNZT1 plasmid at restrictases SacII and PstI digestion sites. The proximal region (442 np) of the *purD* gene adjacent to the 3'-terminus of the *purH* gene was amplified at the next stage using D1

and D2 primers (Table 2), followed by cloning at restrictases PstI and KpnI digestion sites into the pNZT1 plasmid that was obtained at the previous stage and contained the insertion of the *purN* gene fragment. The *E. coli* strain TG1 was transformed by this plasmid. *Em^R* transformants were sampled from a medium with erythromycin (300 µg/mL) at 30°C. The presence of the pNZT1 plasmid with cloned *purN* and *purD* gene fragments was tested in the resulting clones using PCR. The AM764 *purR::neo ΔT-purE* strain was transformed by pNZT1-*purN-purD* plasmids isolated from the inspected clones. The selection of the *Em^R* transformants was carried out on a medium containing erythromycin (3 µg/mL). Several *Em^R* clones were cultured at 37°C for a night, seeded into plates containing the LB medium with erythromycin (3 µg/mL) and incubated for 24 h at 37°C. *Em^R* recombinants were formed by integration of the pNZT1-*purN-purD* plasmid into the corresponding chromosome locus, which was attested by PCR amplification of the fragment consisting of 2413 bp using N1 and D2 primers. Several *Em^R* clones were seeded into an antibiotic-free liquid LB medium and incubated on a shaker at 30°C for 48 h. This was followed by seeding onto plates with an antibiotic-free LB medium and incubation for another 24 h at 30°C. The excision of the integrated pNZT1 plasmid from the

resulting clones was tested. This was detected by the emergence of erythromycin-sensitive clones. As noted above, plasmid excision can be accompanied by either the retention of the wild-type allele of the *purH* gene in the chromosome, or by substitution of this allele for the Δ *purH* deletion (Fig. 3). The integration (transfer) of the Δ *purH* deletion into the chromosome of the AM764 *purR::neo* Δ *T-purE* strain was attested by the production of a PCR fragment (with a size of 2413 np) with the participation of N1 and D2 primers. One of the variants of the AM764 *purR::neo* Δ *T-purE* strain comprising the Δ *purH* deletion and called AM778 was capable of accumulating up to 4–5 g/L of AICAR in CL and grew on the minimal medium only upon addition of hypoxanthine, adenine, or guanine, suchwise the presence of the defect *purH* gene in its genome was confirmed. Simultaneously, the control strain AM793 was constructed: it contained Δ *purH*, but it carried no *purR::neo* and Δ *T-purE* mutations, which provide derepression of the enzymes that involved in purine biosynthesis.

It was reasonable to increase the intracellular content of PRPP, the key precursor of purine biosynthesis; in order to enhance the productivity of the strain obtained (Fig. 1). It is well known that PRPP synthases that are responsible for PRPP synthesis in the cell of both *B. subtilis* [35] and *E. coli* [36] are susceptible to allosteric inhibition by purine nucleotides, including phosphorylated derivatives of AICAR. As previously mentioned in the introduction section, the mutant variant of PRPP synthase of *E. coli*, which is not susceptible to allosteric regulation, has been described [22]. Therefore, the goal was to obtain an analogous mutant enzyme of *E. coli*, to clone it, and to optimize the expression of this enzyme in strain AM778 cells. However, prior to this, the integrative expression vector had to be constructed, which could provide a high level of expression of heterologous *E. coli* genes in *B. subtilis* cells.

Construction of the integrative expression vector based on pDG268 plasmid

The pDG268 plasmid was selected as starting material in order to obtain the integrative expression vector. This plasmid can be replicated in *E. coli* (but not *B. subtilis*) cells. However, when introduced into *B. subtilis* cells, it may integrate into the chromosome locus *amyE* of *B. subtilis*. The pDG268 plasmid comprises a cartridge that includes the polylinker, *lacZ* reporter gene without the intrinsic promoter, and the chloramphenicol (Cm^R) resistance gene (Fig. 4). The cartridge is flanked by fragments of the *amyE* gene, which permits integration of the vector with the cloned fragment into the *amyE* locus on the *B. subtilis* chromosome.

The promoter of the *rpsF* gene encoding the ribosomal protein S6 in bacilla was selected as a promoter

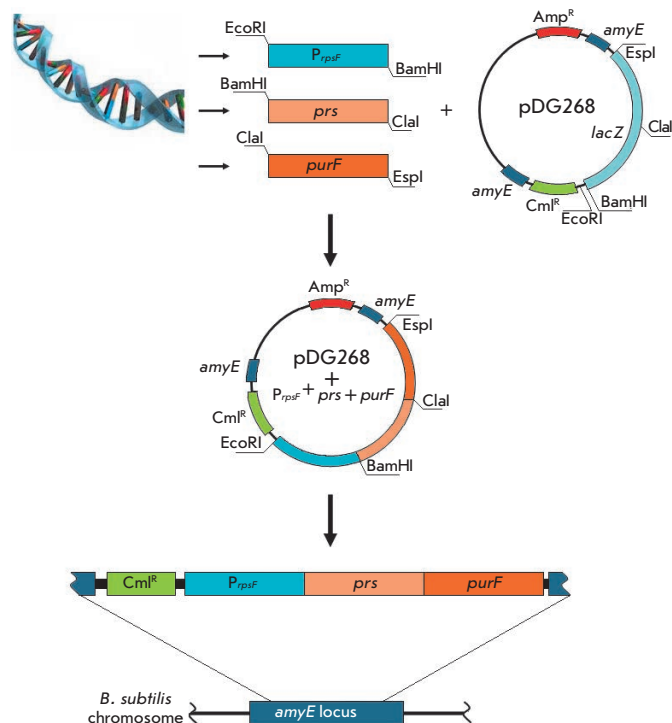


Fig. 4. A schematic representation of cloning procedure of *E. coli* *prS* and *purF* genes under the control of the *B. subtilis* *rpsF* gene promoter in the plasmid pDG268, and their integration into the *B. subtilis* chromosome.

that is capable of providing a high level of expression of the cloned *E. coli* genes in *B. subtilis* cells. The promoters of ribosomal protein genes have been known to belong to the strongest promoters in *B. subtilis*; their expression is coordinated with the bacterial growth rate and attains a maximum level at the logarithmic growth stage [37, 38]. The nucleotide sequence of the *rpsF* gene promoter is shown in Fig. 5. As follows from Fig. 5, the *P_{rpsF}* promoter contains the canonic sequence -70...-50 np, the so-called UP element, which provides a more efficient transcription initiation [39].

With the purpose of cloning the *P_{rpsF}* promoter into the pDG268 plasmid, the DNA fragment containing the promoter region of the *rpsF* gene was amplified by PCR from the *B. subtilis* 168 chromosome using R1 and R2 primers (Table 2). The resulting PCR fragment was digested with the restriction endonucleases *Eco*RI and *Bam*HI and cloned into the pDG268 plasmid digested with the same restrictases (Fig. 4). The *E. coli* TG1 strain was transformed by a ligase mixture. The transformants carrying the insertion of the desired fragment were sampled from an indicator medium containing ampicillin at a concentration of 120 μ g/mL and X-gal. Transformant colonies were bright blue, since it was revealed that the *lacZ* reporter gene was controlled by

the cloned P_{rpsF} promoter. The presence of the insertion was confirmed by PCR using R1 and R2 primers. The resulting plasmid was then integrated into the chromosome *amyE* locus of *B. subtilis* by selecting the chloramphenicol (Cm^R)-resistant transformants. The schematic representation of the integration of the pDG268 vector with the cloned *B. subtilis rpsF* gene promoter is provided in Fig. 4. The determination of the activity of β -galactosidase in these transformants revealed that the *lacZ* reporter gene expression under control of the P_{rpsF} promoter was higher than the expression of this gene when controlled by common promoters, such as the natural *pur*-operon promoter (no data presented), by an order of magnitude. The vector constructed was named pLE1.

Site-directed mutagenesis of the *prs* *E. coli* (*prs_E*) gene

According to the published data, specific mutation in the *prs_E* gene, resulting in the Asp128 → Ala replacement in PRPP synthase, leads to the removal of retroinhibition of the enzyme by purine nucleotides [22]. In order to achieve the analogous mutation, synthesis of the oligonucleotide primers P3 and P4 (Table 2) was performed; the primers contain nucleotide replacements (are denoted by uppercase letters) resulting in the formation of a mutant protein with the Asp128 → Ala replacement. At the first stage, PCR fragments were amplified with the participation of two primer pairs: P4–P1 (it flanks the 5'-terminus of the *prs_E* gene and contains the recognition site for restrictase ClaI). Then, the obtained fragments were joined, and the full-size *prs_E* gene was amplified using the P1 and P2 primers (Table 2). It should be emphasized that the nucleotide sequence of the ribosome recognition site (SD) optimized for expression in bacilli is included into the 5'-region of the P1 primer. At the next stage, the P1–P2 PCR fragment containing the mutant *prs_E* gene was cloned into the earlier obtained pLE1 vector using BamHI and ClaI restrictases. As a result, pLE2 plasmid containing the mutant *prs_E* gene controlled by the P_{rpsF} promoter was obtained. At the final stage, pLE2 plasmid was integrated into the *amyE* *B. subtilis* chromosome locus according to the earlier described scheme (Fig. 4). The strain obtained by integration of the pLE2 plasmid was named AM811 (Table 1).

Site-directed mutagenesis of the *purF* *E. coli* (*purF_E*) gene

The first enzyme of purine biosynthesis, glutamine-PRPP aminotransferase (*purF* gene), plays the primary role in ensuring the normal functioning of the purine biosynthetic path in *E. coli* and *B. subtilis*. In addition, it is susceptible to allosteric regulation with the participa-

tion of nucleotides, which is even more sophisticated in comparison with the PRPP synthase [40]. Therefore, it could be expected that the use of the mutant glutamine-PRPP aminotransferase from *E. coli* that is analogous to that described in [25] will lead to AICAR production. According to [25], Lys326 → Gln and Pro410 → Trp replacements in the protein modify the GMP (A-site) and AMP binding site (C-site), respectively. Combination of these mutations leads to the enzyme being resistant to almost any purine nucleotide. Site-directed mutagenesis of the *purF_E* gene was performed according to the scheme described in the previous section. The F3 and F4 oligonucleotide primers were synthesized to obtain the Lys326 → Gln replacement; and F4 and F5 primers, to obtain the Lys326 → Gln replacement (in Table 2, the corresponding nucleotide replacements are highlighted by uppercase letters and set off in bold). After the PCR amplification of these primers with the flanking primers F1 and F2, followed by the joining of the PCR fragments, the full-size *purF_E* gene encoding the protein with both amino acid replacements was obtained. As found in the case of the *prs_E* gene, the SD site optimized for bacilli was introduced into primer F1. The modified *purF_E* gene was cloned into the pLE1 plasmid under the control of the P_{rpsF} promoter at the ClaI and EspI sites. The modified *purF_E* gene was cloned into the pLE2 plasmid containing the *prs_E* gene using the same procedure. The corresponding plasmids were named pLE3 and pLE4 (Table 1). At the final stage, plasmids pLE3 and pLE4 were integrated into the *amyE* *B. subtilis* chromosome locus according to the scheme described above (Fig. 4). The strains obtained by integrating plasmids pLE3 and pLE4 were named AM813 and AM815, respectively (Table 1).

Determination of the ability of strains to accumulate AICAR

The fermentation experiments were carried out under the conditions described in the experimental section, in order to estimate the ability of the strains obtained in this study to accumulate AICAR. The results of these experiments are summarized in Fig. 6.

As follows from the data given in Fig. 6, the initial AM732 strain accumulates almost no AICAR. Only after the *purH* gene has been removed from the genome of this strain (AM793 strain) is a negligible (< 1 g/L) accumulation of AICAR in CL observed. The mutations of *purR::neo* and ΔT -*purE* (AM788 strain) ensuring complete derepression of the enzymes of purine biosynthesis result in a considerable accumulation of AICAR; up to 4–5 g/L. A subsequent, almost two-fold enhancement of productivity was observed for the AM811 and AM813 strains expressing one of the mutant desensitized *E. coli* proteins — PRPP synthase (*prs* gene) or

obtaining the AICAR producing strain is based on the directed reconstruction of purine metabolism in *B. subtilis* cells. At the first stage of the study, an insertion was introduced into the *purR* gene encoding the *pur*-operon repressor protein, and the transcription attenuator was removed from the leader region of the *pur*-operon, ensuring maximum derepression of the enzymes of *de novo* purine biosynthesis. The *purH* gene encoding formyltransferase/IMP-cyclohydrolase was then removed from the bacterial genome. Inactivation of this enzyme disturbs the reaction of AICAR conversion into IMP and results in its accumulation in the cell. At the next stage, the site-directed mutagenesis of *prs* and *purF* *E. coli* genes encoding the key enzymes of the synthesis of purine precursors was carried out in order to obtain mutant variants of these genes that would not be susceptible to retroinhibition by purine nucleotides. Finally, at the last stage, the modified *prs* and *purF* *E. coli* genes were integrated into the *B. subtilis* chromosome under the control of a strong promoter ensuring a high level of expression of these genes in *B. subtilis* cells. As a result, we obtained a producing strain accumulating 11–13 g/L of AICAR in CL.

To summarize, we would like to note that it was reported recently that AICAR had successfully passed the stage IIa of clinical trials as a antitumor agent [45]. AICAR has a positive effect upon chronic lymphocytic leukemia, multiple myeloma, and mantle cell lymphoma. It should be emphasized that the cost of commercial AICAR substances in catalogues varies from US\$100 to 1,000 per gram, which is likely due to the fact that they are prepared by chemical synthesizing. The high cost makes AICAR inaccessible for research and a fortiori for treatment of the metabolic syndrome. The AICAR-producing strain constructed by us may lay the foundations for industrial microbiological production of an affordable AICAR substance that would cost substantially less. ●

The authors are grateful to N.P. Zakataeva for providing the pNZT1 plasmid and to V.A. Muratova and G.I. Sergeeva for qualified technical assistance. The work was partially supported by the Dynasty Foundation for Non-commercial Programs.

REFERENCES

- Buchanan J.M., Hartman S.C. // *Adv. Enzymol. Relat. Areas Mol. Biol.* 1959. V. 21. P. 199–261.
- Zalkin H., Nygaard P. // *Escherichia coli* and *Salmonella*. Washington, DC.: ASM Press, 1996. P. 561–579.
- Switzer R.L., Zalkin H., Saxild H.H. // *Bacillus subtilis* and its closest relatives: from genes to cells. Washington, DC.: ASM Press, 2002. P. 255–269.
- Hardie D.G., Carling D., Carlson M. // *Ann. Rev. Biochem.* 1998. V. 67. P. 821–855.
- Hardie D.G., Salt I.P., Hawley S.A., Davies S.P. // *Biochem. J.* 1999. V. 338. P. 717–722.
- Rutter G.A., Xavier G.S., Leclerc I. // *Biochem. J.* 2003. V. 375. P. 1–16.
- Gaidhu M.P., Fediuc S., Anthony N.M., So M., Mirpourian M., Ceddia R.B. // *J. Lipid Res.* 2009. V. 50. P. 704–715.
- Swinnen J.V., Beckers A., Brusselmans K., Organe S., Segers J., Timmermans L., Vanderhoydonc F., Deboel L., Derua R., Waelkens E., et al. // *Cancer Res.* 2005. V. 65. P. 2441–2448.
- Pold R., Jensen L.S., Jessen N., Buhl E.S., Schmitz O., Flyvbjerg A., Fujii N., Goodyear L.J., Gotfredsen C.F., Brand C.L., et al. // *Diabetes.* 2005. V. 54. P. 928–934.
- Campas C., Lopez J.M., Santidrian A.F., Barragan M., Bellosillo B., Colomer D., Gil J. // *Blood.* 2003. V. 101. P. 3674–3680.
- Sengupta T.K., Leclerc G.M., Hsieh-Kinzer T.T. // *Mol. Cancer.* 2007. V. 6(46). P. 1–12.
- Matsuno K., Mori Y., Asahara T. // US Patent 7326546 (2008).
- Asahara T., Mori Y., Zakataeva N.P., Livshits V.A., Yoshida K., Matsuno K. // *Appl. Microb. Biotechnol.* 2010. V. 87. P. 2195–2207.
- Ebbole D.J., Zalkin H. // *J. Biol. Chem.* 1987. V. 262. P. 8274–8287.
- Weng M., Nagy P.L., Zalkin H. // *Proc. Natl. Acad. Sci. USA.* 1995. V. 92. P. 7455–7459.
- Ebbole D.J., Zalkin H. // *J. Biol. Chem.* 1988. V. 263. P. 10894–10902.
- Johansen L.E., Nygaard P., Lassen C., Agerso Y., Saxild H.H. // *J. Bacteriol.* 2003. V. 185. P. 5200–5209.
- Mironov A.S., Gusarov I., Rafikov R., Lopez L.E., Shatalin K., Kreneva R.A., Perumov D.A., Nudler E. // *Cell.* 2002. V. 111. P. 747–756.
- Nudler E., Mironov A. S. // *Trends Biochem. Sci.* 2004. V. 29. P. 11–17.
- Mandal M., Boese B., Barrick J.E., Winkler W.C., Breaker R.R. // *Cell.* 2003. V. 113. P. 577–586.
- Lobanov K.V., Korol'kova N.V., Eremina, S. Yu., Er-raïs Lopes L., Mironov A.S. // *Rus. J. Genetics.* 2011. V. 47. P. 785–793.
- Hove-Jensen B., Nygaard P. // *Eur. J. Biochem.* 1982. V. 126. P. 327–332.
- Meyer E., Switzer R.L. // *J. Biol. Chem.* 1979. V. 254. P. 5397–5402.
- Turnbough C.L., Switzer R.L. // *J. Bacteriol.* 1975. V. 121. P. 108–114.
- Zhou G., Smith J.L., Zalkin H. // *J. Biol. Chem.* 1994. V. 269. P. 6784–6789.16. C.L.
- Anagnostopoulos C., Spizizen J. // *J. Bacteriol.* 1961. V. 81. P. 741–746.
- Yoshikawa H., Sueoka N. // *Proc. Nat. Acad. Sci. USA.* 1963. V. 49. P. 559–566.
- Christiansen L.C., Schou S., Nygaard P., Saxild H.H. // *J. Bacteriol.* 1997. V. 179. P. 2540–2550.
- Blattner F.R., Plunkett G. 3rd, Bloch C.A., Perna N.T.,

RESEARCH ARTICLES

- Burland V., Riley M., Collado-Vides J., Glasner J.D., Rode C.K., Mayhew G.F., et al. // *Science*. 1997. V. 277. P. 1453-1474.
30. Zakataeva N.P., Nikitina O.V., Gronskiy S.V., Romanenkov D.V., Livshits V.A. // *Appl. Microbiol. Biotechnol.* 2010. V. 85. P. 1201-1209.
31. Sambrook J., Fritsch E.F., Maniatis T. *Molecular cloning: a laboratory manual*, 2nd ed. N.Y. Cold Spring Harbor: Cold Spring Harbor Lab. Press. 1989.
32. Saito H., Miura K.I. // *Biochim. Biophys. Acta.* 1963. V. 42. P. 619-629.
33. Sanger F., Nicklen S., Coulson A.R. // *Proc. Natl. Acad. Sci. USA.* 1977. V. 74. P. 5463-5467.
34. Shatalin K.Y., Neyfakh A.A. // *FEMS Microbiol. Lett.* 2005. V. 245. P. 315-319.
35. Arnvig K., Hove-Jensen B., Switzer R.L. // *Eur. J. Biochem.* 1990. V. 192. P. 195-200.
36. Hove-Jensen B., Harlow K.W., King C.J., Switzer R.L. // *J. Biol. Chem.* 1986. V. 261. P.6765-6771.
37. Henkin T.M. // *Bacillus subtilis* and other gram-positive bacteria: biochemistry, physiology, and molecular genetics / Eds. Sonenshein A.L., Hoch J.A., Losick R. Washington, D.C.: American Soci. Microbiol., 1993. P. 669-682.
38. Linder C., Nijland R., Hartskamp M. // *J. Bacteriol.* 2004. V. 186. P. 1097-1105.
39. Estrem S.T., Gaal T., Ross W. Gourse R.L. // *Proc. Natl. Acad. Sci. USA.* 1998. V. 95. P. 9761-9766.
40. Chen S., Tomchick D.R., Wolle D., Hu P., Smith J.L., Switzer R.L., Zalkin H. // *Biochemistry.* 1997. V. 36. P. 10718-10726.
41. Sheremet A.S., Gronskiy S.V., Akhmadyshev R.A., Novikova A.E., Livshits V.A., Shakulov R.S., Zakataeva N.P. // *J. Ind. Microbiol. Biotechnol.* 2011. V. 38. P. 65-70.
42. Bochner B.R., Ames B.N. // *Cell.* 1982. V. 29. P. 929-937.
43. Dougherty M.J., Boyd J.M., Downs D.M. // *J. Biol. Chem.* 2006. V. 28. P. 33892-33899.
44. Rebora K., Laloo B., Daignan-Fornier B. // *Genetics.* 2005. V. 170. P. 61-70.
45. The Advancell Company Press Release on 16.02.2011.

Dimeric Structure of the Transmembrane Domain of Glycophorin A in Lipidic and Detergent Environments

K.S. Mineev, E.V. Bocharov*, P.E. Volynsky, M.V. Goncharuk, E.N. Tkach, Ya.S. Ermolyuk, A.A. Schulga, V.V. Chupin, I.V. Maslennikov, R.G. Efremov, A.S. Arseniev

Shemyakin and Ovchinnikov Institute of Bioorganic Chemistry, Russian Academy of Sciences

*E-mail: bon@nmr.ru

Received 24.02. 2011

ABSTRACT Specific interactions between transmembrane α -helices, to a large extent, determine the biological function of integral membrane proteins upon normal development and in pathological states of an organism. Various membrane-like media, partially those mimicking the conditions of multicomponent biological membranes, are used to study the structural and thermodynamic features that define the character of oligomerization of transmembrane helical segments. The choice of the composition of the membrane-mimicking medium is conducted in an effort to obtain a biologically relevant conformation of the protein complex and a sample that would be stable enough to allow to perform a series of long-term experiments with its use. In the present work, heteronuclear NMR spectroscopy and molecular dynamics simulations were used to demonstrate that the two most widely used media (detergent DPC micelles and lipid DMPC/DHPC bicelles) enable to perform structural studies of the specific interactions between transmembrane α -helices by the example of dimerizing the transmembrane domain of the bitopic protein glycophorin A. However, a number of peculiarities place lipid bicelles closer to natural lipid bilayers in terms of their physical properties.

KEYWORDS bitopic membrane proteins; transmembrane domain; dimerization; spatial structure; molecular dynamics; NMR

ABBREVIATIONS TM – transmembrane; GpAtm – TM fragment 61-98 of human protein glycophorin A, GpA₆₁₋₉₈; DPC – dodecylphosphocholine; DMPC – dimyristoylphosphatidylcholine; DHPC – dihexanoylphosphatidylcholine; RMSD – root-mean-square deviation; NOE – nuclear Overhauser effect; NOESY – nuclear Overhauser enhancement spectroscopy experiment; HSQC – heteronuclear single quantum coherence experiment

INTRODUCTION

Membrane proteins constitute more than 25% of the proteome [1], fulfilling some important functions; they ensure the uniqueness of the biological role of each cell membrane and determine its physicochemical properties. The most important cell processes, such as intercellular reception and communication, molecular and ion transport, membrane fusion, etc., are directly associated with the participation of membrane proteins. Interaction between the transmembrane (TM) domains of proteins that are capable of oligomerizing in the membrane is, in many cases, important for the manifestation of their activity. The so-called bitopic membrane proteins, which have a single TM α -helical segment, play the key role in numerous biological processes taking place in the human organism. The regulation of the activity of bitopic proteins in most cases is associated with homo- or hetero-dimerization in the cell membrane, with the active participation of their TM domains [2, 3]. This class of proteins comprises the majority of receptor protein kinases, immunoreceptors, and apopto-

sis proteins, which play a direct part in controlling the development and homeostasis of all organism tissues, both in the normal and pathological states.

In order to study the physical parameters of the interaction between the TM domains of proteins using solution NMR spectroscopy, it is necessary to place them into a medium that can mimic the cell membrane [4]. To record high-quality NMR spectra, the particles in this medium have to be relatively small, while the sample's stability needs to permit the performance of a series of long-term experiments. Meanwhile, the choice of the composition of the membrane-like medium, in which the TM-protein complex would have a biologically significant conformation, is very important. Two classes of membrane mimetics are currently in wide use: detergent micelles with a spherical shape and phospholipid bicelles, which are believed to be disc-shaped [5].

The present work is the first comparative study in the world devoted to the investigation of the effect of various membrane-like media on the conformation of the dimerizing TM domain of bitopic protein. Glyco-

phorin A, an antigen-presenting protein on the surface of human erythrocytes, has been widely used as a model object for fine-tuning experimental and theoretical procedures in the study of the spatial structure and intramolecular dynamics of the interacting TM domains of bitopic proteins. The spatial structure of the TM dimer was first determined for the GpAtm domain solubilized in micelles. However, a number of uncertainties in its structure still remain [6–8]. In order to assess the degree to which the membrane-like environment influences the conformation of interacting TM α -helices, the structural and dynamic characteristics of the homodimer of the GpA_{61–98} TM fragment (GpAtm) were investigated in the following two media: detergent dodecylphosphocholine (DPC) micelles and lipid bicelles consisting of a mixture of dimyristoylphosphatidylcholine / dihexanoylphosphatidylcholine (DMPC/DHPC).

EXPERIMENTAL

Preparation of NMR samples of the recombinant GpA_{61–98} TM fragment (GpAtm) in membrane-like media

The recombinant peptide corresponding to the fragment R⁶¹VQLAHHFSEPEITLIIFGVMAGVIGTILL-ISYGIRRL⁹⁸ of human GpA (GpAtm), comprising the TM domain (underlined), was prepared following the procedure in [9, 10]. In NMR studies, detergent DPC micelles and small DMPC/DHPC bicelles with a molar ratio of lipids of 1 : 4 were used as membrane-like media. A completely deuterated detergent *d*₃₈-DPC (Cambridge Isotope Laboratories, Andover, MA, United States) and lipids *d*₅₄-DMPC and *d*₂₂-DHPC with deuterated acyl chains synthesized in accordance with [11] were used. Dry powders of the protein and detergents, or lipids, were dissolved in a 1 : 1 (v/v) trifluoroethanol–water mixture and lyophilized. The dry powder was dissolved in a buffer containing deuterated sodium acetate (20 mM, pH 5.0, 5% D₂O), EDTA (1 mM) and sodium azide (0.05 mM). Then, five freeze-heat cycles (to ~40°C) followed by suspension in an ultrasonic bath were performed until the solution became completely transparent. All samples were prepared based on 2 mM of mM GpAtm in 0.5 ml of a micelle or bicelle solution with a molar ratio of peptide/detergent or peptides approximately 1 : 35, providing approximately two molecules of the TM peptide per micelle/bicelle (meanwhile, taking into account the critical micelle concentration of lipids, the effective ratio between the amount of long and short lipids in a bicelle $q \approx 0.3$). In each of the two membrane-like media, three GpAtm dimer samples were prepared: using only ¹⁵N-labeled or ¹⁵N/¹³C-labeled TM peptide and the 1 : 1 mixture of ¹⁵N/¹³C-la-

beled and non-labeled TM peptide (“isotopic-heterodimer sample”).

The sizes of micelles and bicelles with embedded GpAtm, as well as its secondary structure, were controlled using optical methods, such as dynamic light scattering and circular dichroism. Dynamic light scattering experiments were performed on a DynaPro Titan instrument (Wyatt Technology Corporation, United States) in a 12 μ l cell at a temperature of 30°C. The circular dichroism spectra for GpAtm embedded into micelles, bicelles, or liposomes (phospholipid bilayer) were ascertained on a J-810 spectropolarimeter (Jasco, Japan) in a 0.1 mm quartz cell at 30°C and with a peptide concentration of 1 mg/ml. The circular dichroism spectra were analyzed using CDSSTTR software [12]. In order to prepare small monolayer vesicles, a liposome-containing slurry from DMPC at a 1 : 50 peptide/lipid ratio was treated with ultrasound in ice using an ultrasonic disintegrator with a titanium tip (VirSonic-600, United States) until the sample became completely transparent (approximately 10 min).

NMR spectroscopy, calculation, and relaxation of the spatial structure of the dimer of a GpA_{61–98} TM fragment solubilized in membrane-like media

The NMR spectra of GpAtm solubilized in DPC micelles and DMPC/DHPC bicelles at pH 5.0 and 40°C were recorded on UNITY (Varian, Palo Alto, CA, United States) and AVANCE-III (Bruker BioSpin, Rheinstetten, Germany) spectrometers with proton operating frequencies of 600 MHz. The NMR spectra were analyzed using CARA software [13]. Assignment of the ¹H-, ¹³C-, and ¹⁵N resonances of the peptide and obtainment of the structural data were carried out using the standard procedure, employing the triple resonance experiments in [14, 15]. The data concerning the intra-molecular dynamics of the TM peptide were obtained by analyzing the ¹⁵N relaxation data: the values of the hetero-nuclear ¹⁵N{¹H} NOE, longitudinal (*T*₁) and transversal (*T*₂) relaxation times, and the effective rotational correlation times (τ_R) were measured in accordance with the procedure described in [16]. The rates of exchange of amide protons for the deuterium of the solvent were estimated from the changes in signal intensities in the ¹H/¹⁵N-HSQC spectral array; the spectra were sequentially collected during a 24 h period for the GpAtm samples that were preliminarily embedded into micelles and bicelles, lyophilized, and then dissolved in D₂O.

The spatial structure was calculated in accordance with the standard procedure in [14], utilizing CYANA 3.0 software [17] and using the method of molecular dynamics in torsion angle space and the simulated annealing algorithm. The restraints on interproton in-

tramer distances were obtained from the NOE cross peak volumes in the $^1\text{H}/^{15}\text{N}$ -NOESY-HSQC and $^1\text{H}/^{13}\text{C}$ -NOESY-HSQC spectra accumulated during a mixing time $t_m = 80$ ms. Intermolecular NOE contacts at the GpAtm dimerization interface were obtained from the 3D $^1\text{H}/^{15}\text{N}/^{13}\text{C}$ -F1-filtered/F3-separated-NOESY-HSQC spectra ($t_m = 80$ ms) using the “isotopic-heterodimer sample” [15]. The ranges of the dihedral angles ϕ , ψ , and χ^1 of the protein backbone were estimated from the values ^1H , ^{15}N , and ^{13}C of the chemical shifts of the NH-, C α H-, and CO groups of GpAtm in TALOS software [18]. The restraints on hydrogen bonds were added after preliminary calculation of the structure based on the analysis of the data on the rates of amide protein exchange for the deuterium of the solvent and the spatial proximity of amide proteins to the oxygen atoms of the GpAtm backbone in the preliminary array of structures. The restraints introduced were as follows: on angles $140^\circ < \text{NHO} < 180^\circ$ and $130^\circ < \text{COH} < 170^\circ$ and on distances $1.9 \text{ \AA} \leq d(\text{O}, \text{H}^{\text{N}}) \leq 2.3 \text{ \AA}$, $3.0 \text{ \AA} \leq d(\text{O}, \text{N}) \leq 3.4 \text{ \AA}$, $3.2 \text{ \AA} \leq d(\text{C}, \text{H}^{\text{N}}) \leq 3.6 \text{ \AA}$ [19]. As a result, based on the upper limits on interprotonic distances (taking into account the stereospecific assignment of peptide groups) and the restraints both on the dihedral angles ϕ , ψ , and χ^1 and on hydrogen bonds, we calculated the arrays consisting of 200 structures for GpAtm embedded into micelles or bicelles. Then, 20 structures with the lowest values of the penalty function were selected from these arrays in order to be used as representative ones.

The energy relaxation of representative NMR structures of the GpAtm dimer was performed in the explicitly specified hydrated DPC micelles (60 molecules) or in the DMPC bilayer (512 molecules), respectively, by the molecular dynamics (MD) method using the GROMACS 3.3.1 software package [20] as was earlier described in [21]. After balancing and minimizing the energy of the system, MD trajectories with a duration of 2 ns and fixed position of GpAtm dimer atoms were calculated. Next, the calculation of MD trajectories with a duration of 10 ns and experimental NMR restraints on distances were performed, followed by the ones with 10 ns duration, without any restraints (in order to assess the system's stability).

The CYANA 3.0, MOLMOL [22], and PYMOL [23] software programs were used to analyze and visualize the spatial structures. The hydrophobic properties of the surface of α -helices were calculated using the molecular hydrophobic potential (MHP) approach [24]. The area of contact surfaces between the α -helices was calculated using the DSSP software [25] as the differential between the surface of GpAtm residues that is accessible to the solvent in the monomeric and dimeric states, respectively.

RESULTS AND DISCUSSION

Spatial structure and intramolecular mobility of the GpAtm dimer

The effect of the membrane-like environment on the interactions between the helices in the GpAtm homodimer was studied on the example of two media that have been frequently used in NMR spectroscopy of membrane proteins (*Figs. 1a,b*): spherical DPC micelles and disc-shaped DMPC/DHPC lipid bicelles ($q \approx 0.3$) [4, 5]. In order to eliminate any possible discrepancies connected with the different procedures of collection of the experimental NMR data and calculation of the spatial structure, the earlier obtained spatial structure of the GpA₆₂₋₁₀₁ TM-fragment in DPC micelles [6] is not taken into account in this study.

The circular dichroism spectra for the GpAtm fragment embedded both into DPC micelles or DMPC/DHPC bicelles and unilamellar DMPC liposomes (phospholipid bilayer) was revealed to be almost identical and as corresponding to an α -helix content of $75 \pm 8\%$. Parameters of the NMR relaxation of the ^{15}N nuclei of the GpAtm backbone: $^{15}\text{N}\{^1\text{H}\}$ NOE, times T_1 and T_2 , and calculated effective rotational correlation times (τ_{R}) of vectors ^{15}N -H (*Fig. 2*) attest to the presence of the stable E⁷⁰-R⁹⁶ TM segment, which is flanked by flexible N- and C-terminal fragments. The overall rotational correlation time for a peptide/micelle or bicelle complex was estimated from the T_1/T_2 ratio at the TM region and is equal to ~ 13 and ~ 16 ns. According to the empirical dependence [26], it corresponds to the GpAtm dimer, which forms a complex with ~ 65 detergent molecules (~ 34 kDa) or ~ 70 lipid molecules (~ 43 kDa). According to the data of dynamic light scattering, both supramolecular systems have a similar hydrodynamic radius of $26 \pm 4 \text{ \AA}$.

In order to gather information on the interactions between GpAtm helices, we used the NMR spectrum acquired for the “isotopic-heterodimer sample” (*Fig. 1c*). This spectrum shows NOE cross peaks corresponding to the magnetization transfer from the protons that are bound to the ^{14}N and ^{12}C atoms to those bound to the ^{15}N and ^{13}C atoms [15]. As a result, 17 and 14 intermonomeric NOE contacts were detected in micelles and bicelles, respectively. The sets of intra- and intermonomeric NOE contacts identified in the NMR spectra demonstrated that GpAtm forms a symmetrical, in the NMR time scale, homodimer in both media; this dimer consists of two parallel helices. It should be noted that most of the differences in the systems of NOE contacts observed for GpAtm in micelles and bicelles can be explained via the changes in the chemical shifts of the signals and associated differences in the overlapping of the cross peaks.

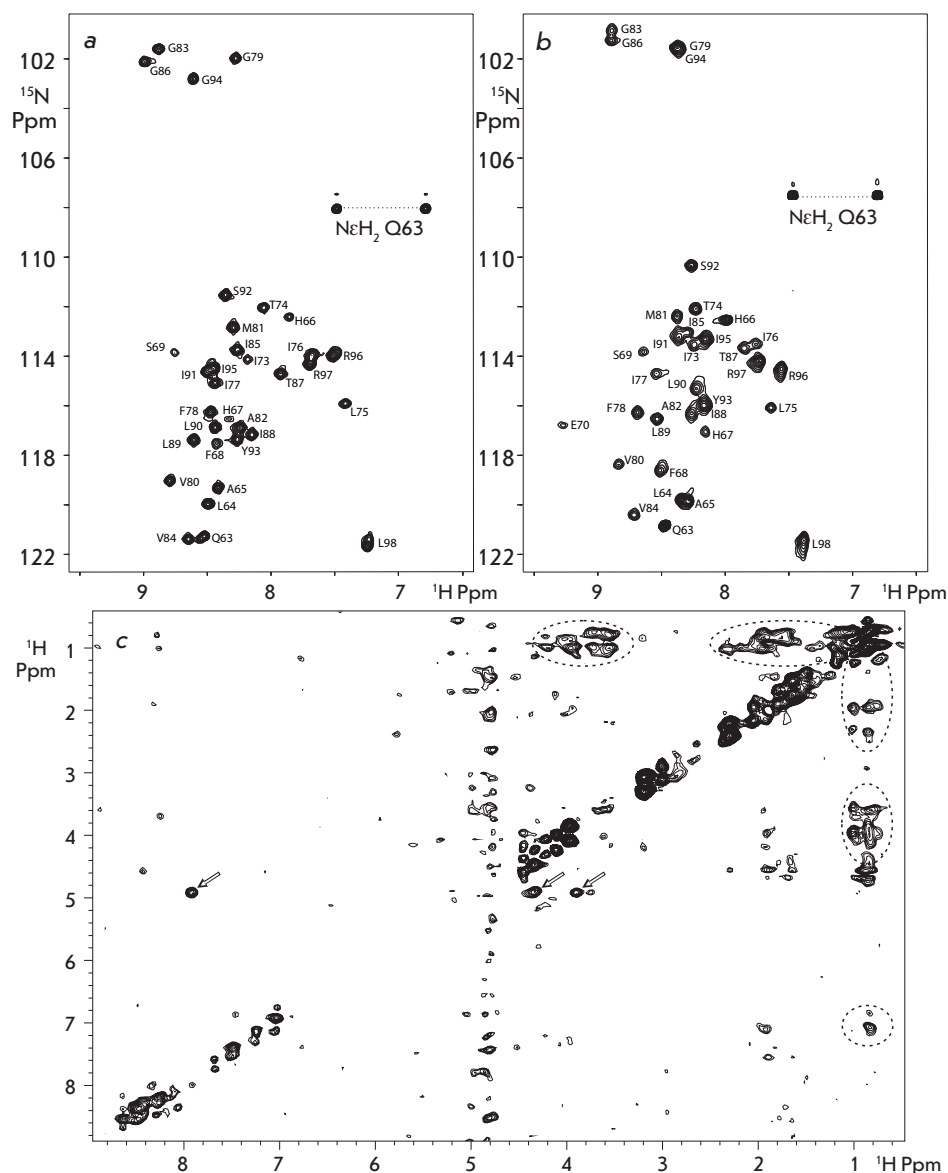


Fig. 1. *a* and *b* – Heteronuclear NMR spectrum ^1H - ^{15}N HSQC of ^{15}N -labeled GpAtm in DPC micelles and DMPC/DHPC (1/4) bicelles, respectively, with a molar peptide/protein ratio of 1:35, at 40°C and pH 5.0. The resonance assignments are shown. *c* – The intermolecular proton-proton NOE contacts are presented on 2D project of the 3D ^{15}N , ^{13}C F1-filtered/F3-edited-NOESY spectrum acquired for the “isotopic-heterodimer” GpAtm sample embedded into the DPC micelles. The NOE cross peaks from the side chain hydroxyl $\text{O}\gamma\text{H}$ group of T^{87} are labeled by arrows, revealing the intramolecular hydrogen-bonding of the hydroxyl group with the carbonyl group of G^{83} in major conformation of the GpAtm dimer.

The spatial GpAtm structures were determined with high quality and resolution (Table, Fig. 3a). The experimental NMR restraints that were used to calculate the spatial structures and the resulting atomic coordinates for the arrays of structures of the GpAtm dimer embedded into DPC micelles and DMPC/DHPC bicelles were deposited in the international RCSB data bank of spatial structures (www.rcsb.org); their IDs are 2kpe and 2kpf, respectively. The representative structures of the GpAtm dimer were subjected to energy MD relaxation in an explicitly specified DPC micelle and DMPC lipid bilayer with experimental restraints imposed on distances. This made it possible to adapt the NMR structure to the model membrane environment (Fig. 3c) and determine whether the force fields that are used in the MD calculation correspond to the ex-

perimental results. In both cases, the extension of the MD trajectory without restraints did not result in any considerable changes in the dimer structure, which indicates both its relative stability and the admissibility of the force fields used.

In general, the spatial structure and intramolecular mobility of the GpA TM domain in micelles and bicelles differ to an insignificant degree: in both cases, the axes of transmembrane α -helices are located at an angle θ that is equal to -40° , the distance d between them being approximately 6.5 \AA . Moreover, a comparison of the spatial structures of the dimer (Fig. 3a) shows that when passing from micelles to bicelles, a small distortion at the C-terminus of the TM-helices occurs. The periodic character of the changes in the chemical shifts of the signals of amide protons ($\Delta\delta_{\text{HN}}$) along the GpAtm

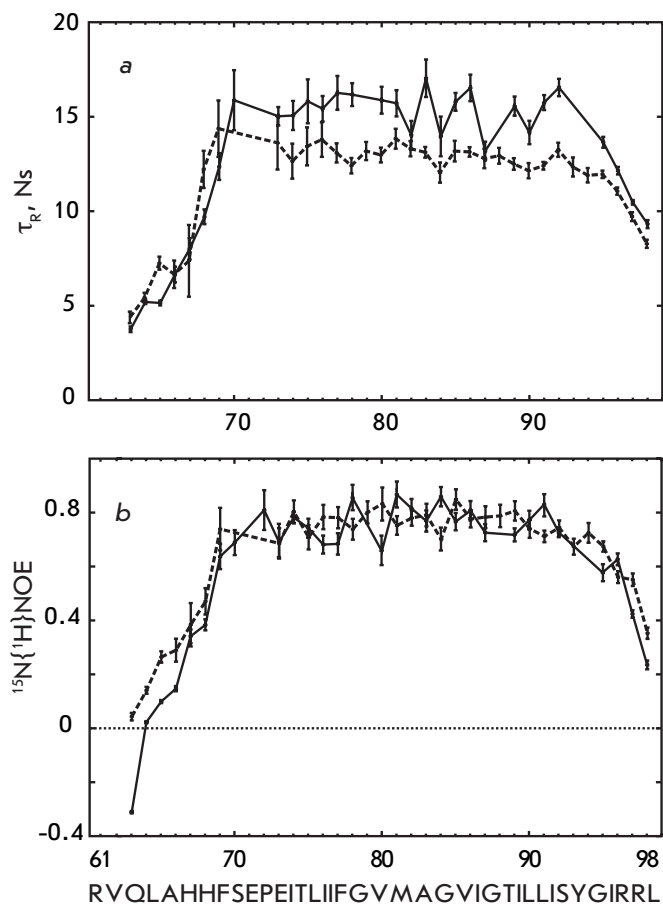


Fig. 2. ^{15}N relaxation data for the amide groups of the GpAtm dimer embedded into detergent DPC micelles (dashed line) and lipid DMPC/DHPC bicelles (solid line): *a* – effective rotation correlation time τ_R calculated from the ratio of the ^{15}N longitudinal T_1 and transverse T_2 relaxation times for the corresponding residues; *b* – steady-state $^{15}\text{N}\{^1\text{H}\}$ NOE values.

amino acid sequence when passing from micelles to bicelles also points to a small distortion at the C-terminus of the helices (Fig. 3b). The tendency towards variation of the average values of $\Delta\delta_{\text{HN}}$ from negative to positive values along the TM helix points to a possible small stretching of its N-terminal fragment before the dimerization interface and compression, after the N-terminal fragment. Along with the general inclination of the GpAtm dimer with respect to the norm of the lipid DMPC bilayer, a small distortion of the C-termini of TM helices was also observed during MD-relaxation (Fig. 3c). On the contrary, no considerable distortions of TM helices in the GpAtm dimer, embedded into a DPC micelle, were detected neither in the set of calculated structures, nor during MD relaxation. Since acyl chains are shorter in DPC (formed by 12 carbon atoms) as compared with DMPC (14 carbon atoms), a longer

TM helix could be expected (e.g., due to the partial transition of the α -helix into helix 3/10) in bicelles as compared with micelles. However, in the resulting set of NMR structures of the GpAtm dimer in micelles and bicelles, no difference in the length of the α -helix fragments was detected. It was only during MD relaxation in an explicitly specified micelle for the first turn of the TM helix of GpAtm that helix-coil transitions were occasionally observed (Fig. 3c). This is in agreement with the fact that micelles are more flexible structures in comparison with bicelles and are capable of adapting, to a larger extent, to the shape and size of the TM protein [27, 28]. In turn, micelles compared with bicelles can provide more freedom to conformational dynamics for the TM protein embedded into them. Indeed, during MD relaxation of GpAtm without the imposition of NMR restraints, the dimer parameters were characterized by amplitudes of random fluctuations in DPC micelles ($\theta 46 \pm 6^\circ$, $d 6.3 \pm 0.8 \text{ \AA}$) that were twice as large as those in the DMPC bilayer ($\theta 42 \pm 3^\circ$, $d 6.4 \pm 0.4 \text{ \AA}$), which points to a denser packing of the TM helices of the dimer in a lipid environment. The changes in the spatial structure of the GpAtm dimer observed by NMR in bicelles as compared with micelles, and the changes in the course of its MD relaxation in the lipid bilayer, seem to be a result of the adaptation of the dimer to the DMPC bilayer in order to prevent the so-called “hydrophobic mismatch” [29, 30].

GpAtm dimerization surface

GpAtm helices embedded into a DPC micelle or DMPC/DHPC bicelle associate into a parallel dimer via the so-called tandem four-membered GG4 motif [31] $\text{G}^{79}\text{VxxG}^{83}\text{VxxT}^{87}$, which is also known as the “glycine zipper” [32]. The motif is formed by the residues with a small side chain, which permits to obtain a tight right-handed packing of the TM helices of GpAtm that contact via their weakly polar surfaces (Figs. 4a,b) in the hydrophobic environment. Meanwhile, the alternative “seven-membered” motif $\text{LI}^{76}\text{xxG}^{79}\text{xxAG}^{83}\text{xxG}^{86}\text{xxLL}^{90}\text{xxY}^{93}$ with left-handed packing of TM α -helices predicted earlier by molecular modelling [33] is not involved.

In both media, there are eight polar intermolecular interactions of $\text{C}\alpha\text{—H}\cdots\text{O}$ type at the GpAtm dimerization interface. These interactions, which can be characterized as non-canonical hydrogen bonds (with the corresponding distance $d(\text{O}, \text{H}) < 3 \text{ \AA}$ and angle $\text{COH} > 120^\circ$ [34]), are formed between $\text{C}\alpha\text{H}$ G^{79} , G^{83} , V^{80} , and V^{84} and the carbonyl groups I^{76} , G^{79} and V^{80} , as well as the O_γH -group of T^{87} , respectively (Fig. 4c). Quantum chemical calculations demonstrated that the presence of interactions of this type should result in a considerable change in the chemical shifts of the proton signals of

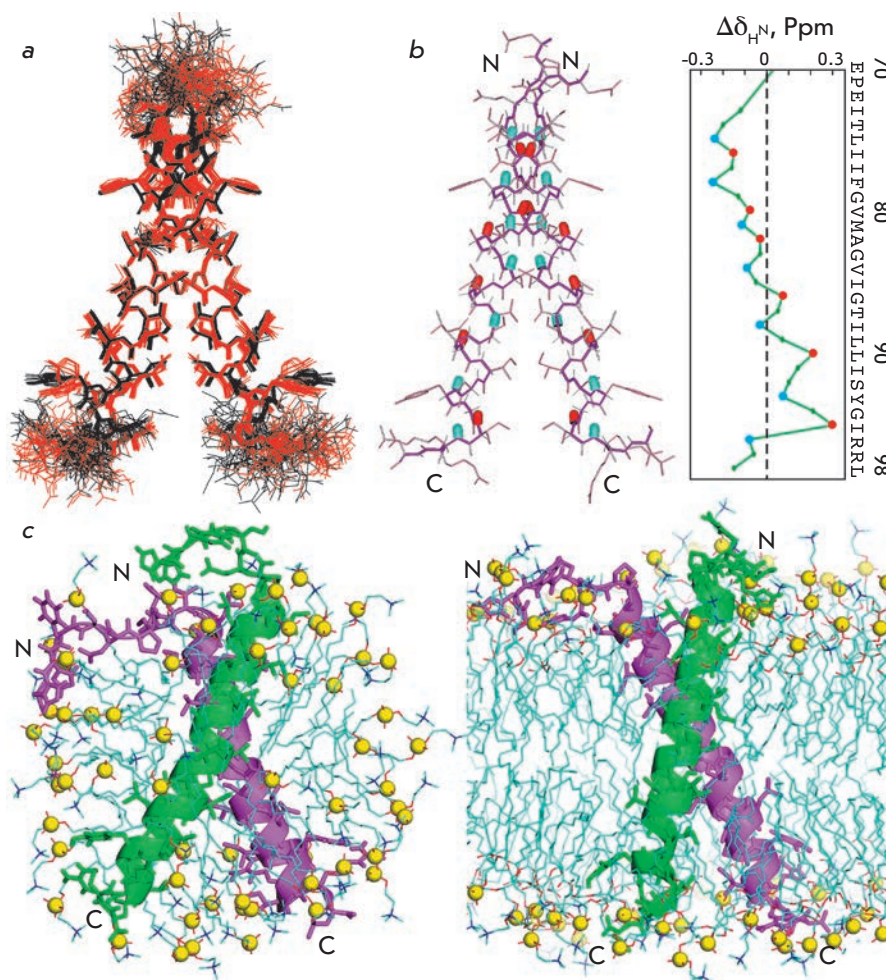


Fig. 3. *a* – Comparison of the 20 NMR-derived structures of the GpAtm dimer in DPC micelles (in *black*) and DMPC/DHPC bicelles (in *red*) after superposition of the backbone atoms of α -helical residues E⁷²–I⁹⁵ of both dimer subunits. The heavy atom bonds of residues (70–98)₂ are shown. *b* – Differences of the amide chemical shifts ($\Delta\delta_{\text{H,N}}$) of GpAtm in bicelles and micelles are shown on the *right*. The amide groups having local minimal and maximal values of $\Delta\delta_{\text{H,N}}$ are highlighted in *blue* and *red*, respectively, in the GpAtm dimer structure shown on the *left*. The $\Delta\delta_{\text{H,N}}$ value strongly depends on the length of the hydrogen bond in which the amide proton participates; thus, the local increase in $\Delta\delta_{\text{H,N}}$ reflects the shortening of the given hydrogen bond [37]. *c* – Ribbon diagrams of the GpAtm dimer after MD-relaxation in an explicit DPC micelle (on the *left*) and DMPC bilayer (on the *right*). Yellow balls show the phosphorus atoms of the detergent and lipid heads. Detergent and lipid tails are shown in *blue*. For the sake of clarity, the structures of the adjacent subunits of the dimer are colored in *green* and *magenta*.

the C α H-groups of the proteins [35]. In other words, the chemical shifts of the proton signals of C α H are a very sensitive sensor determining the distances to the carbonyl groups at the dimerization interface of α -helices. The chemical shifts of protons C α H G⁷⁹, G⁸³, V⁸⁰, and V⁸⁴ almost completely coincide in micelles and bicelles (the maximum difference is 0.05 ppm), which demonstrates a high degree of identity between the structural organizations of the GpAtm dimerization interface in both media. In other words, both the general topology and structural details of the GpAtm dimerization interface are identical in both membrane-like media.

Comparison of the newly obtained GpAtm structures and those published earlier

The structures obtained within the framework of our study agree well with the earlier published data on mutagenesis [31]. On the other hand, the GpAtm structure both in micelle and bicelle turned out to be close (RMSD ~ 1.1 Å on the basis of coordinates of the backbone atoms of residues (72–95)₂) to the earlier published structure of the GpA_{62–101} TM fragment embedded into the

DPC micelle [6]. Later, the conformation of the dimer GpA_{70–98} TM fragment in dried lipid bilayers consisting of DMPC and palmitoyl-oleyl phosphatidylcholine (POPC) was proposed on the basis of the structural restraints obtained using the method of solid-state NMR [7, 8]. In addition to a small decrease in the angle between the axes of the TM helices to -35° and their relative $\sim 25^\circ$ rotation in the dimer, the character of the hydrogen bond that is formed by the side chain of T⁸⁷ is the main distinction from the structure in a DPC micelle. Based on the proximity of the O γ H group of threonine with the carboxyl group V⁸⁴ of the opposite helix, Smith *et al.* [8] arrived at a conclusion that this bond has an intermolecular character. According to the structures of the GpAtm dimer embedded into micelles and bicelles, which was obtained in this study, the distance between the oxygen atoms of the hydroxylic and carbonyl groups of the T⁸⁷ and V⁸⁴ residues in neighboring monomers is equal to ~ 4 Å. Meanwhile, in bicelles, these atoms are juxtaposed to ~ 3.8 Å, which in fact allows this group to form the intermolecular hydrogen bond. However, the system of NOE contacts, which is observed in

Structural statistics for representative ensembles of 20 NMR-derived structures of the GpAtm dimer in the DPC micelles and DMPC/DHPC bicelles

NMR structure	micelle	bicelles
PDB code	2kpe	2kpf
NMR data for structure calculation		
Total unambiguous NOE restraints	484	520
intra-residue	234	278
inter-residue	216	214
sequential ($ i-j =1$)	128	128
medium-range ($1 < i-j \leq 4$)	88	86
long-range ($ i-j > 4$)	0	0
inter-monomeric	34	28
Hydrogen bond restraints (upper/lower)		
intra-monomeric	108/108	108/108
inter-monomeric	0/0	0/0
Total torsion angle restraints	156	156
backbone φ	56	56
backbone ψ	56	56
side chain χ^1	44	44
Structure calculation statistics		
CYANA target function (\AA^2)	0.75±0.15	1.02±0.16
Restraint violations		
distance ($>0.2 \text{\AA}$)	0	0
distance ($>0.1 \text{\AA}$)	6	5
dihedral ($>5^\circ$)	0	0
Average pairwise RMSD (\AA)		
TM α -helix (72-95) ₂		
backbone atoms	0.39±0.17	0.42±0.13
all heavy atoms	0.94±0.18	1.07±0.15
generalized RMSD		
backbone atoms	0.72±0.45	
all heavy atoms	1.25±0.37	
backbone atoms of mean structures	1.03	
Ramachandran analysis		
% residues (70-98) ₂		
in most favored regions	92.7	90.4
in additional allowed regions	7.7	6.4
in generously allowed regions	1.4 [†]	0.2 [†]
in disallowed regions	0.4 [†]	0.7 [†]
Helix-helix packing		
helix-helix contact surface (\AA^2)	370±20	380±20
angle θ (deg.) between the TM helix axes	-40±2	-40±2
distance d (\AA) between the TM helix axes	6.7±0.4	6.4±0.4

Table note:

* Residues from unfolded and flexible regions.

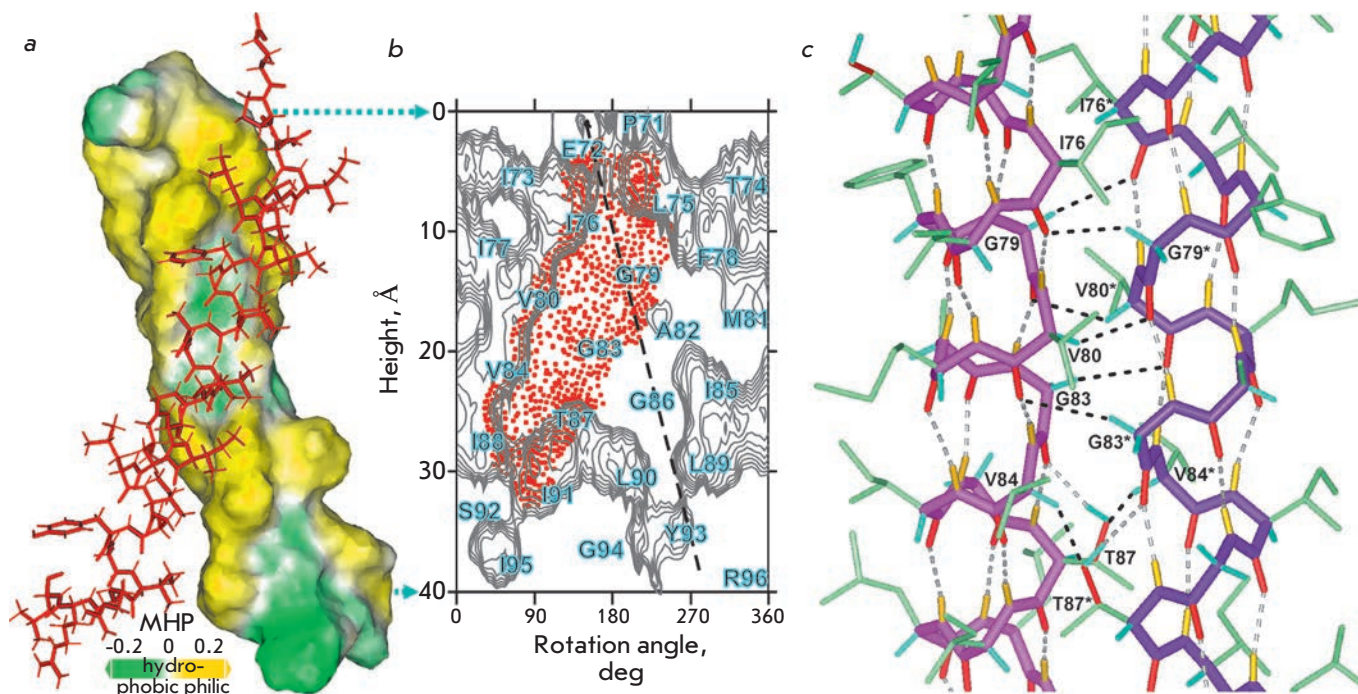


Fig. 4. *a* – Hydrophobic and hydrophilic (polar) surfaces of the TM helix of the GpAtm dimer colored in yellow and green according to the molecular hydrophobicity potential (MHP). The second dimer subunit is presented in red. *b* – Hydrophobicity map for the GpAtm helix surface with contour isolines encircling hydrophobic regions with high values of MHP. Details about map construction are described in [21]. The GpAtm helix packing interface is indicated by a red-point area covering the tetrad repeat GG4-like motif $G^{79}V_{xx}G^{83}V_{xx}T^{87}$ employed upon GpAtm self-association in the DPC micelles and DMPC/DHPC bicelles. The potential dimerization heptad repeat motif $L^{76}V_{xx}G^{79}V_{xx}A^{83}V_{xx}G^{86}V_{xx}L^{90}V_{xx}Y^{93}$ inherent to left-hand helix-helix interactions is marked by a dashed line. *c* – Central part of the dimerization interface of GpAtm. The intramonomeric and noncanonical $C\alpha-H\cdots O$ intermonomeric hydrogen bonds are shown in gray and black, respectively.

the NOESY spectra recorded both in bicelles and micelles (Fig. 1c), unequivocally attests to the fact that in the major conformation of GpAtm, the $O\gamma H$ group of T^{87} forms an intramolecular bond with the carbonyl group G^{83} (juxtaposed to ~ 2 Å) (Fig. 4c). Nevertheless, non-symmetric short-live states with the intermolecular hydrogen bond between the $O\gamma H$ groups of T^{87} (with rotation of the angle χ^1 of the side chain T^{87} from the gauche(+) into gauche(-) position) were detected in both cases during MD relaxation. A similar effect was detected in other studies devoted to simulating the dimerization of the GpA TM domain [33, 36].

CONCLUSIONS

A comparative study of the spatial structure and dynamics in two membrane-like media of different types has been carried out for the first time for specifically interacting TM helices. This significant methodological moment allows one to arrive at the conclusion that in the case of the GpA TM domain, the general topology of the dimer, determined by the specific character of the helix-helix interaction, is independent of the selection of the membrane-like medium; only the local

structures of TM helices are to a certain extent sensitive to this factor. On the other hand, it is known that the disc-shape and lipid composition of bicelles brings them closer to a natural lipid membrane in terms of physical properties, which results in a decrease in both the conformational fluctuations of helices and the fluctuations of the parameters characterizing their relative arrangement (angle θ and distance d between the helices). In turn, other conditions being equal, this should enhance the stability of the spatial structure of the α -helix membrane protein in bicelles, as compared with that in micelles. ●

This work was supported by the Russian Foundation for Basic Research, the Special-Purpose Federal Program “Studies and Designs in the Priority Fields of development of the Scientific-Technological complex of the Russian Federation in 2007–2012” and the programs of the Presidium of the Russian Academy of Sciences “Molecular and cell biology” and “Foundations of fundamental research in nanotechnologies and nanomaterials.”

REFERENCES

1. Frishman D., Mewes H.-W. // *Prog. Biophys. Mol. Biol.* 1999. V. 72. P. 1–17.
2. Li E., Hristova K. // *Biochemistry*. 2006. V. 45. P. 6241–6251.
3. Zviling M., Kochva U., Arkin I.T. // *Biochim. Biophys. Acta*. 2007. V. 1768. P. 387–392.
4. Bocharov E.V., Volynsky P.E., Pavlov K.V., Efremov R.G., Arseniev A.S. // *Cell Adh. Migr.* 2010. V. 4. P. 284–298.
5. Kim H.J., Howell S.C., van Horn W.D., Jeon Y.H., Sanders C.R. // *Prog. Nucl. Magn. Reson. Spectrosc.* 2009. V. 55. P. 335–360.
6. MacKenzie K.R., Prestegard J.H., Engelman D.M. // *Science*. 1997. V. 276. P. 131–133.
7. Smith S.O., Song D., Shekar S., Groesbeek M., Ziliox M., Aimoto S. // *Biochemistry*. 2001. V. 40. P. 6553–6558.
8. Smith S.O., Eilers M., Song D., Crocker E., Ying W., Groesbeek M., Metz G., Ziliox M., Aimoto S. // *Biophys. J.* 2002. V. 82. P. 2476–2486.
9. Goncharuk M.V., Schulga A.A., Ermolyuk Ya.S., Tkach E.N., Goncharuk S.A., Pustovalova Yu.E., Mineev K.S., Bocharov E.V., Maslennikov I.V., Arseniev A.S., Kirpichnikov M.P. // *Mol. Biol. (Mosk)*. 2011. V. 45. № 4. in press.
10. Kirpichnikov M.P., Goncharuk M.V., Ermolyuk Ya.S., Goncharuk S.A., Schulga A.A., Maslennikov I.V., Arseniev A.S. // *Technol. Live Syst.* 2005. V. 2. P. 20–27.
11. Chakrabarti P., Khorana G. // *Biochemistry*. 1975. V. 14. P. 5021–5033.
12. Sreerama N., Woody R.W. // *Anal. Biochem.* 2000. V. 287. P. 252–260.
13. Keller R.L.J. *The computer aided resonance assignment tutorial*. Goldau, Switzerland: CANTINA Verlag, 2004. 81 p.
14. Cavanagh J., Fairbrother W.J., Palmer A.G., Skelton N.J. *Protein NMR spectroscopy: principles and practice*. 2nd ed. San Diego, CA, USA: Acad. Press, 2007. 886 p.
15. Zwahlen C., Legault P., Vincent S.J.F., Greenblatt J., Konrat R., Kay L.E. // *Am. Chem. Soc.* 1997. V. 119. P. 6711–6721.
16. Bocharov E.V., Korzhnev D.M., Blommers M.J., Arvinte T., Orekhov V.Y., Billeter M., Arseniev A.S. // *J. Biol. Chem.* 2002. V. 277. P. 46273–46279.
17. Güntert P. // *Prog. Nucl. Magn. Reson. Spectrosc.* 2003. V. 43. P. 105–125.
18. Cornilescu G., Delaglio F., Bax A. // *J. Biomol. NMR*. 1999. V. 13. P. 289–302.
19. Baker E.N., Hubbard R.E. // *Prog. Biophys. Mol. Biol.* 1984. V. 44. P. 97–179.
20. Lindahl E., Hess B., van der Spoel D. // *J. Mol. Mod.* 2001. V. 7. P. 306–317.
21. Bocharov E.V., Mayzel M.L., Volynsky P.E., Mineev K.S., Tkach E.N., Ermolyuk Ya.S., Schulga A.A., Efremov R.G., Arseniev A.S. // *Biophys. J.* 2010. V. 98. P. 881–889.
22. Koradi R., Billeter M., Wüthrich K.J. // *Mol. Graphics*. 1996. V. 14. P. 51–55.
23. DeLano W.L. *The PyMOL Molecular Graphics System*, Palo Alto, CA, USA: DeLano Scientific, 2002.
24. Efremov R.G., Gulyaev D.I., Vergoten G., Modyanov N.N. // *J. Prot. Chem.* 1992. V. 11. P. 665–675.
25. Kabsch W., Sander C. // *Biopolymers*. 1983. V. 22. P. 2577–2637.
26. Daragan V.A., Mayo K.H. // *Prog. Nucl. Magn. Reson. Spectrosc.* 1997. V. 31. P. 63–105.
27. Bordag N., Keller S. // *Chem. Phys. Lipids*. 2010. V. 163. P. 1–26.
28. Lind J., Nordin J., Måler L. // *Biochim. Biophys. Acta*. 2008. V. 1778. P. 2526–2534.
29. Nyholm T.K., Ozdirekcan S., Killian J.A. // *Biochemistry*. 2007. V. 46. P. 1457–1465.
30. Sparr E., Ash W.L., Nazarov P.V., Rijkers D.T., Hemminga M.A., Tieleman D.P., Killian J.A. // *J. Biol. Chem.* 2005. V. 280. P. 39324–39331.
31. Mackenzie K.R. // *Chem. Rev.* 2006. V. 106. P. 1931–1977.
32. Kim S., Jeon T.-J., Oberai A., Yang D., Schmidt J.J., Bowie J.U. // *Proc. Natl. Acad. Sci. USA*. 2005. V. 102. P. 14279–14283.
33. Efremov R.G., Vereshaga Y.A., Volynsky P.E., Nolde D.E., Arseniev A.S. // *J. Comput. Aided. Mol. Des.* 2006. V. 20. P. 27–45.
34. Senes A., Ubarretxena-Belandia I., Engelman D.M. // *Proc. Natl. Acad. Sci. USA*. 2001. V. 98. P. 9056–9061.
35. Vargas R., Garza J., Dixon D.A., Hay B.P. // *J. Am. Chem. Soc.* 2000. V. 122. P. 4750–4755.
36. Cuthbertson J.M., Bond P.J., Sansom M.S. // *Biochemistry*. 2006. V. 45. P. 14298–14310.
37. Wagner G., Pardi A., Wüthrich K. // *J. Am. Chem. Soc.* 1983. V. 105. P. 5948–5949.

Relationship between the Pathogenic Representatives of Periodontal Pockets Microbiocenosis in Patients with Periodontitis with Varying Degrees of Severity

O. A. Zorina^{1*}, A. A. Kulakov¹, O. A. Boriskina¹, D. V. Rebrikov^{2,3}

¹ Central Research Institute of Dentistry and Oral Surgery

² Vavilov Institute of General Genetics, Russian Academy of Sciences

³ Scientific Production Enterprise «DNA Technology», JSC

*E-mail: zorina-cniis@yandex.ru

Received 09.02.2011

ABSTRACT Periodontitis is a common disease that is considered to be a manifestation of the distortion of the ratio between the normal and conditionally pathogenic microflora of periodontal pockets. In this study, the ratio between the six most important periodontal pathogens and the total microflora of the periodontal pocket in healthy individuals and patients with varying severity of periodontitis was ascertained by quantitative real-time PCR. It was ascertained that the relative content of *Porphyromonas gingivalis*, *Prevotella intermedia*, and *Tannerella forsythensis* (*Bacteroides forsythus*) persistently develops in the total microflora of the periodontal pocket upon progressing periodontitis; this value is higher than that in the control group by more than two orders of magnitude upon a severe degree of chronic generalized periodontitis.

KEYWORDS ecosystem; habitat; periodontitis; periodontopathogenic microflora of periodontal pockets; quantitative polymerase chain reaction

ABBREVIATIONS PCR – polymerase chain reaction; CGP – chronic generalized periodontitis

INTRODUCTION

In terms of the composition of microorganisms, the oral cavity is one of the most sophisticated ecosystems of the human organism. Saliva, gingival fluid, periodontal pocket, biofilm, and a number of other habitats contain approximately 700 different types of microorganisms [1, 2], which can be divided conditionally into three large groups: 1) normoflora, 2) conditionally pathogenic, and 3) pathogenic microorganisms [3].

A number of exogenous and endogenous factors condition the bacterial profile of biocenosis of the oral cavity. The protective mechanisms of the host organism have a considerable effect on the virulence of the conditionally pathogenic and pathogenic microorganisms in each habitat.

It is common knowledge that the distortion of the ratio between the normal and conditionally pathogenic flora leads to the development of dysbacterioses and is characterized by a relative decrease in the content of lacto- and bifidobacteria. The common disease of periodontitis is one of the manifestations of this disbalance. The essential role in the development of periodonti-

tis is known to belong to *Porphyromonas gingivalis*, *Treponema denticola*, *Tannerella forsythensis* (*Bacteroides forsythus*), *Fusobacterium* spp., and a number of other microorganisms [4–6].

Advances in molecular biology techniques, in particular the methods of qualitative and quantitative assessment of the nucleic acid content, have made it possible to determine both the composition and the relative amount of microorganisms in various sub-habitats of the oral cavity rapidly and with a high degree of accuracy [6–8]. A distinctive feature of modern molecular and genetic methods (in particular, quantitative PCR) is their high sensitivity and the possibility for a quantitative determination of anaerobic microorganisms (which is often non-feasible when using conventional culturing methods) [9]. Real-time PCR allows for the simultaneous determination of the qualitative and quantitative composition of microbiota in any habitat of the oral cavity selected.

This work is aimed at a quantitative assessment of the ratio between the most significant (according to [9–11]) representatives of the periodontopathogen-

Table 1. The age structure of the examined groups (%)

Age	Healthy controls (n = 30)	Mild degree (n = 10)	Average degree (n = 29)	Severe degree (n = 35)
Under 35 years old	21	80	24	17
35–44 years old	27	20	35	29
44–55 years old	33	0	31	34
Over 55 years old	19	0	10	20

Table 2. The proportion of positive samples depending on the group of healthy individuals or patients with CGP (%)

Microorganism name	Healthy controls (n = 30)	Mild degree (n = 10)	Average degree (n = 29)	Severe degree (n = 35)
<i>A. actinomycetemcomitans</i>	10	33	48	43
<i>P. gingivalis</i>	47	70	66	86
<i>P. intermedia</i>	33	70	59	71
<i>T. forsythensis</i>	53	80	97	100
<i>T. denticola</i>	60	80	83	83
<i>C. albicans</i>	10	40	38	60

ic microflora of periodontal pockets: *Aggregatibacter actinomycetemcomitans*, *Porphyromonas gingivalis*, *Prevotella intermedia*, *Tannerella forsythensis* (*Bacteroides forsythus*), *Treponema denticola*, *Candida albicans* in healthy people and in patients with periodontitis with varying degrees of severity.

EXPERIMENTAL

The study was carried out in the Periodontology Department of the Central Research Institute of Dentistry and Oral Surgery (Russia). A total of 104 individuals aged 18–65 without severe somatic pathology were examined.

The absence of a dentogingival junction served as the major criterion for the diagnosis of chronic generalized periodontitis (CGP). The degree of severity was determined based on the depth of periodontal pockets and the degree of destruction of bone tissue. Thus, the depth of periodontal pockets was less than 3 mm in cases with a mild degree of CGP; the X-ray pattern confirming signs of initial destruction of the interdental septa.

The depth of periodontal pockets varied from 3 to 6 mm in patients with a moderate degree of CGP; I–II degree of pathologic tooth mobility was frequently revealed during the examination. According to the data obtained by X-ray examination, the destruction of the cortical plate and bone tissue of interdental septa was equal to 1/2–1/3 of the length of the tooth root.

Severe CGP was characterized by the presence of periodontal pockets more than 6 mm deep, II–III degree pathological tooth mobility, destruction of the

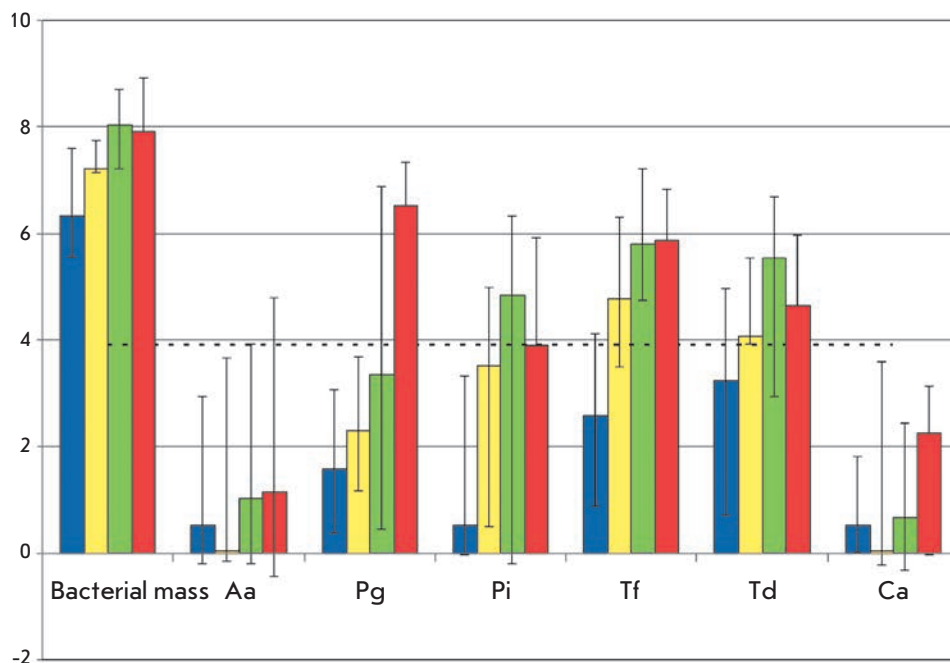
cortical plate and bone tissue by more than 1/3 of the length of the tooth root was revealed by X-ray examination.

The control group consisted of 30 individuals (12 males and 18 females) aged 28–55, without complaints and visible pathological changes in periodontal tissues. The data on the age structure of the groups are listed in *Table 1*.

Microflora of the intact periodontium and periodontal pockets was examined using sterile paper endodontic pins (size no. 25), which were submerged in a gingival sulcus or a pathological pocket until it reached bottom. It was subsequently kept there for 10 s. The pins were then placed into a test tube with a physiological solution, cooled, and transferred to the laboratory. A duplicate sample was taken from each patient.

In order to reveal infectious agents and determine the genomic DNA of the patient (as a normalization index), DNA was extracted from the biological material using the “Proba-GS” kits (DNA Technology JSC, Russia) according to the enclosed manual. The method is based on sorbing DNA on a carrier, washing out the impurities, and eluting nucleic acids from the sorbent. Due to cell lysing by strong chaotropic agents, “Proba GS” destroys the cells with different types of cell walls (gram-positive/gram-negative bacteria, fungi) with almost equal efficacy. The “Proba GS” kit can be used to extract the genomic DNA of eukaryotes as well (it was used as the normalization index).

The previously designed reagent kits, consisting of specific primers and a specific fluorescence-labeled destructible sample (TaqMan type) to six periodontopath-



The relative number of microorganisms in healthy individuals (blue columns) and in patients with CGP of varying degrees of severity (yellow columns – mild, green – medium, and red – severe and aggressive periodontitis). The median values with 25–75 percentile error bars are shown. The data are normalized with respect to the content of human genomic DNA (dotted line). The logarithm of the content of this component in the sample (in arbitrary units) is plotted along the Y axis. Bacterial mass is the total number of bacteria, Aa – *A. actinomycetemcomitans*, Pg – *P. gingivalis*, Pi – *P. intermedia*, Tf – *T. forsythensis*, Td – *T. denticola*, and CA – *C. albicans*.

ogenic agents (*Aggregatibacter actinomycetemcomitans*, *Porphyromonas gingivalis*, *Prevotella intermedia*, *Tannerella forsythensis* (*Bacteroides forsythus*), *Treponema denticola*, and *Candida albicans*) were used in this work. PCR with detection of the conservative region of the 16S rRNA gene was performed simultaneously with the determination of pathogenic microorganisms to estimate the total bacterial mass in the sample. The copy number of the genome equivalents of each type of bacteria (and the total bacterial mass) was normalized per amount of human genomic DNA (a fragment of the growth hormone receptor gene) in order to compare the abundance of pathogens in the samples.

PCR was performed on a DTprime detecting amplifier (OOO DNA Technology, Russia). The results of the reaction were taken into consideration using the software of the DTprime amplifier. The normalized values corresponding to the level of abundance of each microorganism were calculated using the $\Delta\Delta C_t$ method.

RESULTS AND DISCUSSION

The sample to be analyzed was divided into four groups depending on disease severity: 1) healthy control ($n = 30$); 2) mild degree of CGP ($n = 10$); 3) moderate degree of CGP ($n = 29$); and 4) severe degree of CGP ($n = 35$); where n is the number of individuals in a group.

The results of revealing pathogens in each group are listed in Table 2. It is evident that with the progression of the disease, there exists a tendency towards an increase in the number of positive samples with respect

to all microorganisms. The published data on the frequency of detecting periodontopathogens in healthy individuals and in patients with CGP differ considerably [10, 12–14]; however, in most cases a similar tendency is reported. Hence, Braga *et al.* [12] detected *P. intermedia* in 80.0% of healthy individuals ($n = 30$) and in 90.0% of patients with CGP ($n = 30$); *P. gingivalis* was detected in 46.6% of healthy individuals and in 70.0% of patients with CGP; and *A. actinomycetemcomitans* was detected in all individuals in both groups. The differences in the frequencies of detected pathogens can be accounted for by the features of group formation, possible (in certain cases, planned) strain specificity, and the varying sensitivities of the test systems used. It should also be noted that the detection of a pathogenic microorganism in each of the individuals in the control group may attest to contamination of the laboratory with products of earlier reactions; a consideration that should alert the authors.

We used the new approach to quantitatively assess the composition of dental cavity microbiocenoses; therefore, we did not manage to find much published data on the relative content of the pathogens studied. No reliable differences were revealed by Hyvärinen *et al.* [15], who determined the relative content of *A. actinomycetemcomitans*, *P. gingivalis*, *P. intermedia*, *T. forsythensis* and *T. denticola* in saliva samples from patients with periodontitis and healthy individuals.

The results of determining the relative amount of microorganisms in healthy individuals and in patients

with varying degrees of severity of CGP are presented in *Figure*. In order to reduce the amount of biomaterial used for the study to a common denominator, the data were normalized with respect to the content of the unique fragment of human genomic DNA (the fragment of the growth hormone receptor gene) [16, 17]. It is evident from *Figure* that as the disease progresses, there exists a tendency towards an increase in the content of bacteria in general (the “bacterial mass” index) and the content of most representatives of pathogenic microflora (the relative content of pathogens increasing at an anticipatory rate). *P. gingivalis*, *P. intermedia*,

and *T. forsythensis* are the leaders in growth with progressing periodontitis; their content in the total bacterial mass persistently increasing by a factor of more than 100.

The obtained data attest to the possibility of using a quantitative assessment of the ratio between the pathogenic representatives of microbiocenosis of periodontal pockets as a diagnostic tool to predict the development of periodontitis. The determination of the ratio between *P. gingivalis*, *P. intermedia*, *T. forsythensis*, the total bacterial mass, and the genomic DNA of the patient can be recommended as a variant of diagnosticum. ●

REFERENCES

1. Usatova G.N. Adgesia i kolonizatsiya mikroorganizmami polosti rta (Adhesion and Colonization by Microorganisms of the Oral Cavity). Extended Abstract of Cand. Med. Sci. Dissertation. Rostov-on-Don, 1989. 19 p.
2. Paster B.J., Boches S.K., Galvin J.L., Ericson R.E., Lau C.N., Levanos V.A., Sahasrabudhe A., Dewhirst F.E. // *J. Bacteriol.* 2001. V. 183. P. 3770–3783.
3. Kumar P.S., Griffen A.L., Moeschberger M.L., Leys E.J. // *J. Clin. Microbiol.* 2005. V. 43. № 8. P. 3944–3955.
4. Haffajee A.D., Socransky S.S. // *Periodontol* 2000. 1994. V. 5. P. 78–111.
5. Maiden M.F., Cohee P., Tanner A.C. // *Int. J. Syst. Evol. Microbiol.* 2003. V. 53. P. 2111–2112.
6. Takamatsu N., Yano K., He T., Umeda M., Ishikawa I. // *J. Periodontol.* 1999. V. 70. № 6. P. 574–580.
7. Behl Y., Siqueira M., Ortiz J., Li J., Desta T., Faibish D., Graves D.T. // *J. Immunol.* 2008. V. 181. № 12. P. 8711–8718.
8. Boutaga K., Winkelhoff A.J., Vandenbroucke-Grauls I.C., Savelkoul P. // *J. Clin. Microbiol.* 2003. V. 41. № 11. P. 4950–4954.
9. Atieh M.A. // *J. Periodontol.* 2008. V. 79. № 9. P. 1620–1629.
10. Jervoe-Storm P.M., AlAhdab H., Koltzsch M., Fimmers R., Jepsen S. // *Clin. Oral Investig.* 2010. V. 14. № 5. P. 533–541.
11. Naka S., Yamana A., Nakano K., Okawa R., Fujita K., Kojima A., Nemoto H., Nomura R., Matsumoto M., Ooshima T. // *BMC Oral Health.* 2009. V. 9. P. 24.
12. Braga R.R., Carvalho M.A., Bruña-Romero O., Teixeira R.E., Costa J.E., Mendes E.N., Farias L.M., Magalhães P.P. // *Anaerobe.* 2010. V. 16. № 3. P. 234–239.
13. Elamin A., Albandar J.M., Poulsen K., Ali R.W., Bakken V. // *J. Periodontal Res.* 2011. V. 46. № 3. P. 285–291. doi: 10.1111/j.1600-0765.2010.01337.x.
14. Rakić M., Zelić K., Pavlica D., Hadzimihajlović M., Milasin J., Milčić B., Nikolić N., Stamatović N., Matic S., Aleksić Z., Janković S. // *Vojnosanit. Pregl.* 2010. V. 67. № 11. P. 898–902.
15. Hyvärinen K., Laitinen S., Paju S., Hakala A., Suominen-Taipale L., Skurnik M., Könönen E., Pussinen P.J. // *Innate Immun.* 2009. V. 15. № 4. P. 195–204.
16. Zorina O.A., Tumbinskaya L.V., Rebrikov D.V. // *Dentistry for all.* 2011. № 1. P. 46–48.
17. Vandesompele J., De Preter K., Pattyn F., Poppe B., van Roy N., De Paepe A., Speleman F. // *Genome Biol.* 2002. V. 3. № 7. Research0034.

The Effects of β_2 -Adrenoreceptor Activation on the Contractility, Ca-Signals and Nitric Oxide Production in the Mouse Atria

Yu. G. Odnoshivkina, A. M. Petrov*, A. L. Zefirov

Kazan State Medical University, Federal Agency for Health Care and Social Development

*E-mail: fysio@rambler.ru

Received 28.12.2010

ABSTRACT The effects of the selective β_2 -adrenoreceptor agonist (fenoterol) on the functioning of mouse atrial were studied using both tensometry and fluorescent methods. It has been demonstrated that with the use of a high concentration of fenoterol (in the range of 1–50 μM), there is a more significant positive inotropic effect observed within a shorter period of time. In the case of relatively low doses of fenoterol (1 and 5 μM), its contractility effects are observed 20 min after the application of agonist, whereby in the case of high concentrations (25, 50 and 300 μM), the effects appear within the first minutes. During the first 10–15 min, 5 μM fenoterol causes an increase in the amplitude of Ca-signals in cardiomyocytes (this indicates an increase in the concentration of Ca ions during systole) and the activation of NO synthesis. However, after 20 min, the production of NO decreases; while the amplitude of Ca-signals remains high. The application of 50 μM fenoterol leads to a rapid increase in the amplitude of Ca-signals; at the same time, it causes a decrease in the production of NO, which we found to begin to increase after 10 min of agonist application. It is suggested that the dynamics of the positive inotropic effect occurring under pharmacological stimulation of β_2 -adrenoreceptors depend on the rate of increase in the amplitude of Ca-signals and on the degree of NO synthesis.

KEYWORDS β_2 -adrenoreceptor; fenoterol; calcium; nitric oxide; contractility; atrial cardiomyocytes

INTRODUCTION

One of the mechanisms that regulate the action of the heart is based on the interaction of catecholamines (adrenaline and noradrenaline) with G protein-coupled β -adrenoreceptors in cardiomyocytes [1, 2]. Depending on their sensitivity to pharmacological agents and on their structural features, β -adrenoreceptors are divided into three types: β_1 , β_2 , and β_3 . All types of β -adrenoreceptors are expressed within the heart. The function of the β_1 -adrenoreceptors in the heart is well known. Meanwhile, β_2 -adrenoreceptors have been subjected to much less thorough study: only their functions in the regulation of the vascular tone in the heart and the skeletal muscles of bronchial lumen and the metabolism of a body have [3].

The concentration of β_2 -adrenoreceptors is particularly high in atrial cardiomyocytes. While, within the entire heart, the content of β_2 -adrenoreceptors reaches 30–40% of the total amount of β -adrenoreceptors [2], in human atrial cardiomyocytes their content is over 55% [4]. The stimulation of β_2 -adrenoreceptors leads to an increase in the contractility of the ventricular cardiomyocytes in a rat heart, with no significant impact on the rate of relaxation [5]. It is believed that the activa-

tion of β_2 -adrenoreceptors causes a positive inotropic reaction without increasing the risk of arrhythmias and sudden death of the animal [6]. It should be noted that, upon stimulation of β_2 -adrenoreceptors, the inotropic effect might be negative, e.g. in papillary muscles of the guinea pig heart [7].

The effect of the stimulation of β_2 -adrenoreceptors on the contractility of ventricular cardiomyocytes is defined by the interaction of the receptor with the Gs protein, which initiates the adenylyl cyclase cascade causing the activation of protein kinase A. Under the action of this kinase, part of the L-type calcium channels could be opened and the conduction of these channels enhanced, and consequently the amount of Ca ions entering the cytoplasm during action potential could also increase [8, 9]. However, the activated β_2 -adrenoreceptors stimulate also Gi proteins, which inhibit the adenylyl cyclase cascade, thereby limiting the positive inotropic effect produced by the β_2 -adrenoreceptor agonists [10, 11]. The activation of Gi proteins initiates the phosphoinositol-3-kinase (PI3K)/protein kinase B cascade, which is aimed at maintaining cell survival, protecting them from the action of reactive oxygen species and hypoxia [12, 13]. In addition,

the phosphoinositol-3-kinase (PI3K)/protein kinase B cascade may initiate an increase in the production of nitric oxide (NO), which, by affecting the guanylate cyclase system, is capable of inhibiting the effect of β_2 -adrenoceptor agonists [14, 15] and preventing the desensitization of β_2 -adrenoceptors [16] as well. It has been suggested that β_2 -adrenoreceptors play a cardioprotective role, while β_2 -adrenoreceptor agonists can be viewed as promising pharmacological agents [13]. Thus, in mice with overexpression of β_2 -adrenoreceptors, no heart failure develops and no signs of cardiomyocyte damage are revealed against a background of increased frequency and strength of heart contractions, which are observed even in the absence of β_2 -adrenoreceptor activation by endogenous ligands [17]. The point is that β_2 -adrenoreceptors can be spontaneously switched into their active state regardless of whether there are agonists in the extracellular medium or not [18]. It is interesting that, under spontaneous activation of β_2 -adrenoreceptors, contractility increases, but the entering calcium current through L-type calcium channels does not change [19].

β_2 -Adrenoreceptors are very “flexible” molecules with several active states (conformations). The conformations define the properties of the receptors, including their ability to bind to effector signaling proteins, whose role can be played not only by G proteins, but also by tyrosine kinase Src, by the factor that controls the Na-H exchange, by arrestin, by the N-ethylmaleimide factor, and by several scaffold proteins [20–24]. It was demonstrated recently that different agonists can transform β_2 -adrenoreceptors into forms with specific active conformations; hence the reason why the type of agonist defines the cell-mediated response (this phenomenon is called the “functional selectivity” of agonists) [25]. Fenoterol is one of the most widely used drugs in clinical medicine and one of the effective short-acting β_2 -adrenoreceptor agonists. Its effects include a significant increase in the cAMP level and the activation of mitogen-activated protein (MAP) kinase [25] in human airway smooth muscle cells and, in endotheliocytes, intensification of the synthesis of nitric oxide (NO) [26]. It should be noted that, under the action of fenoterol, β_2 -adrenoreceptors undergoes intensive phosphorylation by G protein-coupled receptor kinases, followed by their internalization during clathrin-mediated endocytosis. As a result, long-term use of fenoterol leads to desensitization and a decrease in the amount of the β_2 -adrenoreceptors on the surface of bronchial epithelium [25, 27]. New data on the unique properties of fenoterol and its stereoisomers has appeared; this data can be used to design drugs that have a high selectivity value and pronounced cardioprotective properties [28, 29].

The role of β_2 -adrenoreceptors in atrial cardiomyocytes is not thoroughly understood. There is data indicating that there is an increase in contractility and the rate of intake of the calcium current upon stimulation of the atrial β_2 -adrenoreceptors in guinea pigs, cats, and humans [15, 30, 31]. However, in mice with overexpression of human β_2 -adrenoreceptors, the activation of atrial β_2 -adrenoreceptors by isoprenaline has a negative inotropic effect, while, under normal circumstances, isoprenaline, which affects mostly β_1 -adrenoreceptors, has a positive inotropic effect [32, 33]. In this work, we studied how various doses of racemic fenoterol, a β_2 -adrenoreceptor agonist widely used in medicine, influence the atrial contractility, amplitude of Ca-signals, and NO production.

EXPERIMENTAL

Isolated atria of white mice were used in the experiments. The standard Krebs solution for warm-blooded animals with the following composition was used: 144.0 mM NaCl, 5.0 mM KCl, 0.1 mM $MgCl_2$, 2.0 mM $CaCl_2$, 1.0 mM NaH_2PO_4 , 2.4 mM $NaHCO_3$, 11.0 mM glucose; the solution was saturated with oxygen. The pH value of the solutions was maintained at 7.2–7.4 at a temperature of 20°C. During the experiment, the specimen was stimulated by electrical pulses of suprathreshold amplitude at a frequency of 0.1–1 Hz via platinum electrodes. In the majority of experiments, the application (20 min) of (\pm)-fenoterol (Sigma, USA), a β_2 -adrenoreceptor agonist, at concentrations of 1–300 μ M was used. In some cases, 0.1 μ M ICI-118.551 (Tocris, USA), a selective blocker of β_2 -adrenoreceptors was applied.

Tensometry

The atrial contraction was registered using a PowerLab installation. One end of the isolated atrium was tied to a fixed nail, and the other end was linked to a nail connected to a strain gauge with a sensitivity of 0–25 g (AD Instruments). The signals were treated using Chart software; the contractility was determined in grams.

Fluorescent Microscopy

The fluorescent experiments were carried out using an OLYMPUS CX41 (with exchangeable monochromatic excitation light sources) and an OLYMPUS BX51 (equipped with the DSU confocal system) microscope with a LMPlanFI 20 \times /0.40 and UPlanSApo 60 \times /1.20W objectives. The images were made using high-speed CCD cameras produced by OLYMPUS: a F-View II black and white and DP71 color CCD camera. The images were treated using Cell^A, Cell^P, and ImagePro software. The fluorescence intensity was estimated in relative units (rel. units) that correspond to the brightness value in pixels.

Measurements of the Intracellular Concentration of Calcium Ions. The changes in the concentration of Ca^{2+} were determined using a Fluo-4 dye, which allows the Ca^{2+} concentration to be precisely measured in a range from 1 μM to 1 mM. Fluo-4 is weakly fluorescent in the absence of Ca^{2+} , but its binding to Ca ions leads to an increase in the fluorescence value by a factor over 100 [34]. Fluo-4-AM (Molecular Probes, USA), a membrane-penetrating form of the dye, was used; it was dissolved in DMSO (dimethyl sulfoxide, Sigma, USA) and stored in the frozen form (for not more than a week) in the dark. Just prior to the experiment, a Pluronic F-127 (Molecular Probes, USA) nonionic detergent was added into a Fluo-4-AM batch; the detergent facilitates the dissolving of nonpolar Fluo-4-AM in an aqueous (physiological) solution. In a work solution, the final concentration of Fluo-4-AM was 1 μM , and the content of DMSO and Pluronic F-127 was not more than 0.0005%. The isolated atrial specimen was held in the solution containing 1 μM Fluo-4-AM for 20 min at room temperature. Afterwards, the specimen was perfused with a physiological solution for 40 min (during this period of time, deesterification of Fluo-4-AM in the cytoplasm ended and the formation of hydrophilic Fluo-4, which cannot pass through the membrane into the intracellular medium [34], occurred). Thereafter, measurements of the fluorescence in the cardiomyocytes of the isolated atria were made. The fluorescence of the dye was excited by short (about 1 s) flashes of light with a wavelength of 480 nm and registered using an emission-color filter that transmits light with a wavelength of above 515 nm. During the contraction-relaxation cycle of the atrial specimen, periodic changes in the fluorescence of the Ca sensor, which appeared in the form of flashes (“Ca-signals”), were observed: the intensity of the fluorescence increased during contraction and decreased during relaxation. Ca-signals indicate an increase in the concentration of Ca ions, which initiate contraction of cardiomyocytes. The minimum fluorescence value observed during diastole was subtracted from the maximum fluorescence value observed during systole, in order to estimate the amplitude of the Ca-signals.

Measurements of the Concentration of Nitric Oxide (NO). The production of nitric oxide was detected using a DAF-FM-diacetate marker (Molecular Probes, USA), which was excited by light with a wavelength of $\lambda = 495$ nm; for the registration of fluorescence, an emission filter that transmits light with a wavelength above 515 nm was used. DAF-FM-diacetate easily permeates through the cellular membranes. Inside the cell, DAF-FM-diacetate is deacetylated by intracellular esterase to DAF-FM. Prior to reacting with NO, DAF-FM

almost does not fluoresce; but its interaction with NO leads to an increase in the fluorescence intensity by a factor of more than 160 [29]. DAF-FM was dissolved in DMSO and stored in frozen form in a dark place. The specimen of the isolated atrium was held in a solution containing 2 μM DAF-FM-diacetate for 30 min at room temperature. After that, the atrial specimen was perfused with a physiological dye-free solution for 20 min (the period of time needed for deacetylation of the marker to finish [35]). Thereafter, the measurements of fluorescence in cardiomyocytes of the isolated atria were made.

A statistical analysis was performed using the Origin Pro software. The results of the measurements were presented as mean values \pm standard error (n is the number of independent trials). The significance of the differences was determined in accordance with the Student's test and ANOVA.

RESULTS

Dose-Dependence of the Inotropic Effect of Fenoterol

Amplitude of Contractions. The addition of fenoterol at concentrations ranging from 1 to 300 μM led to a significant increase in contractility (Fig. 1a, b). The application of 1 and 5 μM of fenoterol increased contractility to $134 \pm 4.4\%$ ($p < 0.01$, $n = 5$) and $144.6 \pm 5.1\%$ ($p < 0.01$, $n = 5$), relative to the control value, respectively. Under the action of fenoterol (25 and 50 μM), contractility increased even more; i.e. up to $159.7 \pm 5.5\%$ ($p < 0.01$, $n = 6$) and $176.2 \pm 6.6\%$ ($p < 0.01$, $n = 8$), respectively. However, 300 μM of fenoterol caused an increase in contractility only to $143.3 \pm 6.5\%$ ($p < 0.01$, $n = 5$) (Fig. 1c). Since β_2 -adrenoreceptors are desensitized relatively fast by high doses of agonists, the slight influence of 300 μM of fenoterol on contractility most likely relates to desensitization processes [27, 36].

Time-Course of the Effect. The rate of development of the positive inotropic effect of fenoterol varied depending on its concentration: the higher the concentration, the earlier the increase in contractility was observed (Fig. 1a, b). The amplitude began to grow only 20 min after fenoterol at concentrations of 1 and 5 μM was applied, and maximum contractility was observed after 30–40 min. When fenoterol was used at concentrations of 25 and 50 μM , the contractility increased significantly faster: i.e., 15 and 13 min after the addition of the agonist, contractility reached a maximum. 300 μM of fenoterol led to maximum contractility just after 3 min.

Delayed Effect of Fenoterol. As was mentioned above, at low concentrations of fenoterol, the positive inotropic

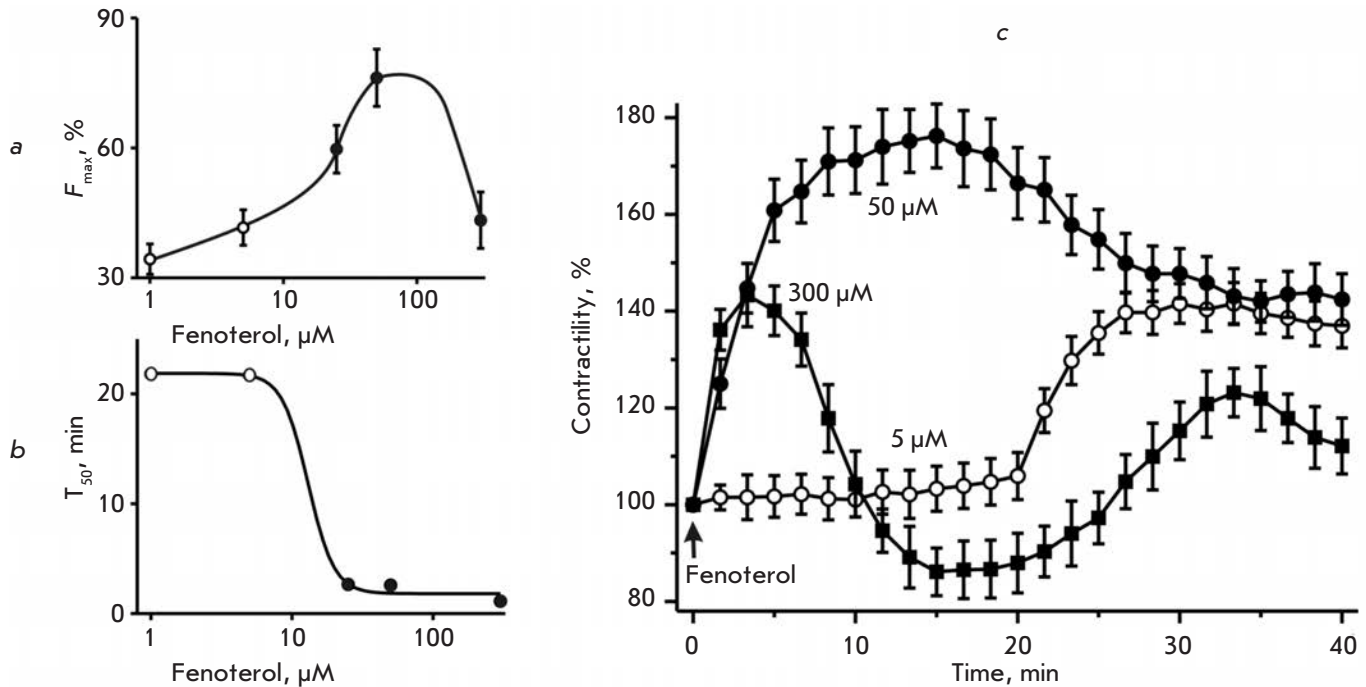


Fig. 1. Effect of fenoterol on the contractility of the isolated atria. The influence of the various doses of fenoterol on contractility (a) and time-course of the effect (b). Y-axis: a is the maximum amplitude of contractions (F_{max} , "0" corresponds to the value observed prior to application of fenoterol); b is the period of time from the moment fenoterol was applied to the moment when the amplitude reached 50% of the maximum amplitude of contractions (T_{50}). X-axis: the logarithmic scale of concentrations (μM). (c) The change in the atrial contractility under the action of 5, 50, and 300 μM of fenoterol (open and filled circles and filled squares, respectively). Y-axis: the force of contraction, (%) (100% corresponds to the level of contractility prior to the application of fenoterol). The beginning of the application of fenoterol is indicated by an arrow. The presented data on the change in the atrial contractility under the action of fenoterol applied at concentrations of 1 ($n = 5$), 5 ($n = 5$), 25 ($n = 6$), 50 ($n = 8$), 300 ($n = 5$) μM were obtained in independent experiments.

effect occurs very late, only after 20–25 min (Fig. 1c). In order to clarify why the development of the effect is so slow, additional experiments in which a solution of fenoterol (5 μM) was replaced by a normal Krebs solution after 20 min (i.e. prior to the beginning of the increase in contractility). The contractility was found to increase despite the absence of fenoterol in the solution. Ten minutes after the removal of fenoterol from the solution surrounding the atrial specimen, the amplitude reached its maximum: $141.6 \pm 4.1\%$ relative to the control value ($p < 0.01$, $n = 8$). It then decreased gradually. This indicates that the delayed effect observed at low concentrations of β_2 -adrenoreceptors is related to the activation of intracellular signal systems, whose action develops at a very low rate.

In further experiments, only two concentrations of fenoterol were used: 5 μM , at which the delayed effect was observed; and 50 μM , at which contractility was found to increase rapidly (Fig. 1c). It should be noted that, in the presence of the selective β_2 -adrenoreceptor blocker (0.1 μM ICI-118.551), no positive inotropic ef-

fect of fenoterol at concentrations of 5 and 50 μM appears (data are not presented).

The Effect of Fenoterol on Ca-Signals

The dynamics of the intracellular concentration of calcium ions, which initiate the contractions of cardiomyocytes, significantly change under the action of fenoterol (Fig. 2). Use of a low concentration of fenoterol (5 μM) leads to a gradual increase in the amplitude of Ca-signals. After 3 min of application of the β_2 -adrenoreceptor agonist, the amplitude of Ca-signals reached $122.6 \pm 4.7\%$ ($p < 0.05$, $n = 7$); and after 10 min, the value of the amplitude was $152.1 \pm 4.9\%$ ($p < 0.01$, $n = 7$) relative to the initial values. After 15 min of application of the agonist, the amplitude of Ca-signals somewhat declined, but after 20 min, it stabilized at a level of 130–140%. Five minutes after the surrounding solution was replaced with a fenoterol-free solution, the amplitude of Ca-signals was $133.6 \pm 4.7\%$ ($p < 0.01$, $n = 7$). The amplitude of Ca-signals returned to the basal level 60–70 min after fenoterol was removed from

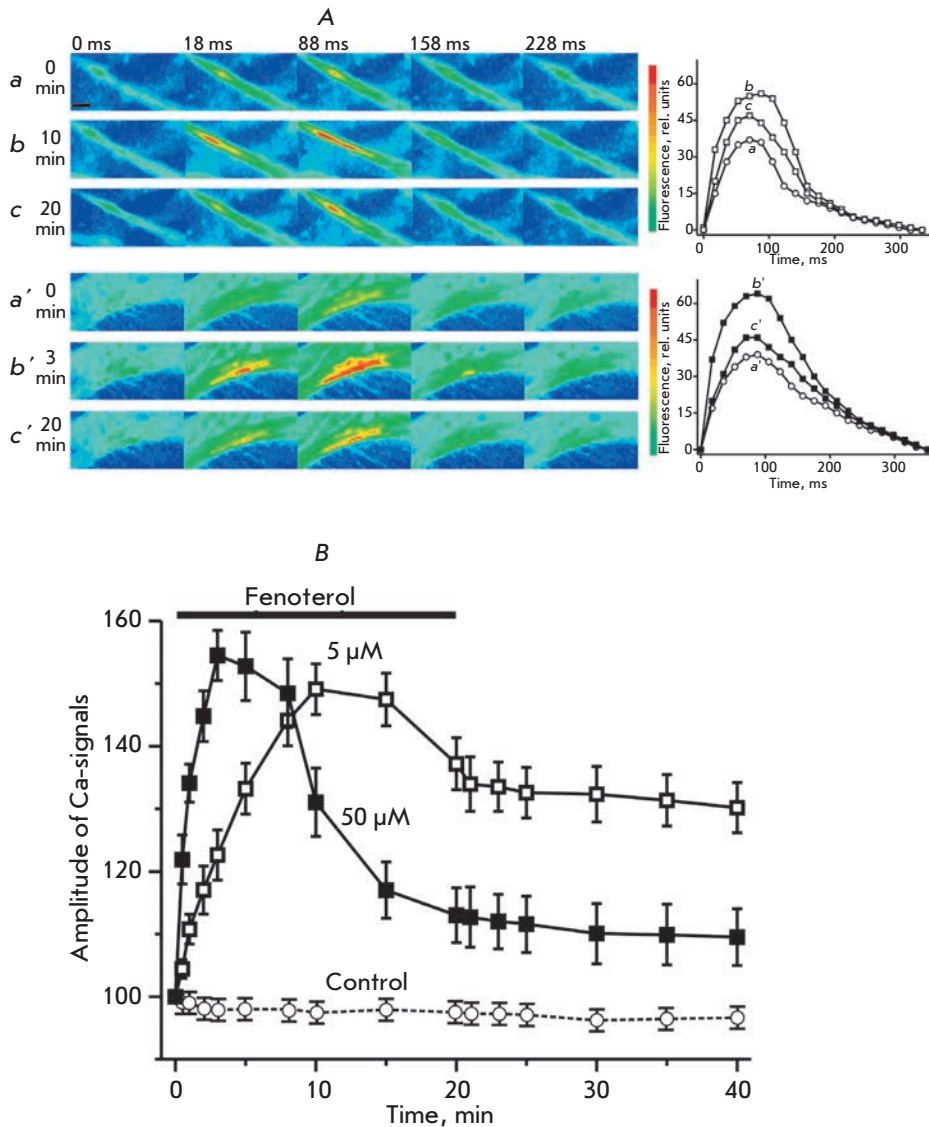


Fig. 2. Effect of fenoterol on the Ca-signals in cardiomyocytes of the isolated atria.

(A) The changes in fluorescence of the Fluo-4 Ca-indicator loaded into cardiomyocytes of the isolated atrium. The pseudo-colored images illustrate Ca-signals occurring in cardiomyocytes of the isolated atria per single atrial contraction before (a, a') and after the application of fenoterol at concentrations of 5 (b, c) and 50 μM (b', c'). Above the images, the time from the stimulus is shown (ms): 0, 18, 88, 158, 228. The scale is 10 μm . On the right, the curves representing changes in the fluorescence of Fluo-4 occurring as a response to the stimulus are shown. Along the Y-axis: the intensity of fluorescence, rel. units ("0" is fluorescence before stimulus); along the X-axis: time in ms from the stimulus. (B) The effect of 5 ($n = 7$) and 50 ($n = 7$) μM fenoterol on the amplitude of Ca-signals (open and filled squares, respectively). Changes in the amplitude of Ca-signals in the absence of fenoterol are shown with open circles connected by a dash line (Control, $n = 5$). Along the Y-axis: fluorescence (%); along the X-axis: time (min). The application of fenoterol is indicated with a line.

the intracellular solution. The application of fenoterol at high concentrations (50 μM) caused an increase in the amplitude of Ca-signals to $121.9 \pm 4.9\%$ ($p < 0.05$, $n = 7$) just after 30 s, and by the third minute, its value reached a maximum, $154 \pm 4.8\%$ ($p < 0.01$, $n = 7$). After 8 min of application, the amplitude began to decline, and 20 min after the application of fenoterol, its value was $111.2 \pm 4.3\%$ ($p < 0.05$, $n = 7$). The amplitude of Ca-signals was brought to its initial value 50–60 min after perfusion of the atrial specimen with a fenoterol solution was begun.

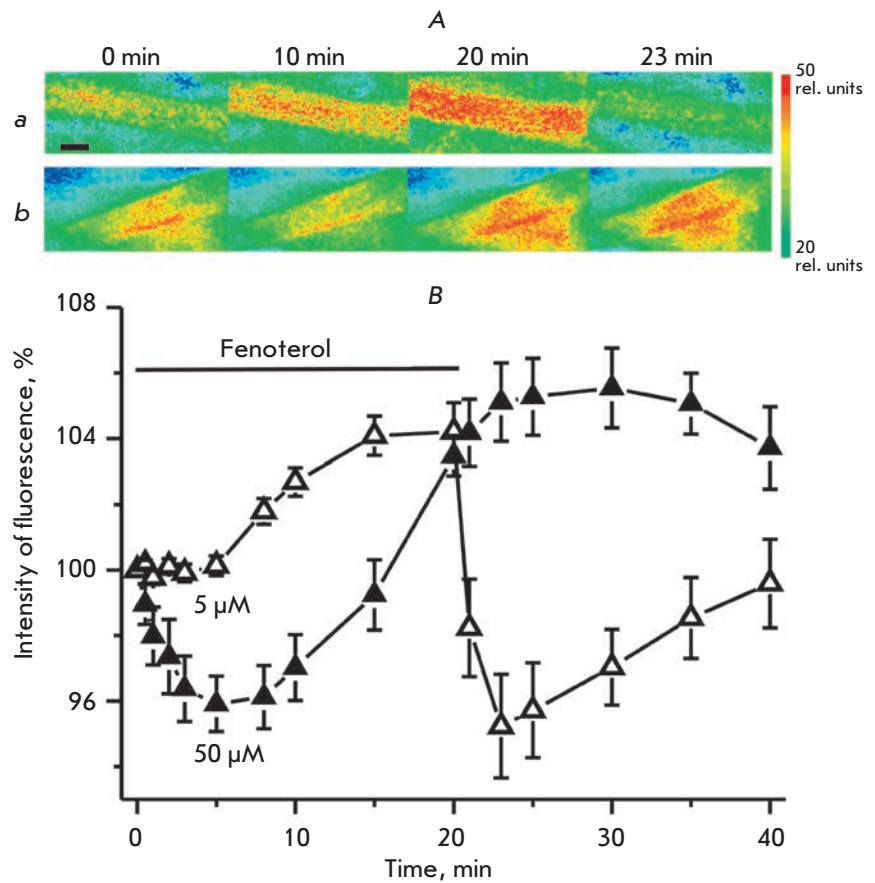
The Effect of Fenoterol on the Production of Nitric Oxide

Under the action of fenoterol, the fluorescence of the DAF-FM marker (an indicator of NO production) in

atrial cardiomyocytes reliably grew (Fig. 3). At low doses, fenoterol initiated a gradual increase in the NO production; and after 20 min of application of fenoterol, the intensity of the fluorescence grew to $104 \pm 0.7\%$ ($p < 0.05$, $n = 6$). After the removal of fenoterol from the surrounding solution, the intensity of the fluorescence dropped to $95.0 \pm 1.4\%$ ($p < 0.05$, $n = 6$) relative to the initial level, after which it returned to the baseline within 5 min. Under the action of a high dose of fenoterol, during the first 5 min of application, a decrease in the intensity of DAF-FM fluorescence was observed (by the fifth minute of application, the intensity was $95.9 \pm 0.8\%$ ($p < 0.05$, $n = 6$)). After 8 min of application of fenoterol, the intensity of the fluorescence began to grow and reached $103.9 \pm 0.6\%$ ($p < 0.05$, $n = 6$) within 20 min. After the atrial specimen was perfused with a

Fig. 3. Effect of fenoterol on the synthesis of nitric oxide in cardiomyocytes of the isolated atrium.

(A) The changes in the fluorescence of the DAF-FM dye pre-loaded into cardiomyocytes of the isolated atrium, occurring as a response to the application of 5 (a) and 50 (b) μM fenoterol. The images of atrial cardiomyocyte bundles are presented (the intensity is shown with a pseudocolor). The scale is 10 μm . (B) The dynamics of the DAF-FM fluorescence (an indicator of nitric oxide production). Along Y-axis: fluorescence intensity (%) (100% corresponds to the value of fluorescence before application of fenoterol). Fenoterol concentrations of 5 ($n = 6$) and 50 ($n = 6$) μM are shown with open and filled triangles, respectively. The X-axis: time (min). The application of fenoterol is indicated with a line.



fenoterol-free solution, the intensity of the fluorescence exceeded the control level for 10–15 min: its value was 104.3–106.7% ($p < 0.05$, $n = 6$) relative to the baseline.

DISCUSSION

The slow development and stability of the effects produced by 1 and 5 μM of fenoterol indicate the activation of the intracellular signal systems with a long-term effect, which is caused by the stimulation of β_2 -adrenoreceptors. In our opinion, the influence of fenoterol on the inotropic atrial function can be explained by the interaction of β_2 -adrenoreceptors with several intracellular signaling cascades that regulate the contractility.

The key factor defining the contractility of the cardiac muscle is the concentration of calcium ions in cardiomyocytes during systole. The contractions of cardiomyocytes are initiated by calcium ions, which enter the cytosol in two ways. Depolarization of the membrane caused by the action potential leads to an opening of voltage-dependent calcium channels, through which calcium ions influx into the cytoplasm, where they bind to the ryanodine receptors (Ca-release channels) of the sarcoplasmic reticulum. As a result, calcium ions are re-

leased from the sarcoplasmic reticulum, and their concentration in the cytoplasm reaches a maximum. In our experiments, the application of fenoterol led to a significant increase in the intensity of Ca-signals (*Fig. 2*); this most likely occurs due to an increase in the amount of Ca^{2+} ions entering through the channels of the plasma membrane. It is known that β_2 -adrenoreceptors, as well as β_1 -adrenoreceptors, bind to Gs proteins, which activate the adenylate cyclase that catalyzes the synthesis of cAMP, a secondary messenger. This process activates cAMP-dependent protein kinases, which phosphorylate the specific target proteins [37]. One of the main substrates for protein kinase A is the L-type calcium channel, which, in the phosphorylated state, has a higher conductance and a higher probability of opening up and is activated when the membrane potential values are more negative [9, 31].

The following interesting fact was denoted. At a concentration of 5 μM , fenoterol causes slow growth in the intensity of Ca-signals, whose amplitude remains high after the removal of fenoterol from the solution surrounding the specimen. Simultaneously, the application of 50 μM of fenoterol leads to an increase in the amplitude of Ca-signals (*Fig. 2*).

There are three possible explanations for this. First, it can be suggested that fenoterol begins to affect not only β_2 -adrenoreceptors at a higher dose, but also β_1 -adrenoreceptors, which activate an additional number of calcium channels under the action of protein kinase A. Thus, the constant characterizing the binding of fenoterol (stereoisomers *R,R*-1 and -2) to the β_1 -adrenoreceptors of HEK cells is estimated to be approximately 15–20 μM [28]. In addition, the most effective concentration of fenoterol, i.e. the concentration that leads to a maximum increase in the contractility of human papillary muscle isolated specimens, was 100 μM ; in this case, the effect of fenoterol depended on β_2 - and β_1 -adrenoreceptors [38]. However, this explanation contradicts our results, according to which the selective β_2 -adrenoreceptor blocker (0.1 μM ICI-118.551) completely eliminates the positive inotropic effect produced by 50 μM fenoterol. The second possible explanation is the involvement of a large number of metabotropic β_2 -adrenoreceptors that cause an increase in the production of cAMP and the activation of a large number of protein kinase A molecules, which in turn intensify the phosphorylation of Ca-channels, rendering them more active [1]. However, the *R,R*-stereoisomer of fenoterol at a concentration of around 0.5 μM activates almost all β_2 -adrenoreceptors in rat ventricular cardiomyocytes [39]. According to the approximate estimations made, even at a concentration of 2 μM , the racemic fenoterol used occupies around 90% of the β_2 -adrenoreceptors of bronchial epithelial cells [27]. Consequently, it is most likely that, under the action of 5 and 50 μM of fenoterol, an equal number of β_2 -adrenoreceptors is activated. The third suggestion is based on the facts noted to date that, for transduction the signal inside a cell, β_2 -adrenoreceptors can use different signal cascades and/or bind differently in terms of efficiency to effector molecules, depending on the dose of the agonist [22]. Thus, upon application of high doses of the agonist (100 μM isoproterenol), the isolated β_2 -adrenoreceptors can exist in two different conformations [40]; in each conformation, the efficiency of the interaction of the activated receptor with G proteins and other proteins is different. It is interesting to note that as a response to the application of selectively high doses of the agonist, the β_2 -adrenoreceptor begins to activate not only Gs proteins, but also tyrosine kinase Src, which is involved in the regulation of signal proteins (e.g., MAP-kinase) and phosphorylates the β_2 -adrenoreceptor. The phosphorylated residues of β_2 -adrenoreceptor tyrosine can play the role of a docking-site for other signal molecules [22]. In addition, Src-kinase is capable of regulating (including the activation) L-type Ca-channel function by binding to the N-terminal region of the channel α_1 -subunit and phosphorylat-

ing it [41]. Most likely, the rapid increase in the amplitude of Ca-signals observed under the action of 50 μM of fenoterol occurs due to the activation of an additional pathway (e.g., involving Src-kinase), which facilitates the function of the L-type Ca-channels. In our opinion, the last suggestion is the most probable and should be studied experimentally in the first place.

In the study we performed, the increase in the production of nitric oxide in atrial cardiomyocytes occurring under the action of fenoterol was revealed for the first time (*Fig. 3*). The production of nitric oxide is an important factor that controls the contractility of cardiomyocytes. An intensification of the NO production may lead to a negative inotropic effect and/or interfere with increasing contractility of cardiomyocytes [42]. Such an effect by nitric oxide might be associated with the activation of cGMP-dependent protein kinases G, which phosphorylate troponin I, thereby decreasing the sensitivity of troponin C to calcium, and influence the Ca-channels, thereby decreasing the calcium conductance [43, 44]. Since the effect of nitric oxide is connected to the activation of the guanylate cyclase that is in the “on” state, it produces thousands of cGMP molecules; thus, even a slight increase in the synthesis of NO can have a significant influence on the cell functions [45].

Several hypotheses regarding the mechanisms of how β_2 -adrenoreceptors are linked with the NO synthase responsible for the production of nitric oxide can be suggested. β_2 -Adrenoreceptors have the ability to interact with the Gi protein. However, the activated receptor binds to the Gi protein less readily than it binds to the Gs protein [46]. It is assumed that for a longer period of time, the activated β_2 -adrenoreceptors are in a state that is characterized by high affinity to the Gs protein, while it is in a state in which it is selectively bound to the Gi protein for a shorter period [47]. According to the other hypothesis, β_2 -adrenoreceptors can interact with the Gi protein only after having been phosphorylated by protein kinase A or kinase of G protein coupled receptors [48]. The α -subunits of the Gi protein inhibit production of cAMP by adenylate cyclases, and the dimers of $\beta\gamma$ -subunits affect some ionic channels and signal molecules; in particular, they activate the PI3K/protein kinase B pathway [1, 49]. One of the effectors in this pathway is NO synthase (neural and endothelial isoforms), whose activity intensifies after its phosphorylation by protein kinase B [50]. In rat endothelial cells, the application of fenoterol causes an increase in the PI3K/protein kinase B-dependent activity of the endothelial NO synthase [26]. However, in rat ventricular and cat atrial cardiomyocytes, fenoterol (0.1 μM) did not activate the pathway associated with the Gi protein and NO production, and its effect on con-

tractility was exclusively associated with the Gs protein [15, 51].

The activation of the Gi-protein in HEK293 cells under the action of fenoterol has been recently found to be independent of ERK1/2 kinase (extracellular signal-regulating kinases) [29]. In rat cardiomyocytes, ERK1/2 is phosphorylated and activated in the NO-dependent pathway [52]. Most likely, β_2 -adrenoreceptors are capable of activating NO synthase independently of the G-protein. The β -arrestin 2 protein, which interacts simultaneously with β_2 -adrenoreceptors and NO synthase, may play the role of a factor that conjugates the activation of the receptor and the increase in NO production [43]. Src kinase stimulated by β_2 -adrenoreceptors phosphorylates the Tyr83 residue of the endothelial NO synthase, thereby increasing the synthesis of NO [54]. In addition, the activation of NO production is facilitated by the complex of calcium ions with calmodulin [42]; that is why an increase in the production of nitric oxide is most likely partially caused by an increase in the concentration of calcium ions due to the high activity of L-type calcium channels.

It should be noted that in this work the production of nitric oxide started to increase almost immediately after the application of a low concentration of fenoterol, while at a high concentration, fenoterol caused a decrease, firstly, and then an increase in NO synthesis. Most likely, in the latter case, a dramatic increase in the production of cAMP firstly had a negative influence on the functioning of NO synthase (our unpublished data), and then the activating action of signals appeared from β_2 -adrenoreceptors and an increased calcium level.

Upon consideration of the effects of the activation of β_2 -adrenoreceptors, it should not be forgotten that β_2 -adrenoreceptors can directly interact with the factor that regulates the Na/H exchange, the N-ethylmaleimide-sensitive factor (that controls the internalization of the receptors and the interaction with Gi-proteins), and the scaffold proteins that connect adrenoreceptors with protein kinase A, C, phosphatase 2A, and L-type calcium channels [20, 22–24]. As a result, the dimers of β_2 -adrenoreceptors can accumulate around the macromolecular signal complex which provides a “coordinated” response by a cell to their activation [55, 56]. Moreover, β_2 -adrenoreceptors, calcium channels, endothelial NO synthase, NADPH oxidase, and other regulatory molecules are colocalized in caveolae, small invaginations of the plasma membrane enriched in cholesterol and caveolin [55]. That is why the effects of β_2 -adrenoreceptor activation *in vivo* can be associated with changes in the activity of a large number of regulatory molecules in limited regions of the cell.

β_2 -Adrenoreceptors are known to exhibit a rapid loss of sensitivity to agonists, followed by a dramatic de-

crease in the number of receptors [27, 36]. Taking this into account, it can be suggested that fenoterol initiates processes that interfere with the desensitization of β_2 -adrenoreceptors, which explains the stability of the effect of fenoterol on the amplitude of contractions and Ca-signals. Nitric oxide directly affects β_2 -adrenoreceptors and the proteins involved in the desensitization of β_2 -adrenoreceptors (G protein-coupled receptor kinases) via S-nitrosylation. As a result, it prevents a decline in the sensitivity of the receptors, which occurs under the action of the agonist, and a decrease in the amount of receptors [16, 53]. As a response to the activation of β_2 -adrenoreceptors, dynamin, a small GT-Pase that participates in endocytosis, undergoes S-nitrosylation; this transformation boosts its ability to polymerize and form a contractive “collar” [57]. Thus, the prolonged effect of fenoterol might be explained by the action of nitric oxide on receptors, G protein-coupled receptors, and dynamin. On the one hand, the increase in NO production that occurs under the action of fenoterol facilitates the closing of caveolae (i.e. the narrowing of the pore that connects an extracellular medium with the cavity of caveolae), in which the agonist molecules are captured; and on the other hand, it provides long-term activity of β_2 -adrenoreceptors. In this case, even the removal of fenoterol from an extracellular medium does not cause a rapid decline in the effects.

CONCLUSIONS

Relying on the data obtained in this work, the following can be suggested. The activation of β_2 -adrenoreceptors with low doses of the agonist simultaneously initiates signal cascades, which have differently directed effects on atrial contractility. That is why the positive inotropic effect produced by the agonist does not occur at the beginning. However, the production of nitric oxide declines, while the amplitude of Ca-signals remains high; this leads to an increase in contractility. In the case of activation of β_2 -adrenoreceptors with high doses of the agonist, the pathway associated with a dramatic increase in the amplitude of Ca-signals is activated first, while the increase in the production of nitric oxide is “delayed”; that is why a significant, positive inotropic effect of the agonist is observed. The hypothetic two-component differently directed mechanism which underlies the changes in the atrial contractility occurring upon activation of β -adrenoreceptors by fenoterol (racemic) requires a more detailed experimental study. The pharmacological approach involving the application of nitric oxide synthesis blockers, the adenylate cyclase system, L-type calcium channels, ryanodine receptors, and probably endocytosis inhibitors would allow to shed more light on the pathways of the effects produced by the β_2 -adrenoreceptors of atrial cardiomy-

ocytes, thereby providing an answer to the questions raised in this work. ●

The authors thank I. R. Efimov and A. V. Gluhov (Washington University, Saint-Louis, USA) for discussions of the results and valuable remarks during the preparation of this paper

This work was supported by grants from the Ministry of Education and Science of the Russian Federation (NSh-5250.2010.4 and MK-3840.2010.4), the Russian Foundation for Fundamental Research (nos. 11-04-00568-a and 11-04-00422-a), and the Federal Targeted Program 02.740.11.0302.

REFERENCES

1. Abramochkin D.V., Sukhova G.S., Rozenshtau L.V. // *Kardiologiya (Cardiology)*. 2006. V.45. № 6. P. 50-53.
2. Buxton B.F., Jones C.R., Molenaar P., Summers R.J. // *Br. J. Pharmacol.* 1987. V. 92. P. 299-310.
3. Vatner S.F., Young M.A. // *Circ. Res.* 1986. V. 59. P. 579-596.
4. Hedberg A., Kempf F.Jr., Josephson M.E., Molinoff P.B. // *J. Pharmacol. Exp. Ther.* 1985. V. 234. P. 561-568.
5. Xiao R.P., Lakatta E.G. // *Circ. Res.* 1993. V. 73. P. 286-300.
6. Sosunov E.A., Gainullin R.Z., Moise N.S., Steinberg S.F., Danilo P., Rosen M.R. // *Cardiovasc. Res.* 2000. V. 48. P. 211-219.
7. Faucher F.A., Gannier F.E., Lignon J.M., Cosnay P., Malécot C.O. // *Am. J. Physiol. Cell. Physiol.* 2008. V. 294. P. 106-117.
8. Davare M.A., Avdonin V., Hall D.D., Peden E.M., Burette A., Weinberg R.J., Horne M.C., Hoshi T., Hell J.W. // *Science*. 2001. V. 293. P. 98-101.
9. Haase H. // *Cardiovasc. Res.* 2007. V. 73. P. 19-25.
10. Jo S.H., Leblais V., Wang P.H., Crow M.T., Xiao R.P. // *Circ. Res.* 2002. V. 91. P. 46-53.
11. Xiao R.P., Ji X., Lakatta E.G. // *Mol. Pharmacol.* 1995. V. 47. P. 322-329.
12. Chesley A., Lundberg M.S., Asai T., Xiao R.P., Ohtani S., Lakatta E.G., Crow M.T. // *Circ. Res.* 2000. V. 87. P. 1172-1179.
13. Zhu W.Z., Zheng M., Koch W.J., Lefkowitz R.J., Kobilka B.K., Xiao R.P. // *Proc. Natl. Acad. Sci. USA*. 2001. V. 98. P. 1607-1612.
14. Danson J.F., Zhang Y.H., Sears C.E., Edwards A.R., Casadei B., Paterson D.J. // *Cardiovasc. Res.* 2005. V. 67. P. 613-623.
15. Dedkova E.N., Wang Y.G., Blatter L.A., Lipsius S.L. // *J. Physiol.* 2002. V. 542. P. 711-723.
16. Whalen E.J., Foster M.W., Matsumoto A., Ozawa K., Violin J.D., Que L.G., Nelson C.D., Benhar M., Keys J.R., Rockman H.A., et al. // *Cell*. 2007. V. 129. P. 511-522.
17. Milano C.A., Allen L.F., Rockman H.A., Dolber P.C., Mc-Minn T.R., Chien K.R., Johnson T.D., Bond R.A., Lefkowitz R.J. // *Science*. 1994. V. 264. P. 582-586.
18. Liggett S.B., Tepe N.M., Lorenz J.N. // *Circulation*. 2000. V. 101. P. 1707-1714.
19. Zhou Y.Y., Cheng H., Song L.S., Wang D., Lakatta E.G., Xiao R.P. // *Mol. Pharmacol.* 1999. V. 56. P. 485-493.
20. Hall R.A., Premont R.T., Chow C.W., Blitzer J.T., Pitcher J.A., Claing A., Stoffel R.H., Barak L.S., Shenolikar S., Weinman E.J., et al. // *Nature*. 1998. V. 392. P. 626-630.
21. Peleg G., Ghanouni P., Kobilka B.K., Zare R.N. // *Proc. Natl. Acad. Sci. USA*. 2001. V. 98. P. 8469-8474.
22. Sun Y., Huang J., Xiang Y., Bastepe M., Jüppner H., Kobilka B.K., Zhang J.J., Huang X.Y. // *EMBO J.* 2007. V. 26. P. 53-64.
23. Wang Y., Lauffer B., von Zastrow M., Kobilka B.K., Xiang Y. // *Mol. Pharmacol.* 2007. V. 72. P. 429-439.
24. Xiang Y., Kobilka B. // *Proc. Natl. Acad. Sci. USA*. 2003. V. 100. P. 10776-10781.
25. Swift S.M., Schwarb M.R., Mihlbachler K.A., Liggett S.B. // *Am. J. Respir. Cell. Mol. Biol.* 2007. V. 136. P. 236-243.
26. Figueroa X.F., Poblete I., Fernández R., Pedemonte C., Cortés V., Huidobro-Toro J.P. // *Am. J. Physiol. Heart. Circ. Physiol.* 2009. V. 297. P. 134-143.
27. Bruce R.W., Roger B., Richard B.C. // *Mol. Pharmacol.* 2000. V. 58. P. 421-430.
28. Jozwiak K., Woo A.Y., Tanga M.J., Toll L., Jimenez L., Kozocas J.A., Plazinska A., Xiao R.P., Wainer I.W. // *Bioorg. Med. Chem.* 2010. V. 18. P. 728-736.
29. Woo A.Y., Wang T.B., Zeng X., Zhu W., Abernethy D.R., Wainer I.W., Xiao R.P. // *Mol. Pharmacol.* 2009. V. 75. P. 158-165.
30. Iijima T., Taira N. // *Eur. J. Pharmacol.* 1989. V. 163. P. 357-360.
31. Skeberdis V.A., Jurevicius J., Fischmeister R. // *J. Pharmacol. Exp. Ther.* 1997. V. 283. P. 452-461.
32. Hasseldine A.R., Harper E.A., Black J.W. // *Br. J. Pharmacol.* 2003. V. 138. P. 1358-1366.
33. Prendergast C.E., Shankley N.P., Black J.W. // *Br. J. Pharmacol.* 2000. V. 129. P. 1285-1288.
34. Harkins A.B., Kurebayashi N., Baylor S.M. // *Biophysic. J.* 1993. V. 65. P. 865-881.
35. Kojima H., Urano Y., Kikuchi K., Higuchi T., Hirata Y., Nagano T. // *Angew. Chem. Int. Ed. Engl.* 1999. V. 38. P. 3209-3212.
36. Liggett S.B. // *Am. J. Respir. Crit. Care Med.* 2000. V. 161. P. 197-201.
37. DiPilato L.M., Zhang J. // *Circ. Res.* 2006. V. 99. P. 1021-1023.
38. Mügge A., Posselt D., Reimer U., Schmitz W., Scholz H. // *J. Mol. Med.* 1985. V. 63. P. 26-31.
39. Jozwiak K., Khalid C., Tanga M.J., Berzetei-Gurske I., Jimenez L., Kozocas J.A., Woo A., Zhu W., Xiao R.P., Abernethy D.R., et al. // *J. Med. Chem.* 2007. V. 50. P. 2903-2915.
40. Swaminath G., Xiang Y., Lee T.W., Steenhuis J., Parnot C., Kobilka B.K. // *J. Biol. Chem.* 2004. V. 279. P. 686-691.
41. Dubuis E., Rockliffe N., Hussain M., Boyett M., Wray D., Gawler D. // *Cardiovasc. Res.* 2006. V. 69. P. 391-401.
42. Balligand J.L., Feron O., Dessy C. // *Physiol. Rev.* 2009. V. 89. P. 481-534.
43. Fiedler B., Wollert K.C. // *Cardiovasc. Res.* 2004. V. 63. P. 450-457.
44. Seddon M., Shah A.M., Casadei B. // *Cardiovasc. Res.* 2007. V. 75. P. 315-326.
45. Urazaev A.Kh., Zefirov A.L. // *Usp. Fiziol. Nauk.* 1999. V. 30. № 1. P. 54-72.
46. Wenzel-Seifert K., Seifert R. // *Mol. Pharmacol.* 2000. V. 58. P. 954-966.

RESEARCH ARTICLES

47. Seifert R., Dove S. // *Mol. Pharmacol.* 2009. V. 75. P. 13–18.
48. Liu R., Ramani B., Soto D., De Arcangelis V., Xiang Y. // *J. Biol. Chem.* 2009. V. 284. P. 32279–32287.
49. Baillie G.S., Sood A., McPhee I., Gall I., Perry S.J., Lefkowitz R.J., Houslay M.D. // *Proc. Natl. Acad. Sci. USA.* 2003. V. 100. P. 940–945.
50. Lynch G.S., Ryall J.G. // *Physiol. Rev.* 2008. V. 88. P. 729–767.
51. Xiao R.P., Zhang S.J., Chakir K., Avdonin P., Zhu W., Bond R.A., Balke C.W., Lakatta E.G., Cheng H. // *Circulation.* 2003. V. 108. P. 1633–1639.
52. Xu Z., Ji X., Boysen P.G. // *Am. J. Physiol. Heart. Circ. Physiol.* 2004. V. 286. P. 1433–1440.
53. Ozawa K., Whalen E.J., Nelson C.D., Mu Y., Hess D.T., Lefkowitz R.J., Stamler J.S. // *Mol. Cell.* 2008. V. 31. № 3. P. 395–405.
54. Fulton D., Church J.E., Ruan L., Li C., Sood S.G., Kemp B.E., Jennings I.G., Venema R.C. // *J. Biol. Chem.* 2005. V. 280. P. 35943–35952.
55. Cherezov V., Rosenbaum D.M., Hanson M.A., Rasmussen S.G., Thian F.S., Kobilka T.S., Choi H.J., Kuhn P., Weis W.I., Kobilka B.K., et al. // *Science.* 2007. V. 318. P. 1258–1265.
56. Liu G., Shi J., Yang L., Cao L., Park S.M., Cui J., Marx S.O. // *EMBO J.* 2004. V. 23. P. 2196–2205.
57. Wang G., Moniri N.H., Ozawa K., Stamler J.S., Daaka Y. // *Proc. Natl. Acad. Sci. USA.* 2006. V. 103. P. 1295–1300.

GENERAL RULES

Actae Naturae publishes experimental articles and reviews, as well as articles on topical issues, short reviews, and reports on the subjects of basic and applied life sciences and biotechnology.

The journal is published by the Park Media publishing house in both Russian and English.

The journal *Acta Naturae* is on the list of the leading periodicals of the Higher Attestation Commission of the Russian Ministry of Education and Science

The editors of *Actae Naturae* ask of the authors that they follow certain guidelines listed below. Articles which fail to conform to these guidelines will be rejected without review. The editors will not consider articles whose results have already been published or are being considered by other publications.

The maximum length of a review, together with tables and references, cannot exceed 60,000 symbols (approximately 40 pages, A4 format, 1.5 spacing, Times New Roman font, size 12) and cannot contain more than 16 figures.

Experimental articles should not exceed 30,000 symbols (20 pages in A4 format, including tables and references). They should contain no more than ten figures. Lengthier articles can only be accepted with the preliminary consent of the editors.

A short report must include the study's rationale, experimental material, and conclusions. A short report should not exceed 12,000 symbols (8 pages in A4 format including no more than 12 references). It should contain no more than four figures.

The manuscript should be sent to the editors in electronic form: the text should be in Windows Microsoft Word 2003 format, and the figures should be in TIFF format with each image in a separate file. In a separate file there should be a translation in English of: the article's title, the names and initials of the authors, the full name of the scientific organization and its departmental affiliation, the abstract, the references, and figure captions.

MANUSCRIPT FORMATTING

The manuscript should be formatted in the following manner:

- Article title. Bold font. The title should not be too long or too short and must be informative. The title should not exceed 100 characters. It should reflect the major result, the essence, and uniqueness of the work, names and initials of the authors.
- The corresponding author, who will also be working with the proofs, should be marked with a footnote *.
- Full name of the scientific organization and its departmental affiliation. If there are two or more scientific organizations involved, they should be linked by digital superscripts with the authors' names. Abstract. The structure of the abstract should be very clear and must reflect the following: it should introduce the reader to the main issue and describe the experimental approach, the possibility of practical use, and the possibility of further research in the field. The average length of an abstract is 20 lines

(1,500 characters).

- Keywords (3 – 6). These should include the field of research, methods, experimental subject, and the specifics of the work. List of abbreviations.

- INTRODUCTION
- EXPERIMENTAL PROCEDURES
- RESULTS AND DISCUSSION
- CONCLUSION

The organizations that funded the work should be listed at the end of this section with grant numbers in parenthesis.

- REFERENCES

The in-text references should be in brackets, such as [1].

RECOMMENDATIONS ON THE TYPING AND FORMATTING OF THE TEXT

- We recommend the use of Microsoft Word 2003 for Windows text editing software.
- The Times New Roman font should be used. Standard font size is 12.
- The space between the lines is 1.5.
- Using more than one whole space between words is not recommended.
- We do not accept articles with automatic referencing; automatic word hyphenation; or automatic prohibition of hyphenation, listing, automatic indentation, etc.
- We recommend that tables be created using Word software options (Table → Insert Table) or MS Excel. Tables that were created manually (using lots of spaces without boxes) cannot be accepted.
- Initials and last names should always be separated by a whole space; for example, A. A. Ivanov.
- Throughout the text, all dates should appear in the “day.month.year” format, for example 02.05.1991, 26.12.1874, etc.
- There should be no periods after the title of the article, the authors' names, headings and subheadings, figure captions, units (s – second, g – gram, min – minute, h – hour, d – day, deg – degree).
- Periods should be used after footnotes (including those in tables), table comments, abstracts, and abbreviations (mon. – months, y. – years, m. temp. – melting temperature); however, they should not be used in subscripted indexes (T_m – melting temperature; $T_{p.t.}$ – temperature of phase transition). One exception is mln – million, which should be used without a period.
- Decimal numbers should always contain a period and not a comma (0.25 and not 0,25).
- The hyphen (“-”) is surrounded by two whole spaces, while the “minus,” “interval,” or “chemical bond” symbols do not require a space.
- The only symbol used for multiplication is “×”; the “×” symbol can only be used if it has a number to its right. The “.” symbol is used for denoting complex compounds in chemical formulas and also noncovalent complexes (such as DNA·RNA, etc.).
- Formulas must use the letter of the Latin and Greek alphabets.

GUIDELINES FOR AUTHORS

- Latin genera and species' names should be in italics, while the taxa of higher orders should be in regular font.
- Gene names (except for yeast genes) should be italicized, while names of proteins should be in regular font.
- Names of nucleotides (A, T, G, C, U), amino acids (Arg, Ile, Val, etc.), and phosphonucleotides (ATP, AMP, etc.) should be written with Latin letters in regular font.
- Numeration of bases in nucleic acids and amino acid residues should not be hyphenated (T34, Ala89).
- When choosing units of measurement, SI units are to be used.
- Molecular mass should be in Daltons (Da, KDa, MDa).
- The number of nucleotide pairs should be abbreviated (bp, kbp).
- The number of amino acids should be abbreviated to aa.
- Biochemical terms, such as the names of enzymes, should conform to IUPAC standards.
- The number of term and name abbreviations in the text should be kept to a minimum.
- Repeating the same data in the text, tables, and graphs is not allowed.

GUIDENESS FOR ILLUSTRATIONS

- Figures should be supplied in separate files. Only TIFF is accepted.
- Figures should have a resolution of no less than 300 dpi for color and half-tone images and no less than 500 dpi.
- Files should not have any additional layers.

REVIEW AND PREPARATION OF THE MANUSCRIPT FOR PRINT AND PUBLICATION

Articles are published on a first-come, first-served basis. The publication order is established by the date of acceptance of the article. The members of the editorial board have the right to recommend the expedited publishing of articles which are deemed to be a priority and have received good reviews.

Articles which have been received by the editorial board are assessed by the board members and then sent for external review, if needed. The choice of reviewers is up to the editorial board. The manuscript is sent on to reviewers who are experts in this field of research, and the editorial board makes its decisions based on the reviews of these experts. The article may be accepted as is, sent back for improvements, or rejected.

The editorial board can decide to reject an article if it does not conform to the guidelines set above.

A manuscript which has been sent back to the authors for improvements requested by the editors and/or reviewers is reviewed again, after which the editorial board makes another decision on whether the article can be accepted for publication. The published article has the submission and publication acceptance dates set at the beginning.

The return of an article to the authors for improvement does not mean that the article has been accepted for publication. After the revised text has been received, a decision is made by the editorial board. The author must return the improved text, together with the original text and responses to all comments. The date of acceptance is the day on which the final version of the article was received by the publisher.

A revised manuscript must be sent back to the publisher a week after the authors have received the comments; if not, the article is considered a resubmission.

E-mail is used at all the stages of communication between the author, editors, publishers, and reviewers, so it is of vital importance that the authors monitor the address that they list in the article and inform the publisher of any changes in due time.

After the layout for the relevant issue of the journal is ready, the publisher sends out PDF files to the authors for a final review.

Changes other than simple corrections in the text, figures, or tables are not allowed at the final review stage. If this is necessary, the issue is resolved by the editorial board.

FORMAT OF REFERENCES

The journal uses a numeric reference system, which means that references are denoted as numbers in the text (in brackets) which refer to the number in the reference list.

For books: the last name and initials of the author, full title of the book, location of publisher, publisher, year in which the work was published, and the volume or issue and the number of pages in the book.

For periodicals: the last name and initials of the author, title of the journal, year in which the work was published, volume, issue, first and last page of the article. Must specify the name of the first 10 authors. Ross M.T., Grafham D.V., Coffey A.J., Scherer S., McLay K., Muzny D., Platzer M., Howell G.R., Burrows C., Bird C.P., et al. // Nature. 2005. V. 434. № 7031. P. 325–337.

References to books which have Russian translations should be accompanied with references to the original material listing the required data.

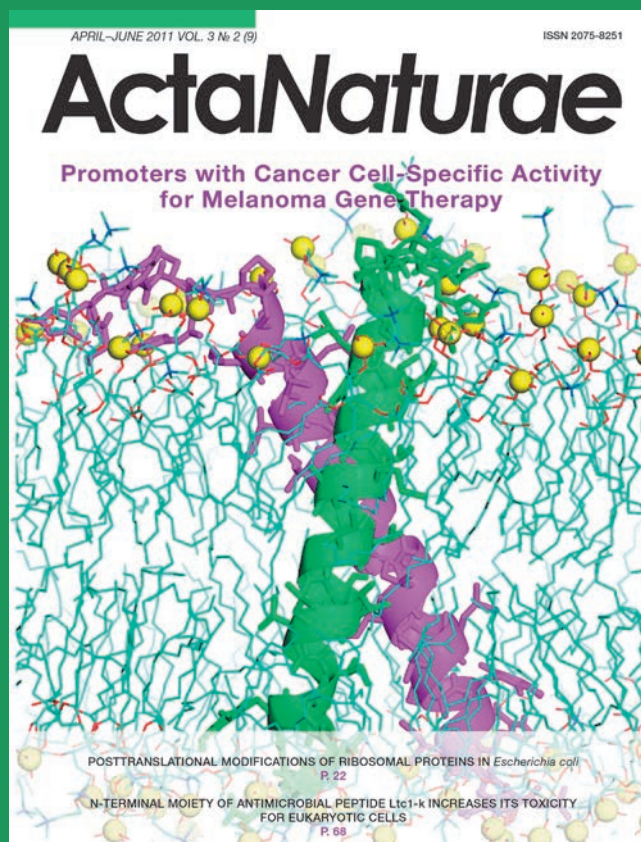
References to doctoral thesis abstracts must include the last name and initials of the author, the title of the thesis, the location in which the work was performed, and the year of completion.

References to patents must include the last names and initials of the authors, the type of the patent document (the author's rights or patent), the patent number, the name of the country that issued the document, the international invention classification index, and the year of patent issue.

The list of references should be on a separate page. The tables should be on a separate page, and figure captions should also be on a separate page.

The following e-mail addresses can be used to contact the editorial staff: vera.knorre@gmail.com, actanaturae@gmail.com, tel.: (495) 727-38-60, (495) 930-80-05

Acta Naturae is a new international journal on life sciences based in Moscow, Russia. Our goal is to present scientific work and discovery in molecular biology, biochemistry, biomedical disciplines and biotechnology. *Acta Naturae* is also a periodical for those who are curious in various aspects of biotechnological business, intellectual property protection and social consequences of scientific progress.



For more information and subscription please contact us at info@biorf.ru

NANOTECHNOLOGIES

in Russia

Peer-review scientific journal

Nanotechnologies in Russia
(*Rossiiskie Nanotekhnologii*)

focuses on self-organizing structures and nanoassemblages, nanostructures including nanotubes, functional nanomaterials, structural nanomaterials, devices and facilities on the basis of nanomaterials and nanotechnologies, metrology, standardization, and testing in nanotechnologies, nanophotonics, nanobiology.

—> **Russian edition:** <http://nanoru.ru>

—> **English edition:** <http://www.springer.com/materials/nanotechnology/journal/12201>

Issued with support from:



The Ministry of Education and Science of the Russian Federation